Departamento de Física Teórica e Instituto de Física Teórica

Universidad Autónoma de Madrid

PROBING THE FOUNDATIONS OF THE STANDARD COSMOLOGICAL MODEL

Memoria de Tesis Doctoral presentada por

Miguel Zumalacárregui Pérez

para optar al título de Doctor en Ciencias Físicas

Programa de Doctorado de Física Teórica

Trabajo supervisado por los Doctores

Juan García-Bellido Capdevila, Profesor Titular
del Departamento de Física Teórica, Universidad Autónoma de Madrid

Pilar Ruiz-Lapuente, Investigadora Científica
del Instituto de Física Fundamental, Consejo Superior de Investigaciones Científicas

y

Tomi S. Koivisto, Investigador Postdoctoral
del Instituto de Astrofísica Teórica, Universidad de Oslo.

Octubre de 2012

A mis padres.

Contents

Statement

The results presented in this dissertation (Chapters 3-6) are based on original work done in collaboration with other researchers during the course of my PhD, from September 2008 to August 2012. The content of these Chapters is based on the released publications [1–6], as well as another ongoing project which is at a mature stage [3]. These references are listed below for convenience. In particular, Chapter 3 is based on Reference [1], Chapter 4 on References [5, 6], Chapter 5 is based on Reference [4] and Chapter 6 is based on References [2, 3]. The introductory Chapters 1 and 2 are mainly a review. The exposition there has been very influenced by References [7–10], as well the works cited in the text. Although they represent my own vision about some of the topics in which the results are framed, no claim of originality is made about the introductory Chapters. Appendices A and B describe some of the tools necessary for the analysis. Appendix D contains some lengthy equations that were not necessary to include in the body of the discussion.

Miguel Zumalacárregui Pérez
Madrid, October 2012

1. **"Tension in the Void: Cosmic Rulers Strain Inhomogeneous Cosmologies"**
   M. Zumalacarregui, J. Garcia-Bellido and P. Ruiz-Lapuente.
   JCAP **1210**, 009 (2012), [arXiv:1201.2790].

2. **"Screening Modifications of Gravity through Disformally Coupled Fields"**
   T. S. Koivisto, D. F. Mota and M. Zumalacarregui. [arXiv:1205.3167].

3. **"DBI Galileons in the Einstein Frame: Local Gravity and Cosmology,"**
   M. Zumalacarregui, T. S. Koivisto and D. F. Mota, [arXiv:1210.8016].

4. **"Disformal Scalar Fields and the Dark Sector of the Universe"**
   M. Zumalacarregui, T. S. Koivisto, D. F. Mota and P. Ruiz-Lapuente.
   JCAP **1005**, 038 (2010), [arXiv:1004.2684].

5. **"Constraining Entropic Cosmology"**
   T. S. Koivisto, D. F. Mota and M. Zumalacarregui.
   JCAP **1102**, 027 (2011), [arXiv:1011.2226].

6. **"Modified Entropic Gravity and Cosmology"**
   M. Zumalacarregui. AIP Conf. Proc. **1458**, 539 (2011), [arXiv:1202.1281].

Preface

You are pooped and demoralized. Why wouldn't you be? Of course it is exhausting, having to reason all the time in a universe which wasn't meant to be reasonable.

Kurt Vonnegut[1]

Astronomy and cosmology are arguably the oldest sciences, and perhaps the second oldest professions in history. After many millenia floating in the darkness of mysticism and speculation, cosmology has finally become an empirical and predictive discipline. The effort of thousands of scientists, from astronomers to theoretical physicists, has carved a Standard Cosmological Model (SCM) that is able to explain a large and increasing set of phenomena. The price to pay is the inclusion of three mysterious elements with no conventional explanation: inflation to account for the large scale homogeneity and initial perturbations of the universe, dark matter to enhance the formation of cosmic structure, and a Cosmological Constant to propel the latter stage of accelerated expansion.

The Standard Cosmological Model is undoubtedly beautiful. The elegance of the General Relativistic geometric description is supplemented by the symmetry of the large scale metric. Despite its simplicity, this scheme seems able to accurately describe the coarse grained evolution of the universe on the largest scales throughout cosmic history. Yet, many questions regarding the nature of the new elements remain unanswered: What is the mechanism behind cosmic inflation and the properties of the dark matter particle(s)? Is cosmic acceleration driven by Einstein's Cosmological Constant? If so, why is its value so small compared to particle physics energy scales but still large enough to be observable? If not, how is its value suppressed and what is the true mechanism for the acceleration?

The Standard Cosmological Model has been extremely successful in explaining a broad set of observables with just a handful of parameters. The evidence supporting cosmic acceleration has grown since the first decisive data from type Ia Supernovae (SNe) pointing towards the existence, and a number of independent observables agree now on the details of this paradigm. Measurements of the Cosmic Microwave Background (CMB) temperature anisotropies support the spatial flatness of the universe. When combined with the determi-

[1] *Breakfast of Champions* (1973)

nation of the local expansion rate, it follows that a smooth component with negative pressure must dominate the cosmic energy budget. Observations of the Large Scale Structure distribution confirm this picture. The formation rate of cosmic structures through gravitational collapse bounds the amount of clustering matter to be well below what is necessary for the universe to be spatially flat. The same physics that produces anisotropies in the CMB imprints a characteristic Baryon Acoustic (BAO) scale in the LSS distribution, which can be measured by galaxy surveys. It provides a standard ruler that tracks the cosmic expansion, further supporting the paradigm of cosmic acceleration.

Cosmology has made the promise of new physics. It not only supports its existence, but also provides means to validate or refute the different scenarios. As in a Gold Rush, myriads of alternatives to the Cosmological Constant have been proposed and studied in recent years. These models necessarily modify some sector of the Standard Cosmological model. It is possible to mimic the observed acceleration without the introduction of new exotic elements, by postulating a metric which is inhomogeneous on large scales. This can be done only at the price of living in a special location within the cosmos: the center of a very large, spherical and underdense region. Another possibility is to extend the Einstein-Hilbert action for General Relativity (GR), allowing the presence of scalar fields or even more dramatic modifications of the gravitational theory. Scalar fields can be uncoupled from other components, in which case they contribute to the universe dynamics only through their energy and pressure density. They may alternatively interact directly with all or some of the matter species, becoming potentially detectable through experiments in our Solar System and the study of the formation of Large Scale Structure.

The present Thesis explores models belonging to each of the categories previously described. A spherically symmetric but inhomogeneous cosmology is found to be discrepant with observations. The matter inhomogeneity necessary to explain the luminosity-redshift relation of type Ia SNe is incompatible with the BAO scale imprinted on the galaxy distribution, because the less dense region near our galaxy expand faster than the more dense ones far away, producing a space dependent stretch of the cosmic ruler. Several departures from General Relativity are also explored. Models based on ideas about the thermodynamical properties of space-time are studied by the modifications of the background cosmological equations that they produce. Theories beyond GR with a full and self consistent description are also considered. They are based on the addition of a scalar degree of freedom, which is introduced by means of a disformal tranformation the metric in some sector of the Lagrangian. The disformal transformation generalizes the well known local rescaling of the metric (confomal transformation), and allows one to establish connections between different theories, including the definition of new physical frames in which to study their consequences. This prescription also allows the construction of models for the cosmic acceleration in which the field is may couple to matter directly or not. In the coupled case, the scalar field mediates a new interaction that affects the growth of structure. However, a disformally coupled field becomes insensitive to the matter distribution in high density, non-relativistic environments, and the additional force is hidden from gravitational experiments in this regime.

Cosmology is not a beauty contest. A model should not be favored because of being simpler, more elegant, or widely accepted. Its validity should depend on the comparison between its predictions and the available data. In order to grant a democratic and fair trial, this comparison should be performed in the least biased possible way. However, cosmic justice is not always blind. Model dependent assumptions are sometimes made in the analysis of raw

data, and certain simplifications which might be compatible with the standard assumptions might not be fulfilled in alternative scenarios. The study of the different alternatives helps to identify these flaws and make the process of comparison between theory and observations as model independent as possible.

Honest empirical science can not prove a model right, but rather disprove its alternatives. Studying the predictions of different models and comparing them with observations provides a way to validate the foundations of the Standard Cosmological Model and quantify departures from the constituent assumptions. This model based approach is complementary to model independent methods: while the latter allow for a general study of the data, which might reveal new phenomenological features, the former allows one to find and study concrete physical mechanisms that produce these phenomena. The study self-consistently formulated models further allows the exploration of a given physical set-up in distinct regimes, within computational limitations.

This considerations will become increasingly important as the cosmological wealth and quality of data increase. It is the observational effort what has awarded physical cosmology its present status, and this effort will continue during the following decades. Keeping in mind alternatives to the Cosmological Constant, or any of the standard assumptions, is a good way to be prepared for new discoveries. Hopefully, forthcoming data might allow us to test the foundations of the Standard Cosmological Model with upgraded independence from each other. Finally, the study of alternative theories often provides a better understanding of the standard paradigm, as different shades might be appreciated in the taste of everyday food after a trip to an exotic land.

Outline

Chapters 1 and 2 introduce the fundamental concepts involved in the study of models for cosmic acceleration and their comparison to observations. Section 1.1 presents the hypotheses behind the Standard Cosmological Model. Arguments to pursue the study of alternatives are given in Section 1.2. Section 1.3 gives an overview of the non-standard scenarios. The observational probes of cosmology are classified based on the type of information that they provide in Section 2.1. The remaining of Chapter 2 presents the most relevant ones for the subsequent analysis.

Several cosmological models that violate the standard assumptions are studied and compared with observations in the following Chapters. The possibility of large scale inhomogeneity and the violation of the Copernican Principle is considered in Chapter 3. After introducing the LTB inhomogeneous models, the effects of the inhomogeneities on the BAO scale are detailed in Section 3.2, and used in Section 3.3 to rule out profiles with space independent Big-Bang. Chapter 4 studies phenomenological modifications of the Friedmann equations (inspired by the entropic gravity proposal) and their observational consequences. Chapter 5 explores theories in which a disformal transformation is performed on a canonical scalar field Lagrangian, including connections between Dark Energy Lagrangians and a thorough study of the cosmological implications of the disformal quintessence model. The use of disformal transformations is extended in Chapter 6, where it is allowed to enter the gravitation and matter sectors. Sections 6.1 and 6.2 contain the derivation of the equations for the theory, and explore the connections between the disformally coupled models and other scalar-tensor theories. Their cosmology is explored for a simple, Disformally Coupled Dark Matter model, both in the homogeneous approximation and including cosmological pertur-

bations, in Sections 6.3 and 6.4. The viability of extending the coupling to visible matter via a disformal screening mechanism is explored in Section 6.5.

The main results and a global discussion are presented in Chapter 7. Several technical results and the description of auxiliary tools have been included in the Appendices A (statistical analysis and Markov Chain Monte Carlo algorithm), B (Boltzmann code to solve cosmological equations), C (equations for k-essence scalar fields) and D (disformal relations).

Resumen y Conclusiones

Cuando una persona tiene la suerte de vivir dentro de una historia, de vivir un mundo imaginario, el dolor de este mundo desaparece. Mientras la historia siga, la realidad deja de existir.

Paul Auster[2]

La cosmología moderna ha alcanzado un gran desarrollo como ciencía empírica y predictiva en las últimas décadas. El incremento en cantidad y calidad de los datos observacionales, unido a una sólida descripción teórica, han permitido el establecimiento de un Modelo Cosmológico Estándar capaz de explicar una gran variedad de fenómenos. Numerosas observaciones cosmológicas apuntan a que el universo está experimentando una época de expansión acelerada. Las supernovas lejanas de tipo Ia son menos luminosas de lo que cabría esperar en un universo que contiene únicamente materia. El estudio de las anisotropías del fondo cósmico de microondas combinado con la medida de la tasa de expansión local, implica que el universo tiene secciones espaciales planas y está dominado por una densidad de energía con presión negativa. Los datos sobre formación de estructuras a gran escala concuerdan con este escenario. La tasa acreción de materia hacia las regiones más densas indica que la cantidad total de materia está muy por debajo de la que se necesita para que el universo sea espacialmente plano. La misma física responsable de las anisotropías del fondo cósmico de microondas imprime una escala característica en la función de correlación de materia, que puede ser medida en catalogos de galáxias en distintas épocas. Esta longitud estándar evoluciona con la expansión del universo y permite medir la tasa de aceleración, que concuerda con los datos de supernovas.

La interpretación de estos datos se han realizado dentro de un paradigma estándard, en el que la gravedad está descrita por la teoría de la Relatividad General, el universo es espacialmente homogeneo e isótropo a grandes escalas y la aceleración es causada por una Constante Cosmológica. Las expectaciones teóricas sobre el valor de dicha constante son superiores al valor observado en muchos ordenes de magnitud. Además de la aceleración, el modelo estándar necesita de otros elementos no convencionales como la materia oscura y

[2] *The Brooklyn Follies* (2005)

la inflación cosmológica para ser fenomenológicamente satisfactorio. El escepticismo sobre el valor de la constante cosmológica, unido a las promesas de nueva física hechas por la cosmología moderna, han favorecido la propuesta de una gran cantidad de modelos alternativos. Éstos pueden clasificarse según las hipótesis que violan dentro del paradigma estándar, y sus prediccions se pueden comparar con observaciones cosmológicas para determinar su viabilidad. Esta Tesis aplica este programa en diferentes casos, para validar los fundamentos del Modelo Cosmológico Estándar y acotar posibles desviaciones de las suposiciones fundamentales. Los resultados incluyen el estudio de modelos sin Constante Cosmológica basados en desviaciones de la homogeneidad, parametrizaciones de las ecuaciones cosmológicas y extensiones de la teoría de la Relatividad General.

Modelos inhomogeneos no Copernicanos: Desde el punto de vista de nueva física, la posibilidad más sencilla consiste en reducir el grado de simetría de la métrica. Postulando un espacio-tiempo esféricamente simétrico alrededor de nuestra galaxía, es posible reinterpretar la aceleración como un espejismo, causado por las diferentes tasas de deceleración, que dependen de la distribución de materia en función de la distancia. En este tipo de modelos es necesario que nuestra galaxia esté situada en un lugar especial del universo: cerca del centro de una región con menor densidad de materia. Cuando la edad del universo y la proporción entre materia bariónica y oscura son independientes de la coordenada radial, estos modelos representan el crecimiento por colapso gravitacional de una perturbacion con una amplitud inicial pequeña. Estos casos particulares están descritos por el perfil de la distribución de materia y la normalización del ritmo de expansión, y se conocen modelos Lemaître-Tolman-Bondi (LTB) adiabáticos.

En el capítulo 3 se estudian modelos LTB adiabáticos con un perfil de tipo GBH, los cuales no son compatibles simultaneamente con observaciones geométricas de supernovas y la escala de oscilaciones acusticas (BAO). Al igual que en el modelo estándar, la escala de BAO evoluciona localmente con el factor de escala, lo que produce una diferencia entre su valor en la dirección radial y angular, así como una dependencia con el radio. Este último efecto hace que la misma inhomogeneidad que permite emular la aceleración, estire de manera diferente la escala de BAO en diferentes puntos, haciendola más grande cerca de nuestra galaxia (donde hay menos materia y el universo se expande más) que a distancias mayores. Los nuevos datos a alto deplazamiento al rojo $z \gtrsim 0{,}5$ permiten explorar ambos regímenes y hacen incompatibles ambos observables. Este efecto ocurre en todos los modelos adiabáticos independientemente del perfil de materia. La comparación con observables geométricos provee un nuevo argumento a favor de la aceleración del universo y en contra de este tipo de modelos, complementario a las medidas del ritmo de expansion en distintas épocas y el efecto Sunyaev Zeldovich cinético.

La discrepancia entre los modelos LTB adiabáticos sin Constante Cosmologica y los observables geométricos puede emplearse para acotar modelos más generales. El estudio de modelos tipo LTB con Constante Cosmológica permite determinar el grado de inhomogeneidad compatible con las observaciones en casos más realistas. También es posible reducir las restricciones del modelo, considerando modelos no adiabáticos (con tiempo desde el Big-Bang o fracción de materiá oscura/radiación sobre bariones dependiente de la posición), desviaciones desde la posición central o incluso métricas más generales. Este programa se beneficiaría en gran medida de la inclusión de observables dinámicos, tales como el efecto Sachs Wolfe integrado o las distorsiones en espacio de desplazamientos al rojo.

Modificaciones fenomenológicas: El estudio de modelos basados en parametrizaciones es útil para simplificar el analisis de ideas teóricas que son dificiles de tratar o no poseen una formulación bien definida. Esta posibilidad se ha explorado en el Capítulo 4 para el caso de modificaciones de las ecuaciones de Friedmann basadas en consideraciones sobre las propiedades termodinámicas del espacio tiempo. Esta aproximación tiene la desventaja de que la obtención de las ecuaciones depende de una serie de hipótesis que son válidas en el marco de Relatividad General, pero que aun no se han comprobado en estos escenarios. A pesar de carecer de una descripción completa y autoconsistente, este típo de estudio permite explorar nuevos mecanismos físicos de manera sencilla, y los resultados son validos en general, para cualquier mecanismo subyacente que introduzca las mismas modificaciones a nivel de las ecuaciones. Por otro lado, la alternativa de emplear una aproximación autoconsistente basada en un modelo concreto tiene la ventaja de que permite explorar los mecanísmos físicos subyacentes en una variedad de situaciones, limitadas por consideraciones computacionales.

Modelos más allá de Relatividad General basados en métricas disformes: El hecho de que la aceleración del universo suceda en escalas en las que no existe una validación independiente de la teoría de la Relatividad General sugiere una revisión en profundidad de sus fundamentos. Una posibilidad de extender la teoría de Einstein es mediante la aplicación de una transformación disforme en algún sector de la acción, dada por los gradientes de un campo escalar. Esta prescripción se empleá sobre un escalar canónico en el Capítulo 5 y sobre el Lagrangiano de materia en el capítulo 6. Las relaciones disformes generalizan las bien conocidas transformaciones locales de escala (o transformaciones conformes) permitiendo una distorsión de la estructura causal en la metríca transformada con respecto a la inicial. Este tipo de relaciones son las más generales posibles entre la métrica gravitatoria y la de materia compatibles con convariancia general, y aparecen la descripcion efectiva de ciertas teorías con dimensiones adicionales extensas.

Las transformaciones disformes permiten construir modelos de energía oscura en los que el campo escalar pierde su energía cinetica, contribuyendo a la expansión del universo únicamente mediante su potencial, que actua como una Constante Cosmológica efectiva. Esto sucede por la tendencia del campo a evitar dinámicamente una singularidad en la metrica disforme, y funciona tanto en el caso de la auto-interacción del propio campo (modelo de quintaesencia disforme) como en el caso de un acoplo con la materia oscura (modelo de materia oscura disformemente acoplada), que fueron estudiados en el caso en el que no hay interacción conforme. El campo de quintaesencia disforme produce únicamente efectos indirectos en la formación de estructura, y su comportamiento se asemeja mucho a una Constante Cosmologica para valores altos de las pendientes de los potenciales, siendo dificil distinguir ambas posibilidades observacionalmente. Sin embargo, el modelo de materia disformemente acoplada experimenta una fuerza adicional mediada por el campo escalar. Aunque es capaz de reproducir la expansión cosmológica en el límite homogeneo, esta fuerza produce efectos importantes en la formación de estructura a gran escala, tornandola incompatible con las observaciones. Afortunadamente, existe mucha libertad en la teoría para producir modelos viables, en los que las modificaciones sean menos dramaticas pero permitan distinguir las diferentes alternativas.

Las transformaciones disformes también permiten relacionar entre si teorías aparentemente disconexas. En ciertos límites, el Lagrangiano de quintaesencia disforme más general se reduce a una serie de modelos de campos escalares no acoplados. Cuando la métrica disforme

entra en el Lagrangiano de materia y el sector gravitatorio corresponde a Relatividad General, se dice que la teoria resultante está en la descripción de Einstein. Es posible invertir la transformación conforme para eliminar el acoplo directo entre el campo escalar y la materia, dando lugar a la descripción de Jordan. En ella, el campo escalar se acopla cinéticamente al escalar de curvatura, y aparecen una serie de términos en segundas derivadas del campo, que sin embargo no introducen inestabilidades en la teoría. Este tipo de Lagrangianos con auto-interacciones no lineales en derivadas son capaces de producir el "effecto de Vainshtein", que alisa los gradientes del campo escalar cerca de objetos masivos, ocultando la interacción adicional.

Las teorías disformemente acopladas en la descripción de Einstein también son capaces de evitar los efectos de la fuerza adicional en entrornos no-relativistas con una densidad de energía elevada, tales como el Sistema Solar. En estos casos, existe un límite bien definido en el que la densidad de materia tiende a infinito (al contrario que en el caso de un acoplo conforme), y en el que la evolución del campo escalar se vuelve independiente de la distribución de materia y los gradientes espaciales del campo. Este "mecanismo de camuflaje disforme", que suprime la fuerza adicional, es debido a la mezcla de términos cinéticos entre campo escalar y los grados de libertad acoplados. Su acción hace muy difícil detectar los efectos inducidos por el acoplo disforme mediante medidas de fenómenos gravitatorios, mientras que permite que éste tenga consecuencias considerables a nivel cosmológico.

La equivalencia entre teorías disformemente acopladas y teorías con interacciones no lineales en derivadas sugiere que el mecanismo de camuflaje disforme y el efecto de Vainshtein son en realidad manifestaciones del mismo fenómeno, pero vistas a la luz de las descripciones de Einstein y Jordan, respectivamente. Esta equivalencia también abre una nueva ventana para el analisis de este tipo de teórias, ya que las ecuaciones en la descripción de Einstein se simplifican considerablemente con respecto a la descripción de Jordan. Asimismo, hay otros aspectos de las teorías disformemente acopladas que merecen ser considerados en detalle. Estos incluyen el estudio de la estabilidad de la teoría, modelos más generales (e.g. añadiendo un acoplo conforme) y otras situaciones en las que puedan producirse signaturas características.

Discusión: El estudio de diferentes modelos es beneficioso para la salud de la ciencia empírica, ya que ésta no puede demostrar la veracidad de una hipótesis, sino únicamente refutar sus alternativas. La comparación de modelos que desafían las suposiciones habituales con las observaciones permite validar los fundamentos del Modelo Cosmológico Estándar y explorar los límites de su validez. Este programa también permite la identificación de las hipótesis que se asumen implicitamente en las distintas etapas del analisis, y permite encontrar ejemplos en los que éstas no se cumplen, facilitando el diseño de estrategias que favorezcan una comparación entre teorías y datos más independiente y menos sesgada. Esto no solo es necesario para obtener resultados fiables, sino que es necesario para comprobar las distintas hipótesis del Modelo Cosmológico Estándar de manera lo más independiente posíble. Por último, el estudio de teorías alternativas a menudo aporta ejemplos que permiten entender mejor el paradigma convencional, enriqueciendo el conocimiento que se tiene sobre él y las tecnicas disponibles para su analisis. Estas consideraciones serán importantes en las próximas décadas, cuando el incremento en la cantidad y calidad de las observaciones cosmológicas valide de manera aún más sólida los fundamentos del Modelo Cosmológico Estándar o nos sorprenda con nuevos datos que indiquen la necesidad de revisarlo.

Acknowledgements

Luckily, I have plenty of reasons to be thankful and many people to express gratitude to, not only for helping me in the course of this Thesis, but also for their support and the unforgettable moments that we have spent together.

First of all, I would like to thank Juan Garcia-Bellido, not only the careful reading of this manuscript, which has greatly contributed to improve it towards the final version, but also for being so generous with his time and sharing his knowledge and physical intuition with me. It was him who awoke my interest for cosmology in the first place, during his inspiring lectures at the UAM, and supported me since the very first time. It has been nothing but the greatest pleasure to be able to discuss and work with him during the last years.

I am also very thankful to my other advisors. Pilar Ruiz-Lapuente has always been extremely supportive, patient, and generous, and I would not have been able to do any of this if it had not been for her. I enjoyed working with Tomi Koivisto and learned a lot from him through his careful explanations, the patient review of my results and the long discussions we held in Heidelberg, Utrecht, Oslo, Barcelona and Madrid, often extending over many drinks. I am especially grateful to David Mota for sharing his vision and giving me very good advice in many occasions, as well as for devising several interesting projects in which I have worked.

Cosmology has allowed me to meet many wonderful people, who have made these four years incredibly fun and enriching. Dani G. Figueroa, my "older brother", has always been a source of inspiration and guidance, and certainly someone who knows where the fun is and how to get there. I've also had great times with my other "siblings" David Alonso and Alicia Bueno-Belloso. All of them have taught me valuable lessons. I can not go any further without thanking the people who I've been meeting everywhere, those who I can not associate to any place in particular: Edoardo Carlesi, who shares the curse of being one of the few CMBeasy users left in the world, Federico Urban, the best chef in Norway and the most patient hiking partner, Jose Beltran, for his good advice and all the inspiring conversations about life and the Cosmological Constant, and Lluis Galbany for his great sense of humor.

During a very important part of my thesis I was working at the Institut de Ciencies del Cosmos (ICC) and the Departament d'Astronomía y Meteorología (DAM) in the University of Barcelona (UB) with a grant associated to the Institut de Estudis Espacials de Catalunya (IECC). I would like to acknowledge the support received from these institutions and all the people whom I met there. I especially appreciated the company of my office mates Andreu Font and Hector Gil-Marin (which was very valuable in our windowless room) as well as the other graduate students at DAM.

There has been some serious traveling these past years, and I've been very fortunate to live and work in several great places. I really enjoyed my stays at the Institutt før Teoretisk

Astrofysikk in the University of Oslo, which has become one of my favourite cities in the World. Being there, I had the pleasure to meet a lot of excellent people, including Nicolaas Groeneboom, Kristin Mikkelsen, Sandro Scodeller, Iain Brown, Hans Winter, Claudio Llinares, Tuva och Ingeborg. *Tusen Takk!* During my time at the Institute of Theoretical Physics in Heidelberg, I had the luck to meet Annika, Nico, Sarah, Richard, Mattias and other nice people who made me feel at home. I am also thankful to Marc Kamionkowski for his kind hospitality at the John Hopkins University during my visits to Baltimore.

One of the strokes of luck I experienced was being able to attend the Cape Town International Cosmology School, thanks to the kind invitation and support of Bruce Bassett. Although it only lasted for two weeks, what I learned and experienced there has had a considerable impact on me as a scientist and a person. It was a real pleasure to work with Sean February and Pranjal Trivedi in the voids project, and I'm really looking forward to work with them again (on that or anything else). And of course I will not forget the fun times I spent with Alvaro de la Cruz-Dombriz, Bryan Nord, Danielle Wills, Michelle Knights, Ze Fonseca and the other people I met there.

The time at the Instituto de Física Teórica in Madrid has been very enriching. I would like to thank my friends from the Master's, Pablo Soler, Javi Abajo, Ana Rodriguez-Sánchez and Bryan Zaldivar, for for all the great times, past, present and future. I'm also very thankful to Chabe, Roxanna and the other people in charge of administration for being so kind and helpful. My undergraduate years at the Universidad Autónoma de Madrid were simply great, and it was a pleasure to study physics there. I would like to thank Arkadi Levanyuk and Andres Cano, who awoke my curiosity for physics and showed me the spirit of critical thinking, during their unforgettable lectures in mathematical methods. I'm also grateful to the great teachers I had, including Miguel Angel Ortega, Paloma Montero, Concha Mozo, Jesus Braña and Javi Holgado from the Colegio Montserrat, as well as Alex and Guillermo from the Colegio Siglo XXI. My cousin Rafa helped me to understand math, and I don't think studying physics would have even been an option without his help.

Many other people need to be properly thanked for the great moments and interesting conversations I had with them, both within and beyond science. I shall not write further without at least mentioning Jaime Alberdi, Santi Barrio, Peri, Jose Frutos, Javi Ramos, Emilio Franco, Zongalo, Pablo Merodio, Alex Molpercebes, Marcos Diaz, Buti, Rogüa, Ana M., Fer de Juan, Hector M., Javi-Teresa, Micky Knife, my cousins Olvido, Felix, Marta and Marcos, Florian und Lidia, Stefan and Michael Friedel, Elsa, Rubén, Dieguito, Marta and Tris. I am also grateful to my uncles Felix and Concha and my grandparents Conchita and Manolo, as well as Teo, Rosi, Marcos Ana, Ramón y Charo and Fátima, who have really become a "non-official family" to me. Mentioning all these people without any details is almost an offense, and I hope to find the time to express my gratitude to them in person.

Very specially, I would like to thank my parents for their invaluable support and understanding as well as for teaching me the most valuable lessons I've learned in life. My gratefulness naturally extends to my uncles and cousins Jesus, Mari Luz, Julia, Jesu, Manuel and Javi, for their endless generosity and their hospitality in Barcelona, and to my grandparents Jesus and Olvido, for their kind affection and the integrity they taught to all who had the luck to know them. My sister Ana, for the great moments and conversations, advice and patience, deserves a very warm mention here. Finally, I would like to thank my dear Lindsey because, among all the things I'm grateful to her, she was the one who made me fall in love with science again.

Notation and Acronyms

The present conventions have been adopted throughout the following Chapters, unless otherwise specified. The metric signature is $(-,+,+,+)$, and the Riemann curvature is defined as in Eq. (1.1). Coordinates are labeled by greek indices x^μ where $\mu = 0$ refers to the time coordinate and latin indices to spatial coordinates only. Sum over contracted indices is implicitly assumed and units in which the speed of light c is set to unity are used.

Partial derivatives with respect to a variable are denoted with commas, $\mathcal{L}_{,\phi} \equiv \partial\mathcal{L}/\partial\phi$. Partial derivatives w.r.t. coordinates are indicated either by commas or by the partial derivative sign $\phi_{,\mu} \equiv \partial_\mu\phi \equiv \partial\phi/\partial x^\mu$, using either the coordinate or its index. A semi-colon will indicate a covariant derivative $\phi_{;\mu\nu} = \nabla_\nu\nabla_\mu\phi$. Derivatives with respect to time coordinates are indicated with a dot $\dot{A}(r,t) \equiv \partial A/\partial t$. t refers to cosmic time, τ to conformal time and both satisfy $dt = a(\tau)d\tau$. In a function of one variable, a prime will denote a derivative $A'(\phi) \equiv A_{,\phi}$, while for functions of space-time, a prime will indicate a derivative with respect to the radial coordinate $A'(r,t) = \partial A/\partial r$. Fourier transforms are defined so that $\partial_i f(t,\vec{x}) = ik_i\tilde{f}(t,\vec{k})$. δ_D, $\delta_D^{(n)}$ denote the Dirac delta function and its n-dimensional generalization. Barred quantities are constructed out of disformal metrics of the form given by Eqs. (6.1, 5.3) (Appendix D contains a compilation of relations that apply to disformal metrics).

The acronyms used throughout the text are summarized in Table 2 below for convenience:

	Name	Reference
BAO	Baryon Acoustic Oscillation(s)	2.4.1
BBN	Big Bang Nucleosynthesis	2.2
CC	Cosmological Constant Λ	1.1.5
CDM	Cold Dark Matter	1.1.4
CGBH	Constrained GBH	3.1.1
C_l	Angular power spectrum	(2.7, 2.9)
CMB	Cosmic Microwave Background	2.3
D_A	Angular Diameter Distance	(2.1)
DC	Disformal Coupling	6.2.2
DCDM	Disformally Coupled Dark Matter	6.3.1
DE	Dark Energy	1.3.2
D_L	Luminosity Distance	(2.2)
DM	Dark Matter	1.1.4
dof	degree of freedom	
EF	Einstein frame	6.2, (1.25)

	Name	Reference
EH	Einsten-Hilbert (action)	(1.2)
eos	equation of state	
FRW	Friedmann-(Lemaître)-Robertson-Walker	(1.5)
GBH	Garcia-Bellido Haugbølle matter profile	3.1.1
GR	General Relativity	1.1.1
Gpc	Gigaparsec ($3.09 \cdot 10^{25}$m)	
H_0	Hubble rate today [km/Mpc/s]	
h	Normalized Hubble rate today [100 km/Mpc/s]	
ISW	Integrated Sachs-Wolfe effect	2.3
JF	Jordan frame	6.2, (1.23)
Λ	Cosmological Constant	1.1.5
lhs	left hand side	
LSS	Large Scale Structure	2.4
LTB	Lemaître-Tolman-Bondi	1.3.1
MCMC	Markov Chain Monte Carlo	A
MG	Modified Gravity	1.3.3
Mpc	Megaparsec ($3.09 \cdot 10^{22}$m)	
OCGBH	Open Constrained GBH	3.1.1
$P(k)$	Power spectrum	(2.17)
rhs	right hand side	
SM	Standard Model (of particle physics)	
	or Standard Matter	1.1.4
SCM	Standard Cosmological Model	1
SNe	Type Ia Supernovae	2.5
WMAP	Wilkinson Microwave Anisotropy Probe	
w_x	Equation of state of the x component	
wrt	with respect to	
z	redshift	
Ω_x	cosmic fraction of the x- component today	(1.8)

Table 2: Acronyms used in the text.

Part I

Foundations

Chapter 1

The Standard Cosmological Model

One should always look for a possible alternative, and provide against it. It is the first rule of criminal investigation.

Arthur Conan Doyle[1]

Recent years have witnessed enormous advance in the quantitative understanding of cosmology and the establishment of a Standard Cosmological Model. In addition to known forms of matter, Einstein's General Relativity and an *ansatz* for the space-time metric (spatially homogeneous and isotropic), two mysterious elements need to be added in order to account for the observations. These give the name to the standard, ΛCDM model: Cold Dark Matter (CDM) to explain the formation and dynamics of cosmic structures and a Cosmological Constant (Λ) to account for the dimming of distant supernovae [11, 12].

The steadily increasing precision and wealth of data and the surprising findings call for a revision of the hypothesis made in the construction of the Standard Cosmological Model. Dropping the large scale homogeneity assumption allows one to reinterpret the observed acceleration as a mirage, allowing in principle for a universe with zero Cosmological Constant [8]. Other alternatives have been proposed in which the Cosmological Constant is substituted by a more general form of dark energy (DE) that fuels the acceleration [9]. Finally, the last major path to address the dynamics of the cosmic acceleration is by postulating modifications of General Relativity acting only on the largest cosmological scales [7].

Comparing these alternative models against cosmological observations does not only provide potential hints to test new physics: it is itself a way to validate the assumptions on which the standard paradigm is formulated. These assumptions will be presented in Section 1.1. A number of reasons to consider alternatives will be discussed in 1.2, and an overview of the possible modifications that deal with the problem of cosmic acceleration in Section 1.3.

[1] *The Return of Sherlock Holmes* (1905)

1.1 Ingredients and Preparation

As a logical construction, the standard cosmological model requires six hypotheses

$$\boxed{\text{Standard Model} = \text{GR} + \text{FRW} + \text{Initial Conditions} + \text{SM} + \text{CDM}{+}\Lambda}$$

1. General Relativity: As gravity is always an attractive interaction, it dominates on macroscopic distances and will be crucial for cosmological phenomena.

2. Friedman-Robertson-Walker metric: GR is a metric theory governed by nonlinear partial differential equations. A simple *ansatz* for the metric is required, which in the standard case is based on maximal spatial symmetry.

3. (Inflationary) Initial Conditions: The paradigm of *cosmic inflation* is able to provide initial conditions for the perturbations around the background metric, explains the observed value of the spatial curvature and further supports the choice of the metric.

4. Standard Matter: The known forms of matter and their cosmological effects have to be accounted for, notoriously baryions (nucleons and electrons), photons and neutrinos.

5. Cold Dark Matter: Structure formation requires the presence of a form of matter does not interact with light, usually assumed to be a new, weakly interacting particle species.

6. Cosmological Constant: The observed acceleration of the universe can be explained in a simple way by the presence of an energy density that does not evolve in time.

Assumptions 1 and 4 are an extrapolation to the cosmological realm of good old earthly physics, assumption 2 is a model simplification justified *a posteriori* and assumptions 3, 5 and 6 require the introduction of new physics, for which so far there is only cosmological and (in the case of dark matter) astrophysical support.

1.1.1 General Relativity

The theory of General Relativity (GR) provides a very elegant framework in which the gravitational interactions can be related to the geometry of the spacetime [13, 14]. The fundamental degree of freedom is the *space-time metric* that determines the physical distances $ds^2 = g_{\mu\nu}dx^\mu dx^\nu$, which is treated as a fully dynamical variable. The theory relates the dynamics of the metric to the matter through the curvature of the space-time, encoded in the *Riemann tensor*

$$R^\alpha{}_{\beta\mu\nu} \equiv \partial_{[\mu}\Gamma^\alpha_{\nu]\beta} + \Gamma^\alpha_{\gamma[\mu}\Gamma^\gamma_{\nu]\beta} \tag{1.1}$$

where $\Gamma^\alpha_{\mu\nu} \equiv g^{\alpha\lambda}(g_{\alpha(\mu,\nu)} - \frac{1}{2}g_{\mu\nu,\lambda})$ is the torsion free ($\Gamma^\alpha_{\mu\nu} = \Gamma^\alpha_{\nu\mu}$) connection that gives a metric compatible ($\nabla_\alpha g_{\mu\nu} = 0$) covariant derivative $\nabla_\mu v^\nu = \partial_\mu v^\nu + \Gamma^\nu_{\mu\alpha}v^\alpha$. Besides the metric formulation, to fully specify the dynamics an action for the metric has to be provided. It turns out that the simplest, nontrivial, theory that can be constructed out of $g_{\mu\nu}$ works superbly

$$S = S_{EH} + S_m = \int d^4x\sqrt{-g}\frac{R}{16\pi G} + S_m\,, \tag{1.2}$$

where an unspecified matter sector has been included, g is the determinant of the metric, and $R \equiv g^{\mu\nu} R^{\alpha}{}_{\alpha\mu\nu}$ is the Ricci scalar. The above equation is known as the Einstein-Hilbert action. The variation wrt the metric lead to Einstein equations

$$G_{\mu\nu} \equiv R_{\mu\nu} - \frac{R}{2} g_{\mu\nu} = 8\pi G T_{\mu\nu} \,. \tag{1.3}$$

The lhs is known as the Einstein tensor. The source term, the *energy momentum* tensor is defined out of the variation of the matter action, which is covariantly conserved by virtue of the Bianchi identities

$$T_{\mu\nu} \equiv -2\frac{\delta S_m}{\delta g^{\mu\nu}} \,, \qquad \nabla_\mu T^{\mu\nu} = 0 \,. \tag{1.4}$$

1.1.2 Metric Ansatz: The Copernican Principle

Einstein equations (1.3) are a set of ten coupled, non-linear, partial differential equations that are very difficult to solve unless some simplifying assumptions are made. Knowing that static metrics are not a solution in the presence of matter, the simplest possible guess is to try to model the "spatial average" and consider the evolution of the mean cosmic density. More precisely, one can assume that the metric is formed by a foliation of maximally symmetric spatial Sections, i.e. *homogeneous* and *isotropic*.[2] This choice gives the Friedman-Lemaître-Robertson-Walker metric

$$ds^2_{\text{FRW}} = -dt^2 + a(t)^2 \frac{dr^2}{1 - kr^2} + a(t)^2 r^2 d\Omega^2 \,, \tag{1.5}$$

where $d\Omega^2 \equiv d\theta^2 + \sin(\theta) d\phi^2$ is the solid angle element, and the *scale factor* $a(t)$ encodes dynamics of the spatial Sections, i.e. the expansion of the universe. The above metric has to be regarded as a large scale, averaged limit of the true universe metric. Inhomogeneities and anisotropies can be introduced as small perturbations within this picture, making the model more predictive on the intermediate scales, at which the perturbations remain sufficiently small.

The assumption of isotropy can be justified by the observations of the Cosmic Microwave Background tempearture fluctuations. After removing the dipolar component (which is likely due to the peculiar motion of our galaxy) the remaining fluctuations deviate at the order of 10^{-5} from the mean and do not show evidence of a preferred direction.[3] The case for homogeneity is trickier, as it is possible to postulate a spherically symmetric universe, which would *seem* isotropic if we are located very close to the center of symmetry, as it will be exploited to construct inhomogeneous cosmological models without a Cosmological Constant. Rather than waiting for observational validation, the assumption of homogeneity is invoked a priori by means of the *Copernican Principle*, i.e. the statement that our location in the universe is not be special (e.g. the center of a large, symmetric region).

There are two independent Einstein equations for the homogeneous metric 1.5, known as the *Friedmann equations*:

$$\left(\frac{\dot{a}}{a}\right)^2 = \frac{8\pi G}{3}\rho - \frac{k}{a^2} \,, \tag{1.6}$$

[2] It is further necessary to specify a global topology for the space-time manifold, for which it is assumed that spatial sections are simply connected. Although the choice of a non-trivial topology does not influence the local gravitational dynamics, it implies the existence of periodicity scales in the universe that violate global isotropy. Such scales must be very large $r \gtrsim 24$Gpc in order to fulfill by CMB observations [15].

[3] Some claims of prefered directions in the CMB have been made and disputed, e.g. references [16, 17].

$$\frac{\ddot{a}}{a} = -\frac{4\pi G}{3}(\rho + 3p) \ . \tag{1.7}$$

Here $\rho = T^{00}$ and $pg^{ij} = T^{ij}$ are the energy and pressure density (1.10). It is conventional to define the *Hubble factor* as $H = \dot{a}/a$ and the fraction of a cosmic component today as

$$\Omega_i = \frac{\rho_i}{\rho_0} \, , \tag{1.8}$$

where $\rho_0 = \frac{3H_0^2}{8\pi G}$ is the critical density, defined in terms of the Hubble rate today H_0.

1.1.3 Inflation: Symmetry and Initial Conditions

There is overwhelming evidence that the universe is not homogeneous on sufficiently small scales. In order to give an accurate cosmological description, it is necessary to consider deviations from the perfect FRW metric

$$ds^2_{\rm PT} = ds^2_{\rm FRW} + \delta g_{\mu\nu} dx^\mu dx^\nu \ . \tag{1.9}$$

In the standard picture, these departures are very small at early times and become increasingly significant as cosmic structures develop by the action of gravity. For a broad range of scales and most of the cosmic evolution, it is sufficient to consider only linear corrections to the Einstein equations, computed using the above perturbed metric to first order in $\delta g_{\mu\nu}$. The CMB shows that these fluctuations had a very small amplitude amplitude $\sim 10^{-5}$ during the recombination epoch.

In order to explain the observed degree of isotropy in the cosmic microwave background radiation, it is postulated that the universe underwent a period of accelerated expansion at very early times, known as *cosmic inflation*. If the inflationary period lasts long enough, it allows for opposite regions in the sky to be causally connected. The fact that they have approximately the same temperature can be then seen as a natural consequence of local physics. As inflation magnifies an initially tiny region into the whole observable universe, it has the additional benefit of diluting away any preexisting feature, such as cosmic relics or initial inhomogeneities. Hence, it provides further support for the choice of a maximally symmetric metric to describe the universe expansion.

In addition to homogenize the universe, inflationary models source initial perturbations in the metric by amplification of quantum fluctuations to macroscopic scales. Each inflationary model provides a set of initial conditions for the perturbation equations that would eventually give rise to the large scale structure of the cosmos through gravitational collapse. Due to the empirical success of these predictions, inflation is often considered an ingredient of the standard cosmological model, even in the absence of a preferred inflationary model. The physical predictions for inflation are:

- ★ Negligible Curvature: Despite it is not a component in itself, it can be quantised in terms of $\Omega_k = \frac{k}{\rho_0 a^2}$. CMB observations combined with H_0 and BAO yield a value compatible with the inflationary prediction $|\Omega_k| < 0.005$ [18].

- ★ Adiabatic, Gaussian and nearly scale invariant initial perturbations: Although the details depend on the inflationary model, the CMB typically constraints departures from this scheme [19].

1.1.4 Standard and Dark Matter

Einstein Equations describe how the space time responds to the distribution of matter and energy. The matter content in the universe can be modeled through an energy-momentum tensor of the perfect fluid form

$$T_{\mu\nu} = (\rho + p)u^\mu u^\nu + p g_{\mu\nu} \,, \tag{1.10}$$

where u^μ is the four velocity and ρ, p the energy and pressure densities respectively. The time component of the covariant energy momentum conservation (1.4) applied to a FRW spacetime yields the *continuity equation*:

$$\dot{\rho} + 3H(\rho + p) = 0 \,. \tag{1.11}$$

For most of the cosmic evolution, the dominant fluids can be treated as *barotropic*, for which $p = w\rho$. This allows the integration of the conservation equation

$$\rho = \rho_0 a^{-3(1+w)} = (1+z)^{3(1+w)} \,. \tag{1.12}$$

The second equality here relates the scale factor to the redshift, which relates the increase in wavelength of photons due to the cosmological expansion as $1 + z \equiv \lambda_\mathrm{r}/\lambda_\mathrm{e} = a(t_\mathrm{r})/a(t_\mathrm{e})$ (i.e. the ratio between the received and the emitted wavelength).

The relevant matter species for the dynamics of the late universe are the following (quoted abundances correspond to reference [20])

- ★ Baryons: The term is used generically for electromagnetic interacting, stable fermions. Its value can be inferred from the primordial deuterium abundance and the CMB $\Omega_b = 0.0225 \pm 0.0006 h^{-2}$.
- ★ Photons: The CMB is the best blackbody observed ever. Its measured temperature $T = 2.7255 \pm 0.0006 K$ translates into a value $\Omega_\gamma = 2.47 \cdot 10^{-5} h^{-2}$.
- ★ Neutrinos: Although the amount of cosmological neutrinos is not directly observed, their properties affect the formation of LSS. Current bounds on neutrino masses are $5.4 \cdot 10^{-4} < \Omega_\nu h^2 < 3.0 \cdot 10^{-3}$, where the upper bound is cosmological and the lower one is obtained in terrestrial neutrino oscillation experiments. The neutrino mass translates to $\Omega_\nu h^2$
- ★ Cold Dark Matter: To correctly explain the formation of cosmic structure, there must be a significant amount of non electromagnetically interacting matter which was non-relativistic (i.e. cold) at the onset of galaxy formation $\Omega_\mathrm{CDM} = 0.112 \pm 0.006 h^{-2}$. Dark matter is also essential to explain the CMB anisotropy pattern, as it is able to cluster before recombination and form potential wells. Other observations, such as the rotational curves of galaxies and the gravitational lensing by galaxy clusters provide independent evidence of its existence.

1.1.5 The Cosmological Constant

The final ingredient is the Cosmological Constant (CC), i.e. a constant term in the Einstein-Hilbert action (1.2) introduced to explain the acceleration of the cosmic expansion

$$S_{\mathrm{EH}+\Lambda} = \int d^4x \sqrt{-g} \frac{1}{16\pi G} \left(R - 2\Lambda\right) \,, \tag{1.13}$$

that modifies Einstein Equations

$$R_{\mu\nu} - \frac{R}{2} g_{\mu\nu} + g_{\mu\nu}\Lambda = 8\pi G T_{\mu\nu} \,. \tag{1.14}$$

The CC term can be incorporated into a redefinition of the energy momentum tensor in the rhs. Its effect then is equivalent to a perfect fluid with $T^{\Lambda}_{\mu\nu} \propto g_{\mu\nu}$, with negative pressure $p = -\rho$ and *constant* energy density $\rho_\Lambda \equiv \Lambda/(8\pi G)$. Hence, the Cosmological Constant represents a source of energy that does not dilute with the cosmic expansion, exactly the properties one would expect from the energy stored in the vacuum [21].

Such a term would be unobservable in a theory based in a static space-time for which only energy differences are observable. In GR, the CC couples to the determinant of the metric in (1.13), thus affecting dynamics of the space-time. In particular, plugging $p = -\rho$ in the second Friedmann equation (1.6) with $k = 0$ shows that it produces a constant positive acceleration

$$\frac{\ddot{a}}{a} = \frac{8\pi G}{3}\rho_\Lambda > 0 \,. \tag{1.15}$$

That is, the effect of the Cosmological Constant on the universe expansion is opposite to the one caused by standard, gravitating matter. Current observations suggest that the Cosmological Constant is the dominant component in the cosmic energy budget, with $\Omega_\Lambda = 0.73 \pm 0.03$ [19].

1.2 The Need to Go Beyond

In this Section I will review some of the arguments to go beyond the standard cosmological model, emphasizing those related with the Cosmological Constant as the source of cosmic acceleration.

1.2.1 Theoretical Issues

The standard cosmological model relies on three pieces of new physics: inflation, dark matter and the Cosmological Constant. Considering alternative paradigms might help to obtain a better understanding of the model and search for possible connections between the different mysterious elements. In this light, the idea of inflation provides the most compelling reason to study alternatives to the Cosmological Constant. Inflationary scenarios require a period of accelerated expansion similar to the one produced by a Cosmological Constant, but at a much higher energy scale. On the other hand, inflation has to end in order to evolve into a universe filled with matter, and hence the inflationary epoch can not be due to a Cosmological Constant term.[4] The fact that there might have been an acceleration mechanism at work in the very early universe different than Λ suggests that a similar mechanism might be at work in the late universe.

The Cosmological Constant also faces two naturalness problems related to its actual value when interpreted as a vacuum energy and due to its time evolution.The lack of a compelling theory for quantum gravity indicates that General Relativity has to be revised, at least in the high-energy/small-scale regime. The modifications introduced in the pursue of

[4] In addition, the running of the spectral index for primordial perturbations $n_s = 0.963 \pm 0.014$ [19] indicates a departure from a "perfect Cosmological Constant" ($n_s = 1$) at the time when the perturbations on the scales probed by the CMB were seeded.

a renormalizable theory of gravity might yield some information on the value and properties of Λ, or whatever mechanism behind cosmic acceleration.

The Cosmological Constant Problem

Since the Cosmological Constant is equivalent to a constant energy density in the action, its effective value receives different contributions. The most problematic of these is the expected from quantum fields in the vacuum [22]. The standard, quantum mechanical harmonic oscillator (or any other bound system) has a energy proportional to the frequency $\hbar\omega$ even in the absence of excitations. As a free quantum field is described as a collection of infinite harmonic oscillators, its energy in the vacuum state is infinite in principle, although it can be renormalized to an arbitrary values by the addition of a suitable counter term Λ_0. Employing dimensional regularization to preserve Lorentz invariance and removing the divergent contribution, the resulting vacuum energy associated to a scalar field of mass m is [23]

$$\Delta\Lambda_{eff} = \frac{Gm^4}{8\pi}\log\left(\frac{m^2}{\mu^2}\right) , \tag{1.16}$$

where μ is a renormalization scale. Although the contribution is dependent on the choice of μ, the above expression shows how the corrections are sensitive to the mass scales present in the theory. The details are different for other types of field, but the conclusion is similar: They all produce an effective contribution to the total Cosmological Constant which is generically much larger than the true value, i.e. Λ is unstable against quantum corrections (technically unnatural).

In addition, the Cosmological Constant receives a *classical contribution* from the field potentials, due to the phase transitions predicted within the standard model of particle physics, e.g. electroweak symmetry breaking. At very early times where the temperature of the universe is $T \gtrsim m_H \approx 125\text{GeV}$, the potential for the Higgs field has a single minimum, and hence the field fluctuates around a unique vacuum state. When the electroweak transition occurs, the Higgs potential is deformed into a Mexican hat form, the central extremum becomes unstable and the vacuum state is displaced towards a degenerate set of minima. Besides being responsible for the masses of the W and Z bosons, this process displaces the minimum of the Higgs potential by $\Delta\rho_{EW} = v^4/4 \sim \mathcal{O}(100\text{GeV})^4$, where v is the vacuum expectation value of the field and λ is the quartic self coupling [23]. A constant term can be added to set the value of the potential energy to zero, but only before or after the transition. According to General Relativity, this offset would produce the same effect as a (perhaps negative) CC with a value much larger than the observed one $\Delta\rho \sim 10^{55}\rho_0$. Similarly, a lower energy phase transition within quantum chromodynamics would induce an imbalance in the effective Cosmological Constant of order $\sim (100\text{MeV})^4$, which is also too large, with $\Delta\rho \sim 10^{45}\rho_0$.

When one considers all the terms that contribute in the same way as the Cosmological Constant

$$\Lambda_{\text{total}} = \Lambda + \sum_{\text{fields}} \Delta\Lambda_{eff} + 8\pi G\Delta\rho_{\text{PT}} + 8\pi G\rho_{QCD} , \tag{1.17}$$

it turns out that the different contributions have to cancel with exquisite precision to yield the observed value today. This fine tuning is known as the *Cosmological Constant problem*.

There are important caveats to these arguments. The quantum corrections have been computed assuming a perturbative expansion in the fields. More importatnly, the whole

computation is performed in a fixed background metric and does not take into account the effects of gravity, which might be crucial to address purely gravitational effects such as the acceleration induced by constant terms in the action. Although the CC problem should be addressed within a consistent framework for quantum gravity, general covariance suggests that local physics can be described by the special relativity in a sufficiently small region, offering some support to the above argument. If the CC problem can not be solved within quantum gravity, it might be pointing towards the existence of a yet unknown principle or mechanism that keeps its value small or zero, and which may have observational consequences.[5]

The Coincidence Problem

The energy densities of matter and Cosmological Constant are similar today, but their relative scaling, $\rho_\Lambda/\rho_m \propto a^3$, implies that Λ was completely negligible in the cosmological past and will be absolutely dominant in the future. If we think of the Cosmological Constant as an initial condition set in the early universe (when the energy density was very high compared with the current one), it seems very unlikely that it acquires a value comparable to matter at the present cosmological epoch, when galaxies and other large scale structures have formed. Had the Cosmological Constant been a couple orders of magnitude higher, the universe would be empty of large scale structure. But if it had been just a couple orders of magnitude smaller it would be hardly measurable.

The lack of an explanation for why the Cosmological Constant becomes relevant at the present epoch is known as the *coincidence problem*. Although this issue is somehow aesthetic, this piece fine tuning might be pointing towards something more complex. The situation is analogous to the inflationary paradigm. Without inflation, the observed value of the spatial curvature $\Omega_k \sim 0$ would seem oddly fine tuned. The inflationary paradigm is able to give a natural explanation for the current bounds and solve the (aesthetic) problem of the small spatial curvature, on top of the more severe problems that lead to the idea in the first place.

1.2.2 Observational Reasons

Even if the standard model turns out to be correct and the only remaining task is to understand the details, the only way to prove it as a physical theory is by disproving the alternatives. This provides an explicit way to test the assumptions behind the standard cosmological model, while searching potential signatures of new physics. In addition, exploring alternative scenarios helps to improve the model independence of cosmological probes, and thus their reliability.

Regardless of its empirical success, the cosmological constant is a very stiff model. If further data becomes incompatible with a non-evolving cosmological constant (even if the evolution is tiny) the cosmological constant would be ruled out and an alternative theory becomes necessary. There are actually some observations that seem at odds with the standard paradigm, which are summarized below. Although these measurements are disputed due to a lack of statistical significance or systematic effects, they might be the first outliers pointing towards necessary modifications.

[5] An argument of symmetry might explain both a vanishing and a small value for Λ, in a similar way as symmetries set certain masses to zero (e.g. the photon by gauge symmetry) or protect their value against quantum corrections (e.g. fermions and broken chiral symmetry). More generally, it is conceivable that a theory of quantum gravity may be pathological if $\Lambda > 0$ and $\Lambda < 0$, in which case $\Lambda = 0$ would be a consistency requirement.

Model Independence of Cosmological Probes

The standard cosmology presented in the previous pages is by far the best worked out model in the market.[6] It is so widely accepted that many observational analyses implicitly include some of the model hypotheses in the treatment of raw data. For example, many cosmological probes of large scale structure require assuming a fiducial cosmology in order to convert redshifts and angles into physical separations, and sometimes effects are tested (or even calibrated) against numerical simulations.

Sometimes, even the quantities used to relate theory and observations are meaningless in a non standard cosmology. Examples of this are the $A(z) = D_V(z)\sqrt{\Omega_m H_0^2}/z$ function [24], that characterizes the Baryon Acoustic Oscillations feature measured in large scale structure surveys, or the CMB shift parameter (2.12). They incorporate a factor $\sqrt{\Omega_m}$ that is useful to eliminate degeneracies of the model. Although practical for standard cases, this extra dependence invalidates $A(z)$ as a way to constrain models for which $\rho_m(z)$ does not evolve as $(1+z)^3$ (e.g. coupled quintessence or inhomogeneous models for which $\rho_m(z) = \rho_m(r,t)\big|_z$). On the other hand, using the ratio between the sound horizon at the drag epoch (which sets the BAO feature initially) and a distance to that redshift makes the measurement much easier to interpret in more general scenarios.

Testing non-standard cosmologies is helpful to realize which quantities make the more sense as physical effects and make observational probes as model-independent as possible. The analysis of raw data should be performed without assuming fiducial cosmological models and aim at the extraction of physical effects that are both observable and possible to compute and interpret within any given cosmology. Chapter 2 introduces several cosmological observables, emphasizing the model independence of the different probes.

Observational Outliers

It is important to bear in mind that the certain sets of evidence pointed towards the existence of mysterious elements in the standard model even before the evidence from supernovae, CMB and large scale structure observations was solid or even existed. Claimed problems of ΛCDM on large scales are the large scale velocity flows, alignment and lack of power of low multipoles in the CMB angular power spectrum and large scale alignment in the QSO optical polarization data. Other potentially problematic features are related to small scale structure formation. These include the tension between dark matter simulations and observations with regard to both the density profiles of dark matter halos and for the number of predicted substructures inside a given host halo, the baryonic Tully-Fisher relation and the constant galactic surface density.[7] The seemingly discrepant measurements might be due to statistical fluctuations, systematic measurement effects or imprecise theoretical models. However, they are useful to keep in mind, for they might be pointing towards a failure of one or more of the standard hypotheses.

[6] For example, non-linear structure formation within the SCM has been worked out using different perturbative schemes (e.g. linear and higher order perturbation theory, Lagrangian and renormalized perturbation theory) and numerical N-body simulations involving increasing resolution. Although some progress has been made, the level of understanding is considerably lower for alternative models.

[7] The reader is referred to reference [17] for an overview.

1.3 Exotic Tastes and Alternative Recipes

In an effort to provide phenomenologically richer and theoretically more pleasant alternatives to Λ, a vast amount of proposals have been considered [7, 9, 25–27]. These alternatives usually appeal to an unknown principle to set the total CC to zero,[8] and provide an alternative mechanism to accelerate the universe, which necessarily requires an additional modification of one of the assumptions behind the standard model:

1. Allowing for large scale inhomogeneity - See Section 1.3.1 and Chapter 3.

2. Extending the Einstein-Hilbert action, Eq. (1.2)

   2.1. Adding a new (dark) energy component - See Section 1.3.2 and Chapter 5.

   2.2. Modifying the gravitational sector or the coupling to matter - See Section 1.3.3 and Chapters 4, 6.

Other possibilities that aim to explain supernovae dimming have been proposed but will not be considered here. These include as axion-photon mixing [31, 32], gray dust and supernovae evolution. Although these models can easily explain the supernovae observations, they generally fail when other probes are taken into account.

An additional approach is to consider parameterizations that extend the theory in certain directions and can be compared with observations, regardless of the physical origin of the modifications. The simplest example is the constant equation of state dark energy model wCDM, which allows one to test the allowed departures from a Cosmological Constant $w = -1$. This approach allows one to test consistency relations and allowed departures observationally. More sophisticated approaches have been proposed in order to encompass very general modifications in a series of free functions (e.g. the Post-Friedmann approach [33]). Choosing a parameterization (e.g. for $w(z)$) has the problem of pre-selecting a very restricted subset of the space of functions that define the theory. More generally, one can try to reconstruct the free functions that define the cosmological model (either fundamental or parametric) without any a-priory restriction. This has been done in the context of cosmic acceleration using genetic algorithms [34] and Gaussian random processes [35]. Parameterizations can capture physical features in a model independent way, but going beyond parameterizations is necessary to have complete, self consistent models that can be explored in different regimes.

The alternatives are described in the following subsections, focusing on the context relevant for the results presented in Chapters 3-6. For a further details and a broader context the reader is referred to the excellent reviews on inhomogeneous cosmologies, dynamical dark energy and alternative theories of gravity by Clarkson [8], Copeland *et al.* [9] and Clifton *et al.* [7] respectively.

1.3.1 Inhomogeneous Models

The cosmological information is gathered through photons from distant sources (e.g. supernovae or galaxies), that were emitted at the time corresponding to a given redshift z and arrive from a given direction $\hat{n}$. Hence, most cosmological probes are only able to explore a

[8] This requires solving the old cosmological constant problem. Several attempts in this direction have been proposed [28–30]

three dimensional submanifold (within the four dimensional space-time), that is, the *light-cone* spanned by the past null geodesics converging to our galaxy at the present time. If the universe is homogeneous on the observed scales, this information can be used to infer the time evolution of the cosmological model. But in general, observations based on direct light can not tell apart time evolution from spatial variation.

The level of CMB isotropy suggests that there is little dependence on the direction of observation $\hat{n}$ on very large scales. It is then justified to consider spherically symmetric but inhomogeneous metrics. If the pressure component can be neglected, the result is the Lemaître-Tolman-Bondi metric

$$ds^2_{\rm LTB} = -dt^2 + \frac{A'^2(r,t)}{1-k(r)}\,dr^2 + A^2(r,t)\,d\Omega^2\,, \tag{1.18}$$

which contains the FRW metric (1.5) as the particular case of no radial dependence $A(r,t) = a(t)A_0(r)$, $k(r) = k$. The above metric is able to explain the supernovae observations without a Cosmological Constant if the matter content represents an underdense region of size comparable to the Hubble radius ($\sim$Gpc) and our galaxy is located very close to the center of symmetry $r = 0$. The apparent acceleration is a spatial effect in these models: the lower matter density around our galaxy decelerate the expansion less at low redshift, while the higher matter density far away increases the deceleration at higher redshift.

Living at the center of an large, underdense region seems unnatural for two reasons. The first one is the choice of a special location (which is contrary to the Copernican Principle), and the second one is that so large and spherically symmetric voids are very unlikely to form out of the standard initial conditions that inflationary models typically predicts (in terms of the size and the amplitude of the initial perturbation). However, the LTB metric is compatible with the Big Bang theory (i.e. very homogeneous universe) if the local expansion rate $H_0(r)$ is chosen to make the age of the universe space independent and the matter components are adiabatically mixed.[9] In that case, the LTB metric describes the growth of an initial perturbation with arbitrarily small amplitude at early times.

On the other hand, any judgment about our underlying cosmological model should rely on observations rather than aesthetic criteria. The modifications on the matter distribution necessary to fit the supernovae data also alter the predictions for several other cosmological observables, which can then be used to test the model. Indeed, combinations of different data sets can be used to rule out inhomogeneous cosmological models without dark energy in four different ways:

1. Tension between local expansion rate and the CMB.

2. Isotropy of the CMB for off-center observers, as constrained from the kinematic Sunyaev-Zel'dovich effect. This probe is very powerful, and can be used to rule out models with inhomogeneous Big-Bang time [36].

3. Tension between SNe and BAO due to the effects of the inhomogeneous expansion.

4. Tension between SNe and galaxy ages [37].

[9] Once the symmetry is reduced, it is possible to extend the inhomogeneity to other degrees of freedom, e.g. baryonic/dark matter ratio or space dependent age of the universe.

Chapter 3 deals with the details of this type of models and their comparison to observations. The results related to the third method are presented together with the references to the work where methods one and two are described.

Effects from Standard Inhomogeneity

Although they are not considered in the present thesis, there are two effects related to the inhomogeneity of the universe that might be relevant for the dark energy problem. The first has to do with the interpretation of observations assuming a homogeneous cosmology. Effects from small scale inhomogeneities, e.g. the lensing of supernovae light by cosmic structures, might affect the recovered value of the cosmological parameters and should in principle be taken into account [27, 38]. The second effect has to do with the non-linear nature of General Relativity and the process of averaging to obtain the FRW cosmological description. Since the Einstein tensor contains higher powers of the metric, its average is different than the Einstein tensor computed out of the average metric, i.e. $\langle G_{\mu\nu}[g_{\mu\nu}]\rangle \neq G_{\mu\nu}[\langle g_{\mu\nu}\rangle]$. If the non-linear corrections were strong enough to explain the cosmic acceleration, they would further provide a solution to the coincidence problem by linking the acceleration to the epoch in which non-linear structures form on small scales. However, the issue of whether these effects can actually modify the background dynamics significantly is still an open question (cf. [39, 40] and references therein for different points of view).

1.3.2 Dynamical Dark Energy

If the universe is homogeneous and general relativity holds, the second Friedmann equation (1.7) shows that cosmic acceleration only requires that the total energy-momentum satisfies $p < -\rho/3$. It is therefore possible that a new kind of cosmological fluid causes the acceleration as long as the strong energy condition is not satisfied [41, 42]. For example, a canonical scalar field

$$S_\phi = -\int d^4x \left(\frac{1}{2} g^{\mu\nu}\phi_{,\mu}\phi_{,\nu} + V(\phi)\right) , \tag{1.19}$$

becomes equivalent to a constant term if the field derivatives (first term above) are negligible with respect to the potential.In the context of cosmology, such a situation is known as *slow roll*. Scalar fields have been used copiously to build models of inflation and late time acceleration. The theory described by the above action is usually known as *quintessence* and is described by the Klein-Gordon equation (with an arbitrary potential)

$$\Box\phi - V'(\phi) = 0 \quad \xrightarrow{\text{FRW}} \quad \ddot{\phi} + 3H\dot{\phi} + V'(\phi) = 0\,. \tag{1.20}$$

Despite the arbitrariness in the choice of V, quintessence models have been fairly well characterized. The energy momentum obtained from the above action $\rho = X + V$, $p = X - V$ restricts the equation of state to $w \geq -1$, with the equality corresponding to the case of a completely homogeneous and non-evolving field (e.g. at the minimum of a potential). One can further distinguish between models *thawing out*, in which the field is initially frozen by the Hubble friction, and starts evolving towards higher values of w when $V' \sim H\dot{\phi}$, and models *freezing in*, when the equation of state is evolving towards $w \sim -1$ [43]. For certain choices of the potential, scalar fields are able of *tracking* the dominant energy component, contributing a fraction of *early dark energy* during most of the cosmic history [9, 44–47]. Tracking models have been used to alleviate the coincidence problem. Their presence throughout the whole

cosmic history increases the Hubble rate at all times, indirectly reducing the clustering rate of ordinary matter. Other than early dark energy, quintessence fields affect very little the growth of cosmological perturbations and are very difficult to distinguish with large scale structure observations. The speed of sound for field perturbations is equal to the speed of light and its mass is of the order of the Hubble constant. Therefore these fields cluster negligibly except on scales comparable to the Hubble radius $H(t)^{-1}$, which produces a small modification on the large scale CMB (see Section 2.3). In addition, the potential can be chosen to satisfy *any* expansion history (with $w \geq -1$), making the general case very unpredictive in the absence of further requirements on V.

More general theories than (1.19) can be considered, as can be described by the *generalized k-essence* action

$$S_K = \int d^4x \, \mathcal{L}(X, \phi) \,, \tag{1.21}$$

where $X \equiv -\frac{1}{2} g^{\mu\nu} \phi_{,\mu} \phi_{,\nu}$ is the standard (or canonical) kinetic term.[10] K-essence fields can have considerably different features than their quintessence cousins (e.g. negative equation of state, variable speed of sound). Many theories derived from the above action are pathological or unstable in some sense (i.e. introduce ghost degrees of freedom or superluminal signal propagation).

Chapter 5 explores a generalized k-essence scalar field derived from a *disformal relation* (1.27) out of which a set of known dark energy models can be derived in some limit.

Coupled Dark Energy

It is also possible to consider theories in which the scalar field modifies the gravitational or the matter sector in the action. This will generally produce a theory of modified gravity (see next Section), unless the coupling is restricted to just *part* of the matter Lagrangian, explicitly violating the weak equivalence principle. That case represents an interaction between the scalar field that provides dark energy and a particular species

$$S = \int d^4x \left(\frac{\sqrt{-g}R}{16\pi G} + \mathcal{L}_\phi(X, \phi) + \mathcal{L}_{\rm c}(g_{\mu\nu}, \phi, \psi_{\rm c}) + \mathcal{L}_{\rm u}(g_{\mu\nu}, \psi_{\rm u}) \right) , \tag{1.22}$$

where $\psi_{\rm c/u}$ denote the coupled/uncoupled matter. An interesting case is given by a scalar field coupled only to dark matter [48, 49] or neutrinos [50]. Since these species can not be used for gravitational experiments, such models can feature an additional, scalar field mediated force with cosmological implications and evade the precision tests of gravity in the Solar System. On the other hand, connecting the dynamics of dark energy to other cosmic constituents offers an interesting possibility to try to alleviate the coincidence problem.

The paradigmatic example is the scalar field conformally coupled to neutrinos, for which the field only enters the matter Lagrangian through a multiplicative factor of the metric tensor $\mathcal{L}_{\rm c}(A(\phi) g_{\mu\nu}, \psi_{\rm c})$ [50, 51]. This coupling modifies the scalar field and neutrino energy conservation equations with a term $A(\phi)(\rho - 3p)$ that vanishes as long as the neutrinos are relativistic ($p = \rho/3$). The coupling is then used to trigger a slow roll phase in the scalar field when the neutrinos become non-relativistic. Since the neutrino mass has a similar order

[10] Even more general theories free of pathologies can be considered (see equation 1.28). However, they generally introduce modifications in the gravitational sector and will hence be described in the next Section. Appendix C summarizes the most important equations for the theory described by the action (1.21).

of magnitude to the energy scale of the observed Cosmological Constant, these *mass varying neutrinos* dark energy models provide a solution to the coincidence problem by relating both scales. Unfortunately, the extra interaction introduced has considerable impact on large scale structure formation and addressing the viability of the model requires considering the non-linear regime [52, 53].

Chapter 6 examines the implications of generalizing the conformal coupling. As a potential application, the cosmological implications of a purely disformal coupling to dark matter are described in Sections 6.3.1, 6.3.1 and 6.4.2.

1.3.3 Modified Gravity

Finally, the dark universe paradigm calls for a revision of Einstein theory. The great empirical success of GR has been to explain gravitational phenomena on the Solar System and compact objects like neutron stars and pulsars. The mysterious elements of the standard cosmological model are introduced to alter the dynamics on scales for which there is little or no independent probe of the workings of gravity. It remains possible that cosmic acceleration is due to a modification of gravitational dynamics manifest on cosmological scales.

It might seem at first that the action for General Relativity (1.2) is rather arbitrary, considering the enormous freedom available in the construction of geometric scalars. However, there are essential limitations in the choice of the theory of gravity. *Ostrogradski's Theorem* [54] states that there exists a linear instability in any non-degenerate theory whose fundamental dynamical variable appears in the action with higher than 2nd order in time derivatives. By constructing the Hamiltonian for this type of theories, the theorem shows that it is not bounded from below and therefore it accepts configurations with arbitrarily large negative energy [55, 56]. It is possible to bypass Ostrogradski's result by considering *degenerate* theories, i.e. those in which the highest derivative term can not be written as a function of canonical variables. The dynamics of this type of theories is described by second order equations of motion, even while the action contains higher derivative terms.

The gravitational action is severely constrained by Ostrogradski's Theorem because the curvature tensors do contain second derivatives of the metric. *Lovelock's Theorem* [57] states that the only action of the form $\int d^4x L[g_{\mu\nu}]$ (i.e. based on a local scalar Lagrangian solely depending on the metric tensor and its derivatives) which gives rise to second order equations of motion is of the Einstein-Hilbert form with a Cosmological Constant (1.13). The introduction of other geometric invariants not only changes the character of the theory substantially, but may render it unstable. The alternative theories can be classified as ways out of Lovelock's Theorem [7]:

T1: Add additional degrees of freedom other than the metric.

T2: Work in a space with dimensionality different from four.

T3: Accept higher than second derivatives of the metric in the field equations.

T4: Give up either rank (2,0) tensor field equations, symmetry of the field equations under exchange of indices, divergence-free field equations or locality.[11]

[11] Certain non-local theories with an infinite number of derivatives provide another way around Ostrogradski's Theorem. These and other T4 theories will not be discussed further here.

Some theories may fall into different categories within the above classification. High derivative theories (T3) that are acceptable in light of Ostrogradski's Theorem can usually be expressed as a second order theory with extra degree(s) of freedom (T1). This includes the $f(R)$ theories in which the Einstein-Hilbert action includes an arbitrary function of the Ricci scalar. These theories can be shown to be safe [55] through its equivalence to a scalar tensor theory with a Lagrangian density $\sqrt{-g}\,(\phi R + U(\phi))$ (plus a kinetic term for ϕ), where $U(\phi)$ depends on the functional form of the original $f(R)$. Certain higher dimensional theories (T2) can also be expressed in terms of additional degrees of freedom (T1) at an effective level.

Scalar-Tensor Bimetric Theories

The addition of scalar degrees of freedom has been extensively exploited to build modifications of gravity. Metric theories already include a scalar d.o.f. in addition to the propagating spin-2 tensor. This scalar mode is non-dynamical if the action has the EH form, but some alternative theories make it active, which is the reason why $f(R)$ can be expressed as a healthy scalar-tensor theory. In addition, scalars do not introduce preferred directions and mediate universally attractive interactions.[12] The paradigmatic example of scalar modifications are the *old school* scalar-tensor theories

$$\int d^4x\sqrt{-g}\left(h(\phi)\frac{R}{16\pi G} + X - V(\phi) + \mathcal{L}_M(g_{\mu\nu},\psi)\right)\,, \tag{1.23}$$

where the field has been redefined as to yield a canonical kinetic term $X = -\frac{1}{2}\nabla_\mu\phi\nabla^\mu\phi$. By a field dependent local rescaling of the metric or *conformal transformation*

$$g_{\mu\nu} \to h^{-1}(\phi)g_{\mu\nu}\,, \tag{1.24}$$

it is possible to remove the field dependent coefficient from the Ricci scalar. The resulting theory reads

$$\int d^4x\sqrt{-g}\left(\frac{R}{16\pi G} + \tilde{X} - V(\tilde{\phi}) + \mathcal{L}_M(h^{-1}(\tilde{\phi})g_{\mu\nu},\psi)\right)\,, \tag{1.25}$$

where $\phi \to \tilde{\phi}$ has been redefined in order to keep the canonical form of the scalar field Lagrangian [7]. Theories related by metric transformations of the form (1.24) are said to be expressed in different *conformal frames*. The examples above show two particularly interesting choices, the *Jordan frame* (Jf) (1.23) in which matter couples to a single rank-2 tensor and the *Einstein frame* (Ef) (1.25) in which the gravitational sector has the Einstein-Hilbert form but matter couples to an effective metric (1.24) which explicitly depends on the scalar field.

The conformal equivalence between the theories (1.23) and (1.25) motivates considering more general *bi-metric theories* for which the effective metric in the gravitational and matter sectors is allowed to be different.[13] An interesting case is when the gravitational sector is of the Einstein-Hilbert form

$$S_{\text{EH}-\text{BM}} = \int d^4x\left(\sqrt{-g^G}R\left[g^G_{\mu\nu}\right] - \sqrt{-g^M}\mathcal{L}_m\left(g^M_{\mu\nu},\psi\right)\right)\,, \tag{1.26}$$

[12] Theories involving vectors have been considered as candidates for cosmic acceleration (e.g. [58, 59]) and modified gravity that attempt to avoid Dark Matter (TeVeS) [60] or spontaneously break Lorentz invariance (Einstein-Aether) [61], among other applications.

[13] Although the term bi-metric often refers to theories with two fundamental rank 2 tensors (tensor-tensor theories) [7], it will be used here in the sense described in the text (e.g. Eq. 1.26 and its extensions).

but the relation between the two metrics is arbitrary $g^G_{\mu\nu} \neq g^M_{\mu\nu}$. An advantage of this choice is the ease to identify in which limits GR can be recovered, which greatly simplifies the construction of phenomenologically viable scenarios. Bekenstein [62] argued that the most general relation between the two metrics that respects general covariance and involves a single scalar degree of freedom has the form

$$g^M_{\mu\nu} = A(\phi, X) g^G_{\mu\nu} + B(\phi, X)\phi_{,\mu}\phi_{,\nu} \,. \tag{1.27}$$

This expression is known as a *disformal relation*, and it generalizes the well known conformal transformation (1.24) by the addition of a term depending on the gradients of the scalar field. Unlike in the conformal case, the above relation establishes different causal structures for the two metrics whenever $B \neq 0$. The class of dark-energy models obtained from a canonical scalar field constructed using a disformal metric are studied in Chapter 5. In Chapter 6 the analysis is generalized to bi-metric theories (1.26) in which matter is directly coupled to a metric of the form (1.27).

Conformally related scalar-tensor bi-metric theories can be classified into the dark energy type and self accelerating (cf. [63]). Viable cosmological theories have to provide acceleration in the Jordan frame metric, where cosmological observations are implicitly performed. Theories of the *dark energy type* are accelerated also in the Einstein frame. Cosmology in the Ef is described by Friedmann equations, and therefore acceleration implies the existence of an energy component with $p < \rho/3$ in this frame. Therefore, those can be thought of as the generalization of the Dark Energy models introduced in Section 1.3.2. On the other hand, *self accelerating* theories are those in which the acceleration occurs *only* in the Jordan frame. These theories imply that there is no effective cosmological constant in Einstein frame and the acceleration is entirely due to the conformal factor. Although this classification is conceptually useful, it does not contemplate the possibility of relating theories by means of disformal transformations, as will be explored in Section 6.2.

One may consider the generalization of Lovelock's Theorem in the case of a scalar tensor theory, i.e. what is the most general local action that produces second order equations of motion. Following Bekenstein, the matter metric can be allowed to have a conformal as well as a disformal contribution (1.27). For the gravitational sector, it is the Horndeski Lagrangian. The most general gravitational sector was first derived by Horndeski [73] and has received considerable attention in recent years [30, 64, 74–78]. It is given by the *Horndeski Lagrangian*

$$\mathcal{L}_H = \sum_{i=2}^{5} \mathcal{L}_i \,. \tag{1.28}$$

The different pieces can be written (up to total derivative terms that do not contribute to the equations of motion) as [76]

$$\mathcal{L}_2 = G_2(X, \phi) \,, \tag{1.29}$$

$$\mathcal{L}_3 = -G_3(X, \phi)\Box\phi \,, \tag{1.30}$$

$$\mathcal{L}_4 = G_4(X, \phi)R + G_{4,X}\left[(\Box\phi)^2 - \phi_{;\mu\nu}\phi^{;\mu\nu}\right] \,, \tag{1.31}$$

$$\mathcal{L}_5 = G_5(X, \phi)G_{\mu\nu}\phi^{;\mu\nu} - \frac{1}{6}G_{5,X}\left[(\Box\phi)^3 - 3(\Box\phi)\phi_{;\mu\nu}\phi^{;\mu\nu} + 2\phi_{;\mu}{}^{;\nu}\phi_{;\nu}{}^{;\lambda}\phi_{;\lambda}{}^{;\mu}\right] . \tag{1.32}$$

Theory	G_2	G_3	G_4	G_5	$g^M_{\mu\nu}$
General Relativity	Λ	0	$\frac{M_p^2}{2}$	0	$g_{\mu\nu}$
Quintessence (1.19)	$X + V(\phi)$	0	$\frac{M_p^2}{2}$	0	$g_{\mu\nu}$
General k-essence[‡] (1.21)	$K(X,\phi)$	0	$\frac{M_p^2}{2}$	0	$g_{\mu\nu}$
Old school Scalar-Tensor					
- Jordan Frame (1.23)	$\tilde{X} + V(\tilde{\phi})$	0	$h(\phi)\frac{M_p^2}{2}$	0	$g_{\mu\nu}$
- Einstein Frame (1.25)	$X + V(\phi)$	0	$\frac{M_p^2}{2}$	0	$h^{-1}(\phi)g_{\mu\nu}$
Covariant Galileon[§] [64]	$c_1\phi - c_2 X$	$\frac{c_3}{M^3}X$	$\frac{M_p^2}{2} - \frac{c_4}{M^6}X$	$\frac{3c_5}{M^9}X^2$	$A(\phi)g_{\mu\nu}$
Kinetic Gravity Braiding [65, 66]	$K(X,\phi)$	$G(X,\phi)$	$\frac{M_p^2}{2}$	0	$g_{\mu\nu}$
Purely Kinetic Gravity [67]	X	0	$\frac{M_p^2}{2}$	$-\lambda\frac{\phi}{M_p^2}$	$g_{\mu\nu}$
DBI Probe Brane[†] [68]	$\lambda\gamma^{-1}$	$-M_5^3$	$\gamma^{-1}M_4^2$	$-\beta\frac{M_5^2}{m^2}\gamma^2$	$g_{\mu\nu}$
Disformally Coupled Scalar [2, 69]	$X + V(\phi)$	0	0	0	$Ag_{\mu\nu} + B\phi_{,\mu}\phi_{,\nu}$

[‡] See Table 5.1 for an assortment of k-essence models constructed using disformal relations.
[§] The usual Galileon [70] is recovered in the absence of curvature. The analysis of these theories often postulates a conformal coupling betwen the matter and the field (a.k.a. conformal Galileon).
[†] References [71, 72] provide generalizations constructed within the probe brane scheme.

Table 1.1: Horndeski projection of Modified Gravity and Dark Energy theories. Here $M_p^2 = (8\pi G)^{-1}$, $X = -\frac{1}{2}\phi_{,\mu}\phi^{,\mu}$ and $\gamma = \frac{1}{\sqrt{1-2X}}$ is a brane Lorentz factor.

On top of a generalized k-essence (1.29), the remaining pieces (1.30-1.32) fix the allowed higher derivative dependences, which rely on the anti-symmetric structure of $\phi_{;\mu\nu}$ terms to cancel higher derivatives in the equations of motion. Note that a constant term in G_4 produces Einstein gravity. One can then consider the scalar-tensor theory

$$S_{\rm H-BM} = \int d^4x \left(\sqrt{-g}\mathcal{L}_H + \sum_i \sqrt{-g^{M,i}}\mathcal{L}_M(g^{M,i}_{\mu\nu}, \psi) \right) , \tag{1.33}$$

as the most general case, where different matter metrics $g^{M,i}_{\mu\nu}$ have been allowed for the different components (e.g. different coupling to dark matter and baryons is allowed) and no particular Frame has been prescribed. Table 1.1 contains several examples that can be described within the Horndeski Lagrangian, including some particular cases studied in the following Chapters. It has been written based on the work of De Felice, Kobayashi and Tsujikawa [76], who considered cosmological perturbations in the quasi-static approximation

for a number of these theories. Table 1.1 includes some further examples and does not implicitly restrict the theory to the Jordan frame.

The higher derivative terms have been found to arise in the effective description of several higher dimensional theories.[14] G_3, G_4 and G_5 are the covariant generalizations of the third, fourth and fifth Galileon terms [70]. The third order Galileon term appears in the decoupling limit of the five-dimensional Dvali-Gabadadze-Porrati model (DGP) [79], and the other two were proposed as an extension. This theories posses Galilean invariance $\phi \to \phi + c + b_\mu x^\mu$ in flat space-time, a symmetry that grants beneficial properties such as the non-renormalization of the coupling by quantum effects [80]. This type of theories were also obtained in a unified way from extra-dimensional models in which matter is confined to a 3+1 dimensional brane embedded in a larger bulk space [68, 71, 72, 81–83].[15] In the case of a single extra dimension [68] the terms obtained out of the brane tension, and extrinsic, Ricci and Gauss-Bonnet curvature fall into G_2, G_3, G_4 and G_5 when projected into the Horndeski's Lagrangian (1.28). In models with large extra dimensions, the dynamics should interpolate between the small scales in which the physics is effectively four dimensional and the large scales in which the existence of a bulk space becomes manifest. The Vainshtein effect described below allows this interpolation by hiding the scalar mediated force within a certain radius from point sources, i.e. it provides a screening mechanism for the modifications to General Relativity on small scales.

Screening mechanisms are central in the construction of gravitational theories that have significant cosmological implications while remain consistent with precision gravity tests. They provide a way to keep the scalar degrees of freedom inactive in environments which are similar to the Solar System. These mechanisms are usually analyzed in a frame where there is a conformal coupling between the field and matter, in which the scalar force is proportional to the spatial gradient of the field. Screening mechanisms can be classified as kinetic or potential:

- **Kinetic screening mechanisms** rely on the kinetic terms of the field to hide the scalar force. In the *Vainshtein mechanism* [84] higher derivative self interactions ($\kappa_1, \kappa_3, \kappa_8 \neq 0$) do not allow large gradients around point sources. The spatial derivatives of the field are suppressed within a certain *Vainshtein radius* from the source. In the simplest case ($G_2 = X, G_3 = m^{-2}, G_4 = M_p^2/2, G_5 = 0$) it reads

$$r_V \approx \left(\frac{2GM}{m^2}\right)^{1/3} \approx 10\text{Mpc}\left[\left(\frac{H_0}{m}\right)^2 \frac{M}{10^{15}M_\odot}\right]^{1/3}, \tag{1.34}$$

  where M is the point source mass and $M_\odot$ is the mass of the Sun.

  A form of kinetic screening can also be achieved if the scalar field coupling to matter involves a disformal part, in which case the higher derivative terms of the field equation acquire an energy density dependence $[(A - 2BX)g^{\mu\nu} - BT^{\mu\nu}]\,\phi_{;\mu\nu}$, and the field decouples in the limit $\rho \to \infty$. The consequences of the *disformal screening mechanism* are explored in Section 6.5.

[14] As these theories should accept an effective, four dimensional representation in certain circumstances, the geometric origin of these terms is plausibly what renders them viable in light of Ostrogradski's Theorem.

[15] The action for this type of theories is constructed using geometric scalars computed out of the *induced metric* $\bar{g}_{\mu\nu} = g_{\mu\nu} + \pi_{,\mu}\pi_{,\nu}$, which has the same form as the disformal relation (1.27) with $A, B = 1$. The field π represents the position of the brane in this scheme. See Section 6.2 for a discussion.

- **Potential screening mechanisms** rely on the interplay between the coupling and the potential to hide the scalar force. When mediated by a scalar particle, the potential associated to the scalar force acquires the Yukawa form

$$\Phi_s(r) = \frac{\alpha}{r} e^{-m_\phi r} \,, \tag{1.35}$$

  where α is the intensity of the coupling and m_ϕ is the mass of the scalar, that determines the range of the interaction. Its value is given by the second derivative with respect to the field of the effective potential $V_{eff}(\phi) = V(\phi) + A(\phi)\rho$ where a conformal coupling to matter has been assumed.

  The *Chameleon mechanism* [85, 86] requires a decreasing potential and an increasing coupling (e.g. $V = M^5/\phi$ and $A \propto e^{\beta\phi/\Lambda}$). It relies on the environment dependent mass of the scalar to grow large in dense environments, so that massive objects contribute to the scalar force only through a thin shell close to the surface. The *Symmetron mechanism* [87, 88] postulates a degenerate potential with two minima and a coupling that vanishes if $\phi = 0$ (e.g. $V \propto (\phi^2 - \phi_0^2)^2$ and $A = 1 + \phi^2/\Lambda^2$). If the energy density is low, the field sits at $\pm\phi_0$ and the coupling is active. If the density is high, the symmetry is restored in the effective potential and $\phi \sim 0$. Therefore, screened objects only contribute to the force through the matter close to their surface.

The cosmology and local gravitational effects of alternative theories of gravity featuring screening mechanisms has been extensively studied (e.g. [89–95]). Theories endowed with mechanisms of the potential type are bound to field ranges $m_\phi^{-1} \lesssim 1$Mpc in order to keep the Sun screened from the scalar force [63], and therefore modifications to structure formation occur only on non-linear scales.

The results on Modified Gravity and Dark Energy models presented in Chapters 5 and 6 concentrate on theories which involve disformal relations (1.27) in their construction. A disformally constructed canonical scalar field Lagrangian encompasses many proposed dark energy models for different choices of the free functions, as it is explored in Section 5.1.1. The existence of two causal structures in this type of theories makes it easy to construct models for cosmic acceleration. In a FRW background, the two metrics are related by $\bar{g}_{00} = -1 + B\dot{\phi}^2$, so the field enters into slow roll whenever $B\dot{\phi}^2$ approaches unity. This has been explored in detail for disformal quintessence (Section 5.2) and canonical quintessence disformally coupled to matter (Sections 6.3.1 and 6.4.2).

Disformal relations also simplify the analysis of certain higher derivative theories, including those of the DBI form, by providing an Einstein frame description in which the gravitational sector is standard but matter appears disformally coupled to the field. This transformations are explored in Section 6.2, where different frames are presented. Disformally coupled theories also provide a screening mechanism that hides the modifications of gravity in high density environments, as it is explored in Section 6.5. Based on the equivalence to some higher derivative theories, this is likely to be the Vainshtein mechanism in disguise, which appears different in the Einstein frame description. Disformal relations offer hence a new way to construct and analyze scalar field extension of the Einstein-Hilbert action that are relevant for the dark energy paradigm.

Chapter 2

Observational Probes of Cosmology

Reality is not always probable, or likely. But if you're writing a story, you have to make it as plausible as you can, because if not, the reader's imagination will reject it.

Jorge Luis Borges[1]

The first compelling evidence in favor of the cosmic acceleration came from the study of high redshift type Ia supernovae (SNe), *standard candles* of similar luminosity which appeared fainter than they would in a spatially flat, matter dominated universe [11, 12]. In the following years, further information obtained from other probes started confirming the standard picture described in the previous Chapter. The Wilkinson Microwave Anisotropy Probe (WMAP) [16, 18, 19] together with several ground based experiments [96–98] measured the anisotropies in the Cosmic Microwave Background (CMB) with great precision. Their data provides accurate information of the initial perturbations that seeded the cosmic structures that formed through gravitational collapse, and have proven very useful to constraint cosmological parameters within the standard cosmological model and its extensions. Galaxy surveys such as SDSS [24, 99–102] and WiggleZ [103, 104] have produced very detailed maps of the Large Scale Structure (LSS) of the universe, including the signature of the Baryon Acoustic Oscillation (BAO) scale in the matter correlation function. This finding provides a *standard ruler*, whose length can be measured at different cosmological epochs and used to track the expansion of the universe.

The precision and consistency of these and other probes allows one to place the standard cosmological model under increasingly stringent tests, which would hopefully allow to establish the validity of the hypotheses as independently as possible from one another. This great effort aimed at observationally determining the physical laws behind cosmic acceleration will continue over the following decades. The Planck satellite will release even more

[1] Quoted in *Worldwide Laws of Life: 200 Eternal Spiritual Principles* (1998) by John Templeton.

detailed maps of the cosmic microwave background [105] and the Dark Energy Survey (DES) will probe the distribution of cosmic LSS during the following years [106]. This international effort will continue with the Euclid satellite mission [107, 108], which will map the whole extragalactic sky as deep as to reach redshifts of 2, before the accelerated expansion began. These galaxy surveys will determine the BAO scale with exquisite precision at different cosmological epochs. In addition, their *multi probe* design makes them capable to extract further cosmological data such as SNe, weak gravitational lensing, clusters of galaxies, that will place even stronger constraints on departures from large scale homogeneity and General Relativity.

The most relevant cosmological probes for the present Thesis are introduced in this Chapter. Section 2.1 gives a general classification of the observables and the type of knowledge that can be gained from them. Sections 2.2 to 2.6 give an overview of the effects and findings that can be used to constraint cosmological models, emphasizing the underlying assumptions introduced in their analysis and how they can be made model independent. The discussion is necessarily brief. More details can be found in the recent review by Weinberg *et al.* [10] and the references included in each Section.

2.1 Geometry and Dynamics

Cosmological probes can be classified into *geometric* and *dynamical* (see Table 2.1). Geometric probes are based on background quantities and measure the zero order expansion, i.e. the predicted quantities to be compared with observations depend only upon the elements of the unperturbed metric, at least to a good enough approximation.[2] A classical example is the *angular diameter distance*

$$D_A(z) = \left.\frac{l_\perp}{\theta}\right|_{O(z)} = \frac{1}{1+z}\int_0^z \frac{dz'}{H(z')}\,, \tag{2.1}$$

where the first equality is observational, i.e. the ratio of the (assumed) known physical length in the transverse direction $l_\perp$ of an object at redshift z and the measured angle it subtends in the sky θ (assumed small), and the second equality is the prediction for a flat FRW cosmology. Another useful geometric probe is the *luminosity distance*:

$$D_L(z) = \left.\sqrt{\frac{L}{4\pi\, F}}\right|_{O(z)} = (1+z)\int_0^z \frac{dz'}{H(z')}\,. \tag{2.2}$$

Here the first equality is the observational value, related to the ratio between the (assumed known) luminosity L and the observed flux F of an object at redshift z. The second equality gives the value within a flat FRW cosmology. The angular diameter distance enters the analysis of the BAO scale, as measured in the CMB and galaxy surveys (Sections 2.3 and 2.4.1), and the luminosity distance is compared with supernovae data (Section 2.5).

Geometric probes can also be applied to inhomogeneous cosmologies rather straightforwardly. The equivalent of the angular diameter and luminosity distances for this type

[2] That means, geometric probes depend only on the scale factor and the Hubble rate in FRW cosmologies, perhaps through integrals or derivatives. In LTB models the cosmological probes may depend on the two scale factors (or expansion rates), which are different in the radial and angular direction due to the inhomogeneity.

Type	Probe	Redshift Range	Section
Geometric	Type Ia SNe	$0.01 - 1.5$	2.5
	Local expansion (H0)	$\lesssim 0.1$	2.5
	CMB priors	z_*	2.3.1, Ref. [19]
	BAO scale from LSS	$0.1 - 0.8(3)$	2.4.1
	Primordial Nucleosynthesis	$\sim 10^{10}$	2.2
Dynamical	CMB primary	$\sim z_*$	2.3
	CMB secondary	$0 \to z_*$	2.3
	CMB kSZ	$0 - 1$	2.4.2, Ref. [109]
	LSS power spectrum	$0.1 - 1(3)$	2.4
	LSS Lensing	$0 - 1$	2.4.2
	LSS Clusters	$0 - 1$	2.4.2
Dynamical	Local Gravity Tests	0	2.6, Ref. [110]

Table 2.1: Summary of cosmological probes. The different observables have been classified into geometric and dynamical. z_* is the recombination redshift, numbers in parenthesis refer to expected limits for future surveys. See reference [10] for details.

of models is presented in equations (3.18,3.19), and the necessary considerations to use the BAO scale are made in Section 3.2 in Chapter 3. Current data allow to rule out LTB models with homogeneous Big-Bang and $\Lambda = 0$ using geometric probes only (Section 3.3).

Dynamical probes are those which crucially depend on the departures from the background metric on cosmological scales. A common coordinate choice to describe metric perturbations is the conformal-Newtonian gauge

$$ds^2_{\rm CN} = a^2(\tau)\left[-(1+2\Phi)d\tau^2 + (1-2\Psi)d\vec{x}^2\right] , \tag{2.3}$$

which has been written in terms of the conformal time $\tau = \int a(t)dt$. The gravitational potentials Φ, Ψ are sourced by the perturbed energy momentum tensor $\delta T^{\mu\nu}(\vec{x}, \tau)$, which is usually expressed in terms of dimensionless variables such as the *density contrast*

$$\delta(\vec{x}, \tau) \equiv \frac{\rho(\vec{x}, \tau)}{\langle\rho\rangle(\tau)} - 1 . \tag{2.4}$$

Cosmological observables sensitive to departures from homogeneity have the potential to probe the gravitational collapse and the formation of cosmic structures. This information is essential for non-standard cosmological models, as it potentially allows one to distinguish modifications from gravity from non-interacting dark energy models with the same background history. Of particular interest are those effects that can be computed within linear perturbation theory. Non-linear effects are more difficult to connect with the models on trial, and the computational tools that allow their exploration have been considerably less developed for non-standard cosmologies than for ΛCDM.

One of the challenges of cosmological model testing is to determine to what extent each cosmological probe is affected by dynamical effects. Some probes, such as the BAO

scale in LSS and CMB distance priors are intrinsically dynamical. But since the physical quantities involved in the comparison can be reliably computed using just the background information, they are considered geometric observables. No probe is purely geometric, as there will always be dyanamical effects if sufficient precision is achieved (e.g. through peculiar motions). However it is a useful classification to bear in mind.

2.2 Primordial Nucleosynthesis

The first event that yields direct information about the early universe involves the formation of the first composite nuclei, a period known as primordial nucleosynthesis or Big-Bang Nucleosynthesis (BBN) [111]. At the onset of BBN, weak interactions keep protons and neutrons in equilibrium, slightly favoring protons due to their lower mass $m_n - m_p = 1.293$ MeV. The formation of composite nuclei is dominated by two body collisions at the BBN temperature scale, and hence deuterium ^{2}H is the first step in the chain of nuclear reactions. The binding energy of deuterium $E_D = 2.224$ MeV is too low for it to be stable until the universe cools down to $T \lesssim 0.1$MeV. This is due to the high photon number density $n_b/n_\gamma = \eta_{10} \cdot 10^{-10}$, which allows a significant population in the high energy tail of the distribution. When the temperature is low enough, the available neutrons combine with protons to form deuterium, and most of it is quickly processed into heavier elements, with a major amount ending in the form of ^{4}He.

The predicted abundances can be compared with observations in low metallicity systems, which have not been significantly affected by stellar nucleosynthesis. The measured abundances can be used to determine certain cosmological parameters and allow the determination of the baryon to photon ratio independently of the CMB. Deuterium and ^{4}He measurements agree well with expectations, but ^{7}Li observations lie a factor 3-4 below the BBN+WMAP prediction, a mismatch known as the "cosmic lithium problem" [20, 112, 113]. BBN is also sensitive to the expansion rate at early times and can be therefore be used to constraint the number of relativistic degrees of freedom N_{eff} [20] as well as non-standard scenarios, such as a possible time variation of the Newton's constant [114], the amount of early dark energy [115], heavy particle decays or the variation of fundamental couplings [116, 117].

2.3 Cosmic Microwave Background Radiation

Similarly to the formation of the first nuclei, no neutral atoms can form in the early universe until the temperature is sufficiently low. The electromagnetic interacting species are tightly coupled and perturbations propagate in the baryon-photon plasma as sound waves . Neutral hydrogen starts forming when the temperature drops below $T \lesssim 1$ eV and the universe starts becoming transparent as light is able to travel without encountering charged particles. This epoch is called *recombination* and occurred at $z \approx 1090$. The photons emitted then have redshifted and diluted since recombination and can be seen today in the form of a *Cosmic Microwave Background* (CMB) with an average temperature ≈ 2.73 K. Several experiments have measured anisotropies of the CMB radiation, whose study is very useful to constraint cosmological models.

The line of sight integration method provides a very direct way to study the physical effects behind the CMB anisotropies [118]. For a spatially flat universe and adopting the

conformal Newtonian gauge (2.3), the linear temperature anisotropy $\Theta \equiv \delta T/T$ due to the Fourier mode k and projected on the multipole l today can be written as

$$\Theta_l^{(s)}(k,\tau_0) = \int_0^{\tau_0} d\tau S_T^{(s)}(k,\tau) j_l(k(\tau_0-\tau))\,, \tag{2.5}$$

where $\mu \equiv \hat{n}\cdot\vec{k}/|k|$. The integrand is a convolution of the l-th spherical Bessel function j_l and the scalar sources

$$S_T^{(s)}(k,\tau) \equiv g\left(\Theta_0+\Phi+\frac{\dot{v}_b}{k}+\frac{\Pi}{4}+\frac{3\Pi}{4k^2}\right)+e^{-\kappa}\left(\dot{\Phi}+\dot{\Psi}\right)+\dot{g}\left(\frac{v_b}{k}+\frac{3\dot{\Pi}}{4k^2}\right)+\frac{3\ddot{g}\Pi}{4k^2}\,. \tag{2.6}$$

Here dots denote derivatives wrt conformal time τ, $\kappa(\tau)=\int_\tau^{\tau_0} n_e\sigma_T a d\tau'$ is the optical depth (determined from the free electron fraction n_e and the Thompson scattering cross section σ_T) and $g \equiv -\dot{\kappa}e^{-\kappa}$ is the visibility function.[3] In addition to the gravitational potentials Φ,Ψ, the sources include the temperature monopole, the baryon velocity v_b and the polarization tensor Π, all of them depending on τ and k. Besides simplifying the computation, the line of sight approach allows the identification of different contributions to the total anisotropy. The terms proportional to the visibility function (which peaks around the recombination epoch) are known as *primary anisotropies*, since they are imprinted at $z\sim 1090$ when the photons decouple:

- Primary monopole Θ_0. The anisotropy is proportional to the local photon energy density fluctuation at the last scattering surface.
- Sachs-Wolfe effect Φ. Photons are redshifted as they climb up the initial potential wells when they are emitted.
- Dopler shift induced by baryon velocity $v_b, \dot{v}_b$.
- Polarization effects $\Pi, \dot{\Pi}, \ddot{\Pi}$. Although these effects are typically small, they are necessary for an accurate description of the anisotropies.

The term proportional to $e^{-\kappa}$ is active since last scattering. This gives rise to a *secondary contribution*

- Integrated Sachs-Wolfe (ISW) effect $\dot{\Phi}+\dot{\Psi}$. This term represents how the photons traveling from the last scattering surface are affected by the potential wells they encounter. If the potential wells were static, the blueshift gained when entering would be compensated by the redshift necessary to escape. But if the potentials are evolving in time, there is a net contribution on the temperature anisotropy.

Gravitational lensing of the CMB provides an additional secondary contribution to the temperature fluctuation [119, 120]. However, lensing effects require a bending of the photon trajectories due to inhomogeneities, which are already an linear effect. Hence they constitute a higher order correction to (2.6).

[3] There is also an equation for the polarization spectrum, featuring different sources. However, dark energy models do not typically affect the CMB polarization, unless there is some specific coupling to photons.

The *angular power spectrum* is obtained by the convolution of the temperature anisotropy (2.5) with the initial power spectrum of the metric perturbation

$$C_l^{(s)} = (4\pi)^2 \int dk k^2 P_\Phi(k) \left|\Theta_l^{(s)}(k,\tau_0)\right|^2 . \tag{2.7}$$

Here $P_\Phi(k)$ is defined for the potential in an analogous way to the matter power spectrum presented below (2.17). Similar expressions exist for the polarization and the tensor sources. To compare with observations, it is useful to project the observed temperature anisotropy into spherical harmonics

$$\Theta^{\rm obs}(\hat{n}) = \sum_{l=0}^{\infty} \sum_{m=-l}^{l} a_{lm} Y_{lm}(\hat{n}) \,, \tag{2.8}$$

so that the coefficients a_{lm} encode the dependence on the direction of observation $\hat{n}$. In a statistically isotropic universe the mean vanishes $\langle a_{lm} \rangle = 0$. If the distribution is Gaussian, it is fully characterized by the variance

$$\langle a_{lm} a_{l'm'} \rangle = C_l^{(\rm obs)} \delta_{ll'} \delta_{mm'} \tag{2.9}$$

The obtained value of $C_l^{(\rm obs)}$ is the quantity to be compared against equation (2.7). It is possible to compute non-Gaussian correlations (e.g. $\langle a_{l_1 m_1} a_{l_2 m_2} a_{l_3 m_3} \rangle$), an information that can be related to the primordial non-Gaussianity induced by inflation and has been bounded by CMB experiments [19, 121].

One of the greatest advantages of the CMB anisotropies is that they can be computed for any cosmological model, provided that there is a reliable linear perturbation theory. Many dark energy models only modify the late time physics substantially, leading to an even simpler implementation. In this cases, the most significant departures come from the low-l end of the spectrum, for which there are less projections m to obtain the angular power spectrum (2.9). Therefore, the CMB is mostly useful to detect significant departures at late times (e.g. the ISW effect), but is limited when it comes to precision measurements of the low redshift dynamics behind cosmic acceleration. Pre-recombination effects such as the presence of early dark energy are still tightly bound by the CMB measurements [122].

2.3.1 CMB Distance Priors

Understanding the CMB physics requires considering the dynamics of the perturbations all the way since the early universe. However, the reason behind the acoustic oscillations that gave rise to the peaks is simple and can be understood in geometric terms. Initial perturbations in the baryon-photon fluid propagate a finite distance until the recombination epoch in which photons decouple. The total length traveled by a sound wave depends on the speed of sound $c_s = \frac{1}{\sqrt{3}} \left(1 + \frac{3\rho_b}{4\rho_\gamma}\right)^{-1/2}$. It is known as the *sound horizon*

$$r_s(z_*) = \int_0^{(1+z_*)^{-1}} \frac{c_s(a)}{a^2 H(a)} da \,. \tag{2.10}$$

The recombination redshift z_* can be calculated using fitting formulae [123] or the full background history, which is recommendable in non-standard cases (e.g. in the presence of early dark energy). The sound horizon is a coordinate distance. To obtain the physical, measurable

distance, it is necessary to multiply by the scale factor at the time of interest $a(t) = 1/(1+z_*)$. Comparing the physical sound horizon at recombination with the angular diameter distance allows one to define the *CMB acoustic scale*

$$l_A = (1 + z_*)\frac{\pi D_A(z_*)}{r_s(z_*)}\,, \tag{2.11}$$

which is inversely proportional to the angle subtended by the sound horizon observed today θ_*. The acoustic scale is a good observable, in the sense that it can be easily defined in any statistically isotropic or spherically symmetric cosmology.

In certain situations it is useful to compare dark energy models against a reduced set of parameters instead of the full angular power spectrum. This allows one to include information from the CMB in the analysis without computing cosmological perturbations. One possibility is then to use the WMAP distance priors l_A, z_*, R [19] where in addition to the already described quantities the shift parameter is defined as

$$R = \sqrt{\Omega_m H_0^2}(1 + z_*)D_A(z_*)\,. \tag{2.12}$$

The use of these parameters is valid for FRW models containing matter, radiation, curvature, dark energy, three neutrinos with minimal mass, and standard initial conditions. Its use is convenient when the model does not affect the clustering of matter significantly (e.g. quintessence) or the equations for the perturbations are not well known (e.g. phenomenological modifications of the Friedmann equations). On the other hand, it misses important effects that may occur in modified gravity and the values of z_*, R can not be used to constraint inhomogeneous models.[4] The shift parameter R is also difficult to interpret in models where the evolution of matter is non-standard (e.g. coupled quintessence). A more model-independent approach to geometric CMB analysis that is valid for inhomogeneous cosmologies can be found in reference [124].

2.4 Large Scale Structure

The gravitational pull exerted by inhomogeneities is responsible for the growth of cosmic large scale structures. An overdense region attracts the matter around it, which in turn enhances the gravitational attraction on its surroundings. By the action of gravitational instability, the matter is always transfered from the underdense to the overdense regions, and the initially quasi-homogeneous universe becomes populated by collapsed non-linear objects and empty regions (voids). The Hubble expansion acts as a friction term and inhibits the growth of perturbation modes which are larger than the Hubble radius at any given time. Therefore, smaller perturbations start growing earlier.

The clustering on cosmological scales is dominated by the dark matter component with zero pressure. In the hydrodynamic limit, it follows the Euler and continuity equation [125]

$$\dot{\delta}_m(\vec{x},\tau) + \nabla\cdot[(1+\delta_m(\vec{x},\tau))\vec{u}(\vec{x},\tau)] = 0\,, \tag{2.13}$$

$$\dot{\vec{u}}(\vec{x},\tau) + \mathcal{H}(\tau)\vec{u}(\vec{x},\tau) + \vec{u}(\vec{x},\tau)\cdot\nabla\vec{u}(\vec{x},\tau) + \nabla\Phi_N(\vec{x},\tau) = 0\,, \tag{2.14}$$

[4] A method to use simplified CMB constraints in inhomogeneous models is explained in Section 3.3.1.

where $u(\vec{x},\tau)$ is the velocity, $\mathcal{H}(\tau) \equiv a^{-1}da/d\tau$ is the conformal Hubble rate and δ_m is defined as in (2.4) . On sub-Hubble scales the Newtonian potential Φ_N is given by the Poisson equation

$$\nabla^2\Phi_N(\vec{x},\tau) = 4\pi G\rho_m(\tau)\delta(\vec{x},\tau)\,. \tag{2.15}$$

Equations (2.13,2.14) are both non-linear. Their general study requires sophisticated techniques such as renormalized perturbation theory, halo model or N-body simulations [126–128]. For linear perturbations $\delta, \vec{u} \ll 1$ on sub-Hubble scales and assuming zero vorticity $\nabla\times\vec{u} = 0$, the above equations can be written in Fourier space as a single, second order equation

$$\ddot{\delta}_m(k) + 2\mathcal{H}(\tau)\dot{\delta}_m(k) = 4\pi G\rho(\tau)\,\delta_m(k)\,. \tag{2.16}$$

The density contrast $\delta_m(\vec{k})$ can be computed for a given cosmological model using perturbation theory. Similarly to the CMB, it is necessary to define statistical quantities in order to compare theoretical predictions and observations. The matter distribution is characterized by the *power spectrum*

$$\langle\delta(\vec{k})\,\delta(\vec{k}')\rangle = (2\pi)^3 P_\delta(k)\,\delta^{(3)}(\vec{k}-\vec{k}')\,, \tag{2.17}$$

where $\delta(\vec{k})$ is the Fourier transform of the density contrast (2.4).[5] The use of the above power spectrum to compare with observations is common. However, projecting the observed redshifts and angular locations of galaxies into physical coordinates $\vec{x}$ (which is necessary to Fourier transform) requires the assumption of a fiducial cosmology.

A model independent approach based on the use of directly measurable quantities was proposed recently[129, 130]. Instead of real or Fourier space, the density contrast is computed as a function of the redshift z and the direction of observation $\hat{n}$

$$\delta_z(\hat{n},z) \equiv \frac{\rho(\hat{n},z)}{\langle\rho\rangle(z)} - 1 = \frac{N(\hat{n},z)}{\langle N\rangle(z)} + \frac{V(\hat{n},z)}{V(z)}\,. \tag{2.18}$$

As a consequence of their observable nature, all the terms in the above equation are themselves gauge invariant. In order to compare with observations, (2.18) can be projected into an angular power spectrum $C_l^{(\delta)}(z,\Delta z)$ for different redshift separations or smearing, and the same procedure can be applied to the data. This is analogous to CMB analysis, except that LSS surveys are three dimensional and have the additional redshift dependence. The study of different angular multipoles and redshift separations allows one to disentangle the different effects contributing to δ_z. The disadvantage of this method is the finite amount of statistics available for each possible correlation. In practice, current surveys take best statistical advantage by condensing all the information in a Fourier power spectrum (2.17) for different redshift slices, although that introduces a spurious, model dependent $(\theta,\hat{n}) \to \vec{x}$ conversion in the analysis.

Galaxy surveys measure galaxies, not the underlying matter density. A galaxy is a very non-linear object, whose formation and evolution depend on its environment in a very complex way. Therefore, galaxies are biased tracers of the underlying matter distribution, i.e. their density contrast is such that

$$\delta_g \approx b_g\delta_m + b_{g(2)}\delta_m^2 + \cdots \tag{2.19}$$

[5] One can also consider higher order statistics, e.g. $\langle\delta\delta\delta\rangle$, which may be sourced by non-linear gravitational clustering or be related to primordial non-Gaussianity [121].

where the *galaxy bias* coefficients can in principle depend on time, scale and galaxy type. Non-linear terms have been included schematically. Although they will not be considered further, realistic bias models should include some non-linear part to distinguish overdense and under-dense regions. Another observational effect is caused by the peculiar velocities of galaxies, which affects the cosmological redshift in a systematic way - galaxies moving towards an overdense cosmic structure will appear redshifted if they are in front of it (wrt the observer) and blueshifted if they are behind. This makes a spherical distribution in real space (e.g. a cluster of galaxies) look squeezed when observed by a survey in $(z, \hat{n})$, an effect known as *Redshift Space Distortions* (RSD). Taking linear galaxy bias and RSD into account allows one to relate the galaxy and matter power spectra [131]

$$P_g(k,\mu) = (b_g + f\mu^2)^2 P_\delta(k)\,, \tag{2.20}$$

where $\mu = \hat{n}\cdot\vec{k}/|k|$ is the angle between the Fourier mode and the line of sight direction and

$$f \equiv \frac{d\log\delta(a)}{d\log a} \equiv \Omega_m(a)^{\gamma(a)}\,, \tag{2.21}$$

is the *growth factor*. The second equality defines an useful parameterization in terms of the *growth index* $\gamma(a)$, that encapsulates the effect of the background matter on the clustering. Its value is very close to a constant and equal to 6/11 in ΛCDM universes, while modified gravity models predict different values. Equation (2.20) can be used to determine f from the angular dependence of the galaxy power spectrum. A compilation of growth factor observational data and the predictions can be found in reference [132].

Non-standard cosmological models can affect considerably the formation of structure. Theories of modified gravity typically incorporate an additional interaction that increases the force and enhances gravitational instability. In certain cases, the growth factor (2.21) might acquire an additional scale dependence at the linear level [133]. Models in which dark energy couples to dark matte do induce an additional bias between the dominant matter component and the baryons. These features are explored in Section 6.4.2 for the case of disformally coupled scalar fields.

The case of inhomogeneous cosmologies has been considerably less explored due to the technical difficulties it poses. These include the lack of a decomposition of linear perturbations into scalar, vector and tensor, together with the need to solve partial differential equations depending on (r, t) insted of ordinary ones [134]. Numerical studies of the growth of structure in LTB spacetimes have been performed using non-linear numerical simulations [135, 136] and linear perturbation theory [137]. Some consequences of these studies are described in Section 3.2.2.

2.4.1 The Baryon Acoustic Oscillation Scale

The large scale distribution of matter also reflects the propagation of perturbations in baryon-photon fluid before recombination as a sequence of oscillations superimposed on the power spectrum. Equivalently, it can be seen as a peak in the two point correlation function, which is related to the power spectrum by a Fourier transform. The BAO scale provides a statistical standard ruler that allows one to reconstruct the expansion history of the low redshift universe using information from galaxy surveys. As the BAO signal is suppressed by the baryon to matter ratio, its determination requires large survey volumes in order to gain

statistical significance. Although it has the same origin as the CMB angular scale (2.10), the LSS-BAO scale is fixed by the sound horizon at the *drag epoch* t_d, which is the time in which the baryons decouple [138]. The high photon to baryon ratio keeps the latter coupled longer, and hence the drag redshift z_d is lower than the recombination one z_*.

The BAO scale is intrinsically three dimensional (like any other LSS quantity and unlike the CMB), and can be measured at different redshifts. Thus, it is possible to observe it parallel to the line of sight (radial BAO) through the correlation in redshift, in addition to the angular correlation (angular BAO). The comparison between the theoretical and predicted BAO scales is presented in detail in Section 3.2 for LTB models, in which new effects arise due to the inhomogeneity. The relevant equations for the projected BAO length in angle and redshift (3.37, 3.40) can be straightforwardly applied to a homogeneous cosmology

$$\theta_{BAO} = \frac{r_s(z_d)}{(1+z)D_A(z)}\,. \tag{2.22}$$

$$\Delta z_{BAO} = H(z) r_s(z_d) \tag{2.23}$$

In order to gain statistical significance, the BAO scale is usually obtained from the raw data by projecting it into spatial coordinates (assuming a fiducial model) instead of using a model independent extraction in the variables $z, \hat{n}$ (2.18).[6] Due to historical reasons and the impossibility to disentangle the different directions after the projection, it is customary to quote the data in terms of the geometric mean of the angular and redshift correlation

$$d_z \equiv \left(\theta_{BAO}^2 \frac{\Delta z_{BAO}}{z}\right)^{1/3} = \frac{r_s(z_d)}{\left((1+z)^2 D_A(z)^2\, z\, H(z)^{-1}\right)^{1/3}}\,. \tag{2.24}$$

The denominator in the second equality is known as the *geometric mean distance* D_V. The angular correlation is squared to account for the two dimensions in the solid angle. Similarly to the product of the correlation in the different distances, it is possible to consider the ratio of the characteristic scales as seen in redshift and angular space. The process of determining whether the $\delta z, \theta$ fulfill the geometric relationships predicted by the FRW metric is called an *Alcock-Paczynski* test. Section 3.2.5 describes it briefly in the context of LTB universes.

Dynamical Effects

The BAO scale is a paradigmatic example of a geometric cosmological probe. The characteristic length remains constant in coordinate space and tracks the background expansion to a very good approximation, since dynamical effects depend on the density variations within ~ 150 Mpc spheres and the universe is very well described by linear perturbation theory on such large scales. In ΛCDM the BAO scale is constant in coordinate space due to the lack of scale dependence of subhorizon perturbations $\delta_k(t) = D(t)\delta_k(t_0)$ (2.16) up to non-linear effects. This preserves the shape of the power spectrum and the two point correlation function, hence making BAO a geometric probe. The first dynamical effects enter non-linearly, broadening the shape of the peak and systematically reducing the BAO scale at the sub percent level [142–146]. Other systematics degenerate with BAO evolution might be caused by scale dependent bias or non-gaussian effects.

[6] This was necessary when the data was scarce. Current galaxy surveys allow for independent determinations of the angular [139] and radial [140, 141] BAO scales

	6dF	SDSS		WiggleZ			Carnero *et al.*	
z	0.106	0.2	0.35	0.44	0.6	0.73	z	0.55
d_z	0.336	0.1905	0.1097	0.0916	0.0726	0.0592	θ_{BAO}	3.90°
Δd_z	0.015	0.0061	0.0036	0.0071	0.0034	0.0032	$\Delta\theta_{BAO}$	0.38°

$$C_{ij}^{-1} = \begin{pmatrix} 4444 & 0. & 0. & 0. & 0. & 0. \\ 0. & 30318 & -17312 & 0. & 0. & 0. \\ 0. & -17312 & 87046 & 0. & 0. & 0. \\ 0. & 0. & 0. & 23857 & -22747 & 10586 \\ 0. & 0. & 0. & -22747 & 128729 & -59907 \\ 0. & 0. & 0. & 10586 & -59907 & 125536 \end{pmatrix}. \tag{2.25}$$

Table 2.2: BAO data. The first six data points are volume averaged and correspond to Table 3 of [103]. Their inverse covariance Matrix is given by (2.25), and was obtained from the covariance data in reference [103] in terms of d_z. The last point corresponds to an angular measurement given in [139].

The evolution of the BAO scale has received considerably less attention in the case of non-standard cosmologies.[7] Sherwin and Zaldarriaga [146] argue that the BAO shift is an intrinsically non-linear effect, as combines the fact that overdense regions expand less *and* contribute more to the two-point correlation function. However, linear perturbations becomes scale dependent in many alternative theories of gravity $\delta_k(t) = D(t,k)\delta_k(t_0)$, and dynamical effects may occur within this approximation. Theories featuring additional forces acting on distances ~ 150 Mpc (e.g. Vainshtein screened models) might enhance the shift of the BAO scale with respect to the standard model.

Current BAO Data

The current BAO data span the redshift interval $0 - 0.8$. The d_z data at lower redshift obtained by SDSS and 6DFGS [101, 147, 148] is complemented with the points provided by the WiggleZ collaboration [103]. An additional point obtained from SDSS DR7 catalog in the range $[0.5 - 0.6]$ has been extracted as a purely angular correlation [139]. It is independent of the other SDSS measurements at $z = 0.2, 0.35$. All d_z data points are summarized in Table 3 of reference [103]. However, the inverse covariance matrix for the data is provided in terms of the variable $A(z)$, which can not be interpreted easily in non-standard cosmologies, as discussed in Section 1.2.1. In order to retain the covariances between the different data points and analyze the models in terms of a meaningful variable, the inverse covariance matrix was obtained in terms of d_z using the correlation matrix. The data are summarized in Table 2.2, and can be also seen in Figure 3.5 compared to several homogeneous and inhomogeneous models.

[7] The discussion here is restricted to the case of modified gravity models. The geometric status of BAO measurements in inhomogeneous cosmologies is discussed in Sections 3.2.1 and 3.2.2.

The likelihood is assumed to be Gaussian and given by

$$\chi^2_{\rm BAO} = \sum_{i,j}(d_i - d(z_i))C^{-1}_{ij}(d_j - d(z_j)) + \frac{(\theta_{\rm BAO}(0.55) - \theta^{0.55}_{\rm BAO})^2}{\Delta\theta^2_{\rm BAO}}\,, \tag{2.26}$$

where the indices i, j are in growing order in z, as in Table 2.2.

The choice of data is convenient because it covers the redshift range $z \leq 0.8$ with a regular spacing and the correlations are known (2.25). Other available BAO scale determinations (e.g. references [100, 102, 149–151]) would add points at intermediate redshifts with similar error bars and unknown covariances, and therefore we expect they will not increase the precision of the constraints. Determinations of the radial BAO scale [140, 141] are particularly interesting to constrain inhomogeneous models [152, 153] due to the distinct radial rescaling factor (3.35), see Section 3.2.4. Nonetheless, they are not included here due to the lack of knowledge about the correlations with other data points.

2.4.2 Other LSS Probes

The previous description has introduced some possible ways to use Large Scale Structure to study cosmology. However, there are other probes that test the dynamical properties of cosmological models, including weak gravitational lensing and galaxy cluster counts.

Weak Gravitational Lensing

One of the consequences of general relativity is the deflection of light by matter. The trajectories of photons traveling over cosmological distances are affected by the intermediate matter distribution, which acts similarly to a lens in geometric optics. It produces a change in the perceived size (magnification) and shape (shear) of background objects.[8] *Magnification* is difficult to use as a cosmological probe, because it requires knowing the intrinsic size of the objects under study with significant precision.

Observing the correlations of shapes within a background set of galaxies allows one to reconstruct the intermediate density distribution. It is then possible to define a *shear power spectrum* analogous to (2.17). Unlike galaxy surveys, this method is directly sensitive to the *total* matter density, and therefore overcomes the difficulties of galaxy bias. Its direct dependence on the gravitational potentials is also very valuable to test theories of modified gravity, for which the Poisson equation (2.15) may be altered [154]. However, systematic effects are important and technically very challenging. These include the difficulties in the shape measurement of the galaxies and the existence of intrinsic alignments between them.

Clusters of Galaxies

Clusters of galaxies form out of the high density fluctuations present in the early times perturbations, and their abundance at a given redshfit can be used to constraint cosmological models [155]. Cluster abundance studies rely on the comparison between the predicted space density of massive halos to the observed space density of clusters, which can be identified via optical, X-ray, or CMB observables that should correlate with halo mass. Their number density is sensitive to a combination of the perturbation normalizations and the matter

[8] Some systems produce *strong gravitational lensing* effects, such as the occurrence of multiple images of a given source. Cosmological constraints usually rely on more subtle modifications (weak lensing), which can be studied statistically over large survey volumes.

energy density, and this dependence can be used to constraint cosmological parameters. As their formation depends on the dynamics of structure formation, they can be used to probe alternative theories of gravity. However, clusters are non-linear objects and their use as cosmological probes in non-standard scenarios is challenging.

Besides galaxies and Dark Matter haloes, clusters of galaxies also contain a large amount of very hot, ionized gas. This gas affects the energy distribution of the CMB photons by inverse Compton scattering processes (energy transfer from an electron to a photon), an effect known as the *thermal Sunyaev-Zel'dovich* effect. Clusters can indeed be detected by distortions in the photon spectrum induced in the CMB. The relative motion of the cluster w.r.t. the CMB rest frame affects the magnitude of this effect, a contribution known as the *kinematic Sunyaev-Zel'dovich* (kSZ) effect. The kSZ effect induced by the relative motion is also produced in any other situation in which the CMB is not isotropic in the cluster reference frame. This property allows one to use bounds on the kSZ effect to probe the large scale homogeneity of the universe [36, 156].

2.5 Type Ia Supernovae

The Type Ia supernovae (SNe) are extremely intense explosions that can be observed up to high redshift $z \sim 1.5$. They are believed to occur when the mass of a white dwarf surpasses the Chandrasekhar limit, either because of matter accretion or through merging with a companion star. At this point the electron degeneracy pressure is not able to compensate the gravitational instability, leading to a collapse and subsequent explosion as the nuclear degeneracy pressure is reached. The existence of this triggering mechanism sets the common energy scale, which can be sharpened through a phenomenological calibration procedure. The corrected SNe luminosity converts them into reliable *standard candles*, which can be used to measure cosmological distances as a function of redshift.

The dimming of distant supernovae constitutes a solid probe of dark energy models in the interval $0.01 \lesssim z \lesssim 1.5$. The difference in magnitude between each observed supernovae at redshift z_i and the theoretical expectation given by (2.1) is

$$\mu^{\rm th}(z_i) - \mu_i^{\rm obs} = 5\log_{10}\left(\frac{D_L(z_i)}{1{\rm Mpc}}\right) + 25 - \mu_0 - \mu_i^{\rm obs} \equiv \Delta\mu_i - \mu_0\,, \tag{2.27}$$

where the last equality defines the quantity $\Delta\mu_i$, used for the observational constraints. The quantity μ_0 is proportional to the intrinsic luminosity of the supernova explosions. Since its value is unknown theoretically, it will be allowed to take arbitrary values. Observational determinations of μ_0 will be used to constrain the local expansion rate, as will be described in Section 2.5.1.

In addition to the intrinsic luminosity, two other unknown quantities are necessary to calibrate the supernovae measurements and obtain a standard candle. These are the stretch (the duration of the supernovae explosion) and the color (to account for dust extinction), which are assumed to be universal and introduce linear corrections on all the SNe $\mu_i^{\rm obs} = \mu_{B,i} - \mu_0 + \alpha(s_i - 1) - \beta c_i$. These factors are calibrated by assuming an FRW-ΛCDM model, and should in principle be allowed to vary if the cosmology changes [157, 158]. However, the result of the analysis should not vary significantly in models which produce luminosity distance curves very similar to the standard model. Considering the covariance matrix between the supernova data should also be beneficial, since it adds information about

this calibration procedure by taking into account the covariance between supernovae with similar color and stretch. Of course, the case would be different in more radical cases, e.g. if the luminosity distance has features or sudden variations.

Supernova are a geometric probe to a very good approximation, granting very direct information on the luminosity distance (2.2). However, there are two ways in which cosmology may affect the SNe distance determinations dynamically:

- Lensing of SNe light induced by cosmic structures, which can induce a systematic magnification. Although lensing is included into the budget of known errors, it is done in a simplified and not completely model independent way [27, 159]. Similarly, SNe redshift determinations are affected by peculiar velocities.
- SNe evolution. If supernovae that originated in older galaxies are intrinsically fainter (or brighter) than their younger counterparts in a way not corrected by stretch and color, then the cosmological parameter estimate would be biased.[9]

Fortunately, spectroscopic analyses show that the supernovae properties have little dependence on their age. These and other systematic uncertainties involved in the use of SNe as cosmological probes have been extensively studied, and the modern wealth and quality of data allow for a consistent study of this systematic error sources and a variety of cross checks that validate their use as standard candles [10, 160–162]. Furthermore, the use of complementary probes (e.g. BAO distance determinations) is able to rule out the models that rely on variable supernovae properties or direct effects on propagating light (e.g. axion-photon mixing).

Current Supernovae Data

Most of the observational constraints presented in the following chapters employ the Union2 supernovae compilation [163], which consists in 557 SNe redshift-magnitude measurements after corrections for color and shape. The likelihood is computed using the covariance matrix including systematic errors C_{ij}

$$-2\log L_{\rm SNe} = \chi^2_{\rm SNe} = \sum_{i,j}(\Delta\mu_i - \mu_0)C^{-1}_{ij}(\Delta\mu_j - \mu_0)\,. \tag{2.28}$$

This result depends on the actual value of the intrinsic luminosity μ_0. Since it is unknown, the likelihood has to be maximized for each model with respect to μ_0 for each model under consideration [162]. Expanding the above expression and substituting back the value of μ_0 such that $\partial(\chi^2)/\partial\mu_0 = 0$, gives the optimal likelihood for each model

$$\chi^2_{\rm SNe} = \sum_{i,j}\Delta\mu_i C^{-1}_{ij}\Delta\mu_j - \frac{\left(\sum_{i,j}C^{-1}_{ij}\Delta\mu_j\right)^2}{\sum_{i,j}C^{-1}_{ij}}\,. \tag{2.29}$$

The Union2 SNe dataset can be seen in Figure 3.4 compared with both homogeneous and inhomogeneous models.

[9] That might happen if different processes producing type Ia SNe (merging vs accretion) occur at different rates depending on the age of the universe. More exotic cases (e.g. time variation of G or other fundamental constants) might involve a variation of the Chandrasekhar mass $M_c \sim M_p^3/m_H^2 \propto G^{-3/2}$.

2.5.1 Local Expansion Rate

Recasting the expression for the luminosity distance (2.27) in units of H_0

$$\mu^{\rm th}(z_i) = 5\log_{10}\left(H_0 D_L(z_i)\right) + 25 - \mu_0 - 5\log_{10}(H_0[{\rm Mpc}^{-1}])\,. \tag{2.30}$$

it is possible to see that the intrinsic luminosity μ_0 is degenerate with the Hubble constant for homogeneous models, for which cosmic distances (2.1, 2.2) only depend on it through a global H_0^{-1} factor. On the other hand, inhomogeneous cosmologies introduce additional scales and allow for more involved dependences [164], and hence the determination of the local expansion rate requires the knowledge of the intrinsic supernovae luminosity. Since the dependence of the expansion rate with redshift in an arbitrary cosmology can be different than in the ΛCDM case (even for low redshifts $z < 0.1$) it is necessary to devise a model independent method.

A recent measurement of the local expansion rate using Ia type supernovae yields a value $H_0 = 73.8 \pm 2.4 {\rm kms}^{-1}{\rm Mpc}^{-1}$ [165]. The supernovae intrinsic luminosity was measured using over 600 Cepheid stars from eight nearby galaxies in which type Ia supernovae have been observed. The Cepheids are calibrated comparing their luminosity to three different distance estimates: 1) the geometric distance to NGC 4258 as obtained from water masers orbiting its central black hole, 2) trigonometric paralaxes to Cepheid stars in the Milky Way and 3) relating the distance to the Large Magellanic Cloud obtained from eclipsing binaries. The local expansion rate is obtained by finding the best fit for a fiducial FRW model with $\Omega_M = 0.3$, $\Omega_\Lambda = 0.7$ to 253 low redshift type Ia supernovae ($z < 0.1$) using the measured intrinsic luminosities. In particular, the quoted value of H_0 is the average of the values obtained from the three different calibrations.

In order to reproduce the method outlined above and provide a fair comparison in an arbitrary cosmology, the constraints on the model are implemented through the supernovae luminosities rather than the model parameter $H_{\rm in}$. The value and the error in the luminosity were obtained by comparing the fiducial model fixing $H_0 = 73.8$ and 73.8 ± 2.4 to the Union2 data in the range $z < 0.1$ (195 SNe) and finding the value of $\mu_0^{\rm obs}$ that gives the best fit, using equation (2.32) below. The result is

$$\mu_0^{\rm obs} = -0.120 \pm 0.071\,. \tag{2.31}$$

The "predicted" intrinsic luminosity that can be compared to the observation is the best fit μ_0 found using the Union2 data for the model under investigation

$$\mu_0^{\rm bf} = \frac{\sum_{i,j} C_{ij}^{-1}\Delta\mu_j}{\sum_{i,j} C_{ij}^{-1}}\,, \tag{2.32}$$

using the distance modulus and the inverse covariance matrix of the data (see previous Section and equations (2.27,2.28). The associated likelihood is assumed to be Gaussian

$$\chi^2_{H_0} = \frac{(\mu_0^{\rm bf} - \mu_0^{\rm obs})^2}{\Delta{\mu_0}^2}\,. \tag{2.33}$$

2.6 Local Gravity Tests

Besides its elegant description of gravity as the dynamics of the space-time geometry, the major strength of General Relativity is to correctly predict a variety of phenomena that occur

in the Solar System and other astrophysical systems at low redshift [110]. Although not truly cosmological probes, local tests of gravity are very useful to constrain departures from GR such as additional scalar forces.

Classical gravity tests may involve null or time-like geodesics, which allow the exploration of different properties. The perihelion precession of Mercury and the precise Lunar laser ranging measurements of the Earth-Moon system are two examples involving massive bodies. Tests based on the trajectory of null geodesics include the gravitational redshift, the deflection of light (including gravitational lensing) and the time delay of a signal passing near the Sun. Laboratory tests of gravity can explore the existence of short range interactions, e.g. of the Yukawa type (1.35), using torsion pendulum experiments. Current bounds limit their coupling strength on scales larger than 0.056 mm [166]. These measurements can achieve the precision necessary to detect small field effects due to the good control of systematic effects and the possibility of collecting considerable statistics. Gravity has also been tested in the strong field regime outside the Solar System, through the observation of binary pulsars (i.e., rotating neutron stars emitting a beam of radio noise). Several systems have been observed in which the orbital period decreases according to the energy emitted in the form of gravitational waves, in great agreement with the General Relativistic expectation.

Many of the aforementioned tests have the advantage of being able to directly translate in to bounds of the *Parameterized Post Newtonian* (PPN) approximation coefficients [110]. The theoretical values can also be computed within alternative theories of gravity in terms of the model parameters, allowing a very neat and direct comparison between theory and experiments. For recent review on gravitational experiments and current bounds on PPN parameters, see Ref. [20].

Part II

Results

Chapter 3

Large Scale Homogeneity and Non-Copernican Void Models

There is nothing more natural than to consider everything as starting from oneself, chosen as the center of the world; one finds oneself thus capable of condemning the world without even wanting to hear its deceitful chatter.

Guy Debord[1]

Recent years have witnessed enormous advance in the quantitative understanding of cosmology and the establishment of a Standard Cosmological Model. Its construction is grounded on the general relativistic description of space-time with the usual Einstein equations. The Ansatz for the space-time is a spatially homogeneous and isotropic Friedmann-Robertson-Walker (FRW) metric, chosen to satisfy the generalized Copernican Principle, or Cosmological Principle. In addition to the known particles (baryons, photons and neutrinos), two mysterious elements need to be added in order to account for all the observations. These give the name to the standard, ΛCDM model: Cold Dark Matter (CDM) plus a cosmological constant (Λ), the last one necessary to explain the dimming of distant supernovae [11, 12]. With the standard choice of the metric, the supernovae data imply that the universe is currently undergoing a phase of accelerated expansion.

The situation changes when the Cosmological Principle Hypothesis is dropped. As the supernovae we observe occur in our past lightcone, the changes in luminosity we interpret as time evolution might be due to spatial variations if the universe is not homogeneous. If the inhomogeneity represents an underdensity with a size comparable to the Hubble radius and our galaxy is located near its center, supernovae observations can be successfully accounted

[1] *Panegyric* (1989)

for without the introduction of new physics. This type of so-called "large void models" can be described by a spherically symmetric Lemaître-Tolman-Bondi (LTB) metric, and have been studied as an alternative to the standard ΛCDM scenario [38, 40, 157, 167–181]. Many different aspect of these alternative models have been considered over the past years, including observational constraints [27, 36, 152, 153, 156, 158, 164, 182–192], the growth of perturbations [134–137, 193, 194], and the physics of the Cosmic Microwave Background (CMB) [109, 195–204]. See reference [8] for a recent review.

If the time to Big Bang and the baryon-mater ratio are independent of the location, the LTB type of metric represents the gravitational growth of an adiabatic perturbation from an initially quasi-homogeneous state [193]. Although a Gigaparsec-sized void is difficult to reconcile with the standard inflationary paradigm, it might still be possible through the production of large non-perturbative inhomogeneities associated with the stochastic nature of the inflaton evolution [205]. The only philosophical problem associated with this type of models is the requirement of being located very close to the center in order to preserve the great degree of isotropy observed in the CMB [196], but ultimately, only cosmological observations can tell us about the geometry and distribution of the cosmos and our position in it, provided that this question is meaningful.

The aim of this work is to analyze LTB models in the light of the most recent cosmological data. The Hubble Space Telescope has made a precise measurement of the local expansion rate [165] that challenges this type of void models, which typically require a low value to fit the CMB power spectrum [153, 187]. The determination of the Hubble parameter relies on the calibration of distant supernovae using Cepheid variable stars and the subsequent fit to a fiducial ΛCDM model in the low redshift range. Although applying priors directly on H_0 is fine for homogeneous cosmologies, LTB universes can have a very different evolution in the relevant redshift range. Therefore, our analysis is based on the intrinsic Ia supernova luminosity instead of the value of the Hubble parameter.

Further restrictions on this model are obtained from the scale of Baryon Acoustic Oscillations (BAO) and its evolution in an inhomogeneous cosmology by including the most recent BAO data up to redshift $z = 0.8$ provided by the WiggleZ collaboration [103] and Carnero *et al.* [139]. In a FRW cosmology, the BAO scale is space-independent and the constraints it yields arise from providing an independent measurement of cosmic distances relative to a *standard ruler*, with an initial length determined by the physics of the early universe. Once baryons decouple, the dominant effect on the observed physical scale is to be stretched by the expansion of the universe. However, in the less symmetric LTB cosmology the initially constant BAO scale grows differently: the physical scale acquires an additional radial dependence and is stretched differently in the longitudinal and transverse direction, due to the existence of two expansion rates.

Adding information about the BAO scale at higher redshift reduces considerably the room for its value in the early universe. If the depth of the void is chosen to fit the supernovae luminosity distances, the inhomogeneous expansion produces a mismatch between the BAO scale at low and high redshift, posing a new problem for these models. Adding information of the CMB increases the discrepancies by restricting the initial acoustic scale, but the constraints are independent of the particular values, i.e, depend only on the *geometric* properties of the model regardless of the calibration of the standard rulers and candles. In particular, these constraints are independent of the primordial power spectrum, a critical assumption necessary to rule out large void models using the tension between the CMB and the local

expansion rate [158] and are therefore complementary to these.

Section 3.1 describes the general LTB void models, giving the corresponding Einstein-Friedmann equations, as well as the standard solution in absence of pressure. In a subsection the adiabatic assumption is introduced, i.e. that the time since Big Bang is space independent, and thus the model only depends on a single function, the inhomogeneous matter profile $\Omega_M(r)$. This is chosen to have the GBH parameterization, which is also presented. Section 3.2 presents in detail the evolution of baryonic features in terms of free-falling trajectories of the background metric and compute the BAO observables. Section 3.3 describes the cosmological data used to analyze the model, including a method to use the supernova luminosity to constrain the local expansion rate. It also contains the results from the comparison of the model and the data and describe the tensions between the different datasets, as well as the result of different model comparison criteria. The conclusions are summarized in Section 3.4, discussing the generality of the results and stating several modifications that might render the model viable.

3.1 Lemaître-Tolman-Bondi Models

The LTB model describes general spherically symmetric space-times and can be used as a toy model for describing voids in the universe [206–208]. The starting point is the general metric

$$ds^2 = -dt^2 + X^2(r,t)\,dr^2 + A^2(r,t)\,d\Omega^2\,, \tag{3.1}$$

where $d\Omega^2 = d\theta^2 + \sin^2\theta d\phi^2$. Units in which $c = 1$ will be assumed in the folowing. Assuming a spherically symmetric matter source with negligible pressure, $T^\mu_{\ \nu} = -\rho_M(r,t)\,\delta^\mu_0\,\delta^0_\nu$, the $(0,r)$ component of the Einstein equations, $G^t_{\ r} = 0$, sets the form of $X(r,t)$. The resulting cosmological metric becomes

$$ds^2 = -dt^2 + \frac{A'^2(r,t)}{1-k(r)}\,dr^2 + A^2(r,t)\,d\Omega^2\,, \tag{3.2}$$

with an arbitrary function $k(r)$ playing the role of the spatial curvature parameter. The other components of the Einstein equations read [173, 182, 184]

$$H_T^2 + 2H_T H_R + \frac{k(r)}{A^2} + \frac{k'(r)}{AA'} = 8\pi\,G\,\rho_M\,, \tag{3.3}$$

$$2\dot{H}_T + 3H_T^2 + \frac{k(r)}{A^2} = 0\,, \tag{3.4}$$

where dots and primes denote ∂_t and ∂_r respectively, and we have defined the transverse (i.e. in the angular direction) and radial Hubble rates as

$$H_T \equiv \dot{A}/A, \quad \text{and} \quad H_R \equiv \dot{A}'/A'\,. \tag{3.5}$$

The reduced Hubble rate can be defined as usual: $H_{R/T} \equiv 100 h_{R/T}\mathrm{Km/Mpc/s}$. It is also useful to consider the normalized *shear*

$$\varepsilon \equiv \frac{H_T - H_R}{H_R + 2H_T}\,, \tag{3.6}$$

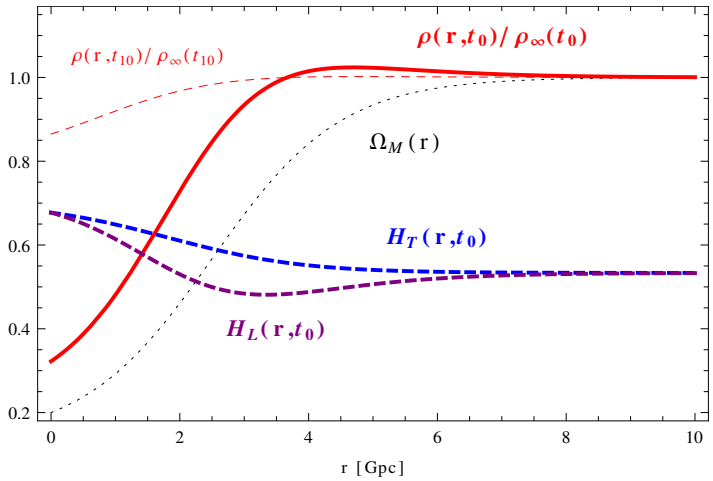

Figure 3.1: Physical parameters in the LTB model. The density contrast at $t(z=0), t(z=10)$ (red) shows the evolution from an initially less inhomogeneous state, and differs from the function $\Omega_M(r)$ (black dotted). The expansion rates in the radial (purple dashed) and transverse (blue dashed) directions differ the most where the void is steeper. The profile shown has $R = 2.5, \Delta R = 1$.

i.e. the difference between the radial and transverse expansion weighted by the total expansion [152]. This variable provides a local quanitfication of the departures with respect to homogeneous cosomologies, e.g. to characterize the growth of structure [136].

Integrating (3.3) yields

$$H_T^2 = \frac{F(r)}{A^3} - \frac{k(r)}{A^2}\,, \tag{3.7}$$

in terms of another arbitrary function $F(r)$. Substituting it into the first equation gives

$$\frac{F'(r)}{A' A^2(r,t)} = 8\pi\, G\, \rho_M(r,t)\,, \tag{3.8}$$

where $\rho_M(r,t)$ is the physical matter density. Since $F(r)$ is time-independent, one can choose $t = t_0$ and compute the integrated matter density in a comoving volume today, $V = 4\pi r^3/3$, as $\bar{\rho}(r) = \frac{1}{V}\int_0^r 4\pi r'^2 dr'\, \rho_M(r', t_0)$, and construct with it the ratio $\Omega_M(r) \equiv \bar{\rho}(r)/\bar{\rho}_c(r)$, where $\bar{\rho}_c(r) = 3H_0^2(r)/8\pi G$ is the critical density in that volume [152].

The boundary condition functions $F(r)$ and $k(r)$ are specified by the nature of the inhomogeneities through the local Hubble rate, the integrated mass ratio and the local spatial curvature,

$$F(r) \;=\; H_0^2(r)\,\Omega_M(r)\,A_0^3(r) = 8\pi G \int_0^r dr' r'^2 \rho_M(r', t_0)\,, \tag{3.9}$$

$$k(r) \;=\; H_0^2(r)\Big(\Omega_M(r) - 1\Big)\,A_0^2(r)\,, \tag{3.10}$$

where functions with subscripts 0 correspond to present day values, $A_0(r) \equiv A(r, t_0)$ and $H_0(r) \equiv H_T(r, t_0)$. With these definitions, the (position dependent) transversal Hubble rate

can be written as [173, 182]

$$H_T^2(r,t) = H_0^2(r)\left[\Omega_M(r)\left(\frac{A_0(r)}{A(r,t)}\right)^3 + (1-\Omega_M(r))\left(\frac{A_0(r)}{A(r,t)}\right)^2\right], \tag{3.11}$$

and we fix the gauge by setting $A_0(r) = r$. For fixed r and $\Omega_M < 0$ the above expression is equivalent to the Friedmann equation, and has an exact parametric solution in terms of the variable η:

$$A(r,t) = \frac{\Omega_M(r)}{2[1-\Omega_M(r)]}[\cosh(\eta)-1]A_0(r)\,, \tag{3.12}$$

$$H_0(r)t = \frac{\Omega_M(r)}{2[1-\Omega_M(r)]^{3/2}}[\sinh(\eta)-\eta]\,. \tag{3.13}$$

Very good approximate solutions can also be found by Taylor expanding around an Einstein de Sitter solution [184].

In addition to the solution of Einstein Equations (3.12,3.13) it is necessary to obtain the coordinates on the lightcone as a function of redshift. For light traveling along radial null geodesics, $ds^2 = d\Omega^2 = 0$ yields

$$\frac{dt}{dr} = \mp\frac{A'(r,t)}{\sqrt{1-k(r)}}\,, \tag{3.14}$$

which, together with the redshift equation [182, 208],

$$\frac{d\log(1+z)}{dr} = \pm\frac{\dot{A}'(r,t)}{\sqrt{1-k(r)}}\,, \tag{3.15}$$

allows us to write a parametric set of differential equations, with $N = \log(1+z)$ being the effective number of e-folds before the present time,

$$\frac{dt}{dN} = -\frac{A'(r,t)}{\dot{A}'(r,t)}\,, \tag{3.16}$$

$$\frac{dr}{dN} = \pm\frac{\sqrt{1-k(r)}}{\dot{A}'(r,t)}\,, \tag{3.17}$$

where the equations are integrated with the initial condition $r(0) = 0$, $t(0)$ obtained from (3.12,3.13) for $r = 0, A = A_0$.

The angular diameter distance is given by the $d\Omega$ element of the metric evaluated on the lighctone, and is related to the luminosity distance by the redshift due to photon redshift and time dilation

$$D_A(z) = A(r(z),t(z))\,, \tag{3.18}$$

$$D_L(z) = (1+z)^2 A(r(z),t(z))\,. \tag{3.19}$$

The dynamics of the LTB metric in the only-matter approximation discussed above are fully specified by the two functions $\Omega_M(r)$, $H_0(r)$ independently of the type of matter present, as long as it exerts no pressure. But by dropping the symmetries of the FRW model

a spherically symmetric but inhomogeneous mixture of baryonic and dark matter can be accommodated. A possible parameterization in terms of the total matter density would be

$$f_b(r) \equiv \frac{\rho_b(r,t)}{\rho_m(r,t)}\,, \tag{3.20}$$

where there is no time dependence because the energy density of baryons and dark matter evolves identically at late times.

Before explaining the choice of matter profile and the physical restrictions on the model, let us briefly summarize the approximations used throughout this work

- Spherical symmetry as given by (3.2) and perfectly central location of our galaxy at $r = 0$, $t = t_0$ as initial conditions for the lightcone integration (3.16).
- Radiation energy and pressure neglected as a source of the expansion (3.11).
- Early time and large radius FRW limit of the model, necessary to compute the BAO scale (Section 3.2) and the relative locations of the CMB peaks (Section 3.3.1).
- Perturbations of the LTB metric neglected. The evolution of the BAO scale from early times is studied by analyzing the geodesics of the background metric (3.2) (Section 3.2).

3.1.1 The Adiabatic GBH Model

General LTB models are uniquely specified by the two functions $k(r)$ and $F(r)$ or equivalently by $H_0(r)$ and $\Omega_M(r)$, but to test them against data it is necessary to parameterize the functions, so that a finite dimensional space is analyzed. In this Chapter we will use the GBH model [184] to describe the matter profile in terms of a reduced number of parameters. In addition to the choice for the free function $\Omega_M(r)$, we further impose that the time to Big Bang is space-independent

$$t_{\rm BB}(r) = H_0(r)^{-1}\left(\frac{1}{\sqrt{\Omega_K(r)}}\sqrt{1+\frac{\Omega_M(r)}{\Omega_K(r)}} - \frac{\Omega_M(r)}{\sqrt{\Omega_K^3(r)}}\,\sinh^{-1}\sqrt{\frac{\Omega_K(r)}{\Omega_M(r)}}\right) = t_0\,, \tag{3.21}$$

where $\Omega_K(r) = 1 - \Omega_M(r)$. The above expression can be obtained from integration of (3.11) [182, 184] or by solving for $A = A_0(r)$ in (3.12,3.13). This condition reduces the functional freedom associated to $H_0(r)$ to a single normalization constant H_0, that is related to the overall age of the universe.

Additionally, we require that there are no large scale baryonic isocurvature modes, i.e. the baryon fraction (3.20) is constant. This type of voids can be regarded as the gravitational collapse of a large scale, adiabatic and spherically symmetric perturbation which has a small amplitude at early times. Its adiabatic nature is related to the fact that there is only one functional degree of freedom that sets the shape of the remaining free functions ($\Omega_M(r)$ in our case, which in turn fixes $H_0(r)$ and the baryon fraction).

The above conditions give a relation between $H_0(r)$, $\Omega_M(r)$ and $f_b(r)$, and hence constrain the models to one free function. Our chosen model is thus given by [184]

$$\Omega_M(r) = \Omega_{\rm out} + \left(\Omega_{\rm in} - \Omega_{\rm out}\right)\left(\frac{1-\tanh[(r-R)/2\Delta R]}{1+\tanh[R/2\Delta R]}\right) \tag{3.22}$$

$$H_0(r) = H_0\left[\frac{1}{\Omega_K(r)} - \frac{\Omega_M(r)}{\sqrt{\Omega_K^3(r)}}\sinh^{-1}\sqrt{\frac{\Omega_K(r)}{\Omega_M(r)}}\right] = H_0\sum_{n=0}^{\infty}\frac{2[\Omega_K(r)]^n}{(2n+1)(2n+3)}\,, \tag{3.23}$$

$$f_b(r) = f_b = \text{constant} \tag{3.24}$$

where the second equation follows from (3.21), and the third by demanding constant baryon to matter ratio. This paremeterization was introduced to lower the shear around the void wall (e.g. with respect to Gaussian profiles) and allow a unified description of cuspy and flat central regions [184]. Each void model is specified by the following parameters:

- $\Omega_{\rm in}$: Matter/curvature fraction at the center of the void (equations 3.8-3.10). As deeper voids produce more fictitious acceleration, this parameter plays a major role in the constraints presented in Section 3.3.
- $\Omega_{\rm out}$: Asymptotic ($r \to \infty$) matter/curvature fraction in which the inhomogeneous region is embedded. Two possibilities will be considered separately depending on the asymptotic curvature of the universe:

  -**CGBH:** Flat $\Omega_{\rm out} = 1$, as suggested by inflationary physics.

  -**OCGBH:** Open $\Omega_{\rm out} \leq 1$, which allows a better fit to the CMB.
- ΔR: Slope of the inhomogeneity. Smaller values of ΔR produce steeper profiles and increase the shear (3.6).
- R: Shape of the void. $\Delta R \ll R$ describes an inhomogeneity with a central plateau of approximately constant density, while $\Delta R \gg R$ produces a cuspy central region.
- H_0: Expansion rate normalization that determines the Big Bang time (3.21).
- f_b: Baryon fraction over the total matter content. Its value affects the pre-recombination physics and determines the value of the BAO scale and CMB peak locations.

The choice of the constrained model is important because, in our gauge, void models with an *inhomogenous* Big Bang would contain a mixture of growing and decaying modes, and consequently the void would not disappear at early times, making them incompatible with the Standard Big Bang scenario [193]. By restricting ourselves to adiabatic LTB models the central void is reduced to an insignificant perturbation in an otherwise homogeneous universe described by an FRW metric, both at large distances *and* early times. This requirement, together with the condition of constant baryon fraction, ensures the space-independence of the early BAO scale, which is a key part of the present analysis.

3.2 The Baryon Acoustic Scale in LTB Universes

Inhomogeneous cosmologies stretch the BAO scale differently than their homogeneous cousins. There are three potential effects to be addressed when computing the BAO scale in LTB models at the background level:

1. Inhomogeneous expansion: The matter distribution will source the expansion of the universe in a position dependent way. Therefore, there will be a radial dependence of the physical scale in addition to the time dependence.

2. Anisotropic expansion: In general the expansion rate in the radial and transverse direction will be different $H_T \neq H_R$, resulting in two different BAO scales $l^T \neq l^R$, as seen by a central observer. The relation between this effect and the Alcock-Paczynski test will be discussed in Section 3.2.5.

3. Radial coordinate drift: Displacements in the radial direction are not a symmetry of the LTB metric and the free-falling baryon features are not ensured to remain at constant r. In Section 3.2.1 we show that this effect does not occur for timelike geodesics.

Possible effects from higher order corrections will be discussed at the end of Section 3.2.2.

Our approach to predict the BAO scale in LTB models with space-independent Big Bang time relies on the homogeneity properties of the metric at large radius (i.e. the profile flattens) and early times (i.e. the Big Bang time and the baryon fraction are independent of the position). Relaxing this assumptions would require a more careful treatment which goes beyond the scope of this work. We first analyze the evolution of the BAO scale in the inhomogeneous cosmology by following the geodesics of the LTB metric (Section 3.2.1). Afterwards, the asymptotic physical scale computed in the limit $r \gg R$, ΔR using the fitting formulae is extrapolated to a suitable early time t_e at which the void is just a negligible perturbation. The obtained value can be then projected to the coordinates of observation $r(z), t(z)$ using the previous results (Section 3.2.3). Finally, the physical scale is related to the observed quantity d_z quoted by the galaxy surveys (Section 3.2.4). The procedure is sketched in Figure 3.2.

The derivation we are presenting avoids using certain concepts that might be equivocal when used for inhomogeneous cosmologies. In particular, we will only use redshift as a coordinate on the lightcone or in the asymptotic region when the FRW limit can be applied. We will also avoid the term "comoving" and will refer to "coordinate" instead, as well as pay special attention to distinguishing physical distances and relative coordinate separations.

3.2.1 Free-falling Scales in the LTB Metric

The propagation of sound waves in the baryon-photon fluid present in the early, expanding, universe leaves an imprint at a characteristic length that will be observable in the late universe as a peak in the correlation function of galaxies [24, 138]. When the universe becomes neutral, baryon-photon interactions become effectively negligible and the baryonic overdensities start behaving as free-falling test bodies. We can therefore analyze the relative separation of the initial baryon clumps and the galaxies they will form by following the geodesics of the LTB metric: $x^\mu(\tau) = \{t(\tau), r(\tau), \theta(\tau), \phi(\tau)\}$, where $\dot{x}^\mu = \frac{dx^\mu}{d\tau}$. The BAO scale can be traced simply by following two nearby trajectories with an initial separation equal to the baryon acoustic scale at a sufficiently early time.

The transverse evolution is the simplest. Since rotations are an isometry of the LTB metric, the momentum in the angular directions is conserved and trajectories with $\dot{\phi}, \dot{\theta} = 0$ initialy will remain at constant angular coordinates. This can be readily seen from the geodesic equation for the θ coordinate

$$\ddot{\theta} + 2\frac{A'}{A}\dot{r}\dot{\theta} + 2\frac{\dot{A}}{A}\dot{t}\dot{\theta} = 0\,, \tag{3.25}$$

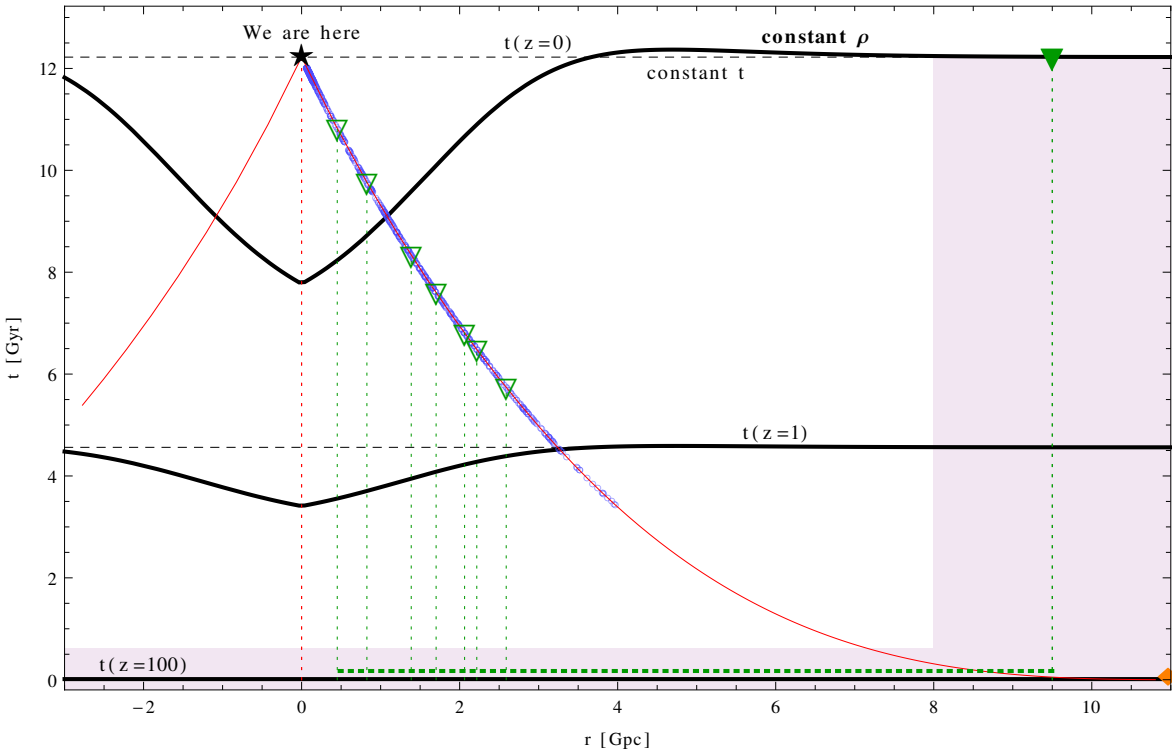

Figure 3.2: The LTB model with space-independent Big Bang. Black lines represent hypersurfaces of constant time $t = t(z)$ for $z = 0, 1, 100$ (dashed) and constant density $\rho(r,t) = \rho(r_\infty, t(z))$ (thick, continuous). The filled areas show schematically the regions in which the void can be considered homogeneous (early times and large radii). Red constant lines represent our lightcone, where the coordinates of SNe (blue circles on the left) and BAO (green triangles on the right) observations has been added. Vertical dotted lines correspond to the geodesic worldlines of our galaxy (red) and the BAO fiducial locations (green). The physical BAO scale at different z is obtained from the asymptotic value (represented by the filled green triangle), extrapolated to early times, for which the universe is approximately homogeneous (horizontal green dotted line) and evaluated at the lightcone coordinates using the LTB metric (see Section 3.2 for the details).

for which $\theta(\tau) = \theta_0$ is a solution. Its stability follows by demanding timelike, slow geodesics for which $\dot{t} \gg \dot{r}$ and noting that the second term is positive in an expanding universe ($\dot{A} > 0$, $H_T > 0$) and acts as a friction against the angular velocity $\dot{\theta}$. Therefore, initial angular separation $\Delta\theta$ is conserved in coordinate space and the associated, transverse physical scale can be obtained integrating the angular element of the metric $l^T_{\rm phys} = A(r,t)\Delta\theta$.

Since shifts in the radial direction are not an isometry of the LTB metric, $\dot{r}$ is not automatically conserved and the determination of the radial acoustic scale requires a more careful treatment. The geodesic equations for a trajectory with $\dot{\phi}, \dot{\theta} = 0$ are

$$\ddot{t} + \frac{A'\dot{A}'}{1-k(r)}\dot{r}^2 = 0\,, \tag{3.26}$$

$$\ddot{r} + \left[\frac{k'(r)}{2(1-k(r))} + \frac{A''}{A'}\right]\dot{r}^2 + 2\frac{\dot{A}'}{A'}\dot{t}\dot{r} = 0\,. \tag{3.27}$$

Similarly to the angular case, a particle initially at rest at some early time t_e, $\dot{r}(t_e) = 0$, will remain at constant radial coordinate location $r(\tau) = r(t_e)$. Timelike, non-relativistic trajectories with $\dot{t} \gg \dot{r}$ are again stable in an expanding universe due to the longitudinal Hubble friction term $\dot{A}'/A' > 0$, and geodesics will remain at constant coordinate separations at different cosmic epochs.[2] The physical distance in the r direction can be obtained simply by integration using the radial element of the metric $l^R_{\rm phys} = \int \sqrt{g_{rr}}dr \approx A'/\sqrt{1-k}\Delta r$.

To summarize, since coordinate locations are conserved in geodesic evolution, we can provide the following relation for freely falling, physical scales in the LTB metric at different times t, t_e in the transverse and longitudinal directions

$$l^T_{\rm phys}(r,t) = \frac{A(r,t)}{A(r,t_e)} l^T_{\rm phys}(r,t_e)\,, \tag{3.28}$$

$$l^R_{\rm phys}(r,t) = \frac{A'(r,t)}{A'(r,t_e)} l^R_{\rm phys}(r,t_e)\,. \tag{3.29}$$

3.2.2 BAO Scale Evolution Beyond Zero Order

The above analysis so far has dealt with the differences between homogeneous and inhomogeneous models at the zero order level. As it was discussed in Section 2.4.1, the BAO scale in homogeneous, GR cosmologies is slightly shifted towards lower values due to non-linear effects on matter clustering. The lack of this effect to linear order is a consequence of the scale independence of the growth function for each Fourier mode.

In inhomogeneous universes the situation is different, since the lack of symmetry produces the failure of the perturbation decomposition and the treatment of scalar perturbations (in the metric and matter density) have to be considered together with vector and tensor perturbations [134, 193]. The vorticity (vector) component is subdominant because the LTB metric is rotationally invariant, but the scalar potential is sourced at linear order by a term proportional to the background shear traced with the tensor perturbations. Fortunately, for the GBH profiles considered here, the background shear is below 5% and these contributions will be subdominant with respect to the much larger effect of the inhomogeneous expansion (see Figure 3.3 and Section 3.2.4). February *et al.* recently presented the numerical computation of the BAO scale in LTB models within linear theory, and considering only scalar perturbations [137]. They found a shift on the BAO scale at the percent level, which is nevertheless considerably smaller than the departures induced by the inhomogeneous and anisotropic expansion discussed above.

Further support for the assumption of a constant BAO scale in coordinate space is provided by N-body numerical studies. Alonso *et al.* [135] run simulations in which inhomogeneous matter profiles are implemented through an initial underdensity of Gpc size. Their results show that the (local) matter density contrast grows with the scale factor in a way analogous to that of an open universe with a value of the matter density $\Omega_M(r)$ corresponding to the appropriate location r, showing an effective decoupling between the small scale clustering and the evolution of the void. Corrections from the large scale inhomogeneity are

[2] The situation would considerably change if Γ^r_{tt} was different from zero in the LTB metric. It might be as well possible to devise profiles for which the first term in (3.27) overcomes the second for sufficiently rapid geodesics, i.e. high $\dot{r}/\dot{t}$, but this is not the case for the models under study.

proportional to the local shear weighted by a factor $\mathcal{O}(1)$ [136], and are hence small for the profiles allowed by observations.

3.2.3 The Physical BAO Scale at Early Times and on the Lightcone

The solutions of the LTB metric with space-independent Big Bang represent an inhomogeneity that grows due to gravitational instability out of a very homogeneous state. For typical voids at $t(z = 100)$ the physical density contrast $\rho_m(r,t)/\rho_m(r_\infty,t)$ is of order 1%, while at $t(z = 1000)$ it shrinks to $\sim 0.1\%$. As the baryionic features develop between $t \sim 0$ and $t \sim t(z = 1000)$, it is a good approximation to consider that the physics responsible for recombination and the origin of the baryon acoustic scale are indistinguishable from their counterparts in homogeneous cosmologies. It will be therefore assumed that for models with space-independent Big Bang the physical BAO scale is isotropic and coordinate independent at early times on constant time hypersurfaces.[3]

$$l_{BAO}(r(z),t_e) \approx l_{BAO}(r_\infty,t_e)\,. \tag{3.30}$$

The early time BAO scale can be obtained from the asymptotic value at different times using equation (3.28) or (3.29). In the $r \to \infty$ limit the universe is indistinguishable from a FRW cosmology, and we can compute the BAO scale using the fitting formulae provided by Eisenstein and Hu [138] in terms of the asymptotic values of the matter density and baryon fraction. These effective values are obtained by projecting the LTB parameters on the lightcone at a very high redshift $z_e \approx 100$, for which 1) $H_T \approx H_R$ and the universe is approximately homogeneous on a constant $t = t(z_e)$ hypersurface, 2) the point $r(z_e)$ is away from the inhomogeneous region and 3) the radiation contribution is still negligible. These values are given by

$$\Omega_m^{\text{eff}} = \frac{\rho(r_\infty,t_0)}{3H_T^2(r_\infty)} \approx \Omega_{\text{out}}\,, \tag{3.31}$$

$$\Omega_b^{\text{eff}} \approx f_b\,\Omega_{\text{out}}\,, \tag{3.32}$$

$$H_0^{\text{eff}} = \frac{2H_T(z_e)+H_R(z_e)}{3\sqrt{\Omega_m^{\text{eff}}(1+z_e)^3+(1-\Omega_m^{\text{eff}})(1+z_e)^2}}\,. \tag{3.33}$$

Here H_0^{eff} can be understood as "rewinding" the LTB value of the average expansion rate $2H_T(z_e)/3 + H_R(z_e)/3$ using the FRW asymptotic value of Ω_m.

The fitting formulae give a comoving scale in a FRW universe which coincides with the physical value at $t = t_0$ for the usual definition of the scale factor in the asymptotic FRW metric $a(t_0) = a_0 = 1$. The corresponding scale at t_0 is valid in the limit $r \to \infty$, but can be related to the radial and transverse physical scales using (3.28,3.29,3.30). For a point located on the past lightcone of the central observer, the values are

$$l^T_{BAO}(z) \equiv \xi_T(z) l_{BAO}(r_\infty,t_0) = \frac{A(r(z),t(z))}{A(r(z),t_e)}\frac{A(r_\infty,t_e)}{A(r_\infty,t_0)} l_{BAO}(r_\infty,t_0)\,, \tag{3.34}$$

$$l^R_{BAO}(z) \equiv \xi_R(z) l_{BAO}(r_\infty,t_0) = \frac{A'(r(z),t(z))}{A'(r(z),t_e)}\frac{A'(r_\infty,t_e)}{A'(r_\infty,t_0)} l_{BAO}(r_\infty,t_0)\,. \tag{3.35}$$

[3] A more physical criterion would be to consider constant density hypersurfaces. Although the difference is of order 0.1% in models with space-independent Big Bang, it might render helpful to generalize the treatment of BAO for profiles with general $H_0(r)$.

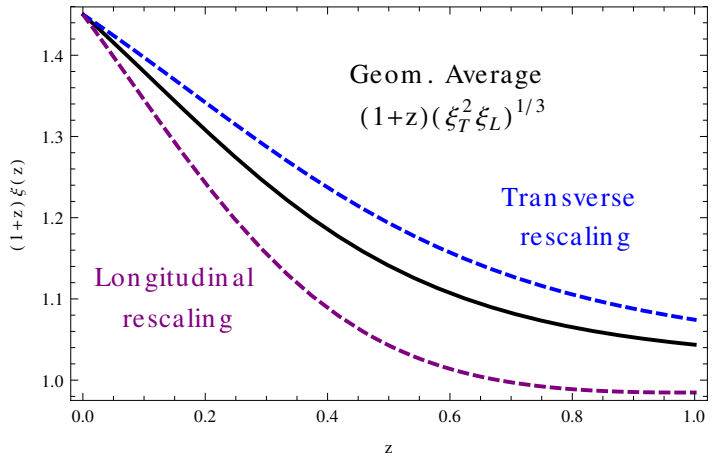

Figure 3.3: Effects on the LTB metric on the BAO scale with respect to their FRW analogue. The difference between the transverse (blue, dashed) and longitudinal (purple, dot-dashed) factors accounts for the anisotropy of the scales in the angular and transverse direction, respectively. The geometric averaged rescaling factor (black solid) is used for volumetric BAO determinations through the quantity $d_z^{\rm LTB} = (1+z)\xi(z)\, d_z^{\rm FRW}$ (3.43). Note that all three curves coincide in $r = 0$, since the void is locally isotropic at the center.

The first equalities define a transversal and longitudinal rescaling factors (see Figure 3.3), which reduce to $(1+z)^{-1}$ in the homogeneous limit.

3.2.4 Comparison with the Observed BAO Scale

The BAO scale can be extracted from the galaxy correlation function measured in galaxy surveys. What is actually observed is a combination of the angular correlation θ_{BAO} and the correlation in redshift space Δz_{BAO} [209]. In order to compare the models with observations, we need to relate the isotropized correlation measured by the surveys

$$d_z = \left(\theta_{BAO}^2 \frac{\Delta z_{BAO}}{z}\right)^{1/3}, \tag{3.36}$$

to the physical scales computed in the previous Section.[4]

The angular correlation can be readily obtained from the definition of the angular diameter distance as the ratio between a known (transverse) length and the angle it subtends

$$\theta_{BAO} = \frac{l_{BAO}^T(z)}{D_A(z)}\,. \tag{3.37}$$

[4]The present discussion follows Section 4.6.3 of Biswas *et al.* [187]. Our result (3.41) has the same form as their equation (4.48) after several coefficients cancel out. However, their computation assumes the BAO scale to be given by the local values of $\Omega_M(r), \Omega_B(r), H_0(r)$ instead of obtaining them from the asymptotic FRW value and the factor $(1+z_{rec})$ is taken to be given by the volume element comparison on the worldline of constant $r = r(z)$ instead of by the asymptotic value $r \to \infty$.

The redshift correlation can be related to the radial coordinate separation by means of the redshift equation (3.15)

$$\Delta z_{BAO} = \int_{r(z)-\Delta r_{\rm BAO}/2}^{r(z)+\Delta r_{\rm BAO}/2} \frac{dz}{dr} dr \approx \frac{(1+z)\dot{A}'(r(z),t(z))}{\sqrt{1-k(r)}} \Delta r_{BAO}\,, \tag{3.38}$$

where in the second equality the integrand has been assumed to be constant.[5] Similarly, the coordinate characteristic scale Δr is given in terms of the physical scale through an integral

$$\Delta r_{BAO} \approx \frac{\sqrt{1-k(r)}}{A'(r(z),t(z))} l^R_{BAO}(z)\,. \tag{3.39}$$

Both equations relate the physical correlation with the redshift correlation

$$\Delta z_{BAO} = (1+z) H_R(z) l^R_{BAO}(z) \tag{3.40}$$

Constructing the geometric mean (3.36) using (3.37,3.40) is straightforward:

$$d_z^{LTB} = \left(\frac{H_R}{z}(1+z)\frac{1}{D_A(z)^2}\right)^{1/3} \xi(z)\, l(r_\infty, t_0)\,, \tag{3.41}$$

where the scale conversion arising from (3.34,3.35) has been introduced in the factor $\xi(z) \equiv (\xi_R(z)\xi_T^2(z))^{1/3}$, given by

$$\xi(z) = \left(\frac{A'(r(z),t(z))}{A'(r(z),t_e)}\frac{A'(r_\infty,t_e)}{A'(r_\infty,t_0)}\right)^{1/3} \left(\frac{A(r(z),t(z))}{A(r(z),t_e)}\frac{A(r_\infty,t_e)}{A(r_\infty,t)}\right)^{2/3}, \tag{3.42}$$

using a suitable early time $t_e = t(z \sim 100)$ to convert the scale as described in the previous Section. Note that due to the FRW limit, the ratios of the factors computed at r_∞ can be expressed as redshift factors $a(t_e)/a_0 = (1+z_e)^{-1}$.

Equation (3.41) can be easily related to the usual expression for d_z

$$d_z^{\rm LTB} = (1+z)\xi(z)\frac{l(r_\infty,t_0)}{D_V(z)} = (1+z)\xi(z)\, d_z^{\rm FRW}\,. \tag{3.43}$$

in terms of the usual volume distance

$$D_V(z) = \left((1+z)^2 D_A(z)^2 \frac{z}{H_R(z)}\right)^{1/3}. \tag{3.44}$$

Relation (3.43) absorbs the effects of the inhomogeneous rescaling in the BAO observations, which pick up a factor $(1+z)\xi(z)$ with respect to the FRW case. The difference between the two rescaling factors accounts for the anisotropy between the transverse and longitudinal BAO scales, while their redshift dependence is a consequence of the inhomogeneity. Both effects are shown in Figure 3.3. Note also that there will be an additional difference because of the modified relations between the angular diameter distance (related to the transverse expansion) and the longitudinal expansion rate entering the geometric mean distance (3.44).

[5] This approximation is justified because the void variation scale is much larger than $\Delta r_{\rm BAO}$. The exact result $\Delta z = z(r+\Delta r_{\rm BAO}) - z(r-\Delta r_{\rm BAO})$ can be obtained by inverting $r(z)$.

3.2.5 The Alcock-Paczynski Effect in LTB Models

The Alcock-Paczynski (AP) effect [210] is the geometric distortion of spherical objects due to cosmological expansion, since distances in the radial direction away from an observer are determined in redshift space, while transverse distances are seen as angular separations in the sky. This motivates the definition of the dimensionless *distortion factor*:

$$f^{\mathrm{AP}}_{\mathrm{FRW}}(z) \equiv \frac{\Delta z}{\Delta \theta} = D_A(z) H_R(z)(1+z)\,. \tag{3.45}$$

In a homogeneous universe, the above relation can be tested against spherical (or spherically distributed) objects for which Δz and $\Delta\theta$ are measured.[6] This technique has been used to constrain cosmological models [104, 151, 211].

In LTB models with space-independent Big Bang time, initially spherical distributions are intrinsically distorted due to the local shear, as discussed in Section 3.2.1. Using the angular and redshift projection of physical distances for the inhomogeneous models given by equations (3.37, 3.40), the analogue of the AP relation is modified by the ratio of the radial and transverse rescaling factors

$$f^{\mathrm{AP}}_{\mathrm{LTB}}(z) = \frac{\xi_R(z)}{\xi_T(z)} D_A(z) H_R(z)(1+z) = \frac{\xi_R(z)}{\xi_T(z)} f^{\mathrm{AP}}_{\mathrm{FRW}}(z)\,. \tag{3.46}$$

The values of these factors in both directions can be seen in Figure 3.3. As the universe expands faster in the transverse than in the radial direction, the distortion factor has a lower value than in FRW models, on top of the different relation between $D_A(z)$ and $H_R(z)$.

The distortion factor (3.46) is sensitive to cosmic shear (3.6) through the ratio of the transverse and radial rescaling (e.g. steeper profiles enhance the asymmetry). In the limit of zero background shear, the ratio of rescaling factors tends to one, and the only difference w.r.t. FRW comes from the different relation between the angular diameter distance and the radial Hubble rate. Therefore, the information one obtains from the AP effect is *complementary* to the geometric mean distance given by Eq. (3.43), which only depends on the expansion, i.e. the product of the rescaling in the three spatial directions, and is unable to tell apart ξ_R from ξ_T. Therefore, the AP effect is not only able to distinguish FRW from LTB models, but could eventually allow to observationally discriminate between different LTB profiles.

3.3 Analysis and Results

In this Section the LTB models described in Section 3.1 will be compared to observations. The present analysis relies on the interplay between the cosmic distances obtained by type Ia supernovae and the distances *and* rescaling constraints from the baryon acoustic oscillation scale. SNe can be regarded as a standard candle and BAO as a standard ruler, which suffers additional effects due to the inhomogeneity (as described in Section 3.2). The measurement of the local expansion rate and the CMB peaks are also considered, their effect being to provide a calibration for the standard candles and rulers, respectively. However, the main result is independent of this calibration.

[6] In practice, the AP test is difficult to perform due to dynamical effects such as the Redshift Space Distortions caused by cosmic structures, which induce peculiar velocities that affect the redshift in a systematic way.

3.3.1 Observational Data

The models were compared against several datasets, which are described below. The BAO, SNe and H0 data have been described in Chapter 2. A simplified method to implement CMB constraints in LTB models without computing cosmological perturbations is presented at the end of this Section.

Type Ia Supernovae

The dimming of distant supernovae constitutes a solid probe of void models in the interval $0.01 \lesssim z \lesssim 1.5$, as the luminosity distance depends on all the parameters of the model in a nontrivial way. One should in principle consider variations on the color and stretch parameters when fitting the model [157, 158]. However, the result of the analysis should not vary significantly since the LTB models we are considering usually give luminosity distance curves very similar to the standard model. The present analysis also includes the covariance matrix between the supernova data, which adds information about this calibration procedure by taking into account the covariance between supernovae with similar color and stretch. The supernovae data will be used as presented in Section 2.5.

Local Expansion Rate

The dependence of the expansion rate with redshift in a LTB cosmology is in general very different than in the ΛCDM case, even for low redshifts $z < 0.1$. In order to reproduce the method used in [165] and provide a more fair comparison, we implement the constraints on the model using supernovae luminosities rather than the model parameter H_{in}. The constraints labeled as H0 are implemented as described in Section 2.5.1.

Baryon Acoustic Scale

Although the use of BAO to constrain LTB models has raised some criticism [27, 164], we will rely on our results from Section 3.2 showing that the baryonic features remain at constant coordinate positions to a good approximation and relating the transverse and radial BAO scales at different redshifts to the asymptotic values. The data used are those presented in Section 2.4.1 and summarized Table 2.2. These measurements are given in terms of the variable d_z, which in our model is computed as (3.41), or alternatively (3.43), (3.44). The additional data point involving the angular correlation is to be compared to the theoretical θ_{BAO} prediction (3.37).

Cosmic Microwave Background

The cosmic microwave background radiation in LTB models has been actively investigated [199–203], as it constitutes the most solid piece of evidence for statistical isotropy and the most powerful tool in cosmological constraints. The obtention of precise constraints from the CMB is beyond the scope of this work, where we focus only on geometric aspects of the model. Therefore and only a relatively simple analysis based on the location of the first peaks will be employed, in order to give an idea of the effects of calibrating the standard rulers. This method yields weaker constraints than using the whole WMAP data and the spectra computed in linear perturbation theory, WMAP distance prior R, l_a, z_* [19] (See Section 3.3 and Figure 3.7) or other model independent determinations [124].

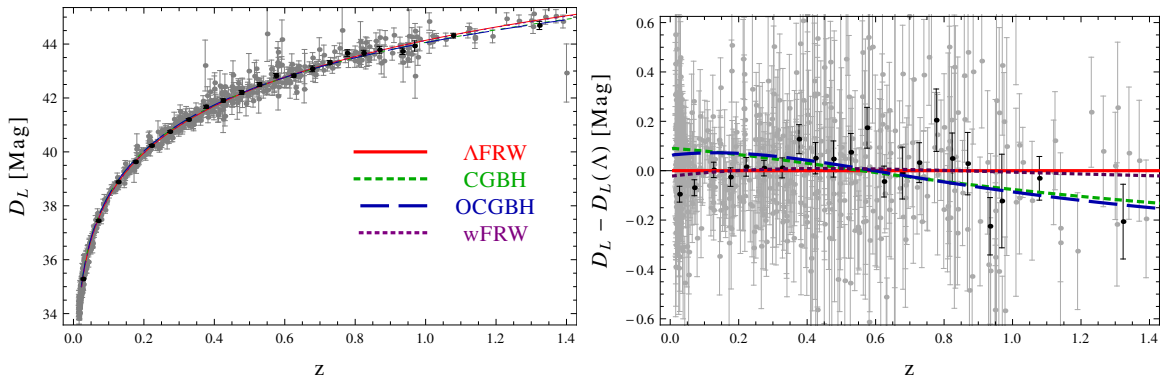

Figure 3.4: Supernovae data and luminosity distance. The gray points correspond to the Union2 compilation [163] used in the computation of the likelihood. The black points correspond to a binning of the same data using the covariance matrix, and are intended only for visual aid. Color lines correspond to the minimum χ^2 models described in Section 3.3, rescaled with the optimal value of μ_0, as described in the text.

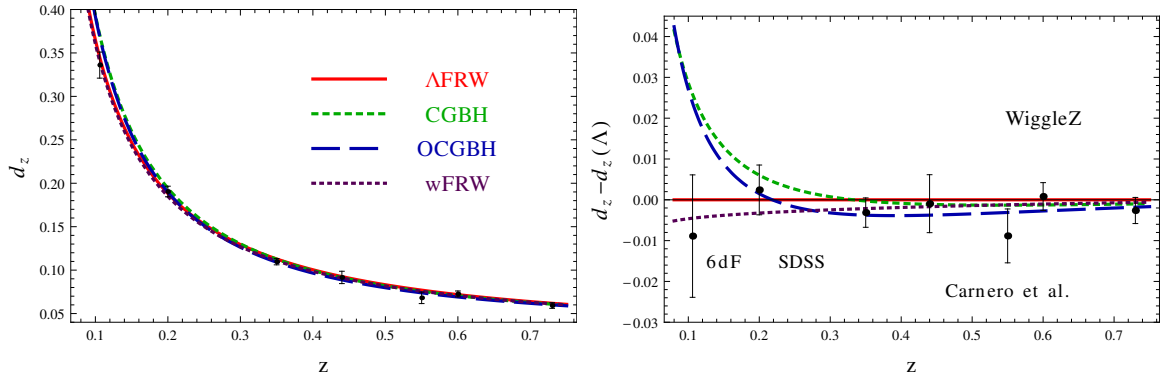

Figure 3.5: BAO data and d_z for the best fit models described in Section 3.3 and residuals with respect to ΛCDM. The point at $z = 0.55$ has been converted from angular to volume distance by means of a fiducial model.

If our galaxy is located very close to the center of the void, the radiation coming from the CMB will be highly isotropic and therefore well described by the angular power spectrum C_l, with no direction dependence. As usual, it will display a characteristic pattern of peaks and troughs located at multipoles

$$l_m = (m - \phi_m)\, l_A \,, \tag{3.47}$$

where integer values of m label the peaks, half integer values correspond to troughs, and ϕ_m are corrections that depends on the details of the cosmology *before* the recombination epoch. The overall factor is fixed by the *CMB acoustic scale*

$$l_A = \pi \frac{D_A(z_*)}{r_s(z_*)(1+z_*)^{-1}} \,, \tag{3.48}$$

determined by the ratio between the observed angular diameter distance until recombination and the sound horizon at that epoch. Further information on the cosmological parameters can be obtained by considering the relative heights of the acoustic peaks compared to the first one $H_a = C_{l_a}/C_{l_1}$.

The decoupling epoch occurs at an early time when the universe is very homogeneous and the primary anisotropies are produced on our past lightcone at a radius much larger than the size of the void $r(z \sim 1100) \gg R$. In this case the pre-recombination physics is effectively the same as in a homogeneous universe, and we can assume that the relative peak positions $(m - \delta\phi_m)$ and heights H_a are those of a FRW universe with the effective asymptotic values of the LTB model discussed in Section Section 3.2.3.[7] On top of modifying these asymptotic parameters, the only effects from the void will be to shift the peaks by varying the acoustic scale l_A through the angular diameter distance $D_A(z_*)$. Our analysis neglects secondary contributions such as the integrated Sachs Wolf effect on the lower multipoles or the action of gravitational lensing, which affects the relative heights of the peaks. Furthermore, we will assume no radiation contribution to the angular distance to recombination.[8]

In order to compare the theoretical predictions and the observations we will follow the approach described by Marra and Pääkkönen [189]. The corrections to the peak locations ϕ_m and heights depend on the effective parameters through the ratio of matter-radiation density and recombination and the physical baryon density $\Omega_m h^2$, as well as the spectral index n_s that characterizes the power spectrum of primordial perturbations. Note that relaxing the common assumption of a nearly scale invariant primordial spectrum considerably reduces the tension between CMB and the local expansion rate [158]. Accurate fitting formulae in terms of these quantities are provided in reference [123] for the recombination epoch z_* and the sound horizon $r_s(z_*)$, reference [214] for l_m with $m = 1, \frac{3}{2}, 2, 3$ and reference [215] for the relative height H_a of the second and first peak $a = 2, 3$. Figure 3.6 shows the location of the peaks reconstructed using this method.

The total likelihood is given by

$$\chi^2_{\rm CMB} = \sum_{m\in\{1,\frac{3}{2},2,3\}} \frac{\left(l_m^{\rm obs} - l_m^{\rm LTB}\right)^2}{2\sigma^2_{l_m}} + \sum_{a\in\{2,3\}} \frac{\left(H_a^{\rm obs} - H_a^{\rm LTB}\right)^2}{2\sigma^2_{H_a}} \,, \tag{3.49}$$

[7] Variations in the effective CMB temperature have not been considered because for the profiles under consideration (compensated voids) there is no significant departure from $T_0 = 2.725K$ [176, 189].

[8] See references [201, 212, 213] for discussions on radiation in the context of LTB models.

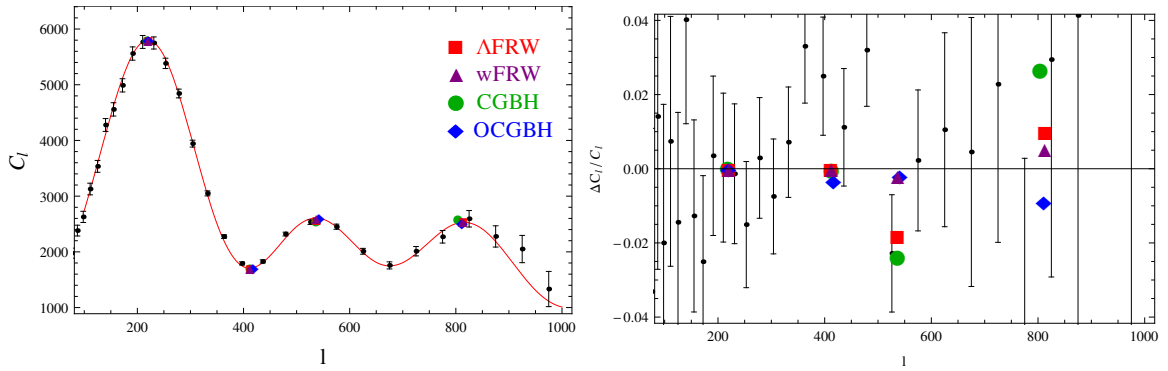

Figure 3.6: CMB spectrum. Black dots and error bars correspond to the binned WMAP7 data and the red line is the CMB only best fit for ΛCDM [18]. The color points are the reconstructed positions of the peaks using the method described in Section 3.3.1 for the minimum χ^2 models (Section 3.3). For visualization aid, the WMAP best fit height has been assumed for the first peak, which is equivalent to a normalization, and the first through due to the lack of a fitting formula (The residuals in $H_{3/2}$ are due to the propagation of $l_{3/2}$). Although the formulae do not exactly recover the values computed in linear perturbation theory, they fall within the assumed errors (1% for l_1, 3% for the rest). Note that the LTB models require values ($f_b \approx 0.7$, $n_s \approx 0.6$ that depart considerably from the standard model (Section 3.3). More precise constraints taken into account the full spectrum would considerably lower the quality of the fit.

where the positions and heights of the peaks are those matching the WMAP 7 year best fit model. As in reference [189], we have taken the errors to be of 1% for the position of the first peak and 3% for the remaining parameters. It is important to note that this likelihood analysis is very simplified and its main aim is to provide an insight on how the information from the CMB helps to sharpen the BAO constraints by fixing the initial size of the standard ruler.

3.3.2 MCMC Analysis

In order to constrain the parameter space and address the viability of the different models, we run several Markov Chain Monte Carlo (MCMC) analysis using a modified version of the publicly available code CMBEasy [216], which includes the integration of the coordinates over the lightcone and the computation of the cosmological observables in the LTB model. The data sets employed are described in Section 3.3.1. CMBEasy's built-in MCMC driver establishes the convergence of the chains through the test of Gelman and Rubin [217], which determines the length of the burn-in sequence and freezes the step-size, which is a necessary condition for the convergence of the MCMC algorithm [218] (see Appendix A). In addition, the chains were monitored manually to ensure a proper sampling of the parameter space.

Additionally to the CGBH and the OCGBH models described in Section 3.1.1, a ΛCDM model and a wCDM model with constant equation of state were studied using the same data. Separate runs were performed for each of the displayed contours corresponding to the constraints of the separate sets (CMB, BAO, SNe) as well as the combined constraints

FRW Models

H_0 [Mpc/km/s]	Ω_M	Ω_Λ	$-w$	$100 f_b$	n_s
$30-90$	$0.05-0.8$	$0-1.2$	$0-5$	$1-25$	$0.05-1.3$

GBH-LTB Models

$H_{\rm in}$ [Mpc/km/s]	$\Omega_{\rm in}$	$\Omega_{\rm out}$	R [Gpc]	ΔR [Gpc]	$100 f_b$	n_s
$30-90$	$0.01-0.5$	$0.1-1$	$0-5$	$0.5-5$	$1-25$	$0.05-1.3$

Table 3.1: Priors on the model parameters used in the MCMCs. In order to facilitate the comparison between the two LTB models, for the CGBH profile we have fixed the value of $H(r=0) \equiv H_{\rm in}$ at the center of the void instead of the more obscure parameter H_0. $\Omega_{\rm out}$ and w are only varied in the OCGBH and wCDM models.

H0+BAO+CMB+SNe. For the inhomogeneous models the additional combinations H0+SNe and BAO+CMB were considered, which combine the information of standard candles/rulers together with their calibrations (as opposed to the SNe/BAO-only). All the runs used flat priors on the model parameters, which are given in Table 3.1.

The results from the combined constraints can be seen in Table 3.2. Figures 3.7, 3.8, 3.9 and 3.10 show the two-dimensional marginalized likelihood contours obtained from the individual and combined data sets. Our discussion starts by considering the homogeneous reference models. Then the results for the inhomogeneous CGBH and OCGBH profiles will be addressed, and the goodness of fit of the different models compared using different criteria.

3.3.3 Homogeneous Models

For ΛCDM the recovered parameters are in good agreement with previous results. However, the region compatible with CMB data (first plot in Figure 3.7) is broader than usual around the flatness line. This lack of precision is caused by the partial use of the CMB data (i.e. only the peaks instead of the whole C_l spectrum), together with the broad parameter priors allowed. When combined with other measurements, it also affects the recovered value of the curvature $\Omega_k = 0.003^{+0.015}_{-0.025}$, which is still very close to flat but has larger error bars than usual. In a computation taking into account the full WMAP7 data, a deviation with respect to the measured values of the peak positions would also displace many of the intermediate points and cause a more dramatic decrease of the likelihood, leading to tighter bounds.

The weakness of the CMB constraints is reflected again in the recovered values for the wCDM model (second and third plots in Figure 3.7). In this case all the parameters except H_0, which is independently constrained by the nearby expansion rate, depart considerably from the standard ones. These allow for lower values of the baryon fraction and the spectral index, which in turn increase the matter fraction and decrease the dark energy content. A very dramatic consequence of the weakness of these constraints can be seen in the recovered value of the curvature $\Omega_k = 0.04 \pm 0.02$, two sigma away from flatness. The low value of

ΛCDM Model

	H_0 [Mpc/km/s]	Ω_M	Ω_Λ	$100 f_b$	n_s
All - Min χ^2	70.7	0.28	0.72	17	0.97
Marginalized	$70.3^{+1.7}_{-1.5}$	0.27±0.03	0.73 ± 0.05	17 ± 0.04	$0.99^{+0.06}_{-0.09}$

wCDM Model

H_0 [Mpc/km/s]	Ω_M	Ω_Λ	w	$100 f_b$	n_s
72.8	0.32	0.66	−1.26	12	0.87
73.5 ± 2.3	0.33 ± 0.04	0.64 ± 0.06	$-1.26^{+0.17}_{-0.22}$	$0.10^{+0.03}_{-0.02}$	$0.82^{+0.08}_{-0.06}$

asymptotically flat Constrained GBH model (CGBH)

	$H_{\rm in}$	$\Omega_{\rm in}$	R [Gpc]	dR [Gpc]	$100 f_b$	n_s
All - Min χ^2	66.4	0.21	0.02	2.78	7.7	0.74
Marginalized	66.0±1.4	0.22 ± 0.04	$0.18^{+0.64}_{-0.18}$	$2.56^{+0.28}_{-0.24}$	7.7 ± 0.4	0.74 ± 0.03
BAO+CMB	61.6±2.4	$0.32^{+0.06}_{-0.04}$	$3.92^{+0.48}_{-3.71}$	$2.76^{+0.50}_{-0.88}$	7.8 ± 0.8	0.73 ± 0.04
SNe+H0	74.0±2.6	0.07 ± 0.04	$1.95^{+1.22}_{-1.82}$	$3.19^{+1.63}_{-1.66}$	-	-

asymptotically Open Constrained GBH model (OCGBH)

$H_{\rm in}$	$\Omega_{\rm in}$	$\Omega_{\rm out}$	R [Gpc]	dR [Gpc]	$100 f_b$	n_s
71.8	0.21	0.87	0.30	1.48	6.3	0.67
71.1 ± 2.8	0.22±0.04	0.86 ± 0.03	$0.20^{+0.87}_{-0.19}$	$1.33^{+0.36}_{-0.32}$	6.2 ± 0.5	0.68 ± 0.03
$63.8^{+4.2}_{-2.8}$	0.35±0.06	$0.98^{+0.02}_{-0.11}$	$0.72^{+2.5}_{-0.67}$	1.79 ± 0.89	6.8 ± 0.9	$0.69^{+0.05}_{-0.03}$
$73.4^{+3.1}_{-2.1}$	0.06±0.04	$0.89^{+0.09}_{-0.25}$	$0.80^{+1.66}_{-0.74}$	$1.63^{+2.04}_{-0.79}$	-	-

Table 3.2: Parameters from the MCMC including H0+SNe+BAO+CMB discussed Section 3.3. The first lines correspond to the minimum χ^2 models, while the second lines corresponds to the best fit model with one sigma errors after marginalizing over the remaining parameters. Note that since the LTB models do not give good fits to the data the errors are apparently very small (see Figures 3.7, 3.8, 3.9 and 3.10). For the sake of comparison, in the case of the LTB models the results from the separate fits using BAO+CMB and SNE+H0 have been added (third and fourth lines).

ΛCDM Model

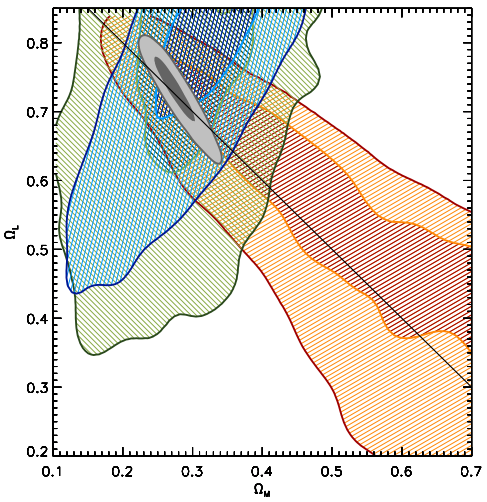

wCDM Model

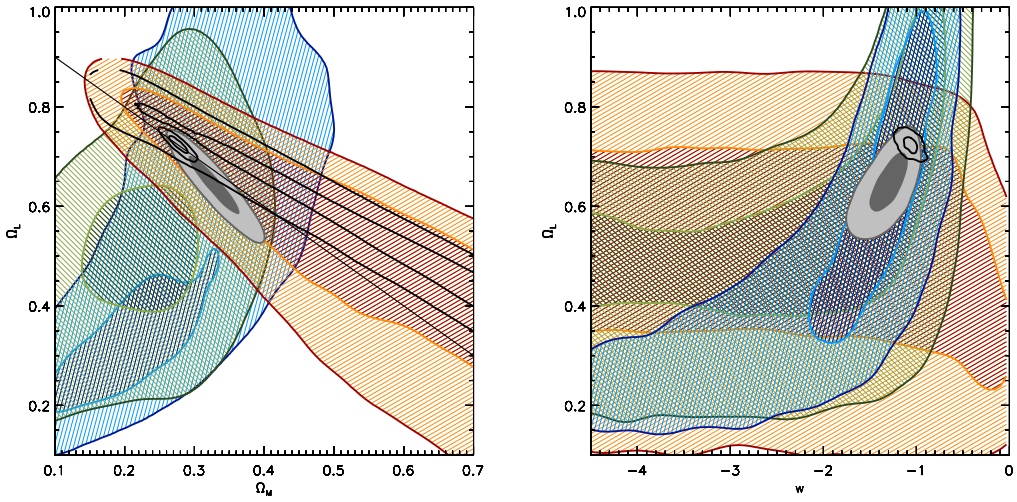

Figure 3.7: One and two sigma regions for the marginalized likelihood function corresponding to the ΛCDM and wCDM homogeneous model as obtained from BAO (green), CMB (Orange) and SNe (blue). Gray contours are the combined constraints H0+BAO+CMB+SNe. Note that the CMB compatible regions are much broader than usual due to the simplification of the method. Black unfilled lines in the wCDM plots correspond to using the WMAP distance prior R, z_*, l_A [19] combined with H0+BAO+SNe or individually (shown only in the $\Omega_\Lambda - \Omega_m$ plane), which recover the standard results.

$\Omega_\Lambda \approx 0.62$ is then compensated with an anomalously low equation of state $w \approx -1.34$.[9]

Note also how the BAO and SNe contours span a similar region in both cases. This is a consequence of them being determined by measurements of standard rulers and candles with *arbitrary* calibration, over a comparable redshift interval (due to the new BAO data provided by the WiggleZ collaboration, up to $z \sim 0.8$). Since in FRW both datasets depend only on the same distance-redshift relation and are consistent with each other, they yield basically the same information and the recovered regions overlap.

3.3.4 Inhomogeneous Models

Discrepancies between the different datasets are encountered for both models regarding the matter content and the expansion rate at the center of the void, as can be seen in Figures 3.8, 3.9, 3.10. This becomes particularly clear for the $\Omega_{\rm in} - h_{\rm in}$ plane.

The most severe problem for both models is the existing tension regarding the value of $\Omega_{\rm in}$ determined from BAO and SNe, which differs by roughly 3σ for the two models (see figures 3.8, 3.9). For example, the asymptotically flat model (CGBH) the BAO-only 1D marginalized likelihood yields $\Omega_{\rm in} = 0.28^{+0.06}_{-0.05}(1\sigma)$, a much higher value than determined by SNe $\Omega_{\rm in} = 0.07 \pm 0.04(1\sigma)$. This discrepancy is showing how the distance redshift relation necessary to explain the supernovae dimming is incompatible with the stretch of the standard ruler inside the void due to the inhomogeneous rescaling discussed in Section 3.2. The low value of $\Omega_{\rm in}$ necessary to fit SNe observations increases the expansion rate and therefore stretches the BAO scale considerably near the center, making it incompatible with the observed values at higher redshift. This is a purely geometric discrepancy, valid for arbitrary calibration of the standard candles and rulers, and is completely independent of the dynamics originating the characteristic length. Figures 3.4, 3.5 show how the best fit models represent a compromise that fails to fit both datasets at low redshift, where the BAO rescaling (Fig. 3.3) is largest.

Naturally, the tension becomes more dramatic when the SNe data are compared to the BAO+CMB combination, because the CMB effectively reduces the allowed range of the initial BAO scale by constraining $H_{\rm in}$, f_b and $\Omega_{\rm out}$. The independence of the constraints on the initial BAO scale is the reason why the asymptotically open model (OCGBH) does not ease the tension between BAO and SNe. This is partly because the apparent freedom gained from allowing $\Omega_{\rm out}$ to vary does not provide essentially different values of the asymptotic BAO scale, already ensured by the freedom in f_b. The other reason is that neither SNe nor BAO-only constraints seem to depend on the value of $\Omega_{\rm out}$. We can regard the dashed green and blue contours in Figures 3.8, 3.9, 3.10) as the purely geometric constraints for *arbitrary* values of the standard rulers/candles, while the filled green and blue contours would correspond to adding priors to those calibrations.

The asymptotically flat model (CGBH) also shows a tension between the value of $H_{\rm in}$ determined by H0+SNe and CMB+BAO, both being discrepant at 3σ. Note that the tension is manifest even using very simplified CMB data, although these yield much looser constraints than the full C_l spectrum. In the asymptotically open model, the additional freedom achieved

[9] The discrepancies disappear when the WMAP7 distance prior R, z_*, l_A [19] are used instead of the peak positions (black, unfilled contours in Figure 3.7), recovering $\Omega_k \approx 0$ and $w \approx -1$. These quantities have been very accurately determined by the WMAP collaboration using the full CMB spectrum, and are able to break the degeneracies in the model (e.g. the baryon fraction). Although they are considerably more precise than the CMB peak information we used (described in Section 3.3.1), the WMAP distance prior can not be directly applied to inhomogeneous models (e.g. LTB models with decoupling redshifts $z_* \gtrsim 1110$ considerably higher than the standard value $z_* = 1091.3 \pm 0.9$ can yield a good fit [199]).

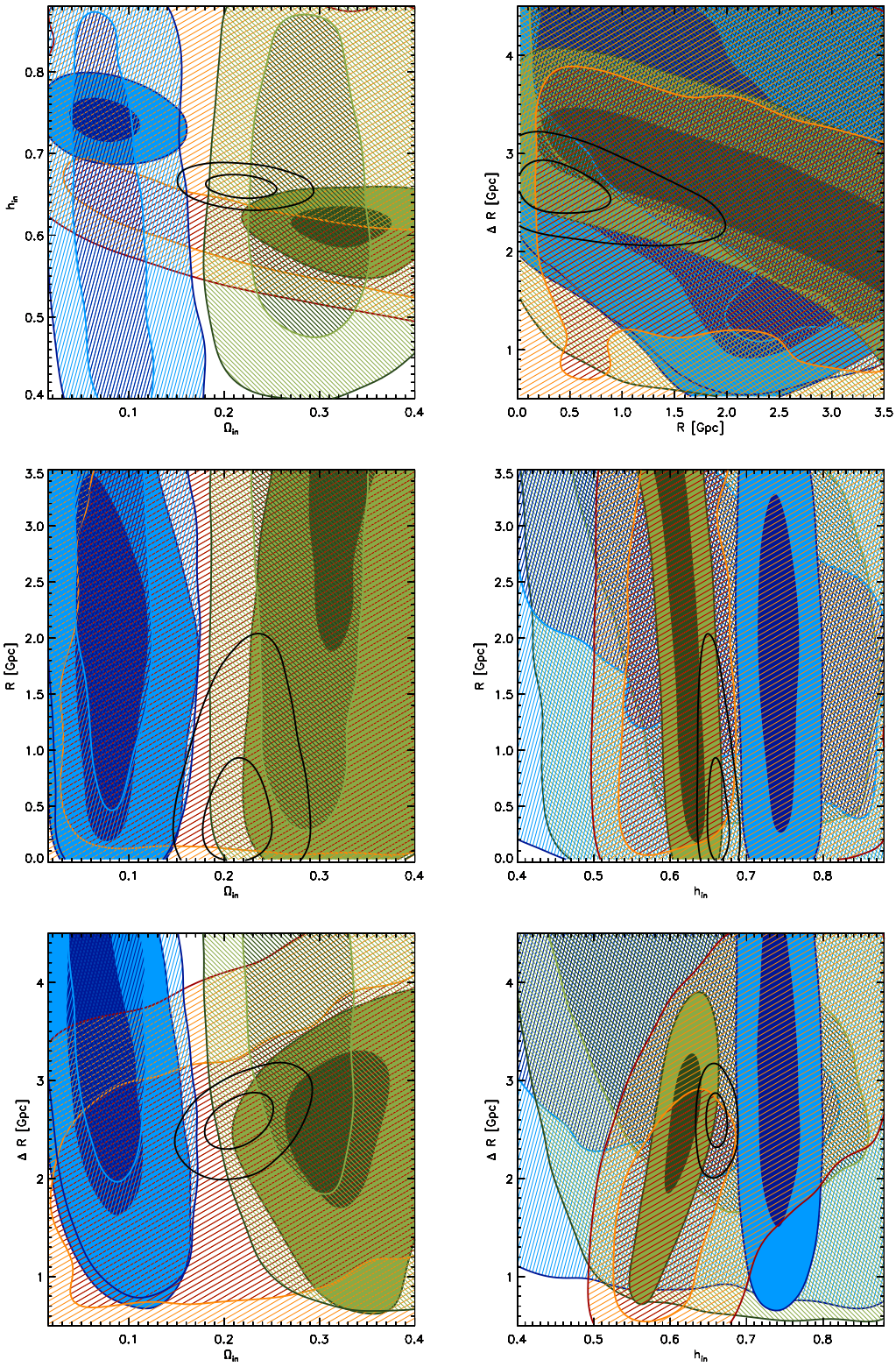

Figure 3.8: CGBH model. One and two sigma regions for the marginalized likelihood function as obtained from BAO (green), CMB (Orange) and SNe (blue). The filled contours represent the combined constraints using SNe+H0 (blue) and BAO+CMB (green). The black lines correspond to the combined data BAO+CMB+SNe+H0.

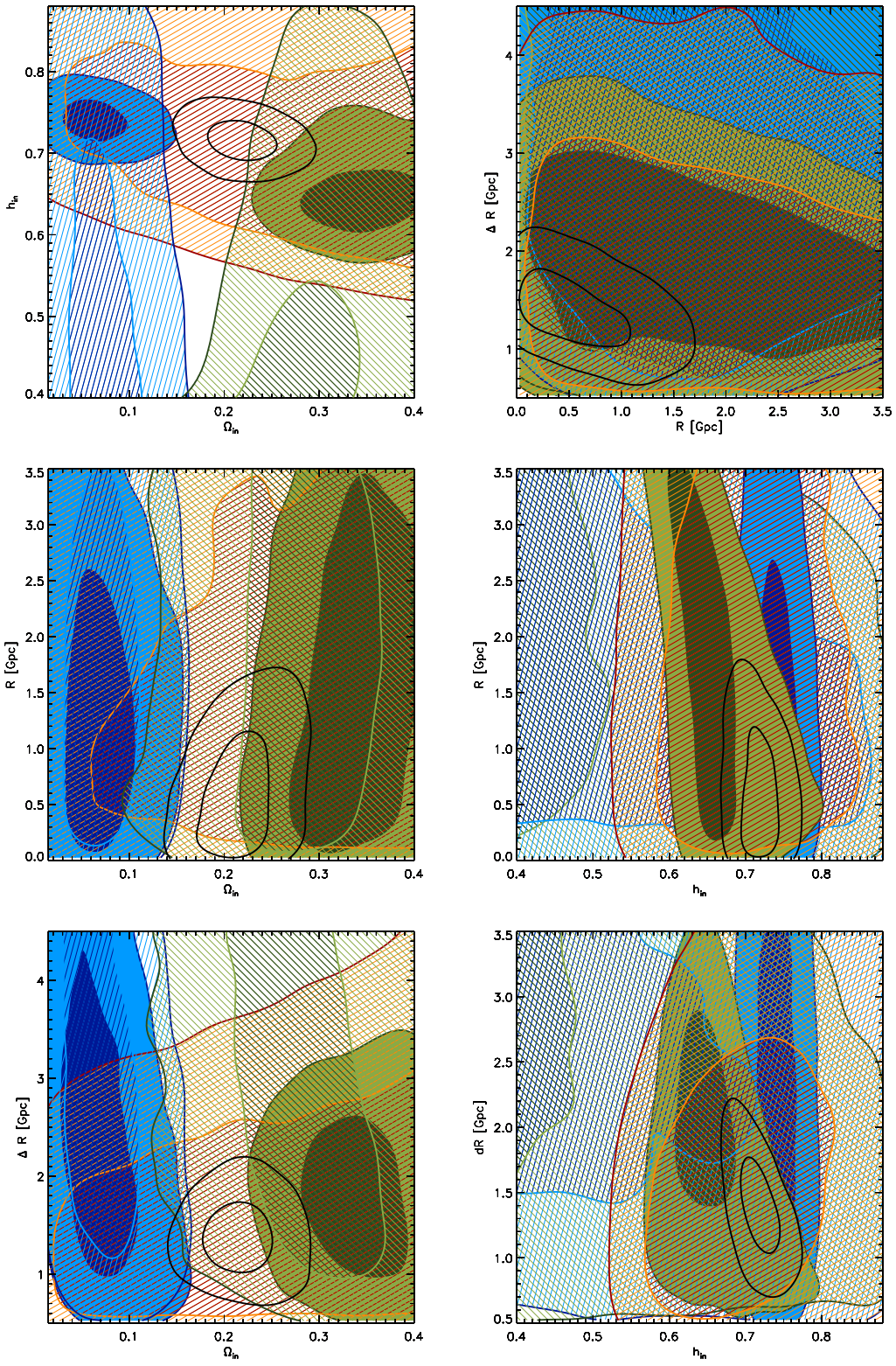

Figure 3.9: OGBH model. One and two sigma regions for the marginalized likelihood function as obtained from BAO (green), CMB (Orange) and SNe (blue). The filled contours represent the combined constraints using SNe+H0 (blue) and BAO+CMB (green). The black lines correspond to the combined data BAO+CMB+SNe+H0.

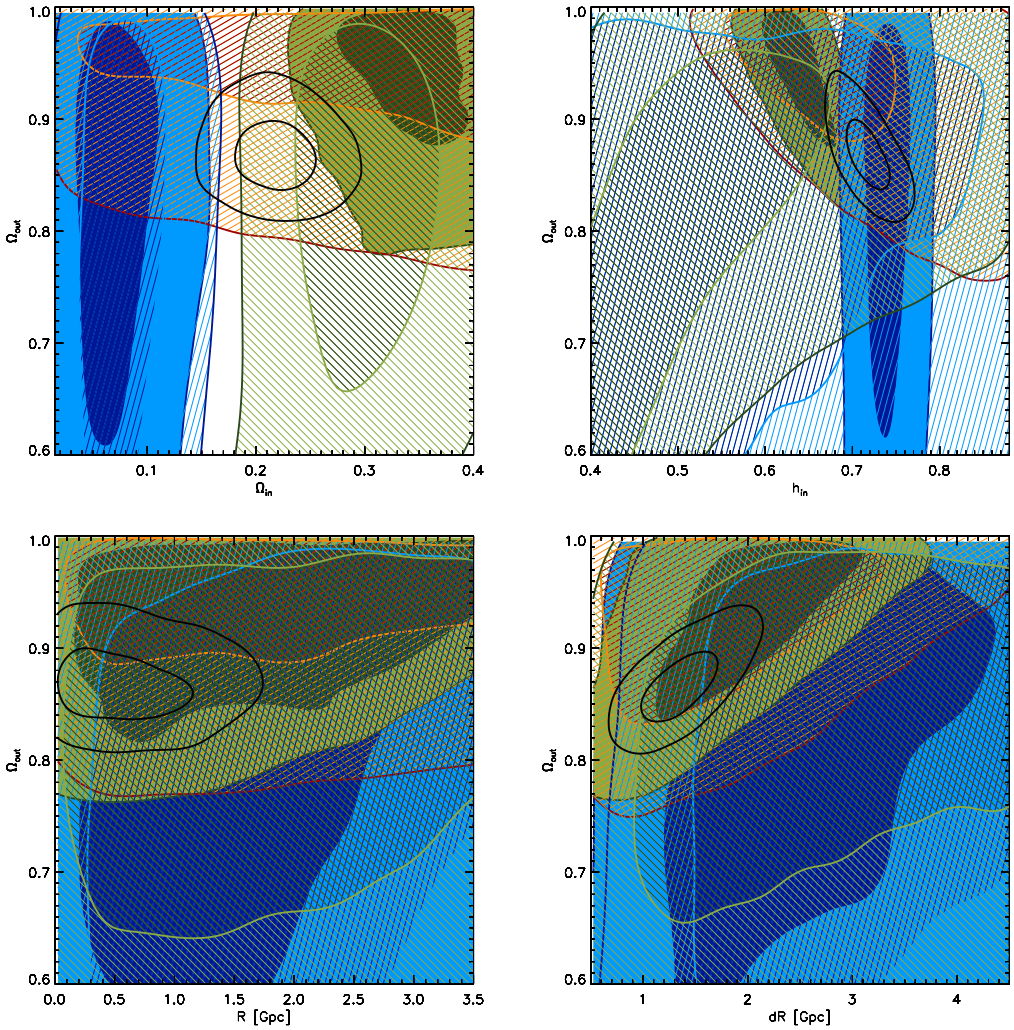

Figure 3.10: Continuation of Figure 3.9.

allows one to recover agreement by reducing the value of $\Omega_{\rm out}$, yielding a concordant value for $H_{\rm in}$ from the different datasets. However, the tension would reappear in more a thorough analysis including the full CMB power spectrum data, which typically require $h_{\rm in} \sim 0.4 - 0.5$ [153]. This increase in the local expansion rate also reduces the age of the universe, which is proportional to $H_0(r)^{-1}$. Although it has not been explicitly accounted for in the MCMC, Figure 3.11 shows how models with a higher expansion rate enter in tension with the limits on the age of the universe obtained from Globular Clusters [219], posing yet another difficulty for this type of models.

The recovered values of the baryon fraction and the spectral index, mainly determined by the CMB, are much lower than in standard cosmologies. This trend agrees with previous studies in which compensated voids are constrained using the full CMB [176]. We note that these features are not relevant to our discussion because 1) the main results are geometric and do not depend on the details of the CMB physics and 2) the obtained values of f_b, n_s

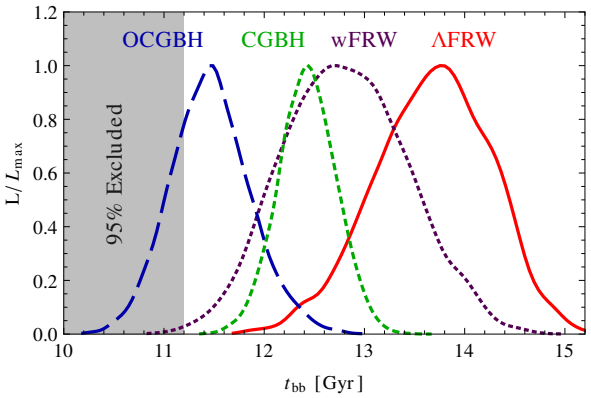

Figure 3.11: Age of the universe for the best fit models. The curves correspond to marginalization of the MCMC chains over the (homogeneous) Big Bang time (note that it is a derived quantity rather than a parameter varied in the exploration). The gray area shows the region excluded by the age of Globular Clusters in the Milky Way.

rely on a simplified treatment of the CMB peaks.

The best fit models turn out to be rather cuspy, as can be seen in the preference towards $R \approx 0$ Gpc in both the asymptotically flat and open voids. Since the fit is not very good and the individual observations are not very restrictive by themselves (including the combinations BAO+CMB, SNe+H0), this feature might well be due to a compromise between the different datasets, and could be related to the fact that cuspy voids achieve better resemblance to an accelerating universe at low redshift [171]. In this case, the size of the void is given by the steepness of the inhomogeneity ΔR, which acquires a value ~ 2.5 Gpc in the flat case but a smaller value ~ 1.5 Gpc in the asymptotically open case. Again, the individual data sets do not yield significant enough information about the value of $R, \Delta R$. Other than the smallness of the asymptotically open void and the better agreement it gives on the value of H_0, there is no significant difference between the two models.

3.3.5 Model Comparison

We now proceed to compare the different models under several criteria. The tensions between the different datasets (Figures 3.8, 3.9 and 3.10) and the poor fit to SNe and BAO (Figures 3.4 and 2.2) will be reflected in poorer figures with respect to the homogeneous models. Furthermore, inhomogeneous models will be additionally penalized because they have a larger number of parameters. Table 3.3 shows the χ^2 values associated to the different observations and the total values, as well as the result of the different model comparison criteria discussed below.

The standard frequentist analysis of parameter estimation, given a set of data, is not very useful for model selection, since it is difficult to compare models with different number of parameters. For instance, the usual method of comparing minimum χ^2 per effective degree of freedom normally misses the point and is not very decisive, as can be seen in the very close values achieved by the different models. Other methods to decide which model gives the best description include various Information Criteria which additionally penalize models

	CGBH	OCGBH	ΛCDM	wCDM
Union SNe	**539.94**	**539.06**	**530.70**	**530.40**
Hubble μ_0	**6.97**	**0.38**	**2.17**	**0.14**
6dF	5.35	4.73	0.35	0.09
SDSS	0.73	0.04	1.29	1.24
WiggleZ	0.65	1.20	0.93	0.63
Carnero *et al.*	0.78	0.12	0.61	0.34
Total BAO	**7.51**	**6.09**	**3.18**	**2.30**
Peak positions	0.87	0.30	0.96	0.07
Peak heights	1.13	0.11	0.24	0.04
Total CMB	**2.00**	**0.41**	**1.20**	**0.11**
Total χ^2	**+19.89**	**+9.40**	**536.56**	**-3.62**
# free parameters	6	7	5	6
χ^2/d.o.f.	0.985	0.968	0.948	0.943
Akaike IC (3.50)	+22	+13	546.6	-1.6
Bayesian IC (3.51)	+26.2	+15.7	568.3	+2.7
Bayes factor (3.53)	+10	+6	282.2	+2.6

Table 3.3: χ^2 contributions to the maximum likelihood models as found by the MCMCs with H0+BAO+CMB+SNe and results from different model comparison criteria discussed in Section 3.3.5. The values χ^2 as well as the model comparison criteria are given show the total value for the ΛCDM best fit, while the other models are given relative to those (minus values are favoured w.r.t. the concordance model, while positive values are disfavoured). The Bayes factor is given by the difference in $-\log E$ (3.53).

described by more parameters. Such include the (corrected) Akaike Information Criterion (AIC) [220] and Bayesian Information Criterion (BIC) [221], given by

$$AIC = \chi^2_{\rm min} + 2k + \frac{2k(k-1)}{N-k-1}\,, \tag{3.50}$$

$$BIC = \chi^2_{\rm min} + k \ln N\,, \tag{3.51}$$

where k is the number of free parameters of a given models and N the number datapoints used in the constraints. The Bayesian evidence

$$E(\mathbf{D}|\mathcal{M}) = \int du\ \mathcal{L}(\mathbf{D}|u,\mathcal{M})\,\pi(u,\mathcal{M})\,, \tag{3.52}$$

is given by the integral of the likelihood $\mathcal{L}(\mathbf{D}|u,\mathcal{M})$ over the values of the model parameters u allowed by the priors $\pi(u,\mathcal{M})$. The computation of the Bayesian evidence is difficult in general, therefore, we will use a simple expression which can be obtained provided that the

likelihood is a single isolated peak, far from the edges of the prior ranges [184]

$$-\ln E = -\ln \mathcal{L}_{\max} + \ln A + \sum_{i}^{n} \ln(u_i^{\max} - u_i^{\min})\,, \tag{3.53}$$

where A is the normalization of the likelihood, and $[u_i^{\min}, u_i^{\max}]$ is the range of parameter u_i allowed in the MCMC exploration (assuming a flat priors), $i = 1 \ldots n$. Moreover, for the case of a Gaussian likelihood,

$$\mathcal{L}(u) = A \exp\Big[-\frac{1}{2}\mathbf{u}^{\mathrm{T}} C^{-1}\mathbf{u}\Big]\,, \tag{3.54}$$

we find $A = (2\pi)^{-n/2}/\sqrt{\det C}$, where C is the covariance matrix and $x_i = u_i - \bar{u}_i$. It is clear that whenever the prior ranges are too big for the likelihood, the Bayesian evidence is penalized. An estimate of the covariance matrix can be obtained assuming that the obtained parameters are independent from each other. In that situation, the covariance matrix is given by the square of the one sigma allowed ranges in each parameter and the determinant becomes $\det C = \prod_i \sigma_i^2$, where we take the average between the upper and lower bounds given in Table 3.2. The determinant computed using the eigenvalues of the covariance matrix used in the MCMC sampling yields similar results.

The bottom part of Table 3.3 shows similar values for the homogeneous models, but the preferred one depends ultimately on the chosen criterion. It is interesting to note that the Bayes factor favors the simpler ΛCDM with a difference of 2.6, despite the slightly better χ^2 fit of the wCDM model. This difference is due to the presence of an additional parameter, w, together with the large prior postulated for it, $[-5, 0]$, relative to the 1σ region, $\Delta w \approx 0.2$.

The logarithm of the Bayes factor for the LTB models w.r.t. to the fiducial ΛCDM is 10 and 6, for the asymptotically flat and open GBH inhomogeneous models respectively, due to the bad fit and the larger parameter range explored. Although the asymptotically open model yields a better Bayes factor, even with an additional parameter, both are strongly disfavored according to Jeffreys' scale, since the difference in the logarithm of the Bayes factor is higher than 5. The Akaike and Bayesian Information Criteria also prefer the homogeneous model, the rejection being significantly stronger for the asymptotically flat case due to the extra tension in the local expansion rate. Increasingly accurate data have significantly worsened the fits of inhomogeneous universes, which were compatible just few years ago (cf. reference [184]).

3.4 Discussion

In this Chapter we presented new constraints on inhomogeneous Lemaître-Tolman-Bondi models in the light of the most recent cosmological data, focusing on profiles of the GBH type with a space-independent Big Bang and baryon fraction. The inclusion of higher redshift BAO data together with type Ia supernovae allows one to reject the models based only on BAO and SNe, independently of other observational data such as the CMB. Additionally, a model independent method to constraint the local expansion rate through a prior on the supernovae luminosity was introduced.

The physical BAO scale at early times was computed in terms of the asymptotic value and then projected to different redshifts using the background LTB metric. This method is

justified due to the existence and stability of constant coordinate geodesic solutions, which are expected to be followed by baryonic overdensities in position space. In addition to the time evolution, the BAO scale is shown to become inhomogeneous and anisotropic due to the different expansion rates in the radial and transverse directions. The dependence of the observed BAO scale on both the cosmic distances *and* the evolution of the scale factor leads generically to different predictions than pure distance indicators such as SNe. The departure is largest near the center of the void, precisely because there is less matter to slow down the expansion that drives the growth of the BAO scale. Ultimately, the difference between the two distances can be regarded as a concrete realization of more general tests of the Copernican Principle [222].

The addition of BAO data at higher redshifts increases considerably their constraining power in this type of models because they help to fix the asymptotic value. The result represents a new drawback for this type of models, as the value of the local matter density $\Omega_{\rm in} \gtrsim 0.2$ preferred by BAO is about 3σ apart from the value $\Omega_{\rm in} \lesssim 0.18$ found using Supernovae, as can be inferred from Figures 3.8 and 3.9. The tension between the two datasets persists when asymptotically open models are studied, and worsens when the information from the CMB is added, since it constraints the parameters involved in the acoustic scale determination $(f_b, h, \Omega_{\rm out})$. Asymptotically flat LTB models show an additional tension regarding the value of the local Hubble rate when CMB and BAO are combined. Allowing $\Omega_{\rm out} \leq 1$ relaxes this incompatibility, but we expect it to re-emerge in a more detailed analysis of the CMB including all scales and secondary contributions such as the ISW effect and gravitational lensing. Additionally, larger values of the expansion rate might render the universe too young to account for the ages of stars in globular clusters. The adiabatic GBH models fail to simultaneously fit the data, and a Bayesian analysis shows that they are ruled out at high confidence.

The above results were obtained for a particular choice of the matter profile. However, the difficulties of the model are manifest in the determined value of matter contrast at the center of the void, while the remaining parameters are poorly constrained by individual datasets. The departure between cosmic rulers and candles becomes most severe at the center of the void, and we expect that $\Omega_{\rm in} \equiv \Omega_M(0)$ captures this tension regardless of other features. Since $\Omega_{\rm in}$ can be defined for any LTB model independently of the parameterization, it is reasonable to expect this result to hold for *all* large void models with space-independent Big Bang and baryon fraction. Nonetheless, we have to keep in mind that the SNe and BAO constraints depend on all the parameters through the distance determinations and the evolution of the BAO scale up to a certain redshift, and therefore different shapes for the profile might soften the tension between the two datasets.[10]

Similarly to the dependence of CMB constraints with the primordial power spectrum [158], it is conceivable that fine tuned initial perturbations could be used to reconcile the BAO observations with SNe in adiabatic voids. However, such conditions would not only need to *provide* an enhanced scale to explain the observed feature in galaxy correlation, but also to *hide* the actual BAO scale that would naturally form due to the existence of a preferred scale (the sound horizon at the recombination epoch). On top of this challenging task, the *fake* BAO scale should be shorter near the center to compensate the inhomogeneous growth and

[10] Recently, genetic algorithms were used to analyze the sensitivity of LTB model profiles to the data without the introduction of a parameterization [34]. The results were not conclusive with respect to the shape of the void profile.

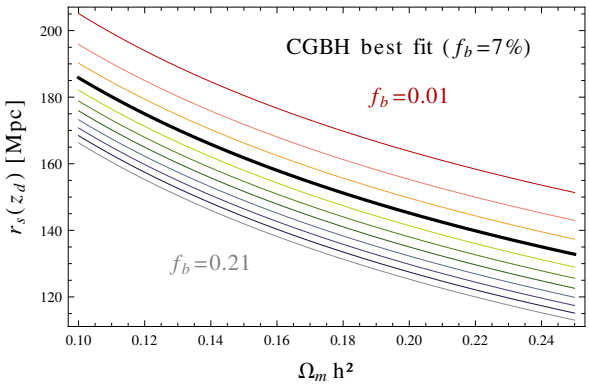

Figure 3.12: FRW, coordinate baryon acoustic scale $r_s(z_d)$ as a function of the physical matter density $\Omega_m h^2$ for different values of the baryon fraction. The mass of the baryons acts lowering the speed of sound in the baryon-photon fluid, and therefore increasing their amount reduces the resulting acoustic scale, which is related to the sound horizon. An LTB model with a higher baryon fraction near the center might render the BAO and SNe observations compatible by lowering the value of $d_z \propto r_s(z_d)$ near the center of the void (see Figure 3.5).

fit the observations, therefore requiring some amount of radial dependence that would be at odds with the (quasi) homogeneous initial state.

The effects of the inhomogeneity on the BAO scale are unavoidable. Even if a different void profile might yield a slightly better fit, more precise data e.g. from future surveys such as Euclid [108, 223] will eventually be able to distinguish adiabatic LTB models from the homogeneous case regardless of the shape of the inhomogeneity. Together with the remaining observational problems for large void models with space-independent Big Bang, this sets the stage for abandoning the adiabatic assumption. A scenario with space dependent Big Bang time would require more careful considerations on the origin of the BAO scale to account for the early time inhomogeneity, but it is still possible that the freedom gained from decoupling $H_0(r)$ from $\Omega_{\rm M}(r)$ renders BAO and SNe observations compatible, although the modulation of the Hubble rate is restricted by the local and asymptotic values, fixed by SNe luminosity priors and the CMB.[11]

A simpler possibility to reconcile SNe and BAO would be to allow for large scale baryon isocurvature modes, and induce a radial dependence on the early time BAO scale through a non-constant baryon to matter ratio $f_b(r)$, a possibility that has been explored as a way to explain the observed abundances of primordial nuclei and attempt to solve the primordial lithium problem [180]. Figure 3.5 suggests that lowering the *local* value near the center of the void would give a nicer fit to the observations, since the value of $d_z \propto r_s/D_V$ is proportional to the physical acoustic scale. A higher baryon fraction acts reducing the speed of sound of the baryon-photon fluid, therefore shortening the sound horizon that determines the observed BAO scale (see Figure 3.12). Adding more baryons at the center of the void would provide the necessary freedom to compensate for the inhomogeneous expansion and render the model

[11] Models with arbitrary $H_0(r)$ also predict a too large kinematic Sunyaev-Zel'dovich effect [36, 203]. It might be still possible to avoid these constraints by including an additional baryon to photon profile $\eta(r)$ [8].

phenomenologically viable, although more involved and less appealing.[12]

To summarize, we have shown how the BAO scale, acting as a standard (but evolving) ruler and the supernovae explosions, acting as standard candles, lead to different predictions in an inhomogeneous universe, which are disfavored by current data. The conclusion of the analysis is that the use of purely geometric probes, that only recently have become sufficiently constraining, is able to rule out the whole class of adiabatic LTB models. This is independent of other dynamical constraints, like those coming from the kinematic Sunyaev-Zel'dovich effect or the integrated Sachs-Wolfe effect, which in the near future can be used to definitely rule out all inhomogeneous models without dark energy. The present results are also relevant for observationaly constraining more general inhomogeneous models [225] including some recent proposals that incorporate dark energy [226–229].

[12]Baryon isocurvature modes are severely constrained by CMB observations [19, 224]. However, these constraints apply to scales much smaller than the size of the void.

Chapter 4

Phenomenological Modifications: Entropic Gravity

Play! Invent the world! Invent reality!

Vladimir Nabokov[1]

henomenological models are a common way to observationally test consistency relations within the standard model. The most known example is the constant equation of state dark energy model wCDM. It is not intended to represent a physically realistic scenario, yet it is useful to encapsulate possible departures form the standard model with the addition of a single parameter. Useful parameterizations should be able to interpolate between different effects, e.g. evolving/static dark energy or scale dependence of gravitational clustering. In addition, they should contain the standard model as a particular point of the parameter space. Testing them against observations is then a simple way to regard the data and their sensitivity to departures from the standard paradigm, and the significance of such departures whenever present.

A different but related idea is to use phenomenological models to describe certain physical situations that are difficult to consider in full detail, or for which a complete, self consistent description does not exist. Hopefully, one can then be able to predict certain physical phenomena and use them to test the underlying principles in a given context. This Chapter undertakes the study of recent ideas about the internal structure of the space-time, namely that gravity is an entropic force of thermodynamical origin. Modifications of gravity can be introduced within this paradigm only phenomenologically, due to a lack of a Lagrangian formulation. The Friedmann equations corresponding to these models have been obtained by several authors from the Newtonian force, following an argumentation that yields the right result in the case of General Relativity. Using this as a starting point, the modified FRW evolution is used to constraint these scenarios.

[1] *Look at the Harlequins!* (1974)

4.1 Gravity and Thermodynamics

The notion of gravity as an emergent force has been contemplated for a long time [230]. The derivation of gravitational field equations from thermodynamics by Jacobson [231] supports this, and has lead to further substantial hints of evidence for the idea [232]. Recently, the proposal was put forward that gravity is a thermodynamic phenomenon emerging from the holographic principle [233]. It was argued that the Newton's law of gravitation can be understood as an entropic force caused by the change of information holographically stored on a screen when material bodies are moving with respect to the screen. This is described by the first law of thermodynamics, $F\Delta x = T\Delta S$, connecting the force F and the displacement Δx to the temperature T of the screen and the change of its entropy, ΔS. T can be then identified with the Unruh temperature without referring to a horizon. Newton's second law follows if the entropy increase is $\Delta S = 2\pi m\Delta x$, m being a particle mass and Δx the distance to a holographic screen. More to the point, assuming equipartition of the energy [234] given by the enclosed mass, Newtonian gravitation emerges.

Cosmology has been also considered in this framework [235, 236]. As is well known, the Friedman equation can be deduced from semi-Newtonian physics. Thus it ensues from the above arguments as shown by reference [237]. Reference [233] has also inspired modifications to the cosmic expansion laws. The purpose of the present Chapter is to uncover the implications of such modifications. Two approaches are investigated. One set of corrections to the Friedmann equations is motivated by the possible connection of the surface terms in the gravitational action to the holographic entropy. Reference [238] noted that (at the present level of the formulation) this is equivalent to introducing sources to the continuity equations, implying non-conservation of energy. In another approach, the derivation of the Friedmann equation as an entropic force from basic thermodynamic principles is generalized by taking into account loop corrections to the entropy-area law [239]. The result is corroborated by its concordance with previous considerations [240], and is consistent with energy conservation though still lacks a covariant formulation. While it might seem preliminary to investigate in detail the predictions of these models whose foundations, at the present stage, are rather heuristic, we believe it is useful to explore their generic consequences. Knowing the possible form of viable extensions to our standard Friedmannian picture along the lines of reference [241] can shed light on the way towards more rigorous derivation of the effective entropic cosmology, and on the prospects of eventually testing these ideas by cosmological observations.

An encouraging result in this respect is that viable cosmologies in realizations of the quite different approaches we focus on, possess an identical expansion rate (in the simplest but relevant setting of a universe filled by a single fluid dominated cosmology). It is also interesting that at high curvatures this expansion rate reduces to a constant. Thus not a big bang singularity, but instead inflation is found in the past. However, we find that the higher curvature terms, motivated by quantum corrections, are not viable as they lack a consistent low-energy limit. Furthermore, we impose bounds on the unknown parameters of the models by considering the scale of inflation, big bang nucleosynthesis (BBN) and from the modified behavior of dark matter in the post-recombination universe.

Although only phenomenologically motivated, an interesting case is a monomial correction to the area-entropy law. Such can result in acceleration without dark energy with a good fit to the data. We perform a full Markov Chain Monte Carlo (MCMC) likelihood analysis

exploiting astronomical data from baryon acoustic oscillations [242], supernovae [163] and cosmic microwave background [19]. A slightly closed universe turns out to be preferred by the data, unlike in the standard ΛCDM model. We consider also the evolution of perturbations, which is determined uniquely if the Jebsen-Birkhoff law is valid. A characteristic feature is then the growth of gravitational potentials in conjunction with the modified growth of overdensities.

The surface term approach is discussed in Section 4.2. In Section 4.3 we consider the implications of a specific form of area-entropy law motivated by quantum gravity, and in Section 4.4 we explore a phenomenological power-law parametrization of this law, including a discussion on the perturbation evolution 4.5. Finally, the results we obtained are concisely summarized in Section 4.6.

4.2 Modifications from Surface Terms

Easson, Frampton and Smoot recently argued that extra terms should be added to the acceleration equation for the scale factor. This was discussed from various points of view, in particular it was conjectured that the additional terms can stem from the usually neglected surface terms in the gravitational action. Present acceleration of the universe [243] and inflation [244] were proposed to be explained by the presence of these terms without introducing new fields. This is obviously an exciting prospect warranting closer inspection.

Slightly different versions of the acceleration equation were introduced in both of the above mentioned papers. The following parametrization of the two Friedmann equations encompass all those versions and their combinations:[2]

$$H^2 = \frac{8\pi G}{3}\rho + \alpha_1 H^2 + \alpha_2 \dot{H} + 8\pi G \alpha_3 H^4 \,, \tag{4.1}$$
$$\dot{H} + H^2 = -\frac{4\pi G}{3}(1+3w)\rho + \beta_1 H^2 + \beta_2 \dot{H} + 8\pi G \beta_3 H^4 \,.$$

The six coefficients α_i, β_i are dimensionless for all $i = 1, 2, 3$. The extrinsic curvature at the surface was argued to result in $\alpha_1 = \beta_1 = 3/2\pi$ and $\alpha_2 = \beta_2 = 3/4\pi$ and quantum corrections in nonzero β_3 [243, 244]. The equations imply that

$$\frac{dH}{dN} = H\left(8\pi G c_2 H^2 - c_1\right) \,, \tag{4.2}$$

where $N = \log(a)$ is the e-folding time and

$$c_1 \equiv \frac{(3-\alpha_1)(1+w) - 2\beta_1}{2 - \alpha_2(1+3w) - 2\beta_2} \,, \tag{4.3}$$
$$c_2 = \frac{\alpha_3(1+3w) + 2\beta_3}{2 - \alpha_2(1+3w) - 2\beta_2} \,. \tag{4.4}$$

Note that c_1 is proportional to the lower order corrections, and c_2 is proportional to the higher order contributions $\sim H^4$. The information lost by having only one differential equation in (4.2) should be compensated by imposing boundary conditions from (4.1) to its solutions.

[2] We will not adress the case in which the two equations degenerate to one by a particular choice of the parameters.

In the general case of multiple fluids, the model does not uniquely determine how to the EoS (equation of state) w evolves. The reason is that the two equations (4.1) result in only one (non)conservation equation for the total density, and we have no unique prescription for how the relative densities behave if the total density consists of a mixture of fluids. From the viewpoint of reference [238], the source terms for the individual fluids are undetermined. However, the most relevant special case of a single-fluid dominated universe allows an exact solution where these ambiguities are absent.

4.2.1 Single Fluid

In the case that w is a constant, Eq.(4.2) can be easily solved:

$$H^2(a) = \frac{c_1}{8\pi G\left[c_0\left(\frac{a}{a_0}\right)^{2c_1} + c_2\right]}\,, \tag{4.5}$$

$$c_0 = \frac{1}{32\pi^2 G^2(1+w)\rho_0}\,. \tag{4.6}$$

We chose the integration constant c_0 in such a way that when the entropic corrections vanish, we recover the standard Hubble law. Although there are six unknown factors in (4.1), the cosmological implications are rather unambiguous and can be encoded in the two numbers c_1 and c_2. Thus it is both feasible and meaningful to constrain them, despite our ignorance of a theoretical prediction. From the form of H in (4.5), it is also transparent that as $a \to 0$, we have a de Sitter solution and the model indeed predicts inflation. As the scale factor grows, (nearly) standard evolution is recovered: so it is also simple to see the present versions of the model do not provide dark energy. At early times, $w = 1/3$, we can obtain constraints from BBN, and from the inflationary scale by estimating the amplitude of fluctuations. Both the scaling modification c_1 and the constant term c_2 can be bounded. At late times, $w = 0$, we can obtain constraints at least from the modified scaling law for dust, c_1. Let us first consider the early universe constraints before adding a cosmological constant to obtain the present acceleration.

Let us consider the constraints from the early universe. During radiation domination, Eq. (4.5) becomes

$$H^2 = 8\pi G\rho \frac{\frac{1}{2}c_1}{a^{2(c_1-2)} + 32\pi G^2 c_2 \rho}\,. \tag{4.7}$$

From this we see that the variation effective Newton's constant is

$$\delta G_{eff}/G \approx (\frac{1}{2}c_1 - 1)(1 - 4c_1 \log a) - 16\pi^2 G^2 c_1 c_2 \rho\,. \tag{4.8}$$

This variation can be bounded by requiring successful BBN. For instance, reference [114] derived that $\delta G_{eff} = 0.09^{+0.22}_{-0.19}$. The radiation energy density is given by

$$\rho = g_* \frac{\pi^2}{30} T^4\,, \tag{4.9}$$

where we use for the number of effective relativistic degrees of freedom g_* at the nucleosynthesis temperature $T \sim 1$ MeV the value $g_* = 10.75$. Plugging in the numbers, we obtain

$$-3.5 \cdot 10^{-3} < 2 - c_1 < 1.1 \cdot 10^{-3}\,. \tag{4.10}$$

$$-2\cdot 10^{84} < c_2 < 6\cdot 10^{84}\,. \tag{4.11}$$

Because of the tremendous hierarchy between the Planck and the BBN scale there is a very poor constraint on the high curvature corrections c_2. This can be also written as $2\sqrt{\pi G}c_2^{1/4} < 457.6\,GeV^{-1}$ by restoring the dimensions.

If inflation is considered to be driven by the entropic corrections, we can estimate their magnitude from the amplitude of perturbations observed in CMB. The amplitude of the spectrum of quantum fluctuations of massless fields is expected to be given by the ratio

$$\langle \delta\phi\delta\phi\rangle = \frac{8\pi G H^2}{\epsilon} \sim 10^{-10}\,, \tag{4.12}$$

where ϵ is the slow-roll parameter and the right hand side is determined from observations. The spectral index as determined from observations gives $\epsilon \sim \mathcal{O}(0.01)$. Since at early times equation (4.5) predicts (nearly) exponential expansion with the Hubble rate $8\pi G H^2 = c_1/c_2$, and we know that c_1 must be of order one, successful generation of observed fluctuations from entropic inflation suggest that $c_2 \sim 10^{12}$. This estimate is much more tentative than the previous, since it depends on the detailed physics of inflation.

4.2.2 Adding a Cosmological Constant

Acceleration at late times can be obtained by the addition of a Λ-term. Then (4.2) generalizes to

$$\frac{dH}{dN} = H\left(8\pi G c_2 H^2 - c_1\right) + c_3\frac{\Lambda}{H}\,, \tag{4.13}$$

$$c_3 = \frac{1+w}{2-\alpha_2(1+3w)+2\beta_2}\,, \tag{4.14}$$

and is solved by

$$H^2 = \frac{c_1}{4\pi G c_2} + \frac{\sqrt{32\pi G c_2 c_3\Lambda - c_1^2}}{16\pi G c_2}\tanh\left(\sqrt{32\pi G c_2 c_3\Lambda - c_1^2}(N-N_0)\right) \tag{4.15}$$

The form of the Friedmann equation above is completely different than in the usual case. This is due to the nonlinearity stemming from the presence of higher curvature corrections. At low curvatures, their effect does not disappear as the most naive expectation would be and the limit $c_2 \to 0$ of Eq.(4.15) is ill defined. The de Sitter solution is recovered at asymptotically late times, but the preceding evolution may not approximate standard cosmology and matter domination is lost. To cure this, we suggest removing the higher curvature corrections ($c_2 = 0$ and consider two scenarios, one with a standard cosmological constant but modified matter scaling, and another one in which matter non-conservation is absorbed by the cosmological constant, which is allowed to evolve in time.

Prescription I - Constant Λ:

In the pressence of a constant Λ term the behavior of the Hubble rate is just what is expected from Eq.(4.5). Now (4.13) is solved by

$$H^2(a) = \frac{8\pi G}{3}\rho_0 a^{-2c_1} + \frac{1}{3-\frac{2}{1+w}\beta_1}\Lambda\,. \tag{4.16}$$

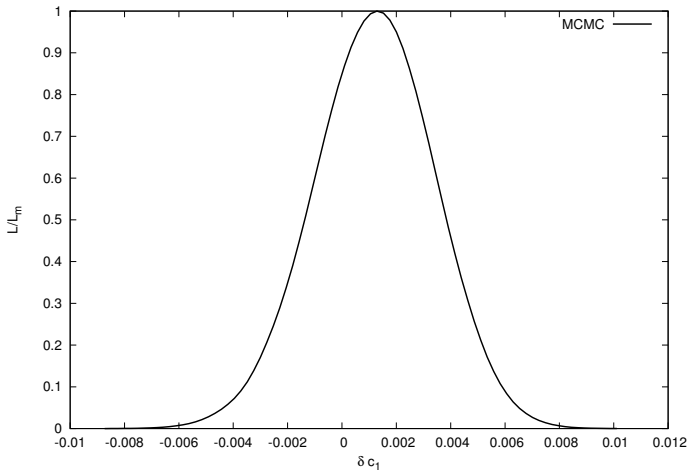

Figure 4.1: Constraints on the modified equation of state for CDM and baryons scaling law by using SNe, BAO and CMB distance priors. Radiation has been assumed to follow the usual scaling. Only very slight deviations from the usual scaling law are allowed.

The integration constant ρ_0 corresponds to the renormalised energy density at $a = 1$. Similarly, the cosmological constant is slightly "dressed". The conclusion is that the observable effect to the expansion is the modified scaling of matter density.

The modified scaling law of dark matter can be used to impose tight bounds from the late universe observations. This has been explored in reference [245], who derived constraints on the EoS for dark matter, taking into account experimental data both on the background and on the perturbations. Adopting the prescription where the Newton frame sound speed vanishes we can translate the result into our case as:

$$-8.78 \cdot 10^{-3} < 2c_1 - 3 < 1.86 \cdot 10^{-3} \,. \tag{4.17}$$

for 99.7% C.L. bounds. Reference [245] took into account the full CMB and LSS data. However, as we cannot deduce the perturbation evolution in these models unambiguously, it is useful to consider constraints ensuing solely from background expansion. It turns out that by including the latest data on SNeIa, BAO and CMB, the reached precision is only slightly lower. The result is shown in Fig. 4.1 and corresponds to the bounds

$$-17.28 \cdot 10^{-3} < 2c_1 - 3 < 20.50 \cdot 10^{-3} \,. \tag{4.18}$$

at 99.7% C.L.

Prescription II - Dynamical Λ: One can also consider the case that matter continuity equation is not violated. Then the Λ-term must be responsible for the non-conservation in a consistent system. The Hubble law can be derived analogously to the above cases and one readily finds that it now has the form

$$H^2 = \frac{8\pi G\rho}{3\left(1 + \frac{2(\alpha_1 - \beta_1)}{3(1+w)}\right)} + \Lambda_0 a^{2(\alpha_1 - \beta_1)} \,. \tag{4.19}$$

So the Λ-term acquires a dynamical behavior. In case $\alpha_1 - \beta_1 < 0$ this would help with the coincidence problems, since one could consider initial large values for Λ, which has diluted to the presently observed scale. Note that this is different from usual dark energy approach, where Λ is tuned to zero (or in any case to an even smaller than the value consistent with observations) and then a new dynamical component is added to explain the acceleration. Reference [246] has also derived this result, which can be equivalently arrived at by imposing only the second Friedmann equation in (4.1). The first one then follows by integration, and the dynamical Λ can be viewed as an integration constant.

In this scenario, the BBN constraint for the effective gravitational constant gives

$$-0.62 < \beta_1 - \alpha_1 < 0.20\,. \tag{4.20}$$

From WMAP7 measurements on the equation of state of dark energy, combined with other cosmological data [19], we obtain an even tighter bound,

$$-0.05 < \beta_1 - \alpha_1 < 0.11\,. \tag{4.21}$$

This is in qualitative agreement with reference [246], where the entropic corrections were bounded with the CMB acoustic scale.

4.3 Modifications from Quantum Corrections to the Entropy-area Law

There is evidence from string theory and from loop quantum gravity that the two leading quantum corrections to the area entropy-law are proportional to the logarithm and the inverse of the area [247, 248]. Reference [239] derived the Friedmann equation from an underlying entropic force taking into account quantum corrections to the entropy formula. We slightly generalize their final result (Equation (25) in [239]) by allowing multiple fluids (labeled i) with constant equations of state w_i and a cosmological constant, and we also allow for spatial curvature:

$$H^2 + \frac{k}{a^2} = \sum_i \left[\frac{8\pi G}{3} - \frac{8\beta(1+3w_i)G^2}{9(1+w_i)}\left(H^2+\frac{k}{a^2}\right) - \frac{2\gamma(1+3w_i)G^3}{3\pi(5+3w_i)}\left(H^2+\frac{k}{a^2}\right)^2\right]\rho_i + \frac{\Lambda}{3}\left[1 - \frac{\beta}{\pi}G(H^2+\frac{k}{a^2})\log a + \frac{\gamma}{4\pi^2}G^2(H^2+\frac{k}{a^2})^2\right]\,. \tag{4.22}$$

As seen in the previous Section, there is a problem recovering the usual evolution at low curvature if we include the high curvature correction proportional to γ. This can be seen easily also in this case. Defining the shorthand notations

$$S_\beta \equiv -\frac{8\beta G^2}{9}\sum_i \frac{1+3w_i}{1+w_i}\rho_i - \beta\frac{G\Lambda}{3\pi}\log a\,, \tag{4.23}$$

$$S_\gamma \equiv -\frac{2\gamma G^2}{3\pi}\sum_i \frac{1+3w_i}{5+3w_i}\rho_i + \gamma\frac{G\Lambda}{12\pi^2}\,, \tag{4.24}$$

the solutions for the Hubble rate may be written as

$$H^2 + \frac{k}{a^2} = \frac{1-S_\beta}{2GS_\gamma} \pm \frac{\sqrt{1-12\pi G^2\rho S_\gamma}}{2GS_\gamma}\,, \tag{4.25}$$

where the total matter density is denoted by $\rho = \sum \rho_i$. It is obvious that in the limit where the corrections tend to zero, we do not recover standard cosmological evolution. Thus the higher order corrections here suffer from a similar problem as we encountered in the previous Section.

Therefore we set $\gamma = 0$ and consider only effect of the leading logarithm correction to the entropy, proportional to β . The solution for the Hubble rate can then be written as, neglecting the cosmological constant,

$$H^2 + \frac{k}{a^2} = \frac{8\pi G}{3}\rho \left[1 + \frac{8\beta G^2}{9}\sum_i \left(\frac{1+3w_i}{1+w_i}\right)\rho_i\right]^{-1} . \tag{4.26}$$

Thus, the corrections occur near the Planck scale. If β is large enough this can support inflation since the RHS tends to a constant when matter is relativistic and $w_i = 1/3$ for all species i. Again, we can constrain this from the effective G at BBN. It is interesting to note that the form of the entropic Friedmann equation assumes the same form as in the previous Section, where the derivation was quite different, the underlying physical assumptions leading to a (non-)conservation and apparently different form of the force law.

From (4.26), the effective variation of the Newton's constant is now given by

$$\delta G_N/G = \frac{1}{1 + \frac{4\beta G^2}{3}\rho_{BBN}} - 1 \approx -\frac{4}{3}\beta G^2 \rho\,. \tag{4.27}$$

Using (4.9) for the radiation density at nucleosynthesis and proceeding analogously to Section 4.2.1, we find that the BBN bound on the magnitude constant β is $|\beta| \lesssim 2.7 \cdot 10^{35}$, translating to

$$|\sqrt{8\pi G\beta}| < 0.0042 \quad 1/GeV\,. \tag{4.28}$$

Again it is clear that BBN is not efficient to constrain the corrections. Furthermore, since the scale of inflation is below the Planck scale, we have to consider very large values of β. However, from considerations of loop quantum gravity and string theory the natural value for β is of order one. Considering such values, inflation takes place at the Planck scale, where we cannot trust the perturbatively entropy-area law, expected to hold only at the limit of large horizon size.

4.4 Dark Energy from a Generalized Entropy-area Law

In the following we consider the possibility of infrared modifications to the large-scale behavior of gravity. Such can ensue from corrections to the $S \sim A$ relation that grow faster than A. Among such is the volume correction that scales as $\sim A^{3/2}$. Interestingly, corrections of this type imply, within the entropic interpretation of gravity, a modified Newton's law which may explain the galactic rotation curves without resorting to dark matter [249]. This motivates us to study whether we may generate modified gravity at the largest scales in such a way that we would avoid the introduction of dark energy field or a cosmological constant.

For this purpose, we consider the area-entropy law of the form

$$S = \frac{A}{4\ell_P^2} + s(A)\,, \tag{4.29}$$

where the function $s(A)$ represents the quantum corrections and $\ell_P^2 = G\hbar/c^3$. We assume that $A = QN$, where Q is a constant to be determined, and that the entropy changes by one fundamental unit (corresponding to unit change in the number of bits on the screen with radius R) when $\Delta r = \eta\hbar/(mc)$, r being the comoving radial coordinate. Then the first law of thermodynamics together with the equipartition of energy leads to the modified Newtonian law of gravitation[3]

$$F = -\frac{Q^2 c^3 Mm}{2\pi k_B \hbar \eta R^2}\left(\frac{1}{\ell_P^2} + \frac{\partial s}{\partial A}\right) = -\frac{GMm}{R^2}\left(1 + 4\ell_P^2 \frac{\partial s}{\partial A}\right), \tag{4.30}$$

where in the second equality we made the identification $Q^2 = 8\pi k_B \eta \ell_P^4$. Let us further assume the power-law correction

$$s(A) = \frac{4\pi\sigma}{n}\left(\frac{ar}{\ell_P}\right)^{2n} \sim A^n\,. \tag{4.31}$$

This type of parametrization for entropic gravity effects has been recently considered by other authors [251]. Taking into account that in the cosmological context the active gravitational mass is given by the Tolman-Komar mass ($M = \frac{4\pi}{3}(\rho + 3p)a^3 r^3$ for a FRW metric), and that the $R = ar = 1/\sqrt{H^2 + k/a^2}$, we obtain the Friedmann equation

$$H^2 + \frac{k}{a^2} = \frac{8\pi G}{3}\sum_i \left[1 + \sigma\frac{(1+3w_i)}{1+3w_i-2n}\left(\frac{1}{\ell_P^2(H^2+\frac{k}{a^2})}\right)^{n-1}\right]\rho_i\,. \tag{4.32}$$

Not surprisingly, the possible infrared corrections, $n > 1$, are precisely those which could be significant in cosmology at late times. The nonperturbative form of $s(A)$ is of course is unknown, but the volume correction is known to be given by $n = 3/2$, so $n > 1$ is not something to exclude a priori.

In the spatially flat case, if the energy density is dominated by a fluid with the EoS w and the corrections dominate over the standard term in (4.32), the expansion is described by the effective EoS

$$w_{eff} = \frac{1+w}{n} - 1\,. \tag{4.33}$$

Thus a matter dominated universe accelerates given $n > 3$. With larger n, the effective EoS is more negative, but phantom expansion can be achieved only when w is itself negative. The exact evolution of w_{eff} including the effects of possible spatial curvature is shown in Figure 4.2.

In order to obtain the bounds on the parameters arising from the modified Friedmann equation, a suitably modified version of CMBeasy [252] was employed together with a MCMC code, taking into account astronomical data from baryon acoustic oscillations [242], supernovae [163] and cosmic microwave background [19]. The results are displayed in Figure 4.3 and Table 4.1. Due to the geometric nature of the modifications, a possible curvature of the spatial Sections was allowed. This revealed a preference towards slightly closed universes,

[3] In Ref.[250] it was instead assumed that the number of bits is directly proportional to entropy, which is not compatible with our assumption $A = QN$. From the former assumption follows instead $F = -GMm/(R^2 + \ell_P^2 s(A)/\pi)$.

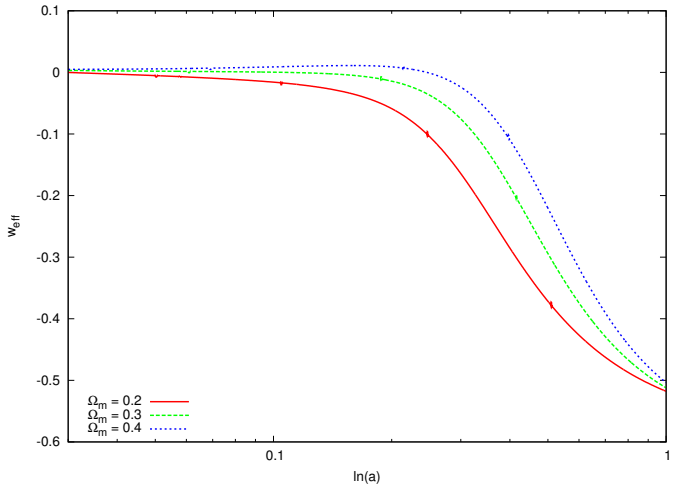

Figure 4.2: Effective equation of state for the generalized entropy-area law DE. The lines correspond to an open, flat and closed universe with $\Omega_S = 0.7$ and $n = 2.5$. Equation (4.33) would give $w = -0.6$ for this case.

	All	BAO	CMB	SNe
h	0.68 ± 0.02	–	0.58 ± 0.06	–
n	3.8 ± 0.7	> 2.9	–	> 3.0
Ω_S	0.69 ± 0.02	–	0.71 ± 0.12	0.76 ± 0.21
Ω_m	0.29 ± 0.02	0.27 ± 0.05	0.33 ± 0.13	0.39 ± 0.10
Ω_k	0.012 ± 0.005	–	-0.04 ± 0.05	-0.16 ± 0.24

Table 4.1: Maximum likelihood values and 1 sigma error bars from the constraints of Section 4.4. Note that $\Omega_k = 1 - \Omega_s - \Omega_m$ is a derived parameter.

which might be due to the appearance of k in the r.h.s. of (4.32). Relatively lower values of n are favoured with respect to higher ones because higher values reproduce a total equation of state which is too close to -1. Note also the existence of degeneracies in the individual datasets, which are broken by the combined constraints.

Table 4.2 shows the results of model comparison with ΛCDM including the Bayesian and the Akaike criteria given by $-2 \log L_{max} + p \log d$ and $-2 \log L_{max} + 2p$ respectively, with p the number of free parameters and d the number of experimental data points. Eventhough a cosmological constant is favoured in all cases, the values of χ^2 are very similar and most of the difference in these cases is due to the additional parameter n in the entropy-corrected model.

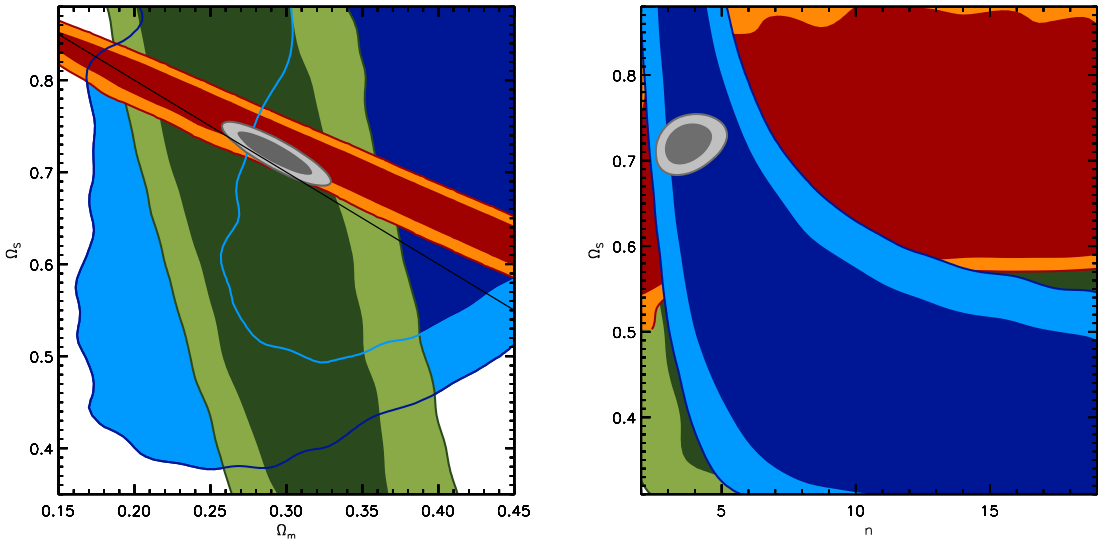

Figure 4.3: Bounds on parameters for the generalized area-entropy law DE using Sne (blue), CMB (orange), BAO (green) and the three combined datasets (gray). Note that closed universes ($\Omega_m + \Omega_S > 1$) are slightly preferred in this model. Entropic corrections gave $\chi^2_S = 533.28$, slightly higher than the value obtained for a similar MCMC for ΛCDM with $\chi^2_\Lambda = 532.34$.

	$S(A)$	Λ
χ^2	533.28	532.34
$\chi^2/d.o.f$	0.956	0.952
Bayesian	558.61	551.31
Akaike	541.28	538.32

Table 4.2: Model comparison according to different criteria.

4.5 On the Evolution of Perturbations

Lue, Roman Scoccimarro and Starkman [253] have shown that by assuming the Jebsen-Birkhoff theorem [254] it is possible to deduce the evolution of the spherical overdensities in a dust-filled universe given the background evolution. It is not clear to us whether the entropic gravity obeys the Jebsen-Birkhoff theorem. Therefore we did not include the constraints from perturbations into the likelihood analysis of Section 4.4.

We will take this approach, which was first developed to study DGP and related models, as a first approximation to gain insight into the clustering of matter in entropic cosmology. The perturbation evolution equation can be derived by tracking the surface of a star in a Schwarzchild metric embedded in the background of FRW, where the expansion is given by some gravity theory deviating from Einstein's GR. At linear order, the density contrast evolves as

$$\ddot{\delta} + 2H\dot{\delta} = \left(2\dot{H} + \frac{\ddot{H}}{H}\right)\delta\,. \tag{4.34}$$

If the same background expansion is due to a smooth dark energy component, the growth of perturbations is governed by

$$\ddot{\delta} + 2H\dot{\delta} = 4\pi G\rho_M\delta\,. \tag{4.35}$$

The difference is thus only the source term in the RHS of Eq.(4.34) due to the clumpiness of the effective fluid, whereas with smooth dark energy only the matter density acts as a gravitational source in the RHS of (4.35). This also determines the behavior of the metric perturbations, which can be probed by various observations, in particular weak lensing and ISW. Following reference [253] one may then find that

$$\frac{\nabla^2}{a^2}\Phi = \dot{H}\delta\,, \tag{4.36}$$

$$\frac{\nabla^2}{a^2}\Psi = -\left(2\dot{H} + \frac{\ddot{H}}{H}\right)\delta\,, \tag{4.37}$$

showing that the entropic corrections can source the temporal and spatial potentials differently, similarly to the effect of anisotropic stress. This is an interesting prediction as it allows to distinguish the possible entropic origin of acceleration from other dark energy models (e.g. quintessence).

As an example, we consider the power-law parametrization (4.31) presented in the previous Section. The growth rate f of the perturbations can be defined as

$$f \equiv \frac{d\log\delta}{d\log a}\,. \tag{4.38}$$

Asymptotically, when the effective EoS is given by (4.33), the growing solution to the evolution equation (4.34) correspond to growth rate

$$f = \frac{3}{2n}\,, \tag{4.39}$$

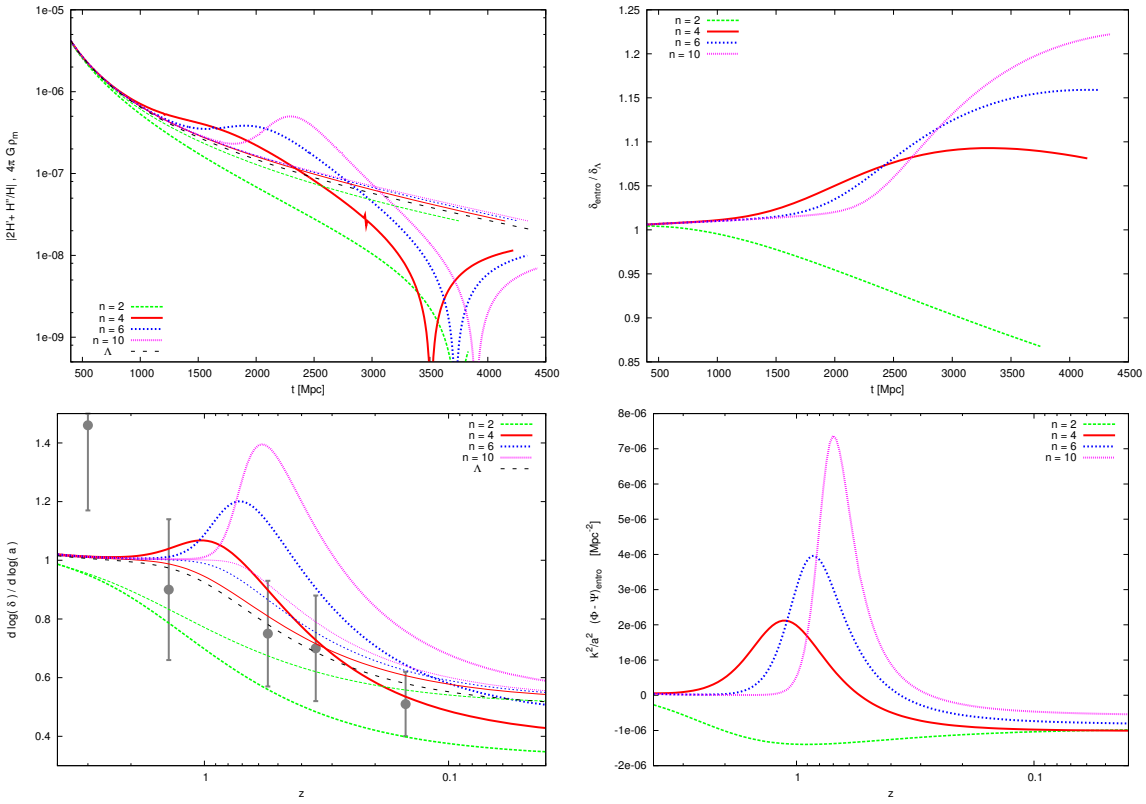

Figure 4.4: Growth of structure in entropic cosmologies. **Top left:** Coefficient of δ in the r.h.s of (4.34) (thick lines) and (4.35) (thin lines) for some values of n. **Top right:** Time evolution of δ normalized to the ΛCDM value. **Bottom left:** Evolution of the growth factor (4.38) obtained using the modified equation (4.34) (thick lines) and the usual one (4.35) (thin lines). Data points correspond to Table 1 in Ref. [132]. **Bottom right:** Anisotropic stress caused by the modified gravitational potentials (4.36,4.37). All lines correspond to flat universes with $\Omega_m = 0.3$, $\Omega_S = 0.7$.

which dominates at late times if $n > 9/4$.[4] As n increases, the decay of perturbations becomes less rapid, and when $n \to \infty$, the background is de Sitter and the matter density is frozen. In dark energy cosmologies described by (4.35), the solution with growing δ is absent and the transition behavior, which is relevant to observations, is different. The growing solution (4.39) corresponds asymptotically to $\Phi, \Psi \sim a^p$, where $p = 2 - 9/(2n)$ if $0 < n < 9/4$ and $p = 0$ if $n > 9/4$. Thus we expect that the gravitational potentials will tend asymptotically to a constant value if the present acceleration stems from entropic nature of gravity.

Numerical solutions for the full evolution of perturbations (4.34, 4.36, 4.37) are plotted in Figure 4.4. Table 4.3 shows the numerical values of the growth factor (4.38) at $a = 1$ and 50, together with the limit previously described. Discrepancies occur for the cases with low n, which have less negative e.o.s. and need longer time to reach the limit. The growth of

[4]The other solution $f = 3/n - 2$ is a decaying mode for the observationally allowed values of n, See Table 4.2.

n	$a=1$	$a=50$	$a\to\infty$
2	0.326	-0.374	-0.5
4	0.390	-0.359	-0.375
6	0.460	-0.246	-0.25
10	0.533	-0.149	-0.15

Table 4.3: Numerical and asymptotic values of the growth factor f.

inhomogeneities can be enhanced or damped depending on the value of n. The weakening of gravity responsible for the acceleration is reflected on smaller scales in the lower value of the r.h.s. factor of (4.34) responsible for gravitational instability. However, that term can become larger than $4\pi G\rho_m$ around the beginning of the acceleration due to the variation of H through its time derivatives.[5] This effect can easily overcome the weakening of gravity if n is large enough (more pronounced transition), leading to higher values of δ. The enhancement effect is also responsible for the resulting anisotropic stress due to the same factors appearing in (4.34) and in (4.37).

4.6 Discussion

Rather than trying to guess the fundamental underlying mechanism describing the microstructure of space time, this Chapter has described some approaches to address simple models of modified gravity inspired by the entropic gravity proposal. These models were argued to introduce parametric modifications of the Friedmann equations, which can have been constrained through their effects on the universe expansion at early and late times

We found that the higher order curvature corrections, motivated by quantum effects, lead to an inflationary graceful exit problem and thus can be excluded, at least in the simplest scenarios. In the surface term approach of Section 4.2, we identified the parameter combinations (4.3) that can be constrained by observations. There c_1 quantifies the lower order and c_2 the higher order contributions. We obtained

$$-17.28\cdot 10^{-3} < 2c_1 - 3 < 20.50\cdot 10^{-3}\,,$$
$$\sqrt{|8\pi G c_2|} < 0.02 \quad 1/GeV\,.$$

from late and early universe constraints, respectively. It was also observed that in two quite different approaches, the higher order corrections lead to a similar expansion law that predicts inflation in the early universe. However, the introduction of a cosmological constant changes the character of the Friedmann equation changes and matter domination is severely modified if $\Lambda, c_2 \neq 0$ simultaneously. In an alternative prescription assuming $c_2 = 0$ and retaining the cosmological matter conservation laws, an estimate for the parameters can be given as

$$\beta_1 - \alpha_1 = 0.02 \pm 0.08\,. \tag{4.40}$$

[5] Ref. [253] argue that slower growth of inhomogeneities follow from the acceleration condition. However, they consider a Friedmann equation which is locally $H^2 \sim \rho^n$ which is inequivalent to (4.32).

In the quantum corrected approach discussed in Section 4.3, the leading logarithm correction to the entropy-area relation was shown to be constrained by BBN in a similar way, and the following inverse area correction was the cause of the graceful exit problem.

In addition, we studied a phenomenological power-law correction to the entropy formula. The addition of a term $\propto A^n$ can produce accelerating expansion in the late universe for certain values of n. Combining the available data to bound the power of the correction, we obtained

$$n = 3.8 \pm 0.7\,. \tag{4.41}$$

We may go significantly further if the evolution of spherical metrics can be argued to depend only on the amount of enclosed matter, as it is the case within General Relativity. Then the features of linearized structure are captured by the three equations (4.34,4.36,4.37), which predict a growth factor and evolution of the gravitational potentials that is different from the general relativistic case.

The origin of the thermodynamical properties of space-time remains mysterious. Even in that case, simple modified theories of gravity based on the entropic gravity proposal can be motivated, constructed and explored to a certain extent using cosmological information. Certain modifications, such as postulating a different entropy-area law can provide mechanisms for dark energy and generically have observable consequences, although there are a number of assumptions that are necessary to extract predictions from the theory. The study of background evolution and comparison with geometrical probes was possible by deriving Friedmann equations from the Newtonian force. Similarly, a prescription for the growth of structure could be obtained only after assuming the Jebsen-Birkhoff theorem. Although these methods are valid for General Relativity, there is no guarantee that they will remain correct in more general theories, and the lack of a complete formulation makes it difficult to check these assumptions, if possible at all. Eventually, a wholesome approach to describe the space-time degrees of freedom would be necessary to properly address the full set of predictions. Only this may ultimately validate or rule out the concept of entropic gravity and its possible variations.

Chapter 5

Standard Matter and Scalar Fields: Disformal Quintessence

You can't just have stuff that is free and escapist, you have to have stuff that is confrontational as well. You need stuff that is mystical but you need the realism too.

Irvine Welsh[1]

Cosmological observations reveal that a mysterious constituent with negative pressure, so called Dark Energy (DE), accounts for about 70% percent of today's mass energy budget and is causing the expansion of the universe to accelerate [19]. A major challenge in present day cosmology is to discover the physical nature of Dark Energy. The quest to find its precise nature, whether as an exotic field or a modification of General Relativity, is ongoing and many possibilities have been explored [9, 25]. The phenomenologically simplest Cosmological Constant is however theoretically problematic [23]. Quintessence provides a dynamical alternative to the static cosmological constant. It can track the background energy density, more naturally resulting in similar orders of magnitude for the Dark Energy and matter energy densities today. However, some mechanism is necessary to end the scaling era and initiate the acceleration. Several possibilities have been considered, such as introducing a suitable bump in the potential [255], coupling the field to the Gauss-Bonnet term [256, 257], coupling the field to other matter components [49, 258], considering non-canonical Lagrangians [259], or introducing several scalar fields [260]. In the following, a disformal relation [62] is applied for this purpose.

Disformal relations have frequently appeared in gravitational theories alternative to dark matter, such as TeVeS [60] or other covariant Modified Newtonian Dynamics formulations [261]. This is necessary to produce gravitational lensing, as light has then to propagate on a

[1] Interview by Alan Black for 3:AM Magazine, 2004

different causal structure than gravity. Disformal relations have also been used to construct inflationary models [69], and are indeed the key to varying speed of light theories that attempt to solve the horizon problem [262, 263]. They generalize the conformal transformations (i.e. local rescalings of the metric), which are well known and have a number of applications, such as relating the simplest scalar-tensor theories to General Relativity with a scalar field entering the matter sector [264]. One can then consider the features of the more general transformation as a model building tool and to examine extended sets of relations between different theories (cf. Chapter 6).

Here a preliminary step is made by exploring one of the simplest possible scenarios: a canonical scalar field self-coupled through a disformal metric. This allows us to uncover many relations between seemingly disconnected Dark Energy models. If only the potential term is considered, one recovers a tachyon or a Chaplygin gas. When the kinetic term is included, some other previously considered models can be recovered in certain limits, as we will discuss in Section 5.1. The rest of the Chapter is devoted to the study of a simple possibility, disformal quintessence, which can act as a viable DE model. Section 5.2 is devoted to study of this model, and contains the main results regarding cosmology. We describe in detail the background evolution of this model in Section 5.2.1. Particular attention is given to the transition mechanism that provides an exit from the scaling era. The details of this transition depend on the two parameters of the model, and thus they can be constrained by cosmological data. The evolution of perturbations is considered in Section 5.2.2 in order to compute the CMB and matter power spectra. Armed with these solutions,a Markov Chain Monte Carlo analysis of the model is performed in Section 5.2.3, combining different geometric and dynamical data. A broad range of the parameter space is found to be compatible with observations, but the region corresponding to a shallow slope of the exponential potential or the disformal factor can be observationally excluded. The model is discussed in Section 5.3.

5.1 Dark Energy from the Disformal Relation

A generic scalar field Lagrangian minimally coupled to gravity is a function of two variables,

$$\mathcal{L} = \mathcal{L}(\phi, X)\,. \tag{5.1}$$

It can be expanded as a series in the kinetic term $X = -\frac{1}{2}g^{\mu\nu}\phi_{,\mu}\phi_{,\nu}$

$$\mathcal{L} = \mathcal{L}(\phi,0) + \mathcal{L}_{,X}(\phi,0)X + \frac{1}{2}\mathcal{L}_{,XX}(\phi,0)X^2 + \dots \tag{5.2}$$

The first term corresponds to the potential and the second term equals one if canonically normalized. The coefficient of the third term has units $1/M^2$ and is suppressed by a factor $(H/M)^2$ for cosmological applications. Unless the prefactor is huge, this term is negligible in the late universe, and a canonical scalar field should be an adequate description of almost any natural case. However, this can be avoided if $\mathcal{L}$ is chosen such that the coefficients in the formal series (5.2) are suitably amplified, e.g. by their dependence on the field.

Let us consider the following generalization of the conformal transformation

$$\bar{g}_{\mu\nu} = A(\phi)g_{\mu\nu} + B(\phi)\phi_{,\mu}\phi_{,\nu} \tag{5.3}$$

defined by a scalar field ϕ. Equation (5.3) constitutes the most general relation between metrics that preserves causality and covariance and is defined through ϕ and its first derivatives

only [62]. Note that the relation (5.3) becomes meaningful only after we have specified the coupling to gravity. Here it will be considered that the gravitational sector is given by the Einstein-Hilbert term of the unbarred metric, and matter couples to the unbarred metric as well.

Throughout the present Chapter, quantities computed or constructed using the metric (5.3) are denoted "barred" or "disformal". Quantities constructed using $g_{\mu\nu}$ are denoted as "unbarred", and do not depend on the scalar field. The dependence on the scalar field will be also omitted from the conformal and disformal factor $A, B \equiv A(\phi), B(\phi)$.

5.1.1 Disformal Dark Energy

The simplest theory where (5.3) appears to be relevant is

$$S_{\bar{\Lambda}} = -\int d^4x\sqrt{-\bar{g}}\Lambda = -\int d^4x\sqrt{-g}A^{3/2}\sqrt{A-2BX}\Lambda\,, \tag{5.4}$$

where the relation between the metric determinants (5.11) has been used. Thus the cosmological term of a disformal metric is a tachyon in a constant potential. Computation of the energy-momentum tensor (C.2) w.r.t. the unbarred metric reveals that $\rho = A^{5/2}\frac{\Lambda}{\sqrt{A-2BX}}$ and $p = A^{3/2}\Lambda\sqrt{A-2BX}$. The above action therefore corresponds to a cosmic component obeying the equation of state

$$p = -A^4(\phi)\frac{\Lambda^2}{\rho}\,. \tag{5.5}$$

If the conformal factor A is constant, the equation of state (5.5) corresponds to Chaplygin gas, which has been applied in cosmology in attempts to unify dark matter and Dark Energy [265]. Our result shows that this rather exotic fluid can be obtained in an extremely simple way from a cosmological constant term by taking into account a possible disformal relation to the gravitational metric.

The Λ term describes the potential of the tachyon, and therefore it seems reasonable to consider it as a field dependent term $V(\phi)$. A straightforward generalization of this scheme is to include also a kinetic term. In the case of canonical kinetic term we obtain the model

$$S_\phi = \int d^4x\sqrt{-\bar{g}}\left(\frac{\varepsilon}{2}\bar{g}^{\mu\nu}\phi_{,\mu}\phi_{,\nu} - V(\phi)\right). \tag{5.6}$$

The sign of the kinetic term ε is kept arbitrary, as it does not complicate the analysis. The case $\varepsilon = 1$ was considered in [266] as a variation of the quintessence scenario. The effect of the disformal relation is then to end the scaling era and begin the accelerated expansion. The canonical field in the disformal metric assumes the rather unappealing form in terms of the unbarred metric

$$\mathcal{L}_\phi = A^{\frac{3}{2}}\left(\frac{\varepsilon X}{\sqrt{A-2BX}} + \sqrt{A-2BX}V(\phi)\right). \tag{5.7}$$

For a derivation of this expression and a variation of the model, see Section 5.1.2. Then, expansion in the kinetic energy follows

$$\begin{aligned}\mathcal{L}_\phi = &-A^2V - AX(\varepsilon - BV) - \frac{1}{2}BX^2(2\varepsilon - BV) \\ &- \frac{B^2X^3}{2A}(3\varepsilon - BV) + \frac{5B^3X^4}{4A^2}(2\varepsilon - BV) + \cdots\end{aligned} \tag{5.8}$$

ε	$B(\phi)$	$V(\phi)$	Model	Remarks
0	0	Λ	Cosmological constant	$w = -1$
1	0	$V(\phi)$	Quintessence	$w > -1$, [41, 42]
-1	0	$V(\phi)$	Phantom quintessence	$w < -1$, [267]
0	> 0	$\pm\Lambda$	(Anti-)Chaplygin gas	Eq. 5.4, [265]
0	1	$V(\phi)$	Tachyon condensate	[268, 269]
-1	$A(\phi)$	0	K-essence‡	$A = B$, [259, 270]
-1	$e^{\beta\phi}$	0	Dilatonic ghost‡	[271]
-1	-	-	Disformal phantom	
1	> 0	$V(\phi)$	Disformal quintessence	[266], Section 5.2

‡ Assuming that the expansion (5.8) is consistent to second order in X. The equivalence is at the level of the Lagrangian rather than dynamically, when the solutions to the equations are considered.

Table 5.1: Disformal Dark Energy models obtained from the action (5.6). The first three models do not use a disformal transformation. The second set contains examples which have been thoroughly studied in the literature. Disformal quintessence will be considered further in this work, while the phantom version is left for further studies. All models are purely disformal ($A = 1$) unless explicitly mentioned. A modification to obtain further variations is briefly discussed in subsection 5.1.2.

Due to the form of the expansion, all terms after first order in X are of the form $X^n B^{n-1} A^{2-n} [p_n \varepsilon - q_n BV]$ with p_n, q_n rational numbers. The argument following (5.2) can be circumvented if the coefficients are adequately enhanced so that the expansion is not valid anymore. One possibility is to choose an exponential form for the disformal function B with $A = 1$.

As it has been shown, the disformal relation has a very simple connection with the Chaplygin gas. It turns out that the theory given by (5.6,5.7) can encompass a broad range of Dark Energy models with non-minimal kinetic term through different choices of ε, B, V and A. Some variations are shown in Table 5.1. Since it contains derivatives of ϕ, the inclusion of the disformal metric $\bar{g}_{\mu\nu}$ makes the scalar field dynamical even in the absence of a canonical kinetic term. Disformal quintessence will be discussed in depth in section 5.2.

5.1.2 A Variation of the Model

By contraction with (5.3), the inverse disformal metric can be shown to be

$$\bar{g}^{\mu\nu} = \frac{1}{A}\left(g^{\mu\nu} - \frac{B}{A - 2BX}\phi^{,\mu}\phi^{,\nu}\right) . \tag{5.9}$$

Then we see that

$$\bar{X} = \frac{X}{A - 2BX} . \tag{5.10}$$

The determinant of the disformal metric is (for a method to obtain the result see Appendix C of Ref.[60])

$$\sqrt{-\bar{g}} = A^2\sqrt{1-2\frac{B}{A}X}\sqrt{-g}\,. \tag{5.11}$$

Using these formulas the form (5.7) follows immediately.

One may also consider an alternative prescription for the canonical field (5.6). The kinetic term is written there is terms of the inverse metric as $\bar{X} = -\frac{1}{2}\bar{g}^{\mu\nu}\phi_{,\mu}\phi_{,\nu}$. The alternative formulation employs the metric in the combination $\hat{X} = -\frac{1}{2}\bar{g}_{\mu\nu}\phi^{,\mu}\phi^{,\nu}$. This is a consistent but not the minimal prescription, since depending on the viewpoint, it is equivalent to 1) mixing the two metrics (since the derivative indices in (5.11) are raised with the unbarred metric), considering non-canonical field (as the unbarred metric can be barred by introducing field combinations) or defining the kinetic energy in terms of differentials with respect to one-forms (and not the coordinate vector as usually). Now $\hat{X} = X(1-2BX)$, and in terms of the matter metric, this Lagrangian corresponding to this model is

$$\hat{\mathcal{L}}_\phi = A^{\frac{3}{2}}\sqrt{A-2BX}\,[X(1-2BX)-V(\phi)]\,. \tag{5.12}$$

We shall not consider this variation further here.

5.2 Disformal Quintessence

We will now explore the model given by action (5.6) and (5.7) with $\varepsilon = 1$. For the sake of simplicity, we will restrict to the purely disformal case $A = 1$. The dynamical equations derived in 5.2.1 and 5.2.2 hold for any choice of B and V, but we will rather focus on an exponential dependence

$$B = M_p^{-4}\, e^{\beta(\phi+\phi_x)/M_p}\,, \tag{5.13}$$

$$V = M_p^4\, e^{-\alpha\phi/M_p}\,, \tag{5.14}$$

for concreteness. The model parameters are chosen so that at early times the disformal features are negligible and the field behaves as normal quintessence. The form for V ensures the existence of scaling solutions in this regime if $\alpha > 2$ [272]. The exponential form for B allows the disformal features to become relevant without introducing a new scale.

5.2.1 Background Evolution

For a flat FRW metric, the energy and density pressure in the Einstein frame read [266]

$$\rho = \frac{1}{\sqrt{\mathcal{L}}}\Big(\varepsilon\frac{\dot{\phi}^2}{2\mathcal{L}} + V\Big) \tag{5.15}$$

$$p = \sqrt{\mathcal{L}}\Big(\varepsilon\frac{\dot{\phi}^2}{2\mathcal{L}} - V\Big) \tag{5.16}$$

where the *lapse function*

$$\mathcal{L} \equiv \frac{\bar{g}_{00}}{g_0 0} = 1 - B\dot{\phi}^2\,, \tag{5.17}$$

measures the relative time flow in the barred metric (5.3) relative to the unbarred one.[2] The *disformal factor*

$$\mathcal{D} = B\dot{\phi}^2 \,, \tag{5.18}$$

is a measurement of the deviation with respect to canonical quintessence.

The field equation can be written in a form analogous to a single harmonic oscillator with coefficients that depend on $\phi, \dot{\phi}$

$$\ddot{\phi} + 3\frac{\mathcal{F}}{\mathcal{M}}H\dot{\phi} + \frac{\mathcal{P}}{\mathcal{M}} = 0 \,. \tag{5.19}$$

The analogs of mass, friction and potential terms can be written in terms of the disformal factor and the lapse as

$$\mathcal{M} = \varepsilon(1 + \frac{1}{2}\mathcal{D}) + \mathcal{L}BV \,, \tag{5.20}$$

$$\mathcal{F} = \mathcal{L}[\varepsilon(1 - \frac{1}{2}\mathcal{D}) + \mathcal{L}BV] \,, \tag{5.21}$$

$$\mathcal{P} = [\varepsilon\frac{3}{4}\dot{\phi}^2 + \frac{1}{2}\mathcal{L}V]B_{,\phi}\dot{\phi}^2 + \mathcal{L}^2 V_{,\phi} \,. \tag{5.22}$$

In addition to the disformal factor (5.18) and the lapse (5.17), the dimensionless *disformal-potential factor* BV offers yet another quantitative estimate of the disformal properties

$$BV = e^{[(\beta-\alpha)\phi + \beta\phi_x]/M_p} \,. \tag{5.23}$$

We assume that the field has reached the tracking solution with before the time of Big Bang Nucleosynthesis. Then the field contributes a constant fraction of the energy density (Early Dark Energy) which depends on the effective equation of state w and the slope of the exponential potential α [9]

$$\Omega_{\rm ede} = \frac{3}{\gamma^2}(1 + w) \,. \tag{5.24}$$

This behavior lasts while $\mathcal{D} \ll 1$ and $BV \ll 1$. If the field is tracking the matter density and $\mathcal{D} \approx 0$, then $V \sim \frac{1}{2}\dot{\phi}^2$ and both conditions hold simultaneously. The disformal factor evolves as

$$B\dot{\phi}^2 = 2^{\frac{\beta}{\alpha}}\left[\Omega_\phi \rho M_p^{-4}\right]^{1-\frac{\beta}{\alpha}} \propto a^{3(1-\frac{\beta}{\alpha})} \,, \tag{5.25}$$

and will be a growing function of time only if $\beta > \alpha$, a condition necessary to push the field out of the attractor. The parameter ϕ_x produces a shift in the transition time and hence Ω_ϕ is a monotonous growing function of it. In the following we will discuss the model in terms of α, β and Ω_ϕ.

When the disformal factor $B\dot{\phi}^2$ becomes of order one, the time slows down in the unbarred metric $\bar{g}_{00} = -1 + B\dot{\phi}^2$ (in which ϕ lives), and the field is pushed towards a slow roll phase (as seen in the unbarred metric). This causes the equation of state to become negative and source the acceleration of the universe. Figure 5.1 displays the effects of the transition in w_ϕ for different values of β/α. High values lead to a rapid slow down of the field and a more negative equation of state while low values are associated with gradual

[2] The lapse function defined here is different than the one appearing in the ADM formalism in General Relativity [273].

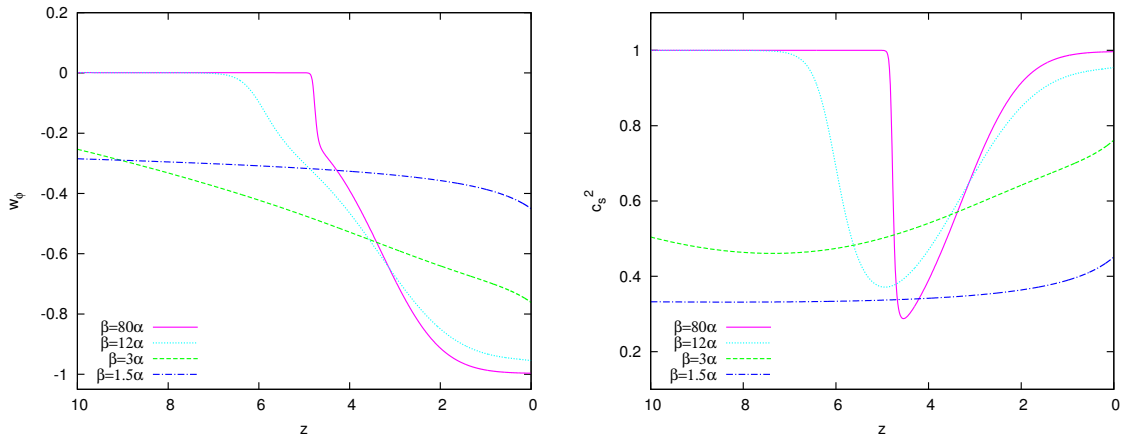

Figure 5.1: Disformal quintessence dependence on β/α as a function of redshift ($\alpha = 10$ and $\Omega_\phi = 0.7$). **Left:** Equation of state for the field. Higher values of β/α produce sharper transitions while low values lead to smoother ones.. **Right:** Speed of sound squared (see section 5.2.2), equivalent to $\mathcal{F}/\mathcal{M} \approx 1 - \mathcal{D}$.

and longer transitions in which the field preserves a significant velocity at later times. The evolution of the disformal factor is similar regardless of the parameters, but becomes more clear for higher values of β/α (See Figure 5.2). The transition is associated with a maximum and a rapid fall towards a certain value, followed by a slower reduction. The existence of a maximum follows from the role of $\mathcal{D}$ in the disformal metric, which implies that $\mathcal{D} < 1$ at any time. Otherwise the metric would run into a singularity and many quantities would blow up, notoriously the energy density (5.15). Hence a slow down of the field is therefore expected whenever $\mathcal{D}$ approaches unity.

No similar bound can be put on the potential disformal factor, which grows exponentially with ϕ and can overcome the small velocity and reach large values after the freeze out. It can be seen how the change of slope in BV roughly corresponds to the transition due to the slow down of the field. This factor represents the dominant contribution to $\mathcal{M}$, increasing the inertia term in the field equation 5.19. Despite the disformal factor is restored to very small values after the transition, the dynamics of the field remain affected by the large value of BV.

If $\beta \ll \alpha$, the disformal factor is much smaller than one, except for some interval around the freeze-out transition. An expansion to first order in $\mathcal{D}$ can be hence used to gain some intuition about the model. Let us regard the terms in (5.19) in the light of this expansion. For the friction term we get a simple correction with respect to the usual quintessence case ($\mathcal{F}/\mathcal{M} = 1$)

$$\frac{\mathcal{F}}{\mathcal{M}} = 1 - \mathcal{D} + \mathcal{O}(\mathcal{D}^2)\,. \tag{5.26}$$

Taking into account the exponential dependence on the field, the expansion of the potential

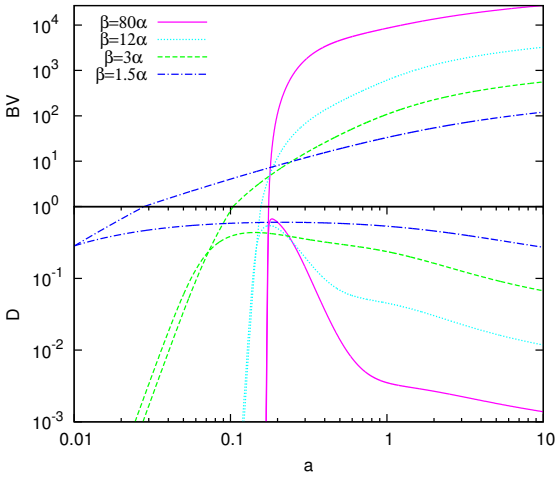

Figure 5.2: Disformal functions $\mathcal{D}$, BV for different β/α as a function of the scale factor ($\alpha = 10$ and $\Omega_\phi = 0.7$). Before the transition both lines evolve together. The disformal factor $\mathcal{D} < 1$ corresponds to the lower lines. The bounce avoids a metric singularity in (5.3). The disformal-potential term BV corresponds to the lines that cross above one. This term dominates $\mathcal{M}$ after the transition. Note that the evolution has been extrapolated to $a = 10$.

yields

$$\frac{\mathcal{P}}{\mathcal{M}} = \frac{V'}{1+BV}\left[1 + 3\mathcal{D}\frac{1-2BV}{2(1+BV)}\right] + B'\dot{\phi}^2\frac{1}{2}\frac{\frac{3}{2}\dot{\phi}^2 + V}{1+BV} + \mathcal{O}(\mathcal{D}^2)\,. \tag{5.27}$$

The first term reduces to the usual $V_{,\phi}$ at early times, but it is suppressed by the BV factor in the denominator at late times (the expression in brackets remains of order one at all times). The second term represents the purely disformal contribution to the potential and is equally suppressed by BV at late times. At early times, it is suppressed by $B'\dot{\phi}^2$, which is small until the transition by construction. With the exponential choice of the functions (5.13, 5.14) $B' = \frac{\beta}{M_p}B$ and $V' = -\frac{\alpha}{M_p}V$ have opposite signs and therefore the two terms push the field in opposite ways. The second, disformal force term is hence able to decelerate the field when it becomes non-negligible.

Neglecting fine details from (5.27), and within our exponential model the "force" acting on the field will flip sign when

$$\mathcal{D} \sim \frac{\alpha}{\beta}\,. \tag{5.28}$$

The contribution from the disformal factor can be much larger than $V_{,\phi}$ if $\beta \gg \alpha$, which is the ultimate cause for the transition to occur so rapidly. Since it is proportional to $\mathcal{D} \propto \phi^2$, it decreases as the field slows down and eventually the usual term will come to dominate the force when (5.28) is fulfilled again (Figure 5.2 shows that the disformal factor stabilizes approximately around this value). As the transition happens, BV increases and strongly suppresses the force term acting on the field. The later and softer slow down would then be driven by the friction term (5.26), which does not suffer from this suppression.

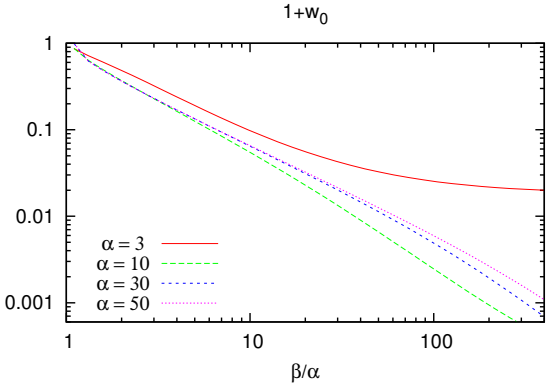

Figure 5.3: Field equation of state at present time as a function of β/α for different values of α. There is a clear trend towards $w_\phi - 1 + \alpha/\beta$ unless α or β/α are very low. Models with early dark energy deviate from this trend because the transition is not complete when $\Omega_\phi \approx 0.7$ is reached.

It is possible to compute the equation of state from equations (5.16, 5.15) to first order in $\dot{\phi}^2/V$ and $\mathcal{D}$

$$w \approx -1 + \mathcal{D} + \frac{1}{2}\dot{\phi}^2/V \approx -1 + \mathcal{D}\,, \tag{5.29}$$

where in the last equality potential domination was assumed. according to (5.28) we expect that $w_0 + 1 \sim \alpha/\beta$. Figure 5.3 confirms this trend for a wide range of parameters. For larger amounts of early Dark Energy (low α) or slow transitions (low β/α) the freeze out does not finish before the required Ω_ϕ is reached. The properties of the accelerated expansion are therefore linked to the quotient β/α. Apparently the only role of α is to regulate the amount of early Dark Energy and therefore shift the transition time to compensate the time interval necessary to achieve Ω_ϕ today.

5.2.2 Cosmological Perturbations

The perturbations were studied in the synchronous gauge [274]. The relevant equations are the same as in Ref. [275] were p is given by the Lagrange density (5.7). With the definitions from the previous section, we can write the energy density and velocity perturbation introduced by the disformal field as

$$\delta\rho_\phi = \mathcal{L}^{-5/2}\left[\mathcal{M}\dot{\phi}\dot{\delta\phi} + \mathcal{P}\delta\phi\right]\,, \tag{5.30}$$

$$(\rho + p)\theta_\phi = -\frac{\mathcal{F}}{\mathcal{L}^{5/2}}\frac{k^2}{a}\dot{\phi}\delta\phi\,, \tag{5.31}$$

where $\delta\phi \equiv \phi(\vec{x},t)/\phi(t)$. The scalar field equation obeyed by such perturbations can be written as

$$\ddot{\delta\phi} + \left[3H + \frac{\dot{\mathcal{M}}}{\mathcal{M}}\right]\dot{\delta\phi} + \left[\frac{\mathcal{F}}{\mathcal{M}}k^2 + m_\phi^2\right]\delta\phi + \frac{1}{2}\frac{\mathcal{F}}{\mathcal{M}}\dot{h}_k\dot{\phi} = 0\,. \tag{5.32}$$

Herre h_k is the interaction with gravity introduced through the covariant derivative and the field mass m_ϕ^2 generalizes the $V_{,\phi\phi}$ term. It is given in terms of the background valuated partial derivatives of (5.7) as

$$m_\phi^2 = \frac{1}{\mathcal{M}}\left[(\ddot{\phi}+3H\dot{\phi})p_{,X\phi}+\dot{p}_{,X\phi}\dot{\phi}+p_{,\phi\phi}\right]. \tag{5.33}$$

As in the homogeneous limit, the smallness of the disformal factor ensures no significant departure from the canonical quintessence case at early times.

The speed of sound characterizes the propagation of fluctuations within the field. For the purely disformal case it is given by [266]

$$c_\phi^2 = \frac{\mathcal{F}}{\mathcal{M}} = \mathcal{L}\frac{1+BV\mathcal{L}-\mathcal{D}/2}{1+BV\mathcal{L}+\mathcal{D}/2}. \tag{5.34}$$

The allowed values of BV and $\mathcal{D}$ bound its value between 0 and 1, see Figure 5.1. It is very close to one before the transition, as for canonical quintessence. Therefore, the growth of perturbations at the tracking stage will be strongly suppressed, and by the time of the transition to slow roll the Dark Energy overdensity will be many orders of magnitude below the matter contrast. As for usual quintessence, the finite amount of early Dark Energy will increase the expansion rate and damp the formation of structure in all epochs. This departure of matter domination is reflected in a slope in the Newtonian gravitational potentials and a slight enhancement of the first acoustic peaks on the CMB.

The transition affects the terms involved in (5.30-5.32). It flips the sign of $\mathcal{P}$ at freeze out and increases its value several orders of magnitude. This variation is compensated by a reduction of $\delta\phi$, which mantains the velocity and energy density perturbations at a similar level, as can be seen in Figure 5.4. The speed of sound drops below unity for a certain time and then stabilizes with a value that depends on β/α, as can be seen in Figure 5.1. Although this enhances the clustering properties of the disformal field, the inhomogeneities in the fluid can grow no faster than the matter ones (for which the speed of sound is zero) and are very suppressed w.r.t. matter inhomogeneities. Therefore, they are completely subdominant.

The main departures from ΛCDM are caused by the different equation of state and transition times, i.e. by purely background physics. Lower values of β/α render the transition slower, but a longer expansion period is required to achieve the same density fraction. Both effects shift the angular scales of the CMB and affect the Integrated Sachs Wolfe signal. Higher values of β/α mimic the Λ behavior at late times. If the value of α is also high (i.e. negligible early DE) matter domination is recovered and disformal quintessence becomes very similar to the standard model.

5.2.3 Observational Constraints

A Markov Chain Monte Carlo simulation was used to obtain constraints on the parameter space of the theory by comparing with WMAP 7 year power spectrum data [19], supernovae from the Union dataset [162], SDSS DR7 baryon acoustic peak position [242] and matter power from the SDSS Luminous Red Galaxies (LRGs) sample [99]. The uncertainty in the galaxy bias factor was treated by choosing the highest likelihood value in the range $(1,3)$ within a linear model. This choice accounts for the uncertainty associated while avoiding too large bias factors. Spatial curvature was set to zero in all the models. The upper bounds in parameter space $\alpha \in (3,20)$ and $\beta/\alpha \in (1.5,30)$ were chosen by sensitivity considerations,

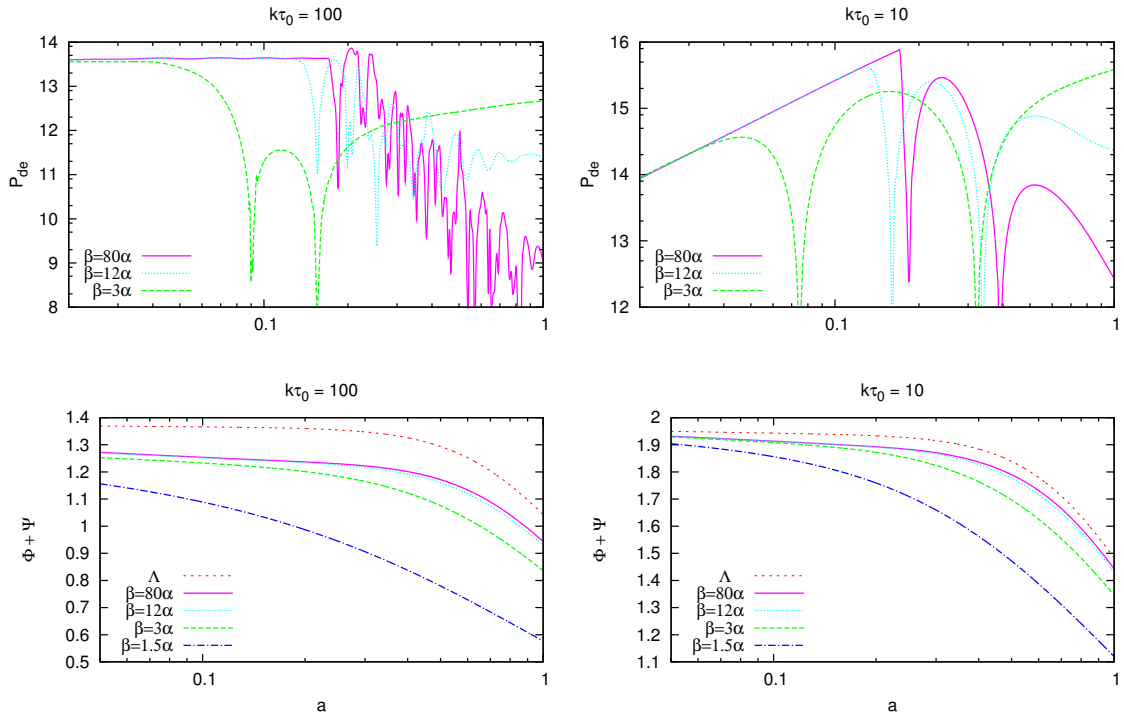

Figure 5.4: Large scale perturbations for $\alpha = 10$. **Top:** Dark energy power spectrum along the scale factor (arbitrary units). **Bottom:** Gauge invariant potentials for the same $k-$modes.

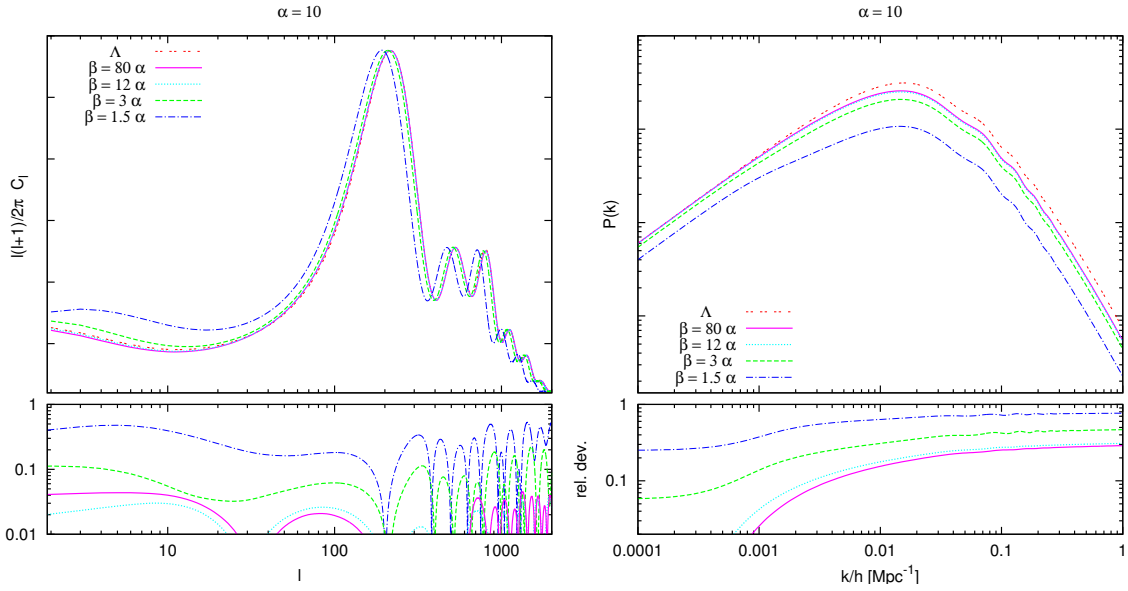

Figure 5.5: CMB (left) and matter power (right) spectra for different values of β/α ($\alpha = 10$) and relative deviation with respect to Λ. The initial amplitude of the perturbations has been chosen to fit the first peak.

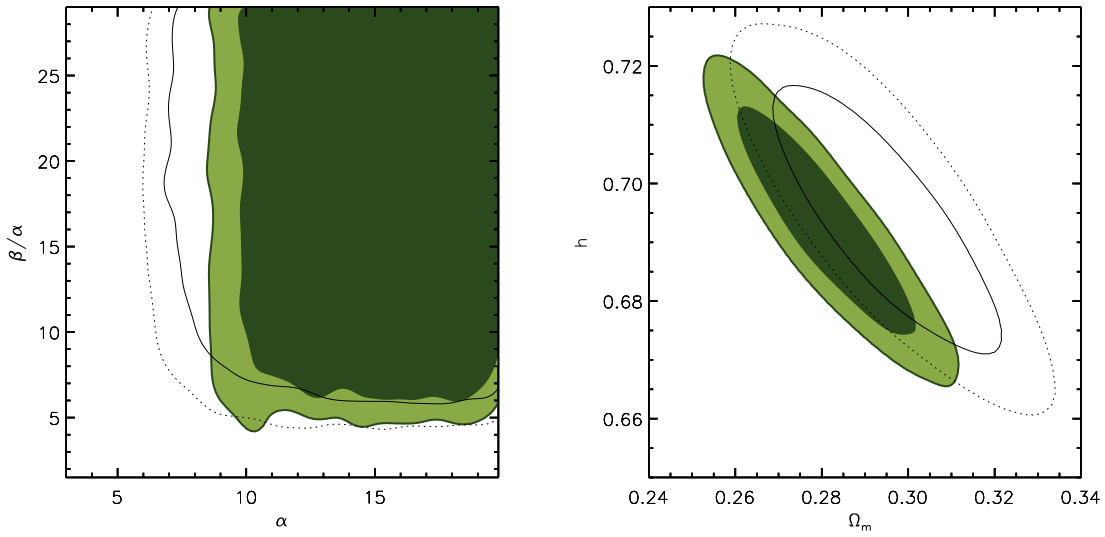

Figure 5.6: Likelihood contours for disformal quintessence. Shaded regions correspond to the 1 and 2-σ obtained by the full MCMC analysis while the black lines correspond to a restricted analysis using only information from the background expansion (SNe, BAO and CMB distance priors). The constraints in α and β/α correspond respectively to high fractions of early Dark Energy and slow disformal transitions towards accelerated expansion.

since very little departure from Λ can be observed for large values. The lower bounds ensure the existence of matter attractor solution for the field ($\alpha > 3$), disformal transition ($\beta > \alpha$) and avoid computational difficulties. The simulation was performed through a modification of the publicly available Boltzmann code CMBeasy [216, 218]. Four chains were run adding up to 20870 accepted models. An additional MCMC using only background information (SNe, BAO and CMB distance priors as described in section 5 of [19]) was run for comparison. The results are displayed in Table 5.2 and Figure 5.6.

Observations are compatible with a large patch of parameter space in the $\alpha, \beta/\alpha$ plane and confirm the preference towards higher values of both parameters where the Λ limit can be achieved. Constraints are tighter on α due to the cumulative effect that early Dark Energy exerts in the growth of perturbations, as can be inferred by a comparison between the runs using the complete and the restricted sets of observations (top plot in Figure 5.6). This difference is likely to arise when the allowed bias factor fails to compensate the effect of early Dark Energy to produce a good fit to LRGs data, as well as due to the effect in the third and further acoustic peaks, as seen in Figure 5.5. The constraints on the properties of accelerated expansion (i.e. on β/α) do not improve significantly in the full analysis because the relevant features affect mostly distance information, encoded in SNe, BAO and CMB angular shift measurements. Other features such as the integrated Sachs-Wolfe effect are significant only for very low values of the parameters and do not introduce relevant differences in the region of interest.

Parameter	Maximum Likelihood	68% C.L.
$100\Omega_b h^2$	2.23	± 0.05
$\Omega_m h^2$	0.135	± 0.004
h	0.690	± 0.014
α	15.9	$\gtrsim 8.5$
β/α	17.2	$\gtrsim 4.9$
τ	0.086	± 0.015
n_s	0.971	± 0.014
Amp.	2.91	± 0.015

Table 5.2: Results from the Monte Carlo Markov Chain analysis. All the usual cosmological parameters lie within one sigma from the WMAP 7 constraints presented in [19]. Amplitude is given by $\ln(10^{10}A_s) - 2\tau$.

5.3 Discussion

Disformal generalizations of the conformal transformation have found several applications in cosmology, particularly in the frameworks of gravitational alternatives to dark matter and varying light speed alternatives to inflation. In this Chapter it has been shown that the disformal relation can be also very prolific in generating alternative explanations for the cosmic acceleration and provide new connections between models. Here we considered the canonical scalar field action where the metric is replaced by the disformal one, i.e. we made the substitution $g_{\mu\nu} \to \bar{g}_{\mu\nu}$ in the Lagrangian. Different choices of the free functions allowed to recover several Dark Energy models proposed in the literature, as can be seen in Table 5.1.

Disformal quintessence arises in a very simple way as an application of this substitution, which results effectively in a non-standard self-interaction of the scalar field. This self-interaction causes the field to accelerate the universe given exponential functions of the field and under the condition $\alpha/\beta < 1$ in (5.13, 5.14). Acceleration can be achieved for models in which the Lagrangian parameters are of order M_p, due to the shift symmetry of the exponential functions. Moreover, the exponential potential allows scaling solutions, so practically no tuning whatsoever of initial conditions for the field is required. The model evolution was studied considering the homogeneous limit and linear perturbations. The dependence of the background dynamics on model parameters allows us to put constraints on them. These become more stringent if we take into account the evolution of linear structures, although the effects are subtle and mostly geometric in nature (i.e. depend on the background properties of the model). A Markov Chain Monte Carlo simulation was used to obtain constraints on the parameter space of the theory by comparing with WMAP 7 year data, SNe from the Union dataset, baryon acoustic peak position and LRGs power spectrum from SDSS. Small values of α can be ruled out because of the effect of early Dark Energy. On the other hand, small values of β/α result in slow transition to acceleration, which is also disfavored by the data. However, when both α and β/α are sufficiently large (the precise

limits shown in Figure 5.6), it becomes very difficult to distinguish the model from ΛCDM.

These results are a first step in the exploration of the disformal relation as a way to connect different theories and build cosmological models. Next Chapter discusses the role of the disformal relation in Dark Energy scenarios by the introduction of couplings to other forms of matter, using the disformal prescription $g_{\mu\nu} \rightarrow \bar{g}_{\mu\nu}$. It turns out that disformal relations allow to relate different scalar tensor theories, and a mechanism similar to the scalar field self coupling is able to initiate a slow roll phase when it couples to non-relativistic matter. Furthermore, such a coupling is in agreement with local gravitational tests by means of a *disformal screening mechanism*.

Chapter 6

General Relativity and Scalar Forces: Disformal Coupling

The only true voyage of discovery would be not to visit strange lands but to possess other eyes, to behold the universe through the eyes of another, of a hundred others, to behold the hundred universes that each of them beholds, that each of them is.

Marcel Proust[1]

In the standard ΛCDM model of cosmology, the universe at the present day appears to be extremely fine tuned. The energy scale of the Λ component is about 10^{-30} times the most naive expectations of the theory. Generalizations of Λ in the form of dynamical scalar fields have been proposed, whose time evolution could more naturally result in the observed energy density today [9]. High energy physics generically predicts an interaction between a scalar degree of freedom and other forms of matter, which in turn could help to explain why the field becomes dynamically important at the present epoch. There are myriad variations of such models, but in most of them the coupling can be effectively described by a field-dependent mass of the coupled particles. Those Yukawa-type couplings can be motivated by a conformal relation to scalar-tensor theories, which includes also the $f(R)$ class of modified gravity [7].

However, for *any* other type of gravity modification, the relation between the matter and gravitational metric will be non-conformal. When given by a scalar field ϕ, the disformal relation can be parametrized as

$$\bar{g}_{\mu\nu} = A(\phi) g_{\mu\nu} + B(\phi)\phi_{,\mu}\phi_{,\nu}\,, \tag{6.1}$$

where commas denote partial derivatives. Considering the most general physical case, Bekenstein [62] argued that both functions A and B may also depend upon $(\partial\phi)^2$, but we will focus

[1] *In Search of Lost Time - The Captive* (1923)

on the simpler case here. Previous applications of such a relation to cosmology include varying speed of light theories [276, 277], inflation [69], massive gravity [278], dark energy [4, 266], gravitational alternatives to [60, 261] and extensions of [279] Dark Matter.

Such a relation can also be motivated in theories with extra dimensions, in which matter is confined to a 3+1 dimensional brane embedded in a larger bulk space [68, 71, 72, 81–83, 280–282]. The action for this type of theories is constructed using geometric scalars computed out of the *induced metric*

$$\bar{g}_{\mu\nu} = g_{\mu\nu} + \pi_{I,\mu}\pi^{I}_{,\nu}\,, \tag{6.2}$$

where the moduli fields π^I represent the coordinates orthogonal to the brane and $g_{\mu\nu}$ is the brane metric prior to the embedding, necessary to describe gravity. In the case of a single extra dimension [68], each curvature invariant is related to a generalized covariant Galileon Lagrangian [64, 74] with a particular form of the Horndeski free functions in (1.28). The usual Galileon terms [70] are then obtained by assuming a flat initial metric $g_{\mu\nu} \to \eta_{\mu\nu}$ and taking the non-relativistic limit (i.e. lower order corrections in $(\partial\pi)^2$). These theories have attracted considerable attention because they capture interesting features of higher dimensional models such as DGP [79], including the Vainshtein screening mechanism [84].

Screening mechanisms are central to the construction of alternative theories of gravity, as they help cover the effects of the additional field in dense environments or around massive, compact objects. Modifications are then allowed to occur over cosmological scales of length and energy density, while the gravitational physics operating in the Solar System are close enough to GR to satisfy the precision tests sketched in Section 2.6. To date three possibilities based on the conformal coupling have been explored, namely the Vainhstein, chameleon and symmetron mechanisms [84, 85, 87]. The chameleon mechanism relies on the high mass of the field in dense surroundings, and the symmetrons are screened in high ambient density due to their field-dependent coupling. The Vainshtein mechanism is somewhat different, as it relies on the non-linear derivative self-interactions of the scalar field to flatten its profile around matter sources within the so-called Vainshtein radius, while keeping it active over cosmological distances.

This Chapter presents results that may simplify considerably the analysis of theories based on higher dimensional models. In Section 6.2 it is argued that by performing a disformal transformation, a theory in which the gravitational sector is standard but the matter metric is constructed disformally (6.1) can be rewritten in a form equivalent to the fourth order covariant Galileon Lagrangian, which arises from the scalar curvature constructed out of the effective metric (6.2) [68]. Disformally coupled theories provide an Einstein frame description of certain brane-world constructions, similar to the way in which the field dependent coefficient of the Ricci scalar can be moved from the gravitational to the matter sector in old-school scalar-tensor theories. In Section 6.2.2, the equations of motion are derived in a frame in which the gravitational sector has the Einstein-Hilbert form but the matter action includes the scalar field as prescribed by Equation (6.1). This Einstein frame description unravels a new screening mechanism in which the coupling vanishes if the field is static and the coupled matter behaves as non-relativistic dust. The properties of the field are discussed in Section 6.5, and some simple solutions are derived. Due to the equivalence between the disformally coupled theory and a covariant Galileon, the *disformal screening mechanism* might just be an alternative way to regard the Vainshtein effect and study its properties.

Even in the absence of a screening mechanism, long range interactions are still phenomenologically viable if they only couple the scalar degree of freedom to Dark Matter particles, which are not involved in local tests of gravity. As a concrete example to analyze the cosmological implications of a *Disformally Coupled Dark Matter* model (DCDM), in which it is assumed that Dark Matter is the only species directly coupled to the field. It is introduced in Section 6.3 where its dynamics and observational compatibility at the background level are analyzed. The intensity of the purely disformal coupling is approximately proportional to the scalar field energy density ρ_ϕ, unlike in the conformally coupled case for which it is proportional to the coupled matter density ρ_m. Cosmological perturbations are analyzed in Section 6.4, including an analytic expression for the small scale effective gravitational constant. The simple DCDM model enhances the growth of the coupled matter density contrast too much to be compatible with observations, but several possibilities to render the model viable are discussed in Section 6.4.3. Although many results would still hold if the coupling is extended to baryons, the results of explicit computations are given for the example DCDM model.

Throughout the present Chapter, quantities computed or constructed using the metric (6.1) are denoted "barred" or "disformal". Quantities constructed using $g_{\mu\nu}$ are denoted as "unbarred" and do not involve the scalar field.

6.1 A Test Particle in a Disformal Metric

Let us start with the simple exercise of determining the dynamics of a point-like particle with mass m coupled to the disformal metric (6.1). A Lagrangian density for such a system is given by

$$\sqrt{-\bar{g}}\bar{\mathcal{L}}_p = -m\sqrt{-\bar{g}_{\mu\nu}\dot{x}^\mu\dot{x}^\nu}\,\delta_D^{(4)}(x^\mu - x^\mu(\lambda))\,, \tag{6.3}$$

where the dot means derivative w.r.t. the affine parameter λ along the trajectory $x(\lambda)$ and the correct weight for the delta function has been taken.[2] The effects from the coupling can be seen from the barred four-velocity modulus in (6.3)

$$\bar{g}_{\mu\nu}\dot{x}^\mu\dot{x}^\nu = A\dot{x}^2 + B(\phi_{,\mu}\,\dot{x^\mu})^2\,. \tag{6.4}$$

Distances are dilated by the conformal factor A, as usual. The disformal factor B gives an additional direction-dependent effect proportional to the projection of the four-velocity along the field gradient. The equations of motion can be obtained by maximizing the proper time of the particle along its path. The result is the *disformal geodesic equation*

$$\ddot{x}^\mu + \bar{\Gamma}^\mu_{\alpha\beta}\dot{x}^\alpha\dot{x}^\beta = 0\,, \tag{6.5}$$

where the barred Levi-Civita connection has been assumed to be torsion-free and such that the metric compatibility relation holds for barred quantities, i.e. $\bar{\nabla}_\alpha\bar{g}_{\mu\nu} = 0$. It can be computed from (6.1) and written in terms of unbarred covariant derivatives of the barred metric in a rather compact form

$$\bar{\Gamma}^\mu_{\alpha\beta} = \Gamma^\mu_{\alpha\beta} + \bar{g}^{\mu\lambda}\left(\nabla_{(\alpha}\bar{g}_{\beta)\lambda} - \frac{1}{2}\nabla_\lambda\bar{g}_{\alpha\beta}\right)\,. \tag{6.6}$$

[2] The one-dimensional definition of the delta function requires that its generalization to higher dimensions cancels out the tensor density in the integrand $\delta_D^{(4)}(x-x_0) = \frac{1}{\sqrt{-g}}\prod_a \delta_D(x^\alpha - x_0^\alpha)$ (e.g. in spherical coordinates $\delta^{(3)}(x) = \delta_D(r)\delta_D(\theta)\delta_D(\phi)/r^2\sin\theta$). Hence it does not matter whether $\sqrt{-g}$ or $\sqrt{-\bar{g}}$ is used in the integration, as long as the delta function is consistent with it.

No assumption about the dependence of A, B has been done to obtain the above expression, which remains valid if A, B depend on X. Note that the difference between the two connections is a tensor, as expected. Appendix D.1 shows the expansion of (6.6) in terms of A, B and its derivatives, which is rather lengthy to be included here.

The stress energy tensor w.r.t. the unbarred metric can be computed by variation of (6.3) with respect to $g_{\mu\nu}$

$$T_p^{\mu\nu} \equiv \frac{2}{\sqrt{-g}} \frac{\delta\left(\sqrt{-\bar{g}}\,\bar{\mathcal{L}}_m\right)}{\delta g_{\mu\nu}} = Am \frac{\dot{x}^\mu \dot{x}^\nu}{\sqrt{g\dot{\bar{x}}^2}} \delta_D^{(4)}\left(x^\mu - x^\mu(\lambda)\right) . \tag{6.7}$$

If the gravitational metric is the unbarred one, this is the energy momentum tensor sourcing the space-time geometry.[3] This result can be used to express the particle Lagrangian in terms of the energy momentum tensor

$$\sqrt{-\bar{g}}\bar{\mathcal{L}}_p = T_p + \frac{B}{A}\phi_{,\mu}\phi_{,\nu}T_p^{\mu\nu} = \bar{g}_{\mu\nu}T_p^{\mu\nu} . \tag{6.8}$$

The above expression gives an effective form for the coupling to matter. It shows how the kinetic term of the scalar mixes with the matter content, a very important property that lies at the heart of disformally coupled theories, including the disformal screening mechanism explored in Section 6.5.

6.2 The Zoo of Disformally Related Theories

The previous Section presented a simple example of a theory in which the matter Lagrangian is constructed using a disformal metric (6.1). Although no gravitational sector was specified, the simplest possibility is to assume that it is given by the Einstein-Hilbert form computed out of the unbarred metric $g_{\mu\nu}$. In this case, Einstein equations retain the usual form and are sourced by the energy momentum tensor (6.7). We shall refer to disformally coupled theories in which the gravitational sector is standard as being expressed in the *Einstein Frame* (EF), in analogy with old-school scalar-tensor theories.

More generally, one wishes to know what kind of theories can be constructed using two metrics that are disformally related and study the relations between them, in analogy to the equivalence between scalar-tensor theories minimally coupled to matter and conformally coupled theories with a standard gravitational sector but with a non-minimal coupling of matter to the scalar field. The starting point is a general *bi-metric theory* where the gravity sector has the EH form, but with unspecified forms for the gravitational and matter metrics

$$S = \int d^4x \left(\sqrt{-g^G}R\left[g^G_{\mu\nu}\right] - \sqrt{-g^M}\mathcal{L}_m\left(g^M_{\mu\nu}, \psi\right)\right) . \tag{6.9}$$

Playing with the disformal relations between $g^G_{\mu\nu}$ and $g^M_{\mu\nu}$ allows one to write it different frames. Besides the Einstein frame, an obvious possibility is to consider the *Jordan Frame* (JF), an equivalent description where matter appears minimally coupled and all the modifications occur in the gravitational part of the action. But since the disformal coupling has

[3] It is possible to write (6.7) in the perfect fluid form $T^{\mu\nu} \equiv \rho u^\mu u^\nu$ if the coupled matter four velocity and the energy density are identified with $u_\mu = \dot{x}_\mu/\sqrt{-\dot{x}^2}$ and $\rho = m\delta_D^{(4)}\left(x^\mu - x^\mu(\lambda)\right)\sqrt{\frac{\dot{x}^2}{g}}\left(1 - \frac{B}{A}(u^\mu\phi_{,\mu})^2\right)^{-1/2}$.

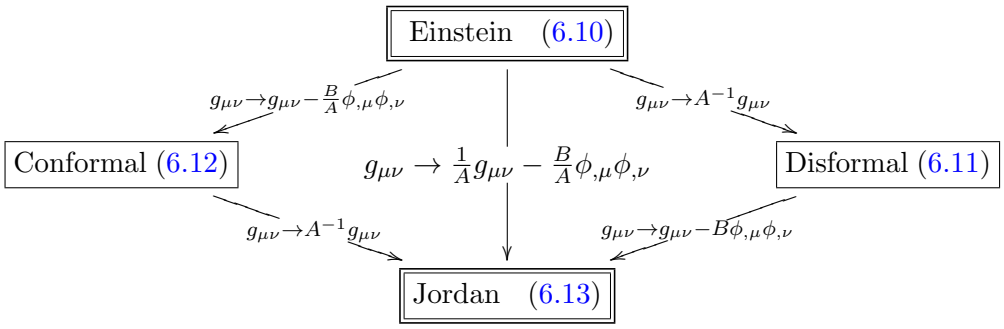

Coupling to ϕ	Uncoupled	Conformal ($Ag_{\mu\nu}$)	Disformal ($B\phi_{,\mu}\phi_{,\nu}$)
Matter	Jordan	Einstein, Conformal frame	Einstein, Disformal frame
Gravity	Einstein	Jordan, Disformal frame	Jordan, Conformal frame

Table 6.1: Physical frames for disformally coupled theories. The conformal and disformal frames refer to the type of coupling present in the matter sector. The transformation rules on top are based on the action 6.9 and given in terms of the definitions (6.10-6.13) (Note that the transformations commute). The lower Table summarizes the type of coupling to the field present in the different sectors depending on the frame.

two parts, two more *intermediate frames* can be defined in which only a certain part of the coupling enters the matter action.The four possibilities are described below and summarized in Table 6.1, together with the transformations that provide the connections between them. For the sake of simplicity, the Einstein frame has been defined using a matter metric of the form (6.1), consistently with the notation used in most of the Chapter (and Section 6.2.2 in particular).

1. **Einstein Frame:**
$$g^G_{\mu\nu} = g_{\mu\nu}, \qquad g^M_{\mu\nu} = Ag_{\mu\nu} + B\phi_{,\mu}\phi_{,\nu}\,. \tag{6.10}$$
This is the formulation used throughout the rest of the Chapter and for which the equations are derived in Sections 6.1 and 6.2.2.

2. **Disformal Frame:**
$$g^G_{\mu\nu} = \frac{1}{A} g_{\mu\nu}, \qquad g^M_{\mu\nu} = g_{\mu\nu} + B\phi_{,\mu}\phi_{,\nu}\,. \tag{6.11}$$
The disformal part enters the matter Lagrangian explicitly. The conformal factor enters the gravitational sector through a coupling to R (e.g. old school scalar-tensor theories).

3. **Conformal Frame:**
$$g^G_{\mu\nu} = g_{\mu\nu} - \frac{B}{A}\phi_{,\mu}\phi_{,\nu}, \qquad g^M_{\mu\nu} = Ag_{\mu\nu}\,. \tag{6.12}$$
The conformal part enters the matter Lagrangian explicitly and the field couples directly to gravity, as described in Section 6.2.1.

4. **Jordan Frame:**
$$g^G_{\mu\nu} = \frac{1}{A} g_{\mu\nu} - \frac{B}{A}\phi_{,\mu}\phi_{,\nu}, \qquad g^M_{\mu\nu} = g_{\mu\nu}\,. \tag{6.13}$$
Matter is minimally coupled to a metric and the field enters the gravitational sector exclusively.

The JF is the most convenient frame to analyze certain properties of the theory and its predictions, as matter follows the geodesics of the simple metric $g_{\mu\nu}$. The matter metric in the remaining frames contains the scalar field explicitly, and therefore matter moves along geodesics that involve the field variations (6.5) in these representations. These frames are still interesting to analyze the theory. For example, the equations simplify considerably in the EF, just like in conformally related theories. Once these are solved, the solutions can be used to transform back to the Jordan Frame.

The explicit computation of the curvature scalar for a metric which includes a disformal part allows one to connect the theory studied in the Einstein frame with a particular sector of the Horndeski Lagrangian (1.28). As anticipated in the introduction, the thus obtained theory is related to a type of covariant Galileon when expressed in the conformal or Jordan frame.

6.2.1 Disformal Curvature: The Conformal Frame

It is possible to get a sense of disformally coupled theories in a different frame by applying the transformations sketched in Figure 6.1 to known actions. These are easy to apply to the terms involving a scalar field, as was described in Chapter 5, where it was shown that applying $g_{\mu\nu} \to A g_{\mu\nu} + B\phi_{,\mu}\phi_{,\nu}$ to a canonical scalar field transforms it into disformal quintessence

$$\sqrt{-g}(X - V) \to A^{3/2}\sqrt{-g}\left(\frac{X}{\sqrt{A - 2BX}} - \sqrt{A - 2BX}V\right), \tag{6.14}$$

up to the ambiguity in the definition of the kinetic term described in Section 5.1.2. This transformation allowed us to relate several dark energy models to disformally self-interacting scalar fields, which were summarized in Table 5.1.

Considering similar relations when the transformations involve the gravitational sector in (6.9) requires the computation of the Ricci curvature for a barred metric that includes the scalar field as in (6.1). The starting point is the difference between the standard and the barred connection (6.6)

$$\mathcal{K}^{\alpha}{}_{\mu\nu} \equiv \bar{\Gamma}^{\alpha}_{\mu\nu} - \Gamma^{\alpha}_{\mu\nu} = \bar{g}^{\alpha\lambda}\left(\nabla_{(\mu}\bar{g}_{\nu)\lambda} - \frac{1}{2}\nabla_\lambda \bar{g}_{\mu\nu}\right) \tag{6.15}$$

where the symmetrization is defined as $t_{(\alpha\beta)} \equiv \frac{1}{2}(t_{\alpha\beta} + t_{\beta\alpha})$. The barred Riemann tensor is obtained from the usual definition, and it can be related to the unbarred one in a manifestly tensorial form in terms of (6.15)

$$\begin{aligned}\bar{R}^{\alpha}{}_{\beta\mu\nu} &\equiv \partial_{[\mu}\bar{\Gamma}^{\alpha}_{\nu]\beta} + \bar{\Gamma}^{\alpha}_{\gamma[\mu}\bar{\Gamma}^{\gamma}_{\nu]\beta} \\ &= R^{\alpha}{}_{\beta\mu\nu} + \nabla_{[\mu}\mathcal{K}^{\alpha}{}_{\nu]\beta} + \mathcal{K}^{\alpha}{}_{\gamma[\mu}\mathcal{K}^{\gamma}{}_{\nu]\beta}\,,\end{aligned} \tag{6.16}$$

where anti-symmetrization is defined without the usual $\frac{1}{2}$ coefficient $A_{[\alpha\beta]} \equiv A_{\alpha\beta} - A_{\beta\alpha}$. The Ricci scalar follows from the contraction

$$\bar{R} \equiv \bar{g}^{\mu\nu}\bar{R}^{\alpha}{}_{\mu\alpha\nu}\,. \tag{6.17}$$

with the inverse barred metric

$$g^{\mu\nu} = \frac{1}{A}\left(g^{\mu\nu} - \frac{B}{A-2BX}\phi^{,\mu}\phi^{,\nu}\right) . \tag{6.18}$$

Finally, the disformal Einstein-Hilbert Lagrangian density requires the barred volume element (D.4) to be covariant

$$\sqrt{-\bar{g}} = \sqrt{-g}A^2\sqrt{1-2\frac{B}{A}X} . \tag{6.19}$$

Note that no assumption has been made about the functions A, B out of which the geometric quantities (6.15-6.17) are computed. However, the general computation is very lengthy, and it is useful to adopt some simplifications.

Let us focus for the time being on a theory in the conformal frame, for which the disformal part is absorbed into the gravitational sector. The following computation assumes thus a gravitational metric of the form (6.12)

$$g^G_{\mu\nu} \equiv \bar{g}_{\mu\nu} = g_{\mu\nu} + D(\phi)\phi_{,\mu}\phi_{,\nu} , \tag{6.20}$$

where the disformal factor $D(\phi)$ is yet to be specified.[4] The Jordan frame can be obtained at the end of the computation by inverting the conformal transformation $g_{\mu\nu} \to A^{-1}(\phi)g_{\mu\nu}$ in the resulting metric and curvature objects. Since the transformation rules for curvature tensors under conformal relations are well known [13], and Galileon-like theories usually retain a conformal coupling to matter in phenomenological applications [283], the Jordan frame curvature will not be computed explicitly.

Let us further redefine the field to simplify the barred metric (6.20)

$$\pi \equiv \int \sqrt{D(\phi)}d\phi \quad \Rightarrow \quad \bar{g}_{\mu\nu} = g_{\mu\nu} + \pi_{,\mu}\pi_{,\nu} . \tag{6.21}$$

The above expression has the same form as the effective metric in probe-brane theories 6.2. It simplifies considerably the computation of the connection tensor (6.15), which now reads

$$\mathcal{K}^{\alpha}{}_{\mu\nu} = \bar{g}^{\alpha\lambda}\left(\pi_{,\lambda}\pi_{;\mu\nu}\right) . \tag{6.22}$$

The barred Riemann tensor can be computed directly from (6.16), rewriting anti-symmetrized derivatives in terms of the curvature $\nabla_{[\mu}\nabla_{\nu]}X^{\cdots\alpha_i\cdots}_{\cdots\beta_j\cdots} = \Sigma_i R^{\alpha_i}{}_{\lambda\mu\nu}X^{\cdots\lambda\cdots}_{\cdots\cdots} - \Sigma_j R^{\lambda}{}_{\beta_j\mu\nu}X^{\cdots\cdots}_{\cdots\lambda\cdots}$. The result is also simple

$$\bar{R}^{\alpha}{}_{\beta\mu\nu} = \bar{g}^{\alpha\lambda}\left(R_{\lambda\beta\mu\nu} + \gamma^2\pi_{;\lambda[\mu}\pi_{;\nu]\beta}\right) . \tag{6.23}$$

Here

$$\gamma = \frac{1}{\sqrt{1+\pi_{,\alpha}\pi^{,\alpha}}} , \tag{6.24}$$

is a Lorentz factor that arises from the inverse metric (6.18). The barred Ricci scalar can be easily obtained by a second contraction

$$\bar{R} = \left(g_{\mu\nu} - 2\gamma^2\pi_{,\mu}\pi_{,\nu}\right)\left[R^{\mu\nu} + \gamma^2\left(\pi^{;\mu\nu}\Box\pi - \pi^{;\mu}_{\ \ ;\alpha}\pi^{;\alpha\nu}\right)\right] . \tag{6.25}$$

[4] Just as in the rest of the Chapter, D has been assumed to be independent of the field derivatives X. This assumption is important in order to simplify the computations performed below. However, given the importance of the X dependence of higher derivative terms in the Horndeski Lagrangian (1.28) and related theories, it is worth considering the more general case $D(\phi, X)$, although in this case the equations would become very involved.

The gravitational Lagrangian $\sqrt{-\bar{g}}\bar{R}$ just requires multiplying by the barred volume factor (6.19) to make it covariant.

The total action for the theory in the Conformal frame is obtained by adding a matter Lagrangian with a conformal factor $A(\phi)$ in the matter metric

$$S_{\rm CF} = \int d^4x\sqrt{-g}\Big[\frac{1}{\gamma}R - 2\gamma\pi_{,\mu}\pi_{,\nu}R^{\mu\nu} + A^2\mathcal{L}_m(Ag_{\mu\nu},\psi) \\ + \gamma\big((\Box\pi)^2 - \pi_{;\mu\nu}\pi^{;\mu\nu}\big) + 2\gamma^3\big(\pi^{,\mu}\pi_{,\mu\alpha}\pi^{;\alpha\nu}\pi_{,\nu} - \pi_{,\mu}\pi^{;\mu\nu}\pi_{,\nu}\Box\pi\big)\Big]. \tag{6.26}$$

These results were previously obtained by de Rham and Tolley [68] in the context of higher dimensional gravity theories. The action (6.26) corresponds to a particular form of the G_4 term in the Horndeski Lagrangian (1.31), which reduces to the fourth covariant Galileon term in the limit $X \ll 1$, with the right non-minimal coupling to gravity. The reader is referred to Section 5 of Ref. [68] for results on other curvature invariants and the relations to other scalar-tensor theories. The Jordan frame expression of covariant Galileons was considered by Appleby & Linder [93], where both the conformal and the disformal coupling to matter were shifted to the gravitational side of the action. The theory studied there is essentially different, as it includes all the covariant Galileon terms, but in the limit of small X, and the authors make no attempt to obtain an Einstein frame description.

6.2.2 Equations in the Einstein Frame

In this Section the equations for a disformally coupled theory which accepts an Einstein frame description will be derived. Such a theory is given by the following action

$$S_{\rm EF} = \int d^4x\left[\sqrt{-g}\left(\frac{R[g_{\mu\nu}]}{16\pi G} + \mathcal{L}_\phi\right) + \sqrt{-\bar{g}}\bar{\mathcal{L}}_m(\bar{g}_{\mu\nu},\psi)\right] \\ = \int d^4x\sqrt{-g}\left[\frac{R[g_{\mu\nu}]}{16\pi G} + \mathcal{L}_\phi + A^2\sqrt{1-2\frac{B}{A}X}\,\bar{\mathcal{L}}_m\big(Ag_{\mu\nu} + B\phi_{,\mu}\phi_{,\nu},\psi\big)\right]. \tag{6.27}$$

The interacting matter sector $\sqrt{-\bar{g}}\bar{\mathcal{L}}_m$ is to be constructed using the barred metric (6.1), as it has been made explicit in the second line using the explicit form of $\bar{g}_{\mu\nu}$ and its determinant (6.19). It will be further assumed that there is no dependence on the barred metric derivatives.[5] A scalar field Lagrangian density of the k-essence type $\mathcal{L}_\phi = \mathcal{L}_\phi(\phi, X)$ has been also included. More general dependence on the field derivatives may be considered (e.g. Kinetic Gravity Braiding [65]), but this term gives relatively simple equations of motion, and is general enough to accommodate the both a canonical $\mathcal{L}_\phi = X - V$ and a disformally self-interacting scalar described in Chapter 5. The matter Lagrangian may include other pieces with different couplings, e.g. an uncoupled matter sector can be included by the addition of a Lagrangian $\sqrt{-g}\mathcal{L}_u$ constructed out of the unbarred metric.

[5] This implies that the disformal connection (6.6) does not appear in the action. This assumption holds for scalar fields and gauge vectors vanishes due to the lack of indices and antisymmetry of the kinetic term, respectively. Although other fields may couple to $\bar{g}_{\mu\nu,\lambda}$, the assumption simplifies the equations considerably and is common in the analysis of scalar tensor theories.

The stress energy tensors for both species will be further defined in terms of the contravariant gravitational metric

$$T^{\mu\nu}_{\phi} \equiv \frac{2}{\sqrt{-g}} \frac{\delta\left(\sqrt{-g}\,\mathcal{L}_{\phi}\right)}{\delta g_{\mu\nu}}\,, \tag{6.28}$$

$$T^{\mu\nu}_{m} \equiv \frac{2}{\sqrt{-g}} \frac{\delta\left(\sqrt{-\bar{g}}\,\bar{\mathcal{L}}_{m}\right)}{\delta g_{\mu\nu}}\,, \tag{6.29}$$

such that the Einstein field equations take the usual form $G^{\mu\nu} = 8\pi G T^{\mu\nu}$ and the *total* energy-momentum is covariantly conserved with respect to the unbarred metric by virtue of the Bianchi identities: $\nabla_{\mu}(T^{\mu\nu}_{m} + T^{\mu\nu}_{\phi}) = 0$. However, the coupling causes that this relation does not occur for each component separately. Instead, only the total energy-momentum for the field and matter is conserved and $\nabla_{\mu} T^{\mu}_{(\phi)\nu} = -\nabla_{\mu} T^{\mu}_{(m)\nu}$. The divergence of the scalar field stress tensor can be re-casted as

$$\nabla_{\mu} T^{\mu}_{(\phi)\nu} = \left(\mathcal{L}_{\phi,\phi} - \nabla_{\mu} \frac{\partial \mathcal{L}_{\phi}}{\partial \phi_{,\mu}}\right) \phi_{,\nu} \equiv Q \phi_{,\nu}\,, \tag{6.30}$$

where the interaction density Q has been defined and is equal to the variation of the uncoupled Lagrangian with respect to the field $\delta\mathcal{L}_{\phi}/\delta\phi$. The equation for the scalar field, $\delta S/\delta\phi = \delta\mathcal{L}_{\phi}/\delta\phi + \delta\mathcal{L}_{m}/\delta\phi = 0$, allows one to write the above expression in terms of the matter Lagrangian

$$Q = \frac{1}{\sqrt{-g}} \left(\nabla_{\mu} \frac{\partial\left(\sqrt{-\bar{g}}\bar{\mathcal{L}}_{m}\right)}{\partial \phi_{,\mu}} - \sqrt{-\bar{g}}\bar{\mathcal{L}}_{m,\phi}\right)\,. \tag{6.31}$$

The coupling can be evaluated by application of the chain rule. For the specific form of the barred metric (6.1), the variation with respect to the field yields

$$\frac{\delta\left(\sqrt{-\bar{g}}\bar{\mathcal{L}}_{m}\right)}{\delta g_{\mu\nu}} \frac{\partial g_{\mu\nu}}{\partial \bar{g}_{\mu\nu}} \frac{\partial \bar{g}_{\mu\nu}}{\partial \phi} = \frac{\sqrt{-g}}{2A} T^{\mu\nu}_{m} \left(A' g_{\mu\nu} + B' b_{\mu} b_{\nu}\right)\,, \tag{6.32}$$

and similarly for the derivative with respect to the field gradient.

After replacing these expressions in (6.31), the coupling reads

$$Q = \nabla_{\mu}\left(\frac{B}{A} T^{\mu\nu}_{m} \phi_{,\nu}\right) - \left[\frac{A'}{2A} T_{m} + \frac{B'}{2A} \phi_{,\mu}\phi_{,\nu} T^{\mu\nu}_{m}\right]\,. \tag{6.33}$$

The equations for the coupled matter component and the field are then

$$\nabla_{\mu} T^{\mu\nu}_{m} = -Q\phi^{,\nu}\,, \tag{6.34}$$

$$\mathcal{M}^{\mu\nu}_{(\phi)} \phi_{;\mu\nu} + \mathcal{L}_{\phi,\phi} - 2X\mathcal{L}_{\phi,X\phi} = Q\,, \tag{6.35}$$

where $\mathcal{M}^{\mu\nu}_{(\phi)} \equiv (\mathcal{L}_{\phi,X} g^{\mu\nu} + \mathcal{L}_{\phi,XX} \phi^{,\mu}\phi^{,\nu})$ is the general kinetic term for the scalar. Einstein equations $G^{\mu\nu} = 8\pi G(T^{\mu\nu}_{m} + T^{\mu\nu}_{(\phi)})$ together with (6.34, 6.35) and (6.33) determine unambiguously the evolution of matter, the scalar field and the metric. These equations naturally contain the case of conformally coupled quintessence, where only the coupling to the trace of energy momentum is present in Q. Note that so far this result is general and does not depend upon the matter content as long as the matter action only depends on the field through the barred metric (6.1) algebraically.

Scalar field equation

The first term in (6.33) contains higher derivatives of the variables $T^{\mu\nu}{}_{;\mu}, \phi_{;\mu\nu}$ due to the kinetic mixing in the mater action, e.g (6.8). These have to be solved for in order to integrate the evolution equations (6.34, 6.35), which can be done after adopting a coordinate system. For the scalar field, it is possible to eliminate the matter derivatives in a general way by contracting (6.34) with $\phi^{,\nu}$ and solving for $\phi_{,\nu}\nabla_\mu T_m^{\mu\nu}$. The result can be inserted back in (6.35) and rearranged as

$$\mathcal{M}^{\mu\nu}\nabla_\mu\nabla_\nu\phi + \frac{A}{A-2BX}\mathcal{Q}_{\mu\nu}T_m^{\mu\nu} + \mathcal{V} = 0\,, \tag{6.36}$$

were we have defined:

$$\mathcal{M}^{\mu\nu} \equiv \mathcal{L}_{\phi,X}g^{\mu\nu} + \mathcal{L}_{\phi,XX}\phi^{,\mu}\phi^{,\nu} - \frac{B\,T_m^{\mu\nu}}{A-2BX}\,, \tag{6.37}$$

$$\mathcal{Q}_{\mu\nu} \equiv \frac{A'}{2A}g_{\mu\nu} + \left(\frac{A'B}{A^2} - \frac{B'}{2A}\right)\phi_{,\mu}\phi_{,\nu}\,, \tag{6.38}$$

$$\mathcal{V} \equiv \mathcal{L}_{,\phi} - 2X\mathcal{L}_{,X\phi}\,. \tag{6.39}$$

The above equation can then be used instead of (6.35) to determine the evolution of the scalar field. It displays very clearly the role of the coupling, which enters not only as a modification to the effective potential (second term), but also in the coefficient for the higher derivatives of the field. This feature will be ultimately responsible for the screening mechanism that disformal models exhibit in high density regions, explored in Section 6.5.

Coupling to Perfect Fluids

The analogue of (6.36) for the covariant matter conservation equation without second order field derivatives can not be obtained without choosing a time slicing due to the different high derivative structure in both equations. Nevertheless, there is no need to do so, since we already found a *bona fide* field equation (6.36) that can be integrated consistently with the corresponding equation for matter (6.34), substituting the appropriate value of Q.[6]

Assuming a perfect fluid in the Einstein frame $T^{\mu\nu} = (\rho+p)u^\mu u^\nu + pg^{\mu\nu}$ with $u^\alpha u_\alpha = -1$, it is instructive to project (6.34) along and perpendicular to the matter four velocity. This determines how the local law of energy conservation and the geodesic equation are modified by the coupling

$$u^\alpha\nabla_\alpha\rho + (\rho+p)\nabla_\alpha u^\alpha = Q\phi_{,\alpha}u^\alpha\,. \tag{6.40}$$

$$(\rho+p)u^\alpha\nabla_\alpha u^\mu + [g^{\mu\alpha} + u^\mu u^\alpha]\,(\nabla_\alpha p + Q\nabla_\alpha\phi) = 0\,. \tag{6.41}$$

In the first equation the coupling the usual energy conservation relation, due to the energy transfered from the scalar field, which is modulated by the projection of the field gradient along the 4-velocity. The second equation determines the departure of geodesic motion w.r.t. the gravitational metric. The first term describes the force arising from the pressure gradient and the second the additional force exerted by the scalar field. Both forces are projected into the direction $\perp u^\mu$ (coefficient in brackets) due to the orthogonality of the four velocity and four acceleration.

[6] It is possible to solve for the time derivatives of all the variables after a metric ansatz has been chosen, as will be done in the study of FRW models and cosmological perturbations, see Sections 6.3, 6.4.

6.3 Background Cosmology

Let us consider an application of the theory (6.27), where the scalar acts as a quintessence fiend and the disformal coupling is used to trigger cosmic acceleration. Using the Einstein frame description the Friedmann equations have the usual form

$$H^2 + K = \frac{8\pi G}{3}(\rho + \frac{\dot\phi^2}{2} + V)\,, \tag{6.42}$$

$$\dot H + H^2 = -\frac{4\pi G}{3}(\rho + 2\dot\phi^2 - 2V)\,, \tag{6.43}$$

but the conservation equations for matter and the scalar field have to be computed from (6.34, 6.36):

$$\dot\rho + 3H\rho = Q_0\dot\phi\,, \tag{6.44}$$

$$\ddot\phi + 3H\dot\phi + V' = -Q_0\,, \tag{6.45}$$

were the background order coupling factor reads

$$Q_0 = \frac{A' - 2B(3H\dot\phi + V' + \frac{A'}{A}\dot\phi^2) + B'\dot\phi^2}{2\left(A + B(\rho - \dot\phi^2)\right)}\rho\,, \tag{6.46}$$

after solving away the higher derivatives. In the following we restrict to flat space, $K = 0$.

At this stage it is possible to understand the difference between the pure conformal ($B = 0$) and disformal ($A = 1$) cases by writing (6.46) in terms of the equation of state and the scalar field energy density:

$$Q_0^{(\mathrm{c})} = \frac{A'}{2A}\rho\,, \tag{6.47}$$

$$Q_0^{(\mathrm{d})} \approx \Big(\frac{B'}{2B}(1+w_\phi) - \frac{V'}{2V}(1-w_\phi)\Big)\rho_\phi + \frac{\sqrt{3}}{M_p}\left((1+w_\phi)\rho_{\rm tot}\rho_\phi\right)^{1/2}\,, \tag{6.48}$$

where in the second line it has been assumed that $B\rho \gg 1 \gtrsim B\dot\phi^2$. This approximation is satisfied by the model under study when the coupling is active, see Figure 6.2. The last term in (6.48) represents the contribution from the Hubble term, which is subdominant when the slopes of B, V are large. The above expressions imply that the conformal and disformal coupling between Dark Energy and Dark Matter are related to essentially different dark energy parameterizations, where the interaction is either proportional to $\rho = \rho_{\rm dm}$ [49, 258] or ρ_ϕ [284, 285].

6.3.1 An Example Model: Disformally Coupled Dark Matter

In what follows it will be assumed that the field is only coupled to Dark Matter, while radiation and baryons follow geodesics of the gravitational metric and do not feel the scalar interaction directly. If baryons are also coupled, then the ratio ρ_{dm}/ρ_b remains fixed, because both species feel the same effective metric.[7] Postulating that the baryonic and electromagnetic

[7] This can also be seen directly from (6.46): in the denominator of Q_0, the energy density has to be substituted by the total one $\rho \to \rho_{dm} + \rho_b$, while the multiplicative coefficient ρ would refer to each individual species.

sectors are constructed out of the gravitational metric also avoids problems with precision gravity tests and the subtleties related to the existence of different frames, hence simplifying the analysis of cosmological observations.

To study the dynamics within a particular example, we focus on a simple *Disformally Coupled Dark Matter* (DCDM) model, constructed with the following prescriptions

- Dark Matter disformally coupled to a canonical scalar field, following Eq. (6.44-6.46).
- An exponential parametrization for the disformal relation and the scalar field potential:

$$B = B_0 e^{\beta(\phi-\phi_0)/M_p}\,, \quad V = V_0 e^{-\gamma\phi/M_p}\,, \quad A = 1\,. \tag{6.49}$$

  with $M_p = (8\pi G)^{-1/2}$. The conformal factor A has been set to the trivial value in order to focus on the novel features. Furthermore, the coupling is chosen to be negligible in the early universe, and hence initial conditions and early evolution are not affected.
- Uncoupled baryons, photons and neutrinos, which follow the usual barotropic scaling relations $\rho = a^{3(1+w)}$. Zero cosmological constant.

Besides being motivated from some high energy scenarios, the exponential forms (6.49) facilitate the choice of natural scales for the constant prefactors by shifting the zero point of the field (e.g. $B_0 \sim M_p^{-4}$, $V_0 \sim M_p^4$, A_0 dimensionless). The model set up is similar to the uncoupled self-interacting field case described in Chapter 5. In particular, the potential ensures a tracking stage for the field and the value of ϕ_0 is chosen to tune the transition time when the disformal coupling becomes relevant. Although only Dark Matter is affected by the coupling, radiation and baryons are included in order to provide a more realistic description.

With this set up, the evolution at early times is as in the usual exponential quintessence model, where the field tracks the dominant fluid component and the slope of the potential γ determines the amount of Early Dark Energy (EDE) [9]

$$\Omega_{\rm ede} = \frac{3}{\gamma^2}(1+w_m)\,, \tag{6.50}$$

which depends on the dominant matter component equation of state parameter w_m. The new features appear when the disformal factor $B\dot\phi^2$ becomes of order one. Then the clocks that tick for Dark Matter, $\bar g_{00} = -1 + B\dot\phi^2$, slow down and make the effective equation of state approach minus unity asymptotically. The field also slows down to avoid a singularity in the effective metric $\bar g_{\mu\nu}$, and the universe enters into a de Sitter stage. This natural resistance to pathology was also observed in the disformal self-coupling scenario described in Chapter 5 and references [4, 266]. The disformal coupling provides then a mechanism that triggers the transition to an accelerated expansion. The relatively steeper the slope of the disformal function is, i.e. the higher the ratio β/γ, the faster the transition happens, as seen in Figures 6.1, 6.2. This transition also produces a short "bump" in the equation of state, which affects the growth of structure.

The departures with respect to the standard ΛCDM model allow the use of cosmological observation to constrain the model parameters in the homogeneous approximation using different datasets. The Union2 Supernovae compilation and the local expansion rate measurement were implemented as described in Section 3.3.1. The BAO scale data was also used as described in Section 3.3.1, but computed using the Dark Matter fraction extrapolated

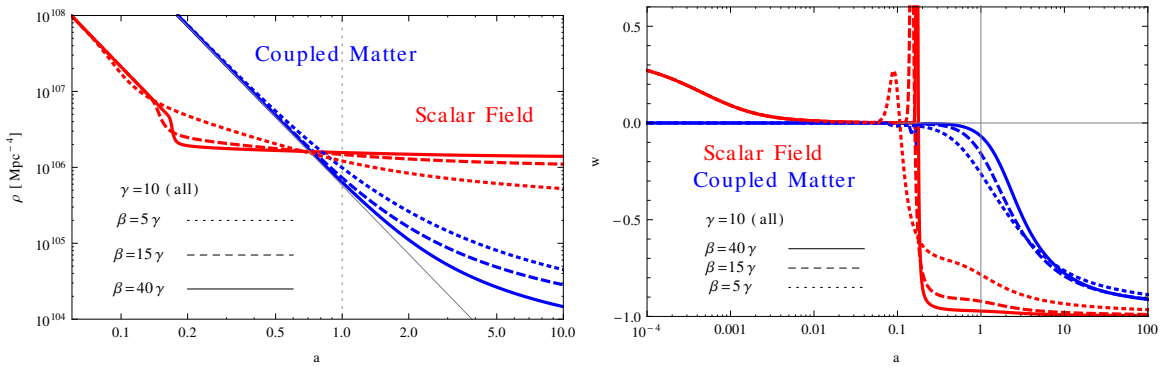

Figure 6.1: Background evolution of disformally coupled matter. **Left:** evolution of the energy density for the field (red) and coupled matter (blue) for different choices of the coupling slope β. **Right:** equation of state for the field (red) and coupled matter (blue). High values of β/γ (solid, dashed) give a good fit to observations, while low values (dotted) do not produce enough acceleration.

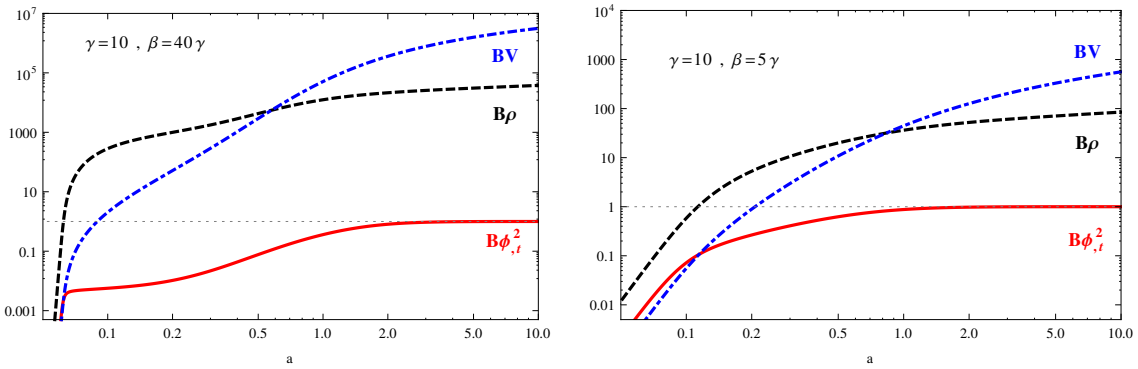

Figure 6.2: Evolution of the dimensionless disformal factors $B\dot{\phi}^2$, $B\rho$ and BV. Higher values of β/α produce a sharper transition and lead to higher B at late times.

from the drag epoch assuming the usual scaling $\rho_{\rm dm} \propto a^{-3}$ in order to ensure the validity of the fitting formulae. The Cosmic Microwave Background constraints include the bound on early dark energy obtained from the South Pole Telescope $\Omega_\phi(z_*) < 0.018$ (95%C.L.) [122] *and* the angular scale, given by the ratio between the physical sound horizon at recombination and the angular diameter distance $\theta_{\rm CMB} = r_s(z_*)(1+z_*)/D_A(z_*) = 0.5952(16)\,{\rm deg}$ [18]. The effects of early dark energy are taken into account by using the model background thermal history to compute r_s, rather than a fitting formula. A prior on $\Omega_b h^2$ obtained from primordial nucleosynthesis [286] was also included. Although this values assumed no Early Dark Energy, the severe CMB bounds constraint the potential impact of neglecting EDE in BBN constraints.

A Markov Chain Monte Carlo analysis with these datasets was performed using a modified version of CMBEasy [216]. The obtained constraints are shown in Figure 6.3 and Table

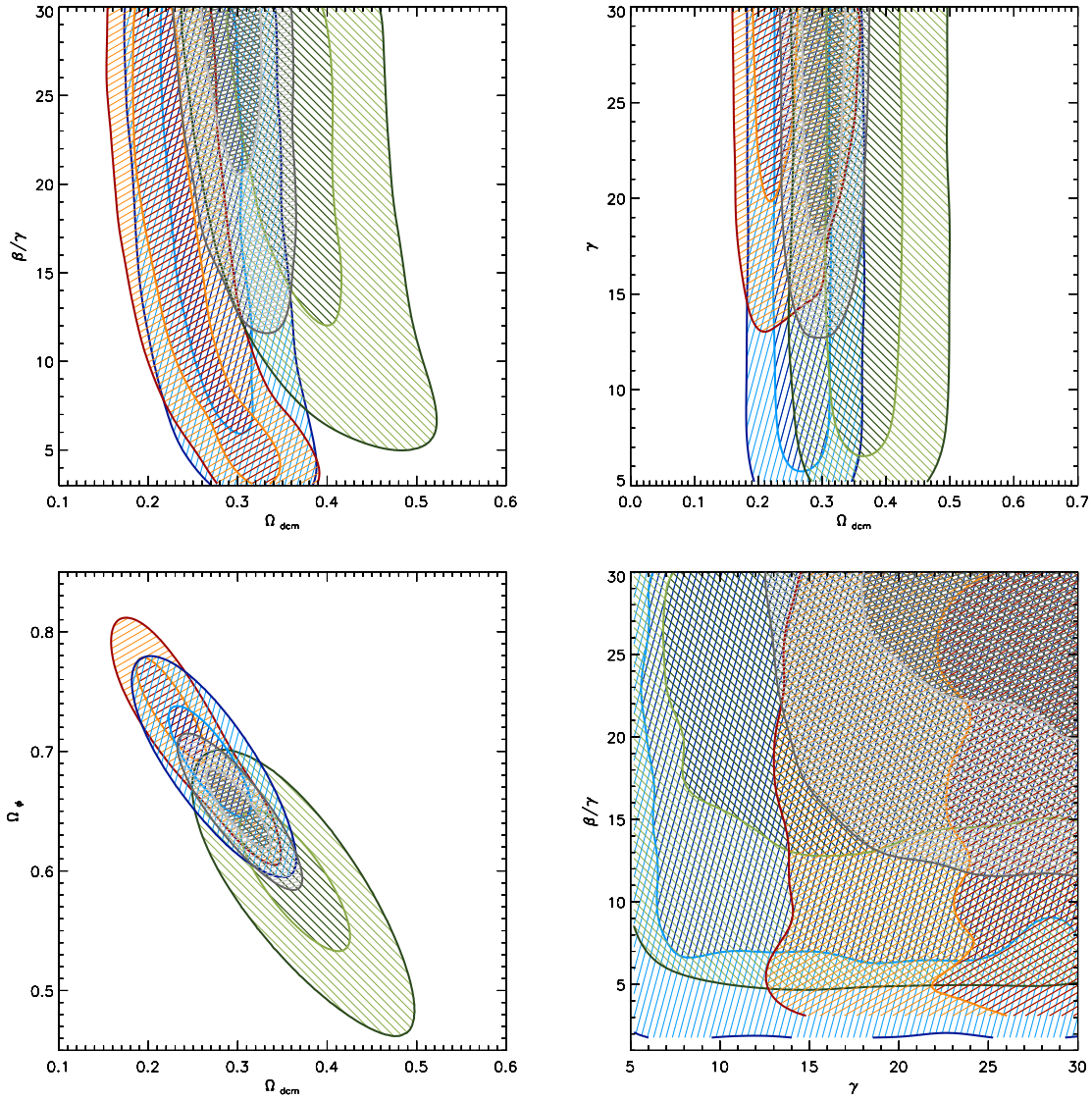

Figure 6.3: Marginalized one and two-sigma regions obtained from Supernovae (Blue), BAO (Green), CMB angular scale + early dark energy bounds (Orange), and combined (Gray). All contours included a prior on H_0 from the HST and $\Omega_b H_0^2$ from Big Bang Nucleosynthesis (see text).

h	$=$	0.738 ± 0.024	Ω_b	$=$	0.0382 ± 0.005
Ω_{dcm}	$=$	$0.263^{+0.033}_{-0.022}$	Ω_ϕ	$=$	$0.698^{+0.025}_{-0.036}$
λ	$>$	18.6	β/λ	$>$	15.6

Table 6.2: Parameter constraints for disformally coupled Dark Matter. Error bars correspond to the one-sigma allowed ranges.

6.2. The slope of the potential γ determines the amount of early dark energy, and is therefore best constrained by the CMB. The ratio β/γ determines the equation of state at late times. Its value is best bound by the combination of all different probes. In the homogeneous approximation there are no higher bounds on the parameters β and γ, and the model is completely viable with $\chi^2_{\rm disf} = 538.79$ versus $\chi^2_{\Lambda\rm CDM} = 538.91$ obtained from the best fit WMAP7 ΛCDM model compared to the same datasets. The lower value of the equation of state parameter for the disformally coupled matter is responsible for the higher value of Ω_{dm}, at the expense of a lower Ω_ϕ than in standard quintessence or cosmological constant cosmologies. These results reproduce closely the constraints on the disformal self-interaction of the (otherwise uncoupled) scalar field described in Chapter 5: For steep slopes γ and β, the background evolution becomes increasingly similar to ΛCDM. However, the model is essentially different from ΛCDM and disformal quintessence, as is quite obvious when one looks at the effective Dark Matter equation of state in Figure 6.1. The growth of perturbations studied in the next Section shows that the model is not viable as it is. A glimpse to alternative, viable models is provided in Section 6.4.3.

6.4 Cosmological Perturbations

A more realistic description of the universe requires considering cosmological perturbations. The starting point is equation (6.31), which can be used to read both the disformal matter non-conservation and the field dynamical equation. Working in the Newtonian gauge

$$ds^2 = -(1+2\Phi)dt^2 + a^2(1-2\Psi)d\vec{x}^2\,, \tag{6.51}$$

the equation for the scalar field is

$$\delta\ddot{\phi} + 3H\delta\dot{\phi} + \left(\frac{k^2}{a^2} + V''\right)\delta\phi = -\delta Q - 2\Phi\left(Q_0 + V'\right) + \dot{\phi}(\dot{\Phi} + 3\dot{\Psi})\,, \tag{6.52}$$

while the perturbed continuity and Euler equations for the disformally coupled matter contrast $\delta_{\rm dc} = \delta\rho/\rho$ (with ρ being the coupled matter component) and the divergence of its velocity $\theta = ik_jT^{0i}_{(m)} = ik_jv^j\rho a^{-1}$ read

$$\dot{\delta}_{\rm dc} + \frac{\theta}{a} + \frac{Q_0}{\rho}\dot{\phi}\delta_{\rm dc} = 3\dot{\Psi} + \frac{Q_0}{\rho}\delta\dot{\phi} + \frac{\delta Q}{\rho}\dot{\phi}\,, \tag{6.53}$$

$$\dot{\theta} + \theta\left(H + \frac{Q_0}{\rho}\dot{\phi}\right) = k^2\left(\Phi + \frac{Q_0}{\rho}\delta\phi\right)\,. \tag{6.54}$$

The coupling perturbation δQ is given in Appendix D.2 for the general case. In the case of a purely disformal coupling, it reduces to

$$\begin{aligned}\delta Q^{(\rm d)} = &-\left(\frac{k^2}{a^2}\frac{B\rho}{M} + (2BV'' - B''\dot{\phi}^2)\frac{\rho}{2M} + \left(2B'(V' + 3H\dot{\phi}) + B'^2\dot{\phi}^2(\rho - \dot{\phi}^2)\right)\frac{\rho}{2M^2}\right)\delta\phi \\ &+(1 - B\dot{\phi}^2)\frac{Q_0}{M}\delta_{\rm dc} + \left(B'\dot{\phi} - B(3H - \rho B'\dot{\phi}) - B^2(2V'\dot{\phi} + 3H(\rho + \dot{\phi}^2))\right)\frac{\rho}{M^2}\delta\dot{\phi} \\ &+\left(-B'\dot{\phi} + B(6H - \rho B'\dot{\phi}) + 2B^2(3H\rho + V'\dot{\phi})\right)\frac{\rho\dot{\phi}}{M^2}\Phi + \frac{3B\rho\dot{\phi}}{M}\dot{\Psi}\,.\end{aligned} \tag{6.55}$$

It is a much more cumbersome combination of the fluid and field perturbations than for the purely conformal coupling

$$\delta Q^{(\mathrm{c})} = \frac{1}{2}\log(A)'\rho\delta_{\mathrm{dc}} + \frac{1}{2}\log(A)''\rho\delta\phi\,. \tag{6.56}$$

Note that, unlike in the conformal case, the first term in (6.55) is proportional to k^2 and hence the coupling is scale dependent. This feature will be reflected in the growth of perturbations and the power spectrum.

6.4.1 Small Scale Limit

To extract the most relevant new features by analytic means, we shall consider the subhorizon approximation. In the small scale limit, taking into account only the matter perturbations and the gradients of the field, there is a simple expression for the perturbed interaction δQ. In this Newtonian limit, we further relate the field gradient to the matter perturbation through the field equation (6.52), which yields the simple expression

$$\delta Q^{(\mathrm{N})} = Q_0\delta_{\mathrm{dc}}\,. \tag{6.57}$$

Combining equations (6.53) and (6.54) together with the usual Poisson equation, we obtain the evolution of the coupled Dark Matter overdensity

$$\ddot{\delta}_{\mathrm{dc}} + \left[2H + \frac{Q_0}{\rho}\dot{\phi}\right]\dot{\delta}_{\mathrm{dc}} = 4\pi G_{\mathrm{eff}}\rho\delta_{\mathrm{dc}}\,. \tag{6.58}$$

In addition to an extra friction term, the source term is modulated. The last effect is captured by defining an effective gravitational constant G_{eff} that determines the clustering of Dark Matter particles on subhorizon scales

$$\frac{G_{\mathrm{eff}}}{G} - 1 = \frac{Q_0^2}{4\pi G\rho^2}\,. \tag{6.59}$$

This approximation has the same expression as the simple conformal case, although with a significantly different functional form of the coupling Q_0, which is now given by Eq. (6.46).

The evolution of G_{eff} for the disformally coupled Dark Matter example model (6.49) is shown in Figure 6.4. It is characterized by a bump at the transition, whose height increases with β, and a further increase when the potential becomes dominant. At the later stage, the dependence is approximately $G_{\mathrm{eff}}/G - 1 \sim (\gamma V/\rho)^2$ and yields a large value since dark energy domination requires $V \gtrsim \rho$ and $\gamma \gtrsim 18$ is necessary to avoid the effects of early dark energy (6.50). This enhancement occurs on observable scales and spoils the formation of large scale structure in this particular case. Problematic growth enhancement also occurs in conformally coupled models that attempt to address the coincidence problem [258]. The observable effects will be analyzed using the full perturbation δQ within the disformally coupled Dark Matter model. Several alternatives to render the model viable will be described in Section 6.4.3.

6.4.2 Structure Formation for Disformally Coupled Matter

The linearized equations (6.52-6.55) were solved using a modified version of the Boltzmann code CMBeasy adapted to the Disformally Coupled Dark Matter model described in Section

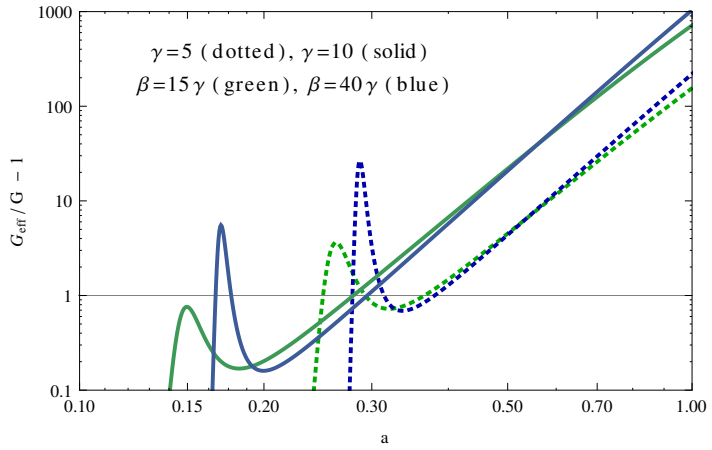

Figure 6.4: Effective gravitational constant on small scales (6.59) for different values of β, γ. The value is large at the transition due to the disformal friction term $B'\dot{\phi}^2$, and latter due to the contribution of the potential term BV' (see text and compare to Figure 6.1).

6.3.1. Since matter is essentially uncoupled until $z \lesssim 10$ there was no need to modify the initial conditions, which have been assumed adiabatic. Figure 6.5 shows the evolution of the density contrast of disformally coupled matter. The baryons, which are uncoupled in this particular example, are also shown for comparison. Figure 6.6 displays the power spectra for disformally coupled matter and baryons at $z = 0$ for different values of the parameters. Figure 6.7 shows the CMB power spectrum and the baryon-DM bias induced by the coupling at $z = 0$.

Besides the effect of early dark energy and late time scalar force captured in G_{eff}, the disformal coupling causes a considerable integrated Sachs-Wolfe effect, a fundamental bias between disformally coupled matter and baryons and cause large scale oscillatory features beyond the BAO scale. The numerical results and the discussion are restricted to the DCDM model, and focus on the role of the potential slope γ, which mostly determines the late time value of G_{eff}. It remains to be studied whether or not similar effects occur in viable models such as the ones described in Section 6.4.3, and to what extent they might be observable by current or future surveys.

Early Dark Energy

Both the baryons and the coupled Dark Matter are indistinguishable as long as the coupling is negligible. They are equally affected by the presence of early dark energy (see Figure 6.5), which produces a departure from the matter domination result $\delta \propto a$: EDE increases the expansion rate without clustering, reducing the formation of structure. This effect was also found for the uncoupled scalar field (Chapter 5), and is most noticeable for models with higher Ω_{ede} (e.g. $\gamma = 4$).

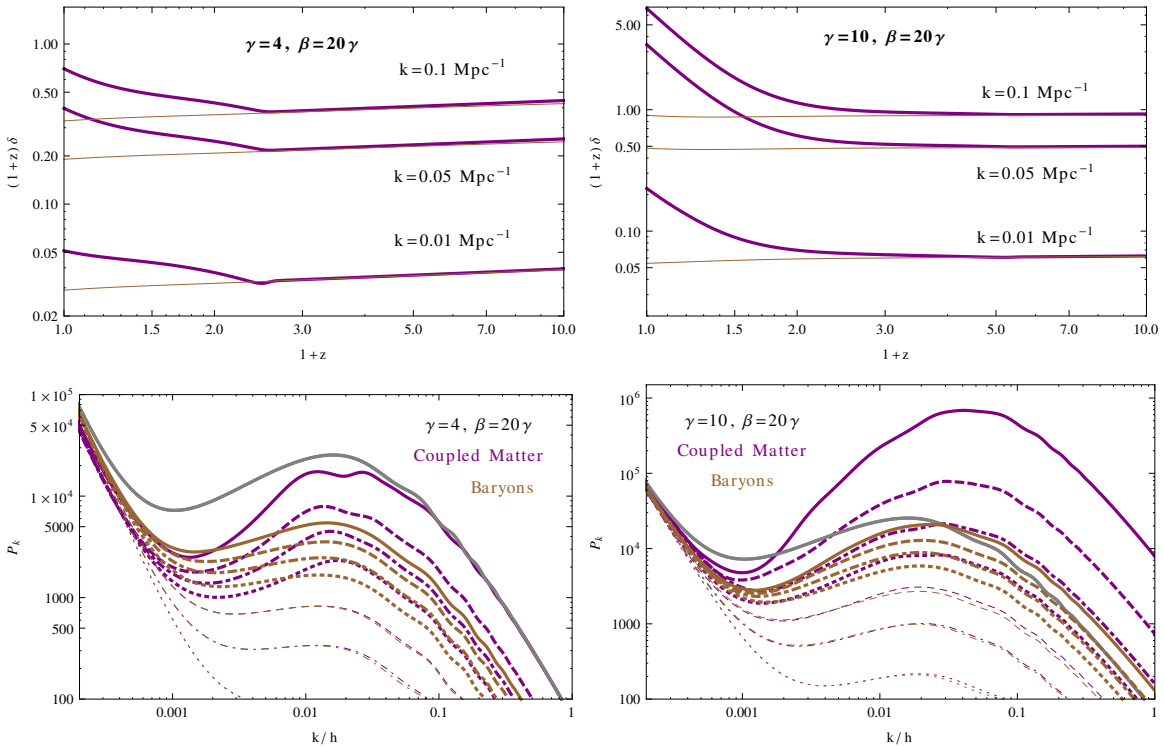

Figure 6.5: Growth of disformally coupled matter and (uncoupled) baryons. **Upper panel:** Thick purple lines cooresponds to the disformally coupled matter and thin brown lines to baryons at the same scales. The pressence of early dark energy affects the slope at early times. Afterwards, the Dark Matter perturbation starts growing rapidly, as deduced in the small scale approximation (see Figure 6.4). **Lower panel:** Evolution of the power spectrum at $z = 0$ (thick, solid), 0.3, 0.6, 1 (thick, dotted), 2, 4 and 10 (thin, dotted). Gray line corresponds to a reference ΛCDM model.

Late Enhanced Growth

The growth of structure is enhanced after the transition takes place, consistently with the small scale approximation (6.59). The large value of $G_{\rm eff}/G$ overcomes the additional friction term, and structures form much faster than in the standard CDM scenario. Models with less EDE suffer a *higher* enhancement, because the effective gravitational constant $G_{\rm eff} \propto \gamma^2$ is larger and the transition occurs earlier (i.e. the field takes longer to dominate the energy content). The effect from the bump in the effective Newton's constant associated to the transition is not obvious in the evolution of δ, and is subdominant with respect to potential domination.

The enhanced growth effect is partly canceled by the early dark energy damping. This degeneracy causes the relative resemblance between DCM power spectra with $\gamma = 4$ and the DM power for the standard model on small scales, but fails anywhere else. It would be worth exploring this cancellation in a more systematic way (e.g. MCMC exploration of the model parameters). This would actually require a better understanding of the baryon bias induced

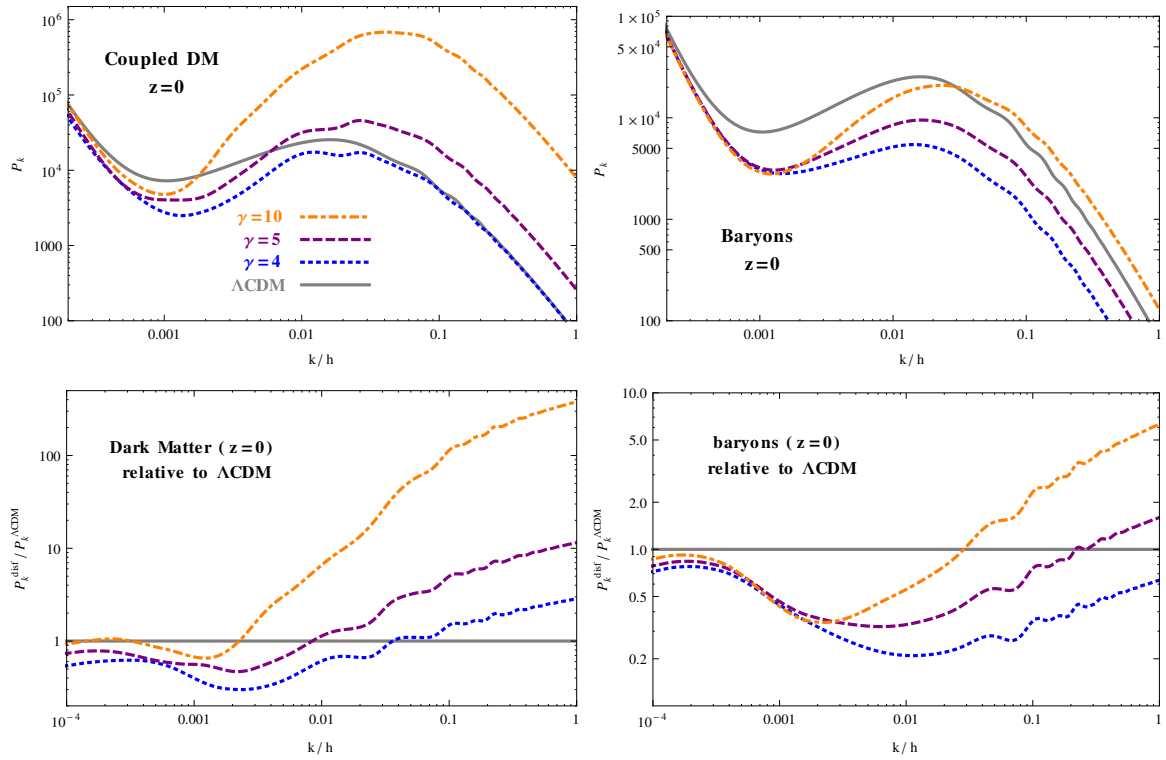

Figure 6.6: Perturbations at $z = 0$ for $\beta = 20\gamma$ and different values of γ. **First line:** Power spectrum for (uncoupled) baryons and (coupled) matter. **Second Line:** Ratio of the power spectra in disformally coupled models relative to ΛCDM. See Section 6.4.2 for a discussion of the different effects.

by the coupling (see below). However, such an exploration is postponed for future work.

Note that Fourier modes reach the non-linear regime earlier due to the enhanced coupling. Upon the failure of linear perturbation theory, the disformal screening mechanism explored in Section 6.5 might hide these dramatic effects and restore the standard growth, softening the deviations on small scales. Although this seems unlikely to save the example model, it might be necessary to take the effect into account to obtain a fair comparison with observations.[8]

Scale Dependent Growth and Bias

The power spectra show scale dependent evolution, as can be seen in the different power spectra normalized to the corresponding ΛCDM (second line of Figure 6.6). In the standard model, the linear growth factor is scale independent and does not distinguish baryons from Dark Matter. For disformally coupled Dark Matter, the scale dependent growth follows from the k-dependent term in the perturbed coupling (6.55). This feature does not appear in

[8]Similar enhanced growth effects have been considered in the context of quintessence conformally coupled to neutrinos, where the necessity of non-linear analysis has been pointed out [53].

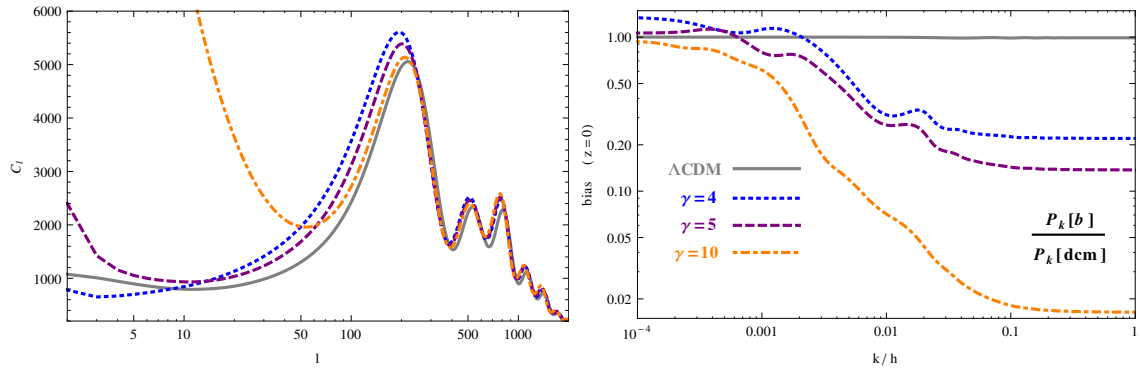

Figure 6.7: CMB power spectrum (left) and bias between baryons and Disformally Coupled DM (DCM) induced by the coupling (right). The enhanced growth of Dark Matter structures on small scales produces a very large ISW effect. Note that the departures are worse for models with *less* early dark energy (higher γ), as derived in the small scale approximation (6.59).

phenomenological coupled models, in which the growth of the coupled matter structures is enhanced, but in a scale independent way, (cf. [284]).

The coupling also modifies the relation between baryonic and Dark Matter structures, since DM couples directly to the field while baryons are only indirectly affected. As baryons are dragged into the potential wells created by the coupled matter, they follow a scale dependent growth pattern, delayed with respect to the dominant matter component. The resulting bias between the two species is shown in Figure 6.7. The scale dependence of the bias vanishes both on super-horizon scales ($k/h \lesssim 0.001$) and the small scales ($k/h \gtrsim 0.1$), which are well described by the scale-independent $G_{\rm eff}$ (6.59). The intermediate region shows the interplay between the scale dependent growth for the coupled matter and the baryons following these structures.

Since galaxies form out of baryons, this fundamental bias modifies the usual DM-galaxy power relation (2.20). Such a correction needs to be taken into account when comparing the observed power spectrum with disformally coupled models. On the other hand, other measurements of the matter distribution such as weak lensing would probe the structures formed by both components, and may be used to break the degeneracy.

CMB: Integrated Sachs-Wolfe Effect

The enhancement of the perturbations after the transition causes the very large Integrated Sachs-Wolfe effect appreciated in Figure 6.7, which becomes most noticeable for the models with higher values of γ. The model with $\gamma = 4$ gives a better fit on the $l \lesssim 10$ multipoles, but departs considerably in the range $10 \lesssim l \lesssim 200$ due to the effect of early dark energy after recombination. The model with less early dark energy has the opposite problem: it produces a better fit in the intermediate range $100 < l < 200$ due to the lower amount of early dark energy, but the ISW enhancement explodes at lower multipoles due to the higher value of $G_{\rm eff}$. The different amounts of early dark energy have an additional effect on the CMB normalization due to the primary Sachs-Wolfe effect: by reducing the potential wells

that redshift the photons, $\Omega_{\rm ede}$ acts increasing the height of the peaks.

Oscillatory Features beyond the BAO Scale

Oscillatory features can be appreciated in the coupled matter power spectrum on very large scales. These are likely created as field oscillations on scales near $k \sim H(z)$, which are then transferred to the coupled component, when the coupling is active. They are most noticeable for the models with a large early dark energy component, e.g. larger field energy density. Although it constitutes a distinctive feature of the model, the oscillations are not significantly imprinted on the baryonic power spectrum. This, together with the large survey volumes necessary to explore such scales would make it difficult to detect them through LSS surveys. However, the large scale oscillations would be a characteristic signature in models where the disformal coupling is universal, in which the same effects occur to DM and Baryons.

6.4.3 Viable Scenarios

The study of cosmological perturbations within the Disformally Coupled Dark Matter model (6.49) shows very drastic departures in the formation of large scale structure, that seem very difficult to reconcile with observations. It would be interesting to obtain a more precise quantification of these discrepancies through an MCMC analysis and explore possible degeneracies (e.g. the growth suppression from early dark energy and the enhancement from the high $G_{\rm eff}$). However, it is necessary to address the existence of alternative, viable scenarios already at this stage.

Luckily, the action (6.27) is very general and there is considerable room for improvement through different choices of the functions A, B and $\mathcal{L}_\phi$. There are at least two possibilities

- Introduce a modulation in the disformal factor $B(\phi) \to f(\phi)B(\phi)$, to make Q_0 small enough after the field enters the slow roll phase. This modification can render $\delta G_{\rm eff}$ arbitrarily small, except for a relatively short time around the transition (see Figure 6.1). This type of models would allow us to study the effects imprinted by the transition bump without the problems caused by the high $G_{\rm eff}$ at late times.

- Constructing the field Lagrangian using a disformal metric, as in the uncoupled model presented in Chapter 5 and references [4, 266]. In this model the transition to slow roll would be partially driven by the scalar field Lagrangian itself, and the effects on matter may be significantly reduced. In the minimal prescription, the matter and field Lagrangian are constructed using the same metric (6.1) and no extra parameters are introduced. If this model turned out not to be viable, a different disformal metric for the field and the coupled matter would offer an alternative that is able to interpolate between disformal quintessence and the disformally coupled Dark Matter presented here (e.g. different disformal factors with $B^{(m)} = \epsilon B^{(\phi)}$).

Other alternatives could be based on the interplay between the conformal and the disformal part of the coupling. Viable scenarios might be exploited to alleviate the claimed problems of ΛCDM with small scale structure formation such as the tension between Dark Matter simulations and observations with regard to both the density profiles of Dark Matter halos and for the number of predicted substructures inside a given host halo, the baryonic Tully-Fisher relation, the constant galactic surface density or the large scale bulk flows (See reference [17] for a summary and references therein for further details).

As a final remark, let us note that the enhanced growth rushes the modes into entering the non-linear regime at earlier times, breaking down the perturbative approach followed here. As it will be explained in the next Section, the disformal coupling comes equipped with a screening mechanism, that hides the effects of the additional force on dense environments. Addressing the consequences of this feature would require considering the non-linear backreaction of the field, which is not properly captured in the approximations considered so far. Chameleon-type theories also show a strengthening of the screening when non-linearities are properly taken into account [287].

6.5 The Disformal Screening Mechanism

In this section we will consider the possibility of extending the disformal coupling to visible matter, as well as other aspects of gravitational theories based on a disformal coupling in the Einstein frame. Due to the stringent bounds on equivalence principle violations [110], some sort of screening mechanism is necessary to hide the coupling in dense environments such as the Solar System. The role of a disformal coupling in the chameleon mechanism was recently investigated by Noller [288], who correctly noted that the disformal contribution to the conservation equations vanishes for static, pressureless configurations. This is obvious from (6.34), since only the T^{00} component is nonzero for dust, and when contracting the field derivatives with the stress tensor a non-vanishing result requires time evolution of the scalar field. Therefore, addressing the effects of disformal couplings requires studying the field dynamics in high density environments.

It is possible to obtain some insight into the dynamics of the field from the analysis of the background cosmology given in Section 6.3, where it was argued that for the purely disformal case the coupling was proportional to the scalar field energy density, cf. Eq. (6.48). This causes the existence of two regimes, a matter dominated regime in which the effects of the coupling are small, and a field dominated regime in which the coupled matter equation of state is modified, as can be seen in Figure 6.1. When denser regions form, the scalar field energy density becomes insufficient to produce large effects on the matter distribution, *unless* the field gradients follow the matter distribution and intensify the additional force. As it will be shown below, the kinetic mixing induced by the disformal coupling makes the scalar field evolution insensitive to the matter distribution, as long as the matter energy density is sufficiently high.

For the sake of concreteness, let us restrict ourselves to a canonical scalar field coupled to a perfect fluid. The general equation (6.36) then reads

$$\left(\mathcal{X} g^{\mu\nu} - B\, T_m^{\mu\nu}\right) \nabla_\mu \nabla_\nu \phi + \left(\frac{A'}{2} g_{\mu\nu} + \left(\frac{A' B}{A} - \frac{B'}{2} \right) \phi_{,\mu} \phi_{,\nu} \right) T_m^{\mu\nu} - \mathcal{X} V' = 0\,, \tag{6.60}$$

where $\mathcal{X} \equiv A - 2BX < A$ is bounded in order to avoid a singularity in the volume element of the barred metric $\sqrt{-\bar{g}} \propto \mathcal{X}^{1/2}$, cf. (6.19). The form of the field equation strongly suggests that the dynamics of the coupled system will be different in high than in low density environments. Since the energy momentum-tensor appears as a coefficient of the higher derivatives as well as in the effective potential, there is a well defined limit $T^{00} = \rho \to \infty$, in which the field equation simplifies considerably. This property will be crucial for the *disformal screening mechanism* analyzed in Section 6.5.2.

6.5.1 Pressure Instability

The above equation also shows that the different components of the energy momentum tensor can modify the character of the coefficient of the second order derivatives of the field. Equation (6.36) is a quasi-linear, diagonal second order equation [289], of the form

$$\phi_{;\mu\nu}\mathcal{M}^{\mu\nu}(\phi,\phi_{,\lambda},T^{\alpha\beta})+f(\phi,\phi_{,\lambda},T^{\alpha\beta})=0\,. \tag{6.61}$$

However, its hyperbolicity relies on the signature of $\mathcal{M}^{\mu\nu}$, which in turn depends on the relative values of the coefficients of the higher spatial and time derivatives. Focusing on the purely disformal case $A=1$ for concreteness, we see that the coefficient of the time derivatives, $\mathcal{M}^{00}=-1+2BX-B\rho$, can only flip sign if B or ρ are negative (because of the bound $2BX<1$). However, a large enough value of the Einstein frame pressure, $p>B^{-1}-X$, may flip the sign of $M^{ii}=1-BX-Bp$. If this happens, the equation becomes non-hyperbolic (at least locally), challenging the good initial value formulation and turning the system unstable.

Addressing the viability of the theory hence requires determining under which conditions the instability may occur dynamically, which in turn requires considering the evolution of the coupled matter components. In certain cases, the system might respond to a situation in which $Bp\lesssim 1-BX$ by diluting the (Einstein frame) pressure below the threshold value or softening the spatial gradients of the scalar field. In this sense, the instability induced by the pressure may be analogous to the potential existence of singularities in the disformal volume element whenever $\bar{g}\propto A-2BX\to 0$. This singularity in the barred metric is avoided by the field evolution, as it slows down whenever $B\dot{\phi}^2\to A$. The mechanism exploited to induce a slow roll phase in cosmological applications (disformal quintessence and the disformal coupling to matter described in Sections 5.2.1 and 6.3.1) is precisely this dynamical resistance to pathology.

Studying the conditions under which the pressure instability can be avoided dynamically might restrict the allowed functional forms of the conformal and disformal factors. In the worst case, it might spoil the disformal screening mechanism, or even completely forbid the occurrence of a disformal coupling. Determining whether or not this is the case will be the objective of future work. The Einstein frame pressure p will be neglected as a part of the approximation scheme in the following analysis, implicitly assuming that the theory is well behaved.

6.5.2 The Scalar Field in Dense, Non-relativistic Environments

The study of Solar System and laboratory tests of gravity requires considering energy densities that are much higher than the cosmological average and pressure is completely sub-dominant. As a first approximation, this regime can be explored using the general scalar field equation (6.60) for a static matter distribution $\rho(\vec{x})$ in the limit $\rho\to\infty$. More precisely, the following ratios will be assumed to be negligible

$$\Gamma^{\mu}_{00}\phi_{,\mu}\;\sim\;\frac{p}{\rho}\;\sim\;\frac{p}{\rho}\left(\frac{\vec{\partial}\phi}{\partial_t\phi}\right)^2\;\sim\;\frac{\mathcal{X}}{B\rho}\;\sim\;\frac{\mathcal{X}}{B\rho}V'\;\sim 0 \tag{6.62}$$

These approximations quantify to what extent the effects of gravity and pressure are disregarded, the requirement of having "soft" spatial gradients relative to the time evolution

and the fact that $B\rho$ is large enough. This conditions will be briefly discussed at the end of the Section, focusing on systems in which their lack of fulfillment might lead to observable signatures.

The set of assumptions (6.62) simplifies the field equation (6.60) considerably

$$\ddot{\phi} \approx -\frac{B'}{2B}\dot{\phi}^2 + A'\left(\frac{\dot{\phi}^2}{A} - \frac{1}{2B}\right) = -\frac{\beta}{2M_p}\dot{\phi}^2\,, \tag{6.63}$$

where the first equality is general and the second applies to a purely disformal coupling with exponential forms (6.49). The above expression departs substantially from the simple conformal coupling, for which the $\rho \to \infty$ limit is ill-defined. Two important features of the above equation endow the theory with the *disformal screening mechanism*:

- The spatial derivatives become irrelevant, as they are suppressed by a p/ρ factor w.r.t. the time derivatives.[9]
- The equation is *independent of the local energy density*, making the field evolution insensitive to the presence and distribution of massive bodies.

These features ensure that *the field rolls homogeneously* and avoids the formation of spatial gradients between separate objects, which would give rise to the scalar force. The above properties are caused by the kinetic mixing between the field and matter degrees of freedom, and lay at the core of the decoupling between both components.

Let us analyze the simpler, purely disformal exponential case. The second equality of equation (6.63) can be easily integrated

$$\dot{\phi}(t) = \frac{M_p}{\beta}\left(t + \frac{M_p}{\beta\dot{\phi}(0)}\right)^{-1}\,. \tag{6.64}$$

In this solution the field time variation is approximately constant while $t \ll \frac{M_p}{\beta\dot{\phi}(0)}$ and slows down afterwards as $\propto 1/t$. Since the coupling to non-relativistic matter is proportional to $\dot{\phi}$, stronger couplings decay earlier. It is possible to obtain an implicit solution for $A = 1$, $\dot{\rho} = 0$ keeping the potential V, but otherwise assuming the simplifications (6.62). It is given as an implicit solution

$$t - t_0 = \int_{\phi_0}^{\phi}\sqrt{\frac{B(\phi')}{C_0 - 2V(\phi')/\rho}}d\phi'\,, \tag{6.65}$$

where $\dot{\phi}^2 = \frac{C_0}{B} - \frac{2V(\phi)}{B\rho}$.[10] The potential appears suppressed with respect to the energy density. In tracking Dark Energy models, V is a decreasing function of the field and $\dot{\phi} > 0$. Therefore, V is of the order of magnitude of the average cosmic density ρ_0 and can be safely neglected for high energy densities, recovering the simpler solution (6.64). As the field slows

[9] Equation (6.63) also follows from taking the limit $\rho \gg A/B, \dot{\phi}^2$ in the FRW coupling density Q_0 (6.45), precisely due to the absence of spatial derivatives.

[10] Under these assumptions, Eq. (6.60) can be written as $\ddot{\phi} + \frac{B'}{2B}\dot{\phi}^2 + \frac{V'}{B\rho} = \frac{1}{B\dot{\phi}}\frac{d}{dt}\left(B\dot{\phi}^2/2 + \frac{V}{\rho}\right) = 0$. The second equality can be directly integrated, giving the constraint $\dot{\phi}^2 = \frac{C_0}{B} - \frac{2V(\phi)}{B\rho}$, which can be integrated again to obtain (6.65).

down with time if $B'/B > 0$, the order of magnitude of the field time derivative is also cosmological.

One of the effects of the coupling is to modify the energy conservation equation for matter in the Einstein frame, cf. Eq. (6.40). This induces a variation of the gravitational mass, that can be bounded by precision gravity tests. In a gravitationally bound two body system, this effect is degenerate with a possible time evolution of Newton's constant $\frac{\dot{G}}{G} \leftrightarrow \frac{\dot{M}}{M} + \frac{\dot{m}}{m}$ to a first approximation, as can be argued by deriving the expression for the Newtoninan force with respect to time. Lunar laser ranging bounds place precise bounds on this effect to the level of $\dot{G}/G < 10^{-3}/\text{Gy}$ [290]. The magnitude of energy density variation induced by a disformal coupling can be estimated as $\dot{\rho} \approx -(\ddot{\phi} + V')\dot{\phi}$. Assuming $\dot{\phi}^2 \sim V \sim \rho_0$ as discussed above, $B\rho_0 \gtrsim 1$ and the solution (6.64), typical mass variation rates $\dot{M}/M$ are as small as $\sim 10^{-6}/\text{Gy}$ for the interstellar medium and $\sim 10^{-29}/\text{Gy}$ for the average Earth density, well beyond the sensitivity of Lunar laser ranging.

Potential Signatures

New local, astrophysical and cosmological signatures may be found by relaxing the approximations (6.62) assumed in the previous analysis. Some situations where the coupling might become observable include:

- **Matter velocity flows:** The spatial component of the matter four-velocity T^{0i} mixes the time and space derivatives of the field, as non-zero velocities introduce terms proporional to $\phi_{;0i}$, $\dot{\phi}\,\phi_{,i}$, which may source the field evolution. These effects are suppressed by a relativistic v/c factor, but they may be important in certain systems such as binary pulsars.

- **Pressure:** Applications of the disformal coupling in the context of Dark Energy arguably require a value $B\rho_0 \gg 1$, where ρ_0 is the average cosmic density. Then, even though the pressure is usually negligible with respect to the energy density, it should be easy to find systems for which Bp is also much larger than one. This might have important consequences for the stability of the theory, as was briefly discussed in Section 6.5.1.

- **Radiation:** Unlike in the conformal case, the disformal coupling has non-trivial effects on ultra-relativistic fields for which $T \approx 0$, cf. (6.33). Some authors have initiated the study of the disformal coupling in scenarios featuring radiation. Brax *et al.* [291] considered high-precision, low-energy photon experiments, which might be able to detect the influence of a disformal coupling on top of a conformal one. The distortions in the baryon-photon chemical potential induced by a disformal coupling and their signatures on the CMB small scale spectrum have been studied by van de Bruck and Sculthorpe [292]. Other effects may follow if Electromagnetism is formulated in terms of the barred metric, such as varying speed of light or modified gravitational light deflection.

- **Strong gravitational fields:** The connection coefficient $\Gamma^{\mu}_{00}\phi_{,\mu}$ in the field derivative term is not suppressed by $B\rho$. It represents the effects of gravity, and was neglected because it is small in most Solar System applications, since $\Gamma^{r}_{00} = \frac{GM}{r^3}(r - 2GM)$ in the Schwarzschild metric. However, this term might become relevant in strong gravitational fields, such as the vicinity of black holes or compact objects.

- **Spatial Field Gradients:** In the $B\rho \gg 1$, $\rho \gg p$ limit, the equation for the scalar field (6.63) becomes independent of the matter content and the field derivatives. Therefore, if the field acquires a spatial modulation before reaching this limit, it will be preserved by the subsequent evolution. Spatial gradients of the field formed when the linear perturbation theory is valid would then be present today, with their actual value depending on the details of the transition between the perturbative (e.g. the small scale limit considered in Section 6.4.1) and the screened regimes. Gradients of cosmological origin might seem as preferred direction effects pointing towards cosmic structures when analyzed in the Solar System.

  Spatial derivatives of the field may also be important if the field is rolling sufficiently slow as to overcome the p/ρ factor in (6.62).

These and other settings might lead to characteristic signatures and new bounds for disformally coupled theories, which will be investigated in the future. It should be also possible to obtain the coefficients of the Parameterized Post Newtonian approximation, which would allow a more systematic comparison to local gravity tests.

6.6 Discussion

The disformal relation provides a generalization of the conformal transformation. It has been used to construct theories of modified gravity, notably those which produce non-trivial effects on null geodesics, such as varying speed of light and gravitational alternatives to Dark Matter. It also appears in the description of branes embedded in a higher dimensional bulk space, in which the scalar fields represent the brane position in a certain set of coordinates. The results of the present Chapter concern the subset of theories which can be expressed as General Relativity plus a matter Lagrangian, which is constructed using the disformal metric. This provides a generalization of the old-school scalar tensor theories in the Einstein frame: Test particles follow geodesics which explicitly involve derivatives of the scalar field, and the energy momentum of the field and coupled matter (computed w.r.t. the gravitational metric) is not conserved separately.

It is possible to restore the theory to a Jordan frame representation by reversing the disformal transformation, as was argued in Section 6.2.1 and computed first in Ref. [68]. The computation of the Einsten-Hilbert action for a disformal metric produces a theory in which the field has a non-minimal derivative coupling to the Ricci scalar and in which new, higher derivative terms appear. The resulting Lagrangian density has the correct Horndeski form (1.28), and the theory is therefore described by second order equations of motion and stable in light of Ostrogradski's Theorem. The existence of additional frames, in which only the conformal or disformal part enter the matter action explicitly, provides new tools to analyze this type of theories and further connections between different models (e.g. a disformal theory in the Jordan frame reduces to a 4^{th} Galileon Lagrangian in the non-relativistic limit). The terms arising from the inverse disformal transformation contain higher derivatives, endowing the theory with the Vainshtein screening in the conformal and Jordan frames, which allows the field to cause effects on cosmological scales while remaining undetectable in the Solar System.

The equivalence between certain higher derivative theories with conformal or minimal coupling and disformally coupled theories with an Einstein-Hilbert gravitational sector provides new means to analyze this type of models. Although the equations for disformally

coupled theories are rather involved, they are much simpler than higher derivative Horndeski theories in the Jordan frame. Hence the analysis of disformal theories in the Einstein frame can be regarded as equivalent to (at least) some scalar-tensor theories featuring the Vainshtein screening mechanism. The kinetic mixing between the coupled degrees of freedom makes it necessary to solve for the higher time derivatives of the different components. Although this generally requires some assumptions, e.g. about the metric, a general equation without derivatives of the energy-momentum tensor can be obtained (6.36). Once solutions are computed, it is possible to restore to the Jordan metric in order to interpret the results and compare to observations.

In high density environments (as measured by the condition $B\rho \gg 1$) the field does not feel the pressence of disformally coupled, non-relativistic matter. This provides a novel *disformal screening mechanism*, which is distinct from screening mechanisms based on the field potential (Chameleon and Symmetron). Our mechanism relies on the existence of a well defined limit $\rho \to \infty$ in the scalar field equation, given by equation (6.63), for which the field evolution is independent of the matter distribution and the field gradients, up to effects of order $\sim p/\rho$, v/c. If the conformal part A is negligible, only a friction term remains and the field coupling density (6.34) is a decreasing function of time. As it evolves below its cosmological value (provided $V' < 0$ and $B'/B > 0$), the effects of the coupling are suppressed by a factor $\sim \rho_0/\rho$ and the theory is consistent with precision gravity tests. Potentially detectable signatures may be obtained in the presence of matter velocity flows, radiation or pressure, strong gravitational fields or gradients of cosmological origin.

The disformal screening mechanism may be related to the Vainhstein effect [84], which suppresses the gradients of the scalar field and hides the additional force near massive sources due to the higher order derivative self-interactions. In the disformal case, the screening relies on the kinetic mixing between the scalar field and the coupled degrees of freedom. This ultimately allow the existence of a well defined $\rho \to \infty$ limit in which the field is free, or only subject to friction(up to conformal interactions). Hence the disformal mechanism belongs to the kinetic screening category. Moreover, the two cases might indeed be the same physical effect expressed in different frames, due to the equivalence between the disformally coupled theories and a particular higher derivative sector of the Horndeski Lagrangian.

The disformal coupling offers interesting possibilities to build models for cosmic acceleration. In the FRW approximation, the same properties that gave rise to the disformal screening mechanism make the background coupling approximately proportional to the dark energy density (6.48) rather than to the coupled matter energy density. This provides a concrete realization of a class of interacting dark matter models which have been extensively studied using phenomenological parameterizations. The equations for linear perturbations around FRW contain scale dependent terms. These are absent in the pure conformally coupled case, and have hence the potential to distinguish the two possibilities. An analytic equation for the coupled matter perturbations was derived in the small scale limit. On top of an additional friction term, the effect of the fifth force can be encapsulated in the definition of an effective gravitational constant (6.59) which depends on the background coupling factor.

In order to investigate the cosmological implications of a disformal coupling in a simple setting, a *Disformally Coupled Dark Matter* (DCDM) example model was proposed. This has the advantage of avoiding the subtleties of the Einstein frame description, since gravity, baryons and photons share the same physical metric. Additionally, the model has the advantage of being compatible with local gravitational phenomena without invoking the dis-

formal screening mechanism. A DCDM model with exponential functions and no conformal coupling (6.49) provides a dark energy model that tracks the dominant energy component at early times. When the coupling to Dark Matter becomes active, the scalar field enters a slow roll phase in order to dynamically avoid a singularity of the disformal metric. The free parameters can be constrained by observations, and the model is successful at the background level. When perturbations are included, the DCDM model introduces a series of new effects. The effective gravitational constant for this model is too large, due to the persistence of the coupling at late times and the domination of the energy budget by the scalar field. This causes a too large enhancement of the growth factor, which affects the normalization of the DM and baryon power spectra, producing a very large ISW effect. Scale dependent effects are reflected on matter oscillatory features on very large scales and a scale dependent bias between the coupled dark matter and (uncoupled) baryonic component.

There is considerable freedom in the model to produce cosmologically viable scenarios. Models of the DCDM type with less dramatic growth of perturbations can be constructed by modifying the functional dependence of the disformal coupling (e.g. tuning it to become negligible after the transition to slow roll), the scalar field Lagrangian (e.g. constructing it with a disformal metric), or perhaps by the interplay between the conformal and the disformal parts of the coupling. Variations or extensions of DCDM may postulate or include disformally coupled neutrinos.

Another phenomenological direction is to consider the disformal screening mechanism in detail. The results presented here considered a purely disformal coupling, monotonically increasing with the field. Certainly, including a conformal coupling and more general functional forms is of interest. These considerations might help to avoid the instability caused by the Einstein frame pressure if $Bp > 1$, as it was discussed in Section 6.5.1. Once different set-ups are formulated, it is worth to explore the observable signatures for the model by quantifying the effects outlined at the end of Section 6.5.2.

The dependence of the free functions in the Horndeski Lagrangian (1.28) on the field kinetic term X has a very special role, as it relates the coupling to gravity to the coefficients of the second derivative field terms. Therefore, it would be worth considering the transformations between frames in the more general case in which the disformal relations are allowed to depend on X. The computation of the Ricci scalar associated to this general disformal metric would provide the Jordan frame representation of the most general scalar-tensor theory that accepts an Einstein frame description. Since the equations simplify considerably in this frame, the phenomenology of these theories would be relatively easy to address.

Finally, the existence of a well behaved $\rho \to \infty$ classical limit in the field equation suggests that disformally coupled theories might introduce new interesting features for the physics of gravitational singularities and other high energy regimes. The implications of kinetic mixing for the formation of black holes or the origin of the universe is beyond the scope of the present work, but it might provide a fruitful exploration to pursue in the future. This discussion provided just a glimpse to the potential applications of the disformal relation. As a generalization of the conformal case, which was very central to the gravitation and cosmology of the 20^{th} Century, the use of disformal transformation might provide novel ways to address the physics of the 21^{th} Century.

Chapter 7

Conclusions and Outlook

People don't want their lives fixed. Nobody wants their problems solved. Their dramas. Their distractions. Their stories resolved. Their messes cleaned up. Because what would they have left? Just the big scary unknown.

Chuck Palahniuk[1]

The present Thesis analyzes several alternatives to the Standard Cosmological Model that attempt to explain the observed cosmic acceleration. The predictions of these scenarios have been compared with current data, in order to determine which mechanism is empirically favored. The simplest explanation is a Cosmological Constant. Although phenomenologically successful, it is nonetheless unsatisfying according to theoretical estimates and there are good reasons to go beyond, even in the absence of discrepant observations. The alternatives considered either drop the assumption of homogeneity on large scales or introduce modifications in the Einstein-Hilbert action. Theories that generalize the gravitational sector introduce new degrees of freedom, either effective or fundamental. They can be roughly classified as Modified Gravity or Dark Energy, depending on whether their effects on standard matter are direct or indirect. It is also possible to consider purely phenomenological modifications of the underlying equations. Each of these possibilities has been explored in the previous Chapters.

The cheapest option in terms of new physics turns out to be the most difficult to reconcile with observations. Adiabatic inhomogeneous cosmologies without Dark Energy, which can be interpreted as the gravitational growth of a spherically symmetric perturbation with an initially small amplitude, are actually ruled out by current data on geometric observables. LTB models with a CGBH matter profile are unable to simultaneously fit Supernovae and Baryon Acoustic Oscillation (BAO) scale observations. In these models, the apparent acceleration is caused by the relatively lower deceleration near the location of our galaxy (lower

[1] *Survivor* (1999)

density region), compared to the asymptotic value (higher density region). If the density contrast is enough to produce the fictitious acceleration demanded by SNe observations, the lower deceleration near the center produces an additional stretching of the low redshift BAO scale with respect to the asymptotic value, which is incompatible with current, higher redshift data. Due to the generality of the effect, it is expected that a similar tension would be found regardless of the matter profile. This discrepancy provides further evidence against inhomogeneous cosmological models with adiabatic initial conditions, e.g. on top of bounds from the kSZ effect and the expansion rate measured at different redshifts.

The inhomogeneous growth of free falling scales such as the BAO correlation length can be used to test inhomogeneity within more general models. It is possible to use inhomogeneous models of the LTB type with a Cosmological Constant (or other form of Dark Energy) to quantify the level of inhomogeneity allowed by observations. More generally, one can further drop assumptions and consider inhomogeneity in other degrees of freedom (age of the universe, baryon-dark matter or baryon-photon ratios), non-central locations or even less symmetric space-times. The general program to test large scale homogeneity and the Copernican Principle requires extending the set of observables and analyzing them without introducing spurious assumptions. The volume-averaged BAO scale discrepancy may be rendered concordant with SNe by the inclusion of Dark Energy or inhomogeneous baryon fraction. However, new data able to separate the radial and angular distances (e.g. the Alcock-Paczynski effect) can potentially break the degeneracy. This program would naturally profit from the inclusion of dynamical observables, such as Redshift Space Distortions and the Integrated Sachs-Wolfe effect.

The model based approach has a number of advantages with respect to phenomenological descriptions of modified theories. It allows one to give a self consistent description which is well connected to the underlying ideas. Additionally, it can be used to extract predictions in different situations, although the possibilities are usually limited by technical or computational difficulties. On the other hand, phenomenological models often require a number of assumptions in order to obtain the background or perturbation equations, as it was the case of the entropic (modified) gravity scenarios. Parameterizations also allow to explore the inter-dependence of the assumptions (e.g. the preference towards slightly closed spatial sections by the Dark Energy model based on a Generalized Entropy-area Law). Concrete models are complementary to phenomenological parameterizations. The former allow to study the link between observational signatures and the underlying physical mechanisms, and provide valuable inspiration for the latter.

Disformal relations tend new bridges between different scalar-tensor theories of gravity. The inclusion of a scalar field generously extends the theory space from the Einstein-Hilbert to the Horndeski Lagrangian, which allows four free functions of the field and its kinetic term. The disformal transformation applied to a canonical scalar field Lagrangian minimally coupled to gravity recovers a variety of Dark Energy models, that belong to the simplest of Horndeski's functions (k-essence). More generally, the disformal prescription applied to the matter sector introduces a new scalar force. If the gravitational sector is standard, these disformally coupled theories are the Einstein Frame representation of a theory in which the field couples to the curvature tensors through its derivatives, together with second order (but safe) derivative terms. This Jordan Frame representation, obtained by undoing the disformal transformation, corresponds to a particular form of the function in the Horndeski Lagrangian which corresponds to the generalized fourth order Galileon term. These theories

have attracted considerable attention because they are endowed with the Vainshtein screening mechanism, which hides the force mediated by the field near massive bodies.

Theories based on a disformal coupling to matter come naturally equipped with a *disformal screening mechanism*, that renders them viable in the Solar System. The kinetic mixing with the disformally coupled degrees of freedom makes the scalar field equation independent of the matter distribution and the field spatial derivatives in high density, non-relativistic environments. Then the field rolls homogeneously and does not develop gradients between massive bodies, hiding the scalar force. If the field is set up for cosmological applications, the effects of the field are suppressed by the ratio between the local and cosmic average energy density. Based on the correspondence between disformally coupled theories and generalized Galileons, the disformal screening mechanism may be just the Vainshtein effect in disguise. The duality between the higher derivative Jordan Frame and the disformally coupled Einstein Frame descriptions would facilitate the exploration of certain sectors in the Horndeski Lagrangian. Just as in old school scalar-tensor theories, the Einstein Frame description considerably simplifies the equations and is hence useful for computational purposes.

Disformal relations also allow the construction of models for cosmic acceleration. These rely on their dynamical resistance to produce singularities in the disformal metric, which drives the scalar field into a slow roll phase. This property was explored explicitly in two cases that avoid the subtleties of working in the Einstein Frame. Disformal quintessence provides a Dark Energy model compatible with current observations, as it converges to a Cosmological Constant if the potentials are very steep, making it very difficult to distinguish from the Standard Cosmological Model. The Disformally Coupled Dark Energy models introduce more dramatic departures due to the direct effect on Dark Matter. The simple model considered is viable a at the background level. However, the evolution of linear perturbations is incompatible with observations, due to the strong effects on the matter power spectrum and the large Integrated Sachs-Wolfe. Fortunately, viable models may be constructed by exploring the freedom in the field Lagrangian and the coupling functions. These alternatives might be distinguishable from other modifications of gravity and coupled Dark Matter models by the additional bias between DM and baryons, as well as for the scale dependence of the perturbations growth, which is different from conformally coupled models.

It is necessary for the health of science to bear in mind alternative models. Regardless of its success, due respect to the Standard Cosmological Model requires the right dose of skepticism. On the observational side, it helps to identify and avoid (or at least control) the inclusion of model dependent assumptions in the analysis of the data. Studying the phenomenological implications of alternative models and comparing them to observations also allows one to explicitly probe the underlying assumptions behind the standard paradigm, as well as to quantify the allowed departures. This is important, as empirical science relies on disproving alternatives rather than confirming hypotheses. Considerable knowledge can be gained from the theoretical point of view, as the study of alternatives helps to understand and clarify the properties of the standard paradigm. These considerations will become even more important for the next generation of cosmological surveys, as they will either validate the foundations of the Standard Cosmological model to higher accuracy, or open Pandora's box again by bringing new surprises.

Part III

Appendices

Appendix A

MCMC Analysis

When confronting cosmological models with observations, the objective is to determine which values of the free parameters (our theory) are compatible with an available set of astronomical data (our Universe). Since measurements are not infinitely precise, the compatible set of parameters will occupy at least a finite volume in the parameter space, which is initially unknown. What is known is the probability of obtaining a certain measurement for a given model, which can be obtained by comparing the theoretical prediction with the experimental value and its uncertainty (e.g. assuming Gaussian errors). This probability $\mathcal{L}(\mathbf{D}|u)$ is known as the likelihood of observing the data $\mathbf{D}$ (a vector in the space of observations) given a model u (a vector in the space of parameters). It has to be inverted in order to obtain the posterior distribution $P(u|\mathbf{D})$, i.e. the probability of u being the true model if $\mathbf{D}$ is observed. Both probabilities are related through Bayes theorem:

$$P(u|\mathbf{D}) = \frac{\mathcal{L}(\mathbf{D}|u)\pi(u)}{\int \mathcal{L}(\mathbf{D}|u')\pi(u')du'} \tag{A.1}$$

Monte Carlo Markov Chain analysis constitute a widely used strategy to invert the likelihood and obtain the posterior distribution. A direct grid sampling of the parameter space requires a great deal of computational effort, since the number of points scales with exponentially with the number of parameters. On the other hand, MCMC execution times increase roughly linearly with the number of parameters. A Markov Chain is a stochastic sampling of the parameter space $\{u_0, ..., u_n\}$ in which the point u_i only depends on u_{i-1}. If the way in which the chain is created is chosen properly, the distribution of its points will converge to the posterior distribution

$$\text{Dist}\{u_0, ..., u_n\} = P(u|\mathbf{D}) \tag{A.2}$$

The sampling method used by CMBEasy is the Metropolis algorithm [293]. For a given point u_i, the next point is chosen as follow:

1. Compute $L(\mathbf{D}|u_i)$; the likelihood of observing $\mathbf{D}$ given the parameters u_i.
2. Propose a new parameter vector by sampling from a proposal distribution $q(u_i, u_{i+1})$ (see below).
3. Compute the likelihood for the proposed parameter $L(\mathbf{D}|u_{i+1})$.

4. If the likelihood is higher $L_{i+1} > L_i$, the point is added to the chain and the procedure goes to step 2.

5. If $L_{i+1} < L_i$, a random variable $u \in [0, 1]$ is generated. If $u < L_{i+1}/L_i$, the step is taken and go to 2. Otherwise go to 2, but reject the actual point u_{i+1}.

The algorithm assumes flat priors $\pi(u)$ and a symmetric proposal distribution $q(u_i, u_{i+1})$. Likelihoods outside the boundaries are assigned zero likelihood. An adaptive stepsize sampler helps to the convergence and mixing of the chains. Too large stepsize will lead to many steps being rejected, while too short stepsize will take a long time to sample the distribution. The function $q(u_i, u_{i+1})$ is Gaussian, and it is estimated from the previous points in the chains. Stepsizes are taking along the principal axes of this distribution to take into account the possible degeneracies among the parameters.

The initial point in the chain is chosen randomly in the parameter space and will move to regions of higher likelihood afterwards. Therefore, the first points in every chain do not reflect the distribution of $P(u|\mathbf{D})$. In order to test the convergence and determine how many points to ignore, the algorithm uses a number m of chains to evaluate their mixing and convergence. CMBeasy uses the test of Gelman and Rubin [217] to calculate the variance of each parameter between chains. We denote by ψ_{ij} the value of one parameter at the point $j = 1, ..n$ of chain i, and a bar over a quantity means average over the missing indices. The variance between chains B and within chains W are given by [218]

$$B = \frac{n}{m-1} \sum_{i=1}^{m} (\bar{\psi}_i - \bar{\psi})^2 \,, \tag{A.3}$$

$$W = \frac{1}{m(n-1)} \sum_{i=1}^{m} \sum_{j=1}^{n} (\psi_{ij} - \bar{\psi}_i) \,, \tag{A.4}$$

where the sums over the point index j are taken over the last n points instead of the whole chain. The quantity

$$R = \frac{\frac{n-1}{n} W + \frac{1}{n} B}{W} \tag{A.5}$$

should converge to one for the stationary distribution. If, for each parameter $R < 1.2$, the chain can be safely considered to be sampling from the posterior distribution.

Appendix B

CMBEasy

CMBEasy [216] is an open source program for the computation of cosmological observables based on CMBFAST [118]. It is written in C++, and its object oriented source code allows very clean modifications of the code by simply re-implementing the desired functions in the proper subclasses. As in its precursor, most quantities are stored in splines, a very efficient structure to contain and manipulate functions of a single variable. The actual version can compute power and CMB spectra within seconds, including tensors and polarization. Two different gauges (synchronous and Newtonian) and several quintessence models are included. A typical CMB computation is done as follows:

1. The background and thermal histories are computed.
2. The perturbations are propagated in Fourier space for different k modes.
3. The line of sight integration (2.5) is used to compute the anisotropy spectrum seen today.

The *Analyze This!* [218] package provides the necessary functions to observationally constraint models. It is based on the `analizethis` class, containing the routines necessary to calculate the likelihoods of the computed model for a wide set of available astronomical data, a program designed to run the MCMCs in a OpenMPI parallel environment. All the computations of cosmological observables contained in this thesis were performed using suitably modified versions of CMBeasy.

Appendix C

Equations for Generalized k-essence

The action for the scalar is specified through a Lagrangian density

$$S_k = \int d^4x\sqrt{-g}\ \mathcal{L}(X,\phi)\,, \tag{C.1}$$

where $X \equiv -\frac{1}{2}g^{ab}\phi_{,a}\phi_{,b}$. With these conventions, canonical quintessence corresponds to $\mathcal{L}(X,\phi) = X - V(\phi)$. The energy momentum tensor is

$$T^{(\phi)}_{ab} = \frac{-2}{\sqrt{-g}}\frac{\delta\sqrt{-g}\mathcal{L}(X,\phi)}{\delta g^{ab}} = \mathcal{L}(X,\phi)g_{ab} + \mathcal{L}_{,X}(X,\phi)\phi_{,a}\phi_{,b}\,, \tag{C.2}$$

where commas denote partial derivatives. The dynamical equation for the scalar field is

$$\mathcal{L}_{,\phi} - \nabla_a(\mathcal{L}_{,X}\partial^a\phi) = 0\,. \tag{C.3}$$

Background equations: For the flat FRW metric using conformal time $ds^2 = a^2(\tau)(-d\tau^2 + d\bar{x}^2)$ and

$$\rho_\phi = \mathcal{L}_{,X}\phi'^2/a^2 - \mathcal{L}\,, \tag{C.4}$$

$$p_\phi = \mathcal{L}\,, \qquad , \tag{C.5}$$

where $f' = f_{,\tau}$. Expanding the covariant derivative in (C.3) for an FRW metric yields the field equation

$$\mathcal{M}\phi'' + \mathcal{H}(3\mathcal{L}_{,X} - \mathcal{M})\phi' + a^2\mathcal{L}_{,\phi} + \mathcal{L}_{,X\phi}\phi'^{\,2} = 0\,, \tag{C.6}$$

where $\mathcal{M} \equiv \mathcal{L}_{,X} - \mathcal{L}_{,XX}\phi'^2/a^2$ is useful to define.

Linear perturbations (syncrhonous gauge): $ds^2 = a^2(\tau)(-d\tau^2 + (\delta_{ij} + h_{ij})\,dx^i dx^j)$ (using Ma & Bertschinger's notation [274]) the relevant terms for Einstein Equations become

$$\delta\rho_\phi = \mathcal{M}\phi'\delta\phi'/a^2 - (\mathcal{L}_{,\phi} - \mathcal{L}_{,X\phi}(\phi'/a)^2)\delta\phi\,. \tag{C.7}$$

$$\delta p_\phi = \mathcal{L}_{,\phi}\delta\phi + \mathcal{L}_{,X}\phi'\delta\phi'/a^2 + \mathcal{L}\,h/3\,, \tag{C.8}$$

$$(\rho + p)\theta_\phi = -\mathcal{L}_{,X}\frac{k^2}{a^2}\phi'\delta\phi\,. \tag{C.9}$$

$\Sigma^i{}_j = \mathcal{O}(\delta\phi^2)$ and $h = \delta^{ij}h_{ij}$. The Equation for the field perturbations is

$$\begin{aligned} &\mathcal{M}\delta\phi'' + \left[2\mathcal{H}\mathcal{M} + \mathcal{M}'\right]\delta\phi' + \tfrac{1}{2}\mathcal{L}_{,X}h'\phi' \\ &+ \left[\mathcal{L}_{,X}k^2 + (\phi'' + 2\mathcal{H}\phi')\mathcal{L}_{,X\phi} + \mathcal{L}'_{,X\phi}\phi' + a^2\mathcal{L}_{,\phi\phi}\right]\delta\phi = 0\,. \end{aligned} \tag{C.10}$$

Since the coefficients are background quantities, we can take its derivatives $M', \mathcal{L}'_{,X\phi}$ through a spline.

Appendix D

Disformal Relations

Consider the disformal relation between two metrics, specified by the two scalar functions A, B, and a vector b_μ,

$$\bar{g}_{\mu\nu} = A g_{\mu\nu} + B b_\mu b_\nu \,. \tag{D.1}$$

The inverse metric can be found by contraction

$$\bar{g}^{\mu\nu} = \frac{1}{A}\left(g^{\mu\nu} - \gamma^2 b^\mu b^\nu\right) \,. \tag{D.2}$$

where

$$\gamma^2 \equiv \frac{B}{A + B b^2} \,, \tag{D.3}$$

and $b^2 \equiv g^{\mu\nu} b_\mu b_\nu \equiv b^\mu b_\mu$. The determinant of the barred and unbarred metrics are related

$$\sqrt{\frac{\bar{g}}{g}} = A\sqrt{\frac{AB}{\gamma^2}} = A^2\sqrt{1 + \frac{B}{A}b^2} \,, \tag{D.4}$$

The above relation is derived in Appendix C of Reference [60].

It is possible to write the relation of stress energy momentum tensor (associated to a Lagrangian $\sqrt{-g}\mathcal{L}$) in the two metrics by using the chain rule

$$T^{\mu\nu} \equiv \frac{2}{\sqrt{-g}}\frac{\delta\left(\sqrt{-g}\mathcal{L}\right)}{\delta g_{\mu\nu}} = \sqrt{\frac{\bar{g}}{g}}\frac{\delta \bar{g}_{\alpha\beta}}{\delta g_{\mu\nu}}\left(\frac{2}{\sqrt{-\bar{g}}}\frac{\delta\left(\sqrt{-g}\mathcal{L}\right)}{\delta \bar{g}_{\alpha\beta}}\right) \,. \tag{D.5}$$

By identifying the quantity in brackets as $\bar{T}^{\mu\nu}$ and using (D.4), the following relation follows

$$T^{\mu\nu} = A^3\sqrt{1 + \frac{B}{A}b^2}\,\bar{T}^{\mu\nu} \,. \tag{D.6}$$

The equivalent relation with lower indices is considerably more involved

$$T_{\mu\nu} = \sqrt{\frac{\bar{g}}{g}} D_{\mu\nu}{}^{\alpha\beta}\bar{T}_{\alpha\beta} \,, \tag{D.7}$$

where

$$D_{\mu\nu}{}^{\alpha\beta} \equiv \frac{\delta \bar{g}^{\alpha\beta}}{\delta g^{\mu\nu}} = \frac{1}{A}\left(\delta^\alpha_\mu \delta^\beta_\nu - 2\gamma^2 b^\alpha b_{(\mu}\delta^\beta_{\nu)} + \gamma^4 b_\mu b_\nu b^\alpha b^\beta\right) \,. \tag{D.8}$$

The inverse relations are provided below for completeness

$$g_{\mu\nu} = \frac{1}{A}\left(\bar{g}_{\mu\nu} - B\bar{b}_\mu\bar{b}_\nu\right) , \tag{D.9}$$

$$g^{\mu\nu} = A\left(\bar{g}^{\mu\nu} + \bar{\gamma}^2\bar{b}^\mu\bar{b}^\nu\right) , \quad \bar{\gamma}^2 \equiv \frac{B}{A - B\bar{b}^2} , \tag{D.10}$$

$$\bar{D}^{\mu\nu}{}_{\alpha\beta} = A\left(\delta^\mu_\alpha\delta^\nu_\beta + 2\bar{\gamma}^2\delta^\mu_{(\alpha}\bar{b}_{\beta)}\bar{b}^\nu + \bar{\gamma}^4\bar{b}^\mu\bar{b}^\nu\bar{b}_\alpha\bar{b}_\beta\right) , \tag{D.11}$$

where $\bar{b}^\mu \equiv \bar{g}^{\mu\nu}b_\nu$. Note that $\bar{b}_\mu = b_\mu$, $\bar{b}^\mu = B/(A\bar{\gamma}^2)b^\mu$ and $\gamma^2 b^2 = B\bar{b}^2$.

D.1 Disformal Geodesics

The expression for the disformal connection (6.6) can be expanded in terms of the functions in the disformal metric

$$\begin{aligned}\bar{\Gamma}^\mu_{\alpha\beta} = \Gamma^\mu_{\alpha\beta} &+ \delta^\mu_{(\alpha}\log A_{,\beta)} - \frac{1}{2}\log A^{,\mu}g_{\alpha\beta} + \frac{1}{A}\left(\phi^{,\mu}B_{,(\alpha}\phi_{,\beta)} - \frac{1}{2}B^{,\mu}\phi_{,\alpha}\phi_{,\beta}\right) \\ &- \frac{\gamma^2}{A}\phi^{,\mu}\Big[A_{,(\alpha}\phi_{,\beta)} - \frac{1}{2}\phi^{,\lambda}A_{,\lambda}g_{\alpha\beta} - 2X\left(B_{,\alpha}\phi_{,\beta} - \frac{1}{2}\phi^{,\lambda}B_{,\lambda}\phi_{,\alpha}\phi_{,\beta}\right)\Big] \\ &+ \frac{B}{A}\Big[\nabla_{(\alpha}\left(\phi_{,\beta)}\phi^{,\mu}\right) - \frac{1}{2}\nabla^\mu\left(\phi_{,\alpha}\phi_{,\beta}\right) - \gamma^2\phi^{,\mu}\phi^{,\lambda}\left(\nabla_{(\alpha}\left(\phi_{,\beta)}\phi_{,\lambda}\right) - \frac{1}{2}\nabla_\lambda\left(\phi_{,\alpha}\phi_{,\beta}\right)\right)\Big] .\end{aligned} \tag{D.12}$$

Here $\gamma^2 \equiv \frac{B}{A-2BX}$ arises from the inverse barred metric, eq. (D.2). The first term is just the connection of the unbarred metric, and the two following terms arise from the purely conformal transformation involving derivatives of A. The fourth term and the second line contain the first order derivative terms from the disformal contribution to the metric B. The third line shows the second order derivative terms $\nabla\nabla\phi$.

D.2 General Disformal Coupling Perturbations

The coupling density perturbation that enters the linear equations (6.52,6.53) in the case where both the conformal and the disformal parts of the coupling are relevant has the rather complicated form

$$\delta Q = Q_\rho\delta_{\rm dc} + Q_\phi\delta\phi + Q_{d\phi}\delta\dot{\phi} + Q_\Phi\Phi + Q_{\dot{\Psi}}\dot{\Psi} , \tag{D.13}$$

where

$$Q_\rho = \rho\left(1-\frac{B}{A}\dot\phi^2\right)\frac{A'(A-2B\dot\phi^2)+B'\dot\phi^2-A(2BV'+6BH\dot\phi)}{2\left(A+B\rho-B\dot\phi^2\right)^2}\,, \tag{D.14}$$

$$\begin{aligned} Q_\phi = &\left((1-2\frac{B}{A}\dot\phi^2)A''+B''\dot\phi^2-2B\left(\frac{k^2}{a^2}+V''\right)\right)\frac{\rho}{2A(A+B\rho-B\dot\phi^2)}\\ &-\Big(\left(\frac{A'}{A}\right)^2(A^2-2B(2A+B\rho)\dot\phi^2+2B^2\dot\phi^4)+A'\left(-2B(V'+3H\dot\phi)+B'(\rho+2\dot\phi^2)\right)\\ &+2AB'(V'+3H\dot\phi)+A^2B'^2\dot\phi^2(\rho-\dot\phi^2)\Big)\frac{\rho}{2(A+B\rho-B\dot\phi^2)^2}\,, \end{aligned} \tag{D.15}$$

$$Q_{d\phi} = -\frac{B(A+2B\rho)\frac{A'}{A}\dot\phi-(A+B\rho)B'\dot\phi+B\left(2BV'\dot\phi+3H(A+B\rho+B\dot\phi^2)\right)}{\left(A+B\rho-B\dot\phi^2\right)^2}\rho\,, \tag{D.16}$$

$$Q_\Phi = \frac{B(A+2B\rho)\frac{A'}{A}\dot\phi-(A+B\rho)B'\dot\phi+2B\left(3H(A+B\rho)+BV'\dot\phi\right)}{(A+B\rho-B\dot\phi^2)^2}\rho\dot\phi\,, \tag{D.17}$$

$$Q_{\dot\Psi} = \frac{3B\rho\dot\phi}{A+B\rho-B\dot\phi^2}\,. \tag{D.18}$$

D.3 Lagrangian Derivatives for Disformal Quintessence

In this appendix, the necessary derivatives of the Lagrangian density for disformal quintessence studied in chapter 5 are given

$$\mathcal{L}(\phi,X) = \frac{X}{\sqrt{1+2B(\phi)X}} - \sqrt{1+2B(\phi)X}V(\phi)\,. \tag{D.19}$$

$$\mathcal{L}_{,X} = \frac{1}{\sqrt{\mathcal{L}}}\left[1+\frac{\mathcal{D}}{2\mathcal{L}}+BV\right] \tag{D.20}$$

$$\mathcal{L}_{,XX}\dot\phi^2 = -\frac{\mathcal{D}}{\mathcal{L}^{3/2}}\left[2+\frac{3\mathcal{D}}{2\mathcal{L}}+BV\right] \tag{D.21}$$

$$\mathcal{L}_{,X\phi} = -\frac{1}{\sqrt{\mathcal{L}}}\left[\frac{\mathcal{D}_{,\phi}}{\mathcal{L}}\left(1+\frac{3\mathcal{D}}{4\mathcal{L}}+\frac{1}{2}BV\right)+B_{,\phi}V+BV_{,\phi}\right] \tag{D.22}$$

$$\mathcal{L}_{,\phi} = -\frac{1}{\sqrt{\mathcal{L}}}\left[\frac{\mathcal{D}_{,\phi}}{2}\left(\frac{X}{\mathcal{L}}+V\right)-\mathcal{L}V_{,\phi}\right] \tag{D.23}$$

$$\mathcal{L}_{,\phi\phi} = -\frac{1}{\sqrt{\mathcal{L}}}\Big[\frac{(D_{,\phi})^2}{4\mathcal{L}}\left(\frac{-3X}{\mathcal{L}}-V\right)-D_{,\phi}V_{,\phi}+\frac{\mathcal{D}_{,\phi\phi}}{2}\left(\frac{-X}{\mathcal{L}}-V\right)+\mathcal{L}V_{,\phi\phi}\Big] \tag{D.24}$$

List of Tables

List of Figures

Bibliography

[1] M. Zumalacarregui, J. Garcia-Bellido, and P. Ruiz-Lapuente, *Tension in the Void: Cosmic Rulers Strain Inhomogeneous Cosmologies*, *JCAP* **1210** (2012) 009, [arXiv:1201.2790].

[2] T. S. Koivisto, D. F. Mota, and M. Zumalacarregui, *Screening Modifications of Gravity through Disformally Coupled Fields*, arXiv:1205.3167.

[3] M. Zumalacarregui, T. S. Koivisto, and D. F. Mota, *DBI Galileons in the Einstein Frame: Local Gravity and Cosmology*, arXiv:1210.8016.

[4] M. Zumalacarregui, T. Koivisto, D. Mota, and P. Ruiz-Lapuente, *Disformal Scalar Fields and the Dark Sector of the Universe*, *JCAP* **1005** (2010) 038, [arXiv:1004.2684].

[5] T. S. Koivisto, D. F. Mota, and M. Zumalacarregui, *Constraining Entropic Cosmology*, *JCAP* **1102** (2011) 027, [arXiv:1011.2226].

[6] M. Zumalacarregui, *Modified Entropic Gravity and Cosmology*, *AIP Conf.Proc.* **1458** (2011) 539–542, [arXiv:1202.1281].

[7] T. Clifton, P. G. Ferreira, A. Padilla, and C. Skordis, *Modified Gravity and Cosmology*, arXiv:1106.2476.

[8] C. Clarkson, *Establishing homogeneity of the universe in the shadow of dark energy*, arXiv:1204.5505.

[9] E. J. Copeland, M. Sami, and S. Tsujikawa, *Dynamics of dark energy*, *Int.J.Mod.Phys.* **D15** (2006) 1753–1936, [hep-th/0603057].

[10] D. H. Weinberg, M. J. Mortonson, D. J. Eisenstein, C. Hirata, A. G. Riess, *et. al.*, *Observational Probes of Cosmic Acceleration*, arXiv:1201.2434.

[11] **Supernova Cosmology Project** Collaboration, S. Perlmutter *et. al.*, *Measurements of Omega and Lambda from 42 high redshift supernovae*, *Astrophys.J.* **517** (1999) 565–586, [astro-ph/9812133]. *http://www-supernova.lbl.gov*.

[12] **Supernova Search Team** Collaboration, A. G. Riess *et. al.*, *Observational evidence from supernovae for an accelerating universe and a cosmological constant*, *Astron.J.* **116** (1998) 1009–1038, [astro-ph/9805201]. *www.cfa.harvard.edu/supernova/HighZ.html*.

[13] S. M. Carroll, *Spacetime and geometry. An introduction to general relativity*. 2004.

[14] V. Mukhanov, *Physical Foundations of Cosmology*. Nov., 2005.

[15] J. Shapiro Key, N. J. Cornish, D. N. Spergel, and G. D. Starkman, *Extending the WMAP Bound on the Size of the Universe*, *Phys.Rev.* **D75** (2007) 084034, [astro-ph/0604616].

[16] C. Bennett, R. Hill, G. Hinshaw, D. Larson, K. Smith, *et. al.*, *Seven-Year Wilkinson Microwave Anisotropy Probe (WMAP) Observations: Are There Cosmic Microwave Background Anomalies?*, *Astrophys.J.Suppl.* **192** (2011) 17, [arXiv:1001.4758].

[17] L. Perivolaropoulos, *LCDM: Triumphs, Puzzles and Remedies*, arXiv:1104.0539.

[18] D. Larson, J. Dunkley, G. Hinshaw, E. Komatsu, M. Nolta, *et. al.*, *Seven-Year Wilkinson Microwave Anisotropy Probe (WMAP) Observations: Power Spectra and WMAP-Derived Parameters*, *Astrophys.J.Suppl.* **192** (2011) 16.

[19] **WMAP** Collaboration, E. Komatsu *et. al.*, *Seven-Year Wilkinson Microwave Anisotropy Probe (WMAP) Observations: Cosmological Interpretation*, *Astrophys.J.Suppl.* **192** (2011) 18, [arXiv:1001.4538]. *http://map.gsfc.nasa.gov*.

[20] **Particle Data Group** Collaboration, J. Beringer *et. al.*, *Review of Particle Physics (RPP)*, *Phys.Rev.* **D86** (2012) 010001. *http://pdg.lbl.gov*.

[21] Y. Zel'dovich, *The Cosmological constant and the theory of elementary particles*, *Sov.Phys.Usp.* **11** (1968) 381–393.

[22] S. Weinberg, *The cosmological constant problem*, *Rev. Mod. Phys.* **61** (Jan, 1989) 1–23.

[23] J. Martin, *Everything You Always Wanted To Know About The Cosmological Constant Problem (But Were Afraid To Ask)*, arXiv:1205.3365.

[24] **SDSS** Collaboration, D. J. Eisenstein *et. al.*, *Detection of the baryon acoustic peak in the large-scale correlation function of SDSS luminous red galaxies*, *Astrophys.J.* **633** (2005) 560–574, [astro-ph/0501171]. *http://www.sdss.org*.

[25] R. Durrer and R. Maartens, *Dark Energy and Dark Gravity*, *Gen. Rel. Grav.* **40** (2008) 301–328, [arXiv:0711.0077].

[26] P. Ruiz-Lapuente, *Dark energy, gravitation and supernovae*, *Class. Quant. Grav.* **24** (2007) R91, [arXiv:0704.1058].

[27] V. Marra and A. Notari, *Observational constraints on inhomogeneous cosmological models without dark energy*, *Class.Quant.Grav.* **28** (2011) 164004, [arXiv:1102.1015].

[28] P. J. E. Peebles and B. Ratra, *The cosmological constant and dark energy*, *Rev. Mod. Phys.* **75** (2003) 559–606, [astro-ph/0207347].

[29] S. Nobbenhuis, *The cosmological constant problem, an inspiration for new physics*, gr-qc/0609011.

[30] C. Charmousis, E. J. Copeland, A. Padilla, and P. M. Saffin, *General second order scalar-tensor theory, self tuning, and the Fab Four*, *Phys.Rev.Lett.* **108** (2012) 051101, [arXiv:1106.2000].

[31] C. Csaki, N. Kaloper, and J. Terning, *Dimming supernovae without cosmic acceleration*, *Phys.Rev.Lett.* **88** (2002) 161302, [hep-ph/0111311].

[32] C. Deffayet, D. Harari, J.-P. Uzan, and M. Zaldarriaga, *Dimming of supernovae by photon pseudoscalar conversion and the intergalactic plasma*, *Phys.Rev.* **D66** (2002) 043517, [hep-ph/0112118].

[33] T. Baker, P. G. Ferreira, and C. Skordis, *The Parameterized Post-Friedmann Framework for Theories of Modified Gravity: Concepts, Formalism and Examples*, arXiv:1209.2117.

[34] S. Nesseris and J. Garcia-Bellido, *A new perspective on Dark Energy modeling via Genetic Algorithms*, arXiv:1205.0364.

[35] G.-B. Zhao, R. G. Crittenden, L. Pogosian, and X. Zhang, *Examining the evidence for dynamical dark energy*, arXiv:1207.3804.

[36] P. Bull, T. Clifton, and P. G. Ferreira, *The kSZ effect as a test of general radial inhomogeneity in LTB cosmology*, arXiv:1108.2222.

[37] R. de Putter, L. Verde, and R. Jimenez, *Testing LTB Void Models Without the Cosmic Microwave Background or Large Scale Structure: New Constraints from Galaxy Ages*,

arXiv:1208.4534.

[38] G. F. Ellis, *Inhomogeneity effects in Cosmology*, arXiv:1103.2335.

[39] S. R. Green and R. M. Wald, *A new framework for analyzing the effects of small scale inhomogeneities in cosmology*, *Phys.Rev.* **D83** (2011) 084020, [arXiv:1011.4920].

[40] T. Buchert and S. Rasanen, *Backreaction in late-time cosmology*, arXiv:1112.5335.

[41] C. Wetterich, *Cosmology and the Fate of Dilatation Symmetry*, *Nucl.Phys.* **B302** (1988) 668.

[42] P. J. E. Peebles and B. Ratra, *Cosmology with a Time Variable Cosmological Constant*, *Astrophys. J.* **325** (1988) L17.

[43] R. Caldwell and E. V. Linder, *The Limits of quintessence*, *Phys.Rev.Lett.* **95** (2005) 141301, [astro-ph/0505494].

[44] E. J. Copeland, A. R. Liddle, and D. Wands, *Exponential potentials and cosmological scaling solutions*, *Phys. Rev. D* **57** (Apr, 1998) 4686–4690.

[45] M. Doran and G. Robbers, *Early dark energy cosmologies*, *JCAP* **0606** (2006) 026, [astro-ph/0601544].

[46] P. G. Ferreira and M. Joyce, *Cosmology with a Primordial Scaling Field*, *Phys. Rev.* **D58** (1998) 023503, [astro-ph/9711102].

[47] C. Skordis and A. J. Albrecht, *Planck-scale quintessence and the physics of structure formation*, *Phys. Rev.* **D66** (2002) 043523, [astro-ph/0012195].

[48] J. Casas, J. Garcia-Bellido, and M. Quiros, *Scalar - tensor theories of gravity with phi dependent masses*, *Class.Quant.Grav.* **9** (1992) 1371–1384, [hep-ph/9204213].

[49] L. Amendola, *Coupled quintessence*, *Phys.Rev.* **D62** (2000) 043511, [astro-ph/9908023].

[50] R. Fardon, A. E. Nelson, and N. Weiner, *Dark energy from mass varying neutrinos*, *JCAP* **0410** (2004) 005, [astro-ph/0309800].

[51] A. W. Brookfield, C. van de Bruck, D. Mota, and D. Tocchini-Valentini, *Cosmology of mass-varying neutrinos driven by quintessence: theory and observations*, *Phys.Rev.* **D73** (2006) 083515, [astro-ph/0512367].

[52] N. Afshordi, M. Zaldarriaga, and K. Kohri, *On the stability of dark energy with mass-varying neutrinos*, *Phys.Rev.* **D72** (2005) 065024, [astro-ph/0506663].

[53] N. Wintergerst, V. Pettorino, D. Mota, and C. Wetterich, *Very large scale structures in growing neutrino quintessence*, *Phys.Rev.* **D81** (2010) 063525, [arXiv:0910.4985].

[54] M. Ostrogradski.

[55] R. P. Woodard, *Avoiding dark energy with 1/r modifications of gravity*, *Lect.Notes Phys.* **720** (2007) 403–433, [astro-ph/0601672].

[56] T.-j. Chen and E. A. Lim, *Higher derivative theories with constraints: A strengthening of Ostrogradski's Theorem*, arXiv:1209.0583.

[57] D. Lovelock, *The Einstein tensor and its generalizations*, *J.Math.Phys.* **12** (1971) 498–501.

[58] J. Beltran Jimenez and A. L. Maroto, *Cosmological evolution in vector-tensor theories of gravity*, *Phys.Rev.* **D80** (2009) 063512, [arXiv:0905.1245].

[59] J. Beltran Jimenez and A. L. Maroto, *A cosmic vector for dark energy*, *Phys.Rev.* **D78** (2008) 063005, [arXiv:0801.1486].

[60] J. D. Bekenstein, *Relativistic gravitation theory for the MOND paradigm*, *Phys.Rev.* **D70** (2004) 083509.

[61] T. Jacobson and D. Mattingly, *Gravity with a dynamical preferred frame*, *Phys.Rev.* **D64** (2001) 024028, [gr-qc/0007031].

[62] J. D. Bekenstein, *The Relation between physical and gravitational geometry*, *Phys.Rev.* **D48** (1993) 3641–3647.

[63] J. Wang, L. Hui, and J. Khoury, *No-Go Theorems for Generalized Chameleon Field Theories*, arXiv:1208.4612.

[64] C. Deffayet, G. Esposito-Farese, and A. Vikman, *Covariant Galileon*, *Phys.Rev.* **D79** (2009) 084003, [arXiv:0901.1314].

[65] C. Deffayet, O. Pujolas, I. Sawicki, and A. Vikman, *Imperfect Dark Energy from Kinetic Gravity Braiding*, *JCAP* **1010** (2010) 026, [arXiv:1008.0048].

[66] O. Pujolas, I. Sawicki, and A. Vikman, *The Imperfect Fluid behind Kinetic Gravity Braiding*, *JHEP* **1111** (2011) 156, [arXiv:1103.5360].

[67] G. Gubitosi and E. V. Linder, *Purely Kinetic Coupled Gravity*, *Phys.Lett.* **B703** (2011) 113–118, [arXiv:1106.2815].

[68] C. de Rham and A. J. Tolley, *DBI and the Galileon reunited*, *JCAP* **1005** (2010) 015, [arXiv:1003.5917].

[69] N. Kaloper, *Disformal inflation*, *Phys.Lett.* **B583** (2004) 1–13, [hep-ph/0312002].

[70] A. Nicolis, R. Rattazzi, and E. Trincherini, *The Galileon as a local modification of gravity*, *Phys.Rev.* **D79** (2009) 064036, [arXiv:0811.2197].

[71] G. Goon, K. Hinterbichler, and M. Trodden, *A New Class of Effective Field Theories from Embedded Branes*, *Phys.Rev.Lett.* **106** (2011) 231102, [arXiv:1103.6029].

[72] G. Goon, K. Hinterbichler, and M. Trodden, *Symmetries for Galileons and DBI scalars on curved space*, *JCAP* **1107** (2011) 017, [arXiv:1103.5745].

[73] G. W. Horndeski, *Second-Order Scalar-Tensor Field Equations in a Four-Dimensional Space*, *International Journal of Theoretical Physics* **10** (Sept., 1974) 363–384.

[74] C. Deffayet, S. Deser, and G. Esposito-Farese, *Generalized Galileons: All scalar models whose curved background extensions maintain second-order field equations and stress-tensors*, *Phys.Rev.* **D80** (2009) 064015, [arXiv:0906.1967].

[75] C. Deffayet, X. Gao, D. Steer, and G. Zahariade, *From k-essence to generalised Galileons*, *Phys.Rev.* **D84** (2011) 064039, [arXiv:1103.3260].

[76] A. De Felice, T. Kobayashi, and S. Tsujikawa, *Effective gravitational couplings for cosmological perturbations in the most general scalar-tensor theories with second-order field equations*, *Phys.Lett.* **B706** (2011) 123–133, [arXiv:1108.4242].

[77] T. Kobayashi, M. Yamaguchi, and J. Yokoyama, *Generalized G-inflation: Inflation with the most general second-order field equations*, *Prog.Theor.Phys.* **126** (2011) 511–529, [arXiv:1105.5723].

[78] L. Amendola, M. Kunz, M. Motta, I. Saltas, and I. Sawicki, *Observables and unobservables in dark energy cosmologies*, arXiv:1210.0439.

[79] G. Dvali, G. Gabadadze, and M. Porrati, *4-D gravity on a brane in 5-D Minkowski space*, *Phys.Lett.* **B485** (2000) 208–214, [hep-th/0005016].

[80] L. Hui and A. Nicolis, *An Equivalence principle for scalar forces*, *Phys.Rev.Lett.* **105** (2010) 231101, [arXiv:1009.2520].

[81] K. Hinterbichler, M. Trodden, and D. Wesley, *Multi-field galileons and higher co-dimension branes*, *Phys.Rev.* **D82** (2010) 124018, [arXiv:1008.1305].

[82] M. Trodden and K. Hinterbichler, *Generalizing Galileons*, *Class.Quant.Grav.* **28** (2011) 204003, [arXiv:1104.2088].

[83] K. Van Acoleyen and J. Van Doorsselaere, *Galileons from Lovelock actions*, *Phys.Rev.* **D83** (2011) 084025, [arXiv:1102.0487].

[84] A. Vainshtein, *To the problem of nonvanishing gravitation mass*, *Phys.Lett.* **B39** (1972) 393–394.

[85] J. Khoury and A. Weltman, *Chameleon fields: Awaiting surprises for tests of gravity in space*, *Phys.Rev.Lett.* **93** (2004) 171104.

[86] J. Khoury and A. Weltman, *Chameleon cosmology*, *Phys.Rev.* **D69** (2004) 044026, [astro-ph/0309411].

[87] K. Hinterbichler and J. Khoury, *Symmetron Fields: Screening Long-Range Forces Through Local Symmetry Restoration*, *Phys.Rev.Lett.* **104** (2010) 231301, [arXiv:1001.4525].

[88] K. Hinterbichler, J. Khoury, A. Levy, and A. Matas, *Symmetron Cosmology*, *Phys.Rev.* **D84** (2011) 103521, [arXiv:1107.2112].

[89] J. Khoury, *Theories of Dark Energy with Screening Mechanisms*, arXiv:1011.5909.

[90] N. Chow and J. Khoury, *Galileon Cosmology*, *Phys.Rev.* **D80** (2009) 024037, [arXiv:0905.1325].

[91] D. F. Mota, M. Sandstad, and T. Zlosnik, *Cosmology of the selfaccelerating third order Galileon*, *JHEP* **1012** (2010) 051, [arXiv:1009.6151].

[92] A. De Felice and S. Tsujikawa, *Cosmological constraints on extended Galileon models*, *JCAP* **1203** (2012) 025, [arXiv:1112.1774].

[93] S. Appleby and E. V. Linder, *The Paths of Gravity in Galileon Cosmology*, *JCAP* **1203** (2012) 043, [arXiv:1112.1981].

[94] C. Llinares and D. F. Mota, *Shape of Clusters as a Probe of Screening Mechanisms in Modified Gravity*, arXiv:1205.5775.

[95] A. Barreira, B. Li, C. Baugh, and S. Pascoli, *Linear perturbations in Galileon gravity models*, arXiv:1208.0600.

[96] **CBI** Collaboration, J. L. Sievers, C. Achermann, J. Bond, L. Bronfman, R. Bustos, *et. al.*, *Implications of the cosmic background imager polarization data*, *Astrophys.J.* **660** (2007) 976–987, [astro-ph/0509203]. *http://www.astro.caltech.edu/∼tjp/CBI*.

[97] **QUIET** Collaboration, C. Bischoff *et. al.*, *First Season QUIET Observations: Measurements of CMB Polarization Power Spectra at 43 GHz in the Multipole Range 25 ¡l ¡ 475*, *Astrophys.J.* **741** (2011) 111, [arXiv:1012.3191]. *http://quiet.uchicago.edu*.

[98] M. Lueker, C. Reichardt, K. Schaffer, O. Zahn, P. Ade, *et. al.*, *Measurements of Secondary Cosmic Microwave Background Anisotropies with the South Pole Telescope*, *Astrophys.J.* **719** (2010) 1045–1066, [arXiv:0912.4317]. *http://pole.uchicago.edu*.

[99] **SDSS** Collaboration, M. Tegmark *et. al.*, *Cosmological Constraints from the SDSS Luminous Red Galaxies*, *Phys. Rev.* **D74** (2006) 123507, [astro-ph/0608632]. *http://www.sdss.org*.

[100] **SDSS** Collaboration, E. A. Kazin *et. al.*, *The Baryonic Acoustic Feature and Large-Scale Clustering in the SDSS LRG Sample*, *Astrophys.J.* **710** (2010) 1444–1461, [arXiv:0908.2598]. *http://www.sdss.org*.

[101] **SDSS** Collaboration, W. J. Percival *et. al.*, *Baryon Acoustic Oscillations in the Sloan Digital Sky Survey Data Release 7 Galaxy Sample*, *Mon.Not.Roy.Astron.Soc.* **401** (2010) 2148–2168, [arXiv:0907.1660]. *http://www.sdss.org*.

[102] L. Anderson, E. Aubourg, S. Bailey, D. Bizyaev, M. Blanton, *et. al.*, *The clustering of galaxies in the SDSS-III Baryon Oscillation Spectroscopic Survey: Baryon Acoustic Oscillations in the Data Release 9 Spectroscopic Galaxy Sample*, arXiv:1203.6594.

[103] C. Blake, E. Kazin, F. Beutler, T. Davis, D. Parkinson, *et. al.*, *The WiggleZ Dark Energy Survey: mapping the distance-redshift relation with baryon acoustic oscillations*, *Mon.Not.Roy.Astron.Soc.* **418** (2011) 1707–1724.

[104] C. Blake, K. Glazebrook, T. Davis, S. Brough, M. Colless, *et. al.*, *The WiggleZ Dark Energy Survey: measuring the cosmic expansion history using the Alcock-Paczynski test and distant supernovae*, arXiv:1108.2637.

[105] **Planck** Collaboration, *The Scientific programme of planck*, astro-ph/0604069. *http://www.esa.int/SPECIALS/Planck/index.html*.

[106] **Dark Energy Survey** Collaboration, T. Abbott *et. al.*, *The dark energy survey*, astro-ph/0510346. *http://www.darkenergysurvey.org*.

[107] **Euclid** Collaboration, R. Laureijs, J. Amiaux, S. Arduini, J.-L. Augueres, J. Brinchmann, *et. al.*, *Euclid Definition Study Report*, arXiv:1110.3193. .

[108] L. Amendola, S. Appleby, D. Bacon, T. Baker, M. Baldi, *et. al.*, *Cosmology and fundamental physics with the Euclid satellite*, arXiv:1206.1225.

[109] J. Garcia-Bellido and T. Haugboelle, *Looking the void in the eyes - the kSZ effect in LTB models*, *JCAP* **0809** (2008) 016, [arXiv:0807.1326].

[110] C. M. Will, *The Confrontation between general relativity and experiment*, *Living Rev.Rel.* **9** (2006) 3, [gr-qc/0510072].

[111] R. Alpher, H. Bethe, and G. Gamow, *The origin of chemical elements*, *Phys.Rev.* **73** (1948) 803–804.

[112] R. H. Cyburt, B. D. Fields, and K. A. Olive, *An Update on the big bang nucleosynthesis prediction for Li-7: The problem worsens*, *JCAP* **0811** (2008) 012, [arXiv:0808.2818].

[113] B. D. Fields, *The primordial lithium problem*, *Ann.Rev.Nucl.Part.Sci.* **61** (2011) 47–68, [arXiv:1203.3551].

[114] C. Bambi, M. Giannotti, and F. L. Villante, *The response of primordial abundances to a general modification of G_N and/or of the early universe expansion rate*, *Phys. Rev.* **D71** (2005) 123524, [astro-ph/0503502].

[115] R. Bean, S. H. Hansen, and A. Melchiorri, *Early universe constraints on a primordial scaling field*, *Phys.Rev.* **D64** (2001) 103508, [astro-ph/0104162].

[116] J. Casas, J. Garcia-Bellido, and M. Quiros, *Nucleosynthesis bounds on Jordan-Brans-Dicke theories of gravity*, *Mod.Phys.Lett.* **A7** (1992) 447–456.

[117] C. M. Muller, G. Schafer, and C. Wetterich, *Nucleosynthesis and the variation of fundamental couplings*, *Phys.Rev.* **D70** (2004) 083504, [astro-ph/0405373].

[118] U. Seljak and M. Zaldarriaga, *A Line of sight integration approach to cosmic microwave background anisotropies*, *Astrophys.J.* **469** (1996) 437–444, [astro-ph/9603033].

[119] U. Seljak, *Gravitational lensing effect on cosmic microwave background anisotropies: A Power spectrum approach*, *Astrophys.J.* **463** (1996) 1, [astro-ph/9505109].

[120] A. Lewis and A. Challinor, *Weak gravitational lensing of the cmb*, *Phys.Rept.* **429** (2006) 1–65, [astro-ph/0601594].

[121] N. Bartolo, E. Komatsu, S. Matarrese, and A. Riotto, *Non-Gaussianity from inflation: Theory and observations*, *Phys.Rept.* **402** (2004) 103–266, [astro-ph/0406398].

[122] C. L. Reichardt, R. de Putter, O. Zahn, and Z. Hou, *New limits on Early Dark Energy from the South Pole Telescope*, *Astrophys.J.* **749** (2012) L9, [arXiv:1110.5328].

[123] W. Hu and N. Sugiyama, *Small scale cosmological perturbations: An Analytic approach*, *Astrophys.J.* **471** (1996) 542–570, [astro-ph/9510117].

[124] M. Vonlanthen, S. Rasanen, and R. Durrer, *Model-independent cosmological constraints from the CMB*, *JCAP* **1008** (2010) 023, [arXiv:1003.0810].

[125] F. Bernardeau, S. Colombi, E. Gaztanaga, and R. Scoccimarro, *Large scale structure of the universe and cosmological perturbation theory*, *Phys.Rept.* **367** (2002) 1–248, [astro-ph/0112551].

[126] M. Crocce and R. Scoccimarro, *Renormalized cosmological perturbation theory*, *Phys.Rev.* **D73** (2006) 063519, [astro-ph/0509418].

[127] A. Cooray and R. K. Sheth, *Halo models of large scale structure*, *Phys.Rept.* **372** (2002) 1–129, [astro-ph/0206508].

[128] V. Springel, *The Cosmological simulation code GADGET-2*, *Mon.Not.Roy.Astron.Soc.* **364** (2005) 1105–1134, [astro-ph/0505010].

[129] C. Bonvin and R. Durrer, *What galaxy surveys really measure*, *Phys.Rev.* **D84** (2011) 063505, [arXiv:1105.5280].

[130] A. Challinor and A. Lewis, *The linear power spectrum of observed source number counts*, *Phys.Rev.* **D84** (2011) 043516, [arXiv:1105.5292].

[131] N. Kaiser, *Clustering in real space and in redshift space*, *Mon.Not.Roy.Astron.Soc.* **227** (1987) 1–27.

[132] S. Nesseris and L. Perivolaropoulos, *Testing LCDM with the Growth Function $\delta(a)$: Current Constraints*, *Phys. Rev.* **D77** (2008) 023504, [arXiv:0710.1092].

[133] H. Motohashi, A. A. Starobinsky, and J. Yokoyama, *Cosmology based on f(R) Gravity admits 1 eV Sterile Neutrinos*, arXiv:1203.6828.

[134] C. Clarkson, T. Clifton, and S. February, *Perturbation Theory in Lemaitre-Tolman-Bondi Cosmology*, *JCAP* **0906** (2009) 025, [arXiv:0903.5040].

[135] D. Alonso, J. Garcia-Bellido, T. Haugbolle, and J. Vicente, *Large scale structure simulations of inhomogeneous LTB void models*, *Phys.Rev.* **D82** (2010) 123530, [arXiv:1010.3453].

[136] D. Alonso, J. Garcia-Bellido, T. Haugboelle, and A. Knebe, *Halo abundances and shear in void models*, arXiv:1204.3532.

[137] S. February, C. Clarkson, and R. Maartens, *Galaxy correlations and the BAO in a void universe: structure formation as a test of the Copernican Principle*, arXiv:1206.1602.

[138] D. J. Eisenstein and W. Hu, *Baryonic features in the matter transfer function*, *Astrophys.J.* **496** (1998) 605, [astro-ph/9709112].

[139] A. Carnero, E. Sanchez, M. Crocce, A. Cabre, and E. Gaztanaga, *Clustering of Photometric Luminous Red Galaxies II: Cosmological Implications from the Baryon Acoustic Scale*, *Mon.Not.Roy.Astron.Soc.* **419** (2012) 1689–1694, [arXiv:1104.5426].

[140] E. Gaztanaga, A. Cabre, and L. Hui, *Clustering of Luminous Red Galaxies IV: Baryon Acoustic Peak in the Line-of-Sight Direction and a Direct Measurement of H(z)*, *Mon.Not.Roy.Astron.Soc.* **399** (2009) 1663–1680, [arXiv:0807.3551].

[141] E. Gaztanaga, R. Miquel, and E. Sanchez, *First Cosmological Constraints on Dark Energy from the Radial Baryon Acoustic Scale*, *Phys.Rev.Lett.* **103** (2009) 091302, [arXiv:0808.1921].

[142] M. Crocce and R. Scoccimarro, *Nonlinear Evolution of Baryon Acoustic Oscillations*, *Phys.Rev.* **D77** (2008) 023533, [arXiv:0704.2783].

[143] R. E. Smith, R. Scoccimarro, and R. K. Sheth, *Eppur Si Muove: On The Motion of the Acoustic Peak in the Correlation Function*, *Phys.Rev.* **D77** (2008) 043525, [astro-ph/0703620].

[144] H.-J. Seo, J. Eckel, D. J. Eisenstein, K. Mehta, M. Metchnik, *et. al.*, *High-precision predictions for the acoustic scale in the non-linear regime*, *Astrophys.J.* **720** (2010) 1650–1667, [arXiv:0910.5005].

[145] N. McCullagh and A. S. Szalay, *Nonlinear Behavior of Baryon Acoustic Oscillations from the Zel'dovich Approximation Using a Non-Fourier Perturbation Approach*, *Astrophys.J.* **752** (2012) 21, [arXiv:1202.1306].

[146] B. D. Sherwin and M. Zaldarriaga, *The Shift of the Baryon Acoustic Oscillation Scale: A Simple Physical Picture*, *Phys.Rev.* **D85** (2012) 103523, [arXiv:1202.3998].

[147] B. A. Reid, W. J. Percival, D. J. Eisenstein, L. Verde, D. N. Spergel, *et. al.*, *Cosmological Constraints from the Clustering of the Sloan Digital Sky Survey DR7 Luminous Red Galaxies*, *Mon.Not.Roy.Astron.Soc.* **404** (2010) 60–85, [arXiv:0907.1659].

[148] F. Beutler, C. Blake, M. Colless, D. H. Jones, L. Staveley-Smith, *et. al.*, *The 6dF Galaxy Survey: Baryon Acoustic Oscillations and the Local Hubble Constant*, *Mon.Not.Roy.Astron.Soc.* **416** (2011) 3017–3032, [arXiv:1106.3366].

[149] A. G. Sanchez, C. M. Baugh, and R. Angulo, *What is the best way to measure baryonic acoustic oscillations?*, *Mon.Not.Roy.Astron.Soc.* **390** (2008) 1470–1490, [arXiv:0804.0233].

[150] K. T. Mehta, A. J. Cuesta, X. Xu, D. J. Eisenstein, and N. Padmanabhan, *A 2% Distance to $z = 0.35$ by Reconstructing Baryon Acoustic Oscillations - III : Cosmological Measurements and Interpretation*, arXiv:1202.0092.

[151] X. Xu, A. J. Cuesta, N. Padmanabhan, D. J. Eisenstein, and C. K. McBride, *Measuring D_A and H at $z = 0.35$ from the SDSS DR7 LRGs using baryon acoustic oscillations*, arXiv:1206.6732.

[152] J. Garcia-Bellido and T. Haugboelle, *The radial BAO scale and Cosmic Shear, a new observable for Inhomogeneous Cosmologies*, *JCAP* **0909** (2009) 028, [arXiv:0810.4939].

[153] A. Moss, J. P. Zibin, and D. Scott, *Precision Cosmology Defeats Void Models for Acceleration*, *Phys.Rev.* **D83** (2011) 103515, [arXiv:1007.3725].

[154] L. Amendola, M. Kunz, and D. Sapone, *Measuring the dark side (with weak lensing)*, *JCAP* **0804** (2008) 013, [arXiv:0704.2421].

[155] S. W. Allen, A. E. Evrard, and A. B. Mantz, *Cosmological Parameters from Observations of Galaxy Clusters*, *Ann.Rev.Astron.Astrophys.* **49** (2011) 409–470, [arXiv:1103.4829].

[156] P. Zhang and A. Stebbins, *Confirmation of the Copernican principle at Gpc radial scale and above from the kinetic Sunyaev Zel'dovich effect power spectrum*, *Phys.Rev.Lett.* **107** (2011) 041301, [arXiv:1009.3967].

[157] T. Clifton, P. G. Ferreira, and K. Land, *Living in a Void: Testing the Copernican Principle with Distant Supernovae*, *Phys.Rev.Lett.* **101** (2008) 131302, [arXiv:0807.1443].

[158] S. Nadathur and S. Sarkar, *Reconciling the local void with the CMB*, *Phys.Rev.* **D83** (2011) 063506, [arXiv:1012.3460].

[159] C. Clarkson, G. Ellis, A. Faltenbacher, R. Maartens, O. Umeh, *et. al.*, *(Mis-)Interpreting supernovae observations in a lumpy universe*, arXiv:1109.2484.

[160] L. Ostman and E. Mortsell, *Limiting the dimming of distant Type Ia supernovae*, *JCAP* **0502** (2005) 005, [astro-ph/0410501].

[161] B. Leibundgut, *Supernovae and Cosmology*, *Gen. Rel. Grav.* **40** (2008) 221, [arXiv:0802.4154].

[162] **Supernova Cosmology Project** Collaboration, M. Kowalski *et. al.*, *Improved Cosmological Constraints from New, Old and Combined Supernova Datasets*, *Astrophys.J.* **686** (2008) 749–778, [arXiv:0804.4142]. *http://www-supernova.lbl.gov*.

[163] R. Amanullah, C. Lidman, D. Rubin, G. Aldering, P. Astier, *et. al.*, *Spectra and light curves of six type ia supernovae at 0.511 ¡ z ¡ 1.12 and the union2 compilation*, *Astrophys.J.* **716** (2010) 712–738, [arXiv:1004.1711].

[164] S. February, J. Larena, M. Smith, and C. Clarkson, *Rendering Dark Energy Void*, *Mon.Not.Roy.Astron.Soc.* **405** (2010) 2231, [arXiv:0909.1479].

[165] A. G. Riess, L. Macri, S. Casertano, H. Lampeitl, H. C. Ferguson, *et. al.*, *A 3% Solution: Determination of the Hubble Constant with the Hubble Space Telescope and Wide Field Camera 3*, *Astrophys.J.* **730** (2011) 119.

[166] D. Kapner, T. Cook, E. Adelberger, J. Gundlach, B. R. Heckel, *et. al.*, *Tests of the gravitational inverse-square law below the dark-energy length scale*, *Phys.Rev.Lett.* **98** (2007) 021101, [hep-ph/0611184].

[167] N. Mustapha, C. Hellaby, and G. Ellis, *Large scale inhomogeneity versus source evolution: Can we distinguish them observationally?*, *Mon.Not.Roy.Astron.Soc.* **292** (1997) 817–830, [gr-qc/9808079].

[168] M.-N. Celerier, *Do we really see a cosmological constant in the supernovae data?*, *Astron.Astrophys.* **353** (2000) 63–71, [astro-ph/9907206].

[169] K. Tomita, *A local void and the accelerating universe*, *Mon.Not.Roy.Astron.Soc.* **326** (2001) 287, [astro-ph/0011484].

[170] H. Alnes, M. Amarzguioui, and O. Gron, *An inhomogeneous alternative to dark energy?*, *Phys.Rev.* **D73** (2006) 083519, [astro-ph/0512006].

[171] R. A. Vanderveld, E. E. Flanagan, and I. Wasserman, *Mimicking dark energy with Lemaitre-Tolman-Bondi models: Weak central singularities and critical points*, *Phys.Rev.* **D74** (2006) 023506, [astro-ph/0602476].

[172] D. Garfinkle, *Inhomogeneous spacetimes as a dark energy model*, *Class.Quant.Grav.* **23** (2006) 4811–4818, [gr-qc/0605088].

[173] K. Enqvist, *Lemaitre-Tolman-Bondi model and accelerating expansion*, *Gen.Rel.Grav.* **40** (2008) 451–466, [arXiv:0709.2044].

[174] T. Mattsson, *Dark energy as a mirage*, *Gen.Rel.Grav.* **42** (2010) 567–599, [arXiv:0711.4264].

[175] S. Sarkar, *Is the evidence for dark energy secure?*, *Gen.Rel.Grav.* **40** (2008) 269–284, [arXiv:0710.5307].

[176] J. Zibin, A. Moss, and D. Scott, *Can we avoid dark energy?*, *Phys.Rev.Lett.* **101** (2008) 251303, [arXiv:0809.3761].

[177] J. Moffat, *Void or Dark Energy?*, arXiv:0910.2723.

[178] M.-N. Celerier, K. Bolejko, and A. Krasinski, *A (giant) void is not mandatory to explain away dark energy with a Lemaitre – Tolman model*, *Astron.Astrophys.* **518** (2010) A21, [arXiv:0906.0905].

[179] R. A. Vanderveld, E. E. Flanagan, and I. Wasserman, *Lemaitre-Tolman-Bondi cosmological*

models, smoothness, and positivity of the central deceleration parameter, arXiv:0904.4319.

[180] M. Regis and C. Clarkson, *Do primordial Lithium abundances imply there's no Dark Energy?*, arXiv:1003.1043.

[181] T. Buchert, *Toward physical cosmology: focus on inhomogeneous geometry and its non-perturbative effects*, arXiv:1103.2016.

[182] K. Enqvist and T. Mattsson, *The effect of inhomogeneous expansion on the supernova observations*, *JCAP* **0702** (2007) 019, [astro-ph/0609120].

[183] S. Alexander, T. Biswas, A. Notari, and D. Vaid, *Local Void vs Dark Energy: Confrontation with WMAP and Type Ia Supernovae*, *JCAP* **0909** (2009) 025, [arXiv:0712.0370].

[184] J. Garcia-Bellido and T. Haugboelle, *Confronting Lemaitre-Tolman-Bondi models with Observational Cosmology*, *JCAP* **0804** (2008) 003, [arXiv:0802.1523].

[185] A. E. Romano, *Mimicking the cosmological constant for more than one observable with large scale inhomogeneities*, *Phys.Rev.* **D82** (2010) 123528, [arXiv:0912.4108].

[186] M. Quartin and L. Amendola, *Distinguishing Between Void Models and Dark Energy with Cosmic Parallax and Redshift Drift*, *Phys.Rev.* **D81** (2010) 043522, [arXiv:0909.4954].

[187] T. Biswas, A. Notari, and W. Valkenburg, *Testing the Void against Cosmological data: fitting CMB, BAO, SN and H0*, *JCAP* **1011** (2010) 030, [arXiv:1007.3065].

[188] P. Dunsby, N. Goheer, B. Osano, and J.-P. Uzan, *How close can an Inhomogeneous Universe mimic the Concordance Model?*, *JCAP* **1006** (2010) 017, [arXiv:1002.2397].

[189] V. Marra and M. Paakkonen, *Observational constraints on the LLTB model*, *JCAP* **1012** (2010) 021, [arXiv:1009.4193].

[190] C.-M. Yoo, T. Kai, and K. ichi Nakao, *Redshift Drift in LTB Void Universes*, *Phys.Rev.* **D83** (2011) 043527, [arXiv:1010.0091].

[191] A. E. Romano, *Do recent accurate measurements of H_0 really rule out void models as alternatives to dark energy?*, arXiv:1105.1864.

[192] H. Wang and T.-J. Zhang, *Constraints on Lemaître-Tolman-Bondi models from Observational Hubble Parameter data*, arXiv:1111.2400.

[193] J. P. Zibin, *Scalar Perturbations on Lemaitre-Tolman-Bondi Spacetimes*, *Phys.Rev.* **D78** (2008) 043504, [arXiv:0804.1787].

[194] R. Nishikawa, C.-M. Yoo, and K. ichi Nakao, *Evolution of density perturbations in large void universe*, arXiv:1202.1582.

[195] J. W. Moffat, *Cosmic microwave background, accelerating Universe and inhomogeneous cosmology*, *JCAP* **0510** (2005) 012, [astro-ph/0502110].

[196] H. Alnes and M. Amarzguioui, *CMB anisotropies seen by an off-center observer in a spherically symmetric inhomogeneous Universe*, *Phys.Rev.* **D74** (2006) 103520, [astro-ph/0607334].

[197] R. Caldwell and A. Stebbins, *A Test of the Copernican Principle*, *Phys.Rev.Lett.* **100** (2008) 191302, [arXiv:0711.3459].

[198] T. Clifton, P. G. Ferreira, and J. Zuntz, *What the small angle CMB really tells us about the curvature of the Universe*, *JCAP* **0907** (2009) 029, [arXiv:0902.1313].

[199] C.-M. Yoo, K. ichi Nakao, and M. Sasaki, *CMB observations in LTB universes: Part I: Matching peak positions in the CMB spectrum*, *JCAP* **1007** (2010) 012, [arXiv:1005.0048].

[200] C.-M. Yoo, K. ichi Nakao, and M. Sasaki, *CMB observations in LTB universes: Part II – the*

kSZ effect in an LTB universe, *JCAP* **1010** (2010) 011, [arXiv:1008.0469].

[201] C. Clarkson and M. Regis, *The Cosmic Microwave Background in an Inhomogeneous Universe - why void models of dark energy are only weakly constrained by the CMB*, *JCAP* **1102** (2011) 013, [arXiv:1007.3443].

[202] J. P. Zibin and A. Moss, *Linear kinetic Sunyaev-Zel'dovich effect and void models for acceleration*, *Class.Quant.Grav.* **28** (2011) 164005, [arXiv:1105.0909].

[203] J. P. Zibin, *Can decaying modes save void models for acceleration?*, *Phys.Rev.* **D84** (2011) 123508, [arXiv:1108.3068].

[204] T. Clifton, C. Clarkson, and P. Bull, *The isotropic blackbody CMB as evidence for a homogeneous universe*, arXiv:1111.3794.

[205] A. D. Linde, D. A. Linde, and A. Mezhlumian, *Do we live in the center of the world?*, *Phys.Lett.* **B345** (1995) 203–210, [hep-th/9411111].

[206] G. Lemaitre, *The expanding universe*, *Gen.Rel.Grav.* **29** (1997) 641–680.

[207] R. C. Tolman, *Effect of imhomogeneity on cosmological models*, *Proc.Nat.Acad.Sci.* **20** (1934) 169–176.

[208] H. Bondi, *Spherically symmetrical models in general relativity*, *Mon.Not.Roy.Astron.Soc.* **107** (1947) 410–425.

[209] B. A. Bassett and R. Hlozek, *Baryon Acoustic Oscillations*, arXiv:0910.5224.

[210] C. Alcock and B. Paczynski, *An evolution free test for non-zero cosmological constant*, *Nature* **281** (1979) 358–359.

[211] E. A. Kazin, A. G. Sanchez, and M. R. Blanton, *Improving measurements of H(z) and Da(z) by analyzing clustering anisotropies*, *Mon.Not.Roy.Astron.Soc.* **419** (2012) 3223–3243, [arXiv:1105.2037].

[212] P. D. Lasky and K. Bolejko, *The effect of pressure gradients on luminosity distance - redshift relations*, *Class.Quant.Grav.* **27** (2010) 035011, [arXiv:1001.1159].

[213] V. Marra and M. Paakkonen, *Exact spherically-symmetric inhomogeneous model with n perfect fluids*, *JCAP* **1201** (2012) 025, [arXiv:1105.6099].

[214] M. Doran and M. Lilley, *The Location of CMB peaks in a universe with dark energy*, *Mon.Not.Roy.Astron.Soc.* **330** (2002) 965–970, [astro-ph/0104486].

[215] W. Hu, M. Fukugita, M. Zaldarriaga, and M. Tegmark, *CMB observables and their cosmological implications*, *Astrophys.J.* **549** (2001) 669, [astro-ph/0006436].

[216] M. Doran, *CMBEASY: an object oriented code for the cosmic microwave background*, *JCAP* **0510** (2005) 011.

[217] A. Gelman and D. B. Rubin, *Inference from Iterative Simulation Using Multiple Sequences*, *Statist. Sci.* **7** (1992) 457–472.

[218] M. Doran and C. M. Mueller, *Analyze This! A Cosmological constraint package for CMBEASY*, *JCAP* **0409** (2004) 003, [astro-ph/0311311].

[219] L. M. Krauss and B. Chaboyer, *Age Estimates of Globular Clusters in the Milky Way: Constraints on Cosmology*, *Science* **299** (2003) 65–70.

[220] H. Akaike, *A new look at the statistical model identification*, *IEEE Transactions on Automatic Control* **16 (6):716–723** (1974).

[221] G. Schwarz., *Estimating the dimension of a model*, *Annals of Statistics* **6 (2):461–464** (1978).

[222] C. Clarkson, B. Bassett, and T. H.-C. Lu, *A general test of the Copernican Principle*,

Phys.Rev.Lett. **101** (2008) 011301, [arXiv:0712.3457].

[223] A. B. Belloso, J. Garcia-Bellido, and D. Sapone, *A parametrization of the growth index of matter perturbations in various Dark Energy models and observational prospects using a Euclid-like survey*, *JCAP* **1110** (2011) 010, [arXiv:1105.4825].

[224] M. Beltran, J. Garcia-Bellido, J. Lesgourgues, A. R. Liddle, and A. Slosar, *Bayesian model selection and isocurvature perturbations*, *Phys.Rev.* **D71** (2005) 063532, [astro-ph/0501477].

[225] K. Bolejko, M.-N. Celerier, and A. Krasinski, *Inhomogeneous cosmological models: Exact solutions and their applications*, *Class.Quant.Grav.* **28** (2011) 164002, [arXiv:1102.1449].

[226] J. Grande and L. Perivolaropoulos, *Generalized LTB model with Inhomogeneous Isotropic Dark Energy: Observational Constraints*, *Phys.Rev.* **D84** (2011) 023514, [arXiv:1103.4143].

[227] J. C. Bueno Sanchez and L. Perivolaropoulos, *Topological Quintessence*, *Phys.Rev.* **D84** (2011) 123516, [arXiv:1110.2587].

[228] M. Roos, *Quintessence-like Dark Energy in a Lemaître-Tolman-Bondi Metric*, arXiv:1107.3028.

[229] V. Marra, M. Paakkonen, and W. Valkenburg, *Bias on w from large-scale structure*, arXiv:1203.2180.

[230] M. Visser, *Sakharov's induced gravity: A modern perspective*, *Mod. Phys. Lett.* **A17** (2002) 977–992, [gr-qc/0204062].

[231] T. Jacobson, *Thermodynamics of space-time: The Einstein equation of state*, *Phys. Rev. Lett.* **75** (1995) 1260–1263, [gr-qc/9504004].

[232] T. Padmanabhan, *Thermodynamical Aspects of Gravity: New insights*, *Rept. Prog. Phys.* **73** (2010) 046901, [arXiv:0911.5004].

[233] E. P. Verlinde, *On the Origin of Gravity and the Laws of Newton*, arXiv:1001.0785.

[234] T. Padmanabhan, *Equipartition of energy in the horizon degrees of freedom and the emergence of gravity*, arXiv:0912.3165.

[235] T. Padmanabhan, *Why Does the Universe Expand ?*, arXiv:1001.3380.

[236] M. Li and Y. Wang, *Quantum UV/IR Relations and Holographic Dark Energy from Entropic Force*, *Phys. Lett.* **B687** (2010) 243–247, [arXiv:1001.4466].

[237] R.-G. Cai, L.-M. Cao, and N. Ohta, *Friedmann Equations from Entropic Force*, *Phys. Rev.* **D81** (2010) 061501, [arXiv:1001.3470].

[238] U. H. Danielsson, *Entropic dark energy and sourced Friedmann equations*, arXiv:1003.0668.

[239] A. Sheykhi, *Entropic Corrections to Friedmann Equations*, arXiv:1004.0627.

[240] R.-G. Cai, L.-M. Cao, and Y.-P. Hu, *Hawking Radiation of Apparent Horizon in a FRW Universe*, *Class. Quant. Grav.* **26** (2009) 155018, [arXiv:0809.1554].

[241] G. Dvali and M. S. Turner, *Dark energy as a modification of the Friedmann equation*, astro-ph/0301510.

[242] W. J. Percival *et. al.*, *Baryon Acoustic Oscillations in the Sloan Digital Sky Survey Data Release 7 Galaxy Sample*, *Mon. Not. Roy. Astron. Soc.* **401** (2010) 2148–2168, [arXiv:0907.1660].

[243] D. A. Easson, P. H. Frampton, and G. F. Smoot, *Entropic Inflation*, arXiv:1003.1528.

[244] D. A. Easson, P. H. Frampton, and G. F. Smoot, *Entropic Accelerating Universe*, arXiv:1002.4278.

[245] C. M. Muller, *Cosmological bounds on the equation of state of dark matter*, *Phys. Rev.* **D71** (2005) 047302, [astro-ph/0410621].

[246] R. Casadio and A. Gruppuso, *CMB acoustic scale in the entropic accelerating universe*, arXiv:1005.0790.

[247] A. W. Peet, *TASI lectures on black holes in string theory*, hep-th/0008241.

[248] S. Carlip, *Black Hole Entropy and the Problem of Universality*, arXiv:0807.4192.

[249] L. Modesto and A. Randono, *Entropic corrections to Newton's law*, arXiv:1003.1998.

[250] Y. Zhang, Y. gui Gong, and Z.-H. Zhu, *Modified gravity emerging from thermodynamics and holographic principle*, arXiv:1001.4677.

[251] A. Sheykhi and S. H. Hendi, *Power-Law Entropic Corrections to Newton's Law and Friedmann Equations From Entropic Force*, arXiv:1011.0676.

[252] M. Doran, *CMBEASY:: an Object Oriented Code for the Cosmic Microwave Background*, *JCAP* **0510** (2005) 011, [astro-ph/0302138].

[253] A. Lue, R. Scoccimarro, and G. Starkman, *Differentiating between Modified Gravity and Dark Energy*, *Phys. Rev.* **D69** (2004) 044005, [astro-ph/0307034].

[254] N. Voje Johansen and F. Ravndal, *On the discovery of Birkhoff's theorem*, *Gen. Rel. Grav.* **38** (2006) 537–540, [physics/0508163].

[255] A. Albrecht and C. Skordis, *Phenomenology of a realistic accelerating universe using only Planck-scale physics*, *Phys. Rev. Lett.* **84** (2000) 2076–2079, [astro-ph/9908085].

[256] T. Koivisto and D. F. Mota, *Gauss-Bonnet quintessence: Background evolution, large scale structure and cosmological constraints*, *Phys. Rev.* **D75** (2007) 023518, [hep-th/0609155].

[257] T. Koivisto and D. F. Mota, *Cosmology and astrophysical constraints of Gauss-Bonnet dark energy*, *Phys. Lett.* **B644** (2007) 104–108, [astro-ph/0606078].

[258] T. Koivisto, *Growth of perturbations in dark matter coupled with quintessence*, *Phys.Rev.* **D72** (2005) 043516.

[259] C. Armendariz-Picon, V. F. Mukhanov, and P. J. Steinhardt, *Essentials of k-essence*, *Phys. Rev.* **D63** (2001) 103510, [astro-ph/0006373].

[260] E. J. Copeland, N. J. Nunes, and F. Rosati, *Quintessence models in supergravity*, *Phys. Rev.* **D62** (2000) 123503, [hep-ph/0005222].

[261] M. Milgrom, *Bimetric MOND gravity*, *Phys.Rev.* **D80** (2009) 123536, [arXiv:0912.0790].

[262] M. Clayton and J. Moffat, *Dynamical mechanism for varying light velocity as a solution to cosmological problems*, *Phys.Lett.* **B460** (1999) 263–270.

[263] M. A. Clayton and J. W. Moffat, *A scalar-tensor cosmological model with dynamical light velocity*, *Phys. Lett.* **B506** (2001) 177–186, [gr-qc/0101126].

[264] V. Faraoni and S. Nadeau, *The (pseudo)issue of the conformal frame revisited*, *Phys. Rev.* **D75** (2007) 023501, [gr-qc/0612075].

[265] A. Y. Kamenshchik, U. Moschella, and V. Pasquier, *An alternative to quintessence*, *Phys. Lett.* **B511** (2001) 265–268, [gr-qc/0103004].

[266] T. S. Koivisto, *Disformal quintessence*, arXiv:0811.1957.

[267] R. R. Caldwell, *A Phantom Menace?*, *Phys. Lett.* **B545** (2002) 23–29, [astro-ph/9908168].

[268] T. Padmanabhan, *Accelerated expansion of the universe driven by tachyonic matter*, *Phys. Rev.* **D66** (2002) 021301, [hep-th/0204150].

[269] T. Padmanabhan and T. R. Choudhury, *Can the clustered dark matter and the smooth dark energy arise from the same scalar field?*, *Phys. Rev.* **D66** (2002) 081301, [hep-th/0205055].

[270] T. Chiba, T. Okabe, and M. Yamaguchi, *Kinetically driven quintessence*, *Phys. Rev.* **D62** (2000) 023511, [astro-ph/9912463].

[271] F. Piazza and S. Tsujikawa, *Dilatonic ghost condensate as dark energy*, *JCAP* **0407** (2004) 004, [hep-th/0405054].

[272] E. J. Copeland, A. R. Liddle, and D. Wands, *Exponential potentials and cosmological scaling solutions*, *Phys. Rev.* **D57** (1998) 4686–4690, [gr-qc/9711068].

[273] R. L. Arnowitt, S. Deser, and C. W. Misner, *Dynamical Structure and Definition of Energy in General Relativity*, *Phys.Rev.* **116** (1959) 1322–1330.

[274] C.-P. Ma and E. Bertschinger, *Cosmological perturbation theory in the synchronous and conformal Newtonian gauges*, *Astrophys. J.* **455** (1995) 7–25, [astro-ph/9506072].

[275] J. chan Hwang and H. Noh, *Classical evolution and quantum generation in generalized gravity theories including string corrections and tachyon: Unified analyses*, *Phys. Rev.* **D71** (2005) 063536, [gr-qc/0412126].

[276] J. Magueijo, *New varying speed of light theories*, *Rept.Prog.Phys.* **66** (2003) 2025.

[277] P. Brax, *Lorentz Invariance Violation in Modified Gravity*, *Phys.Lett.* **B712** (2012) 155–160, [arXiv:1202.0740].

[278] C. de Rham and G. Gabadadze, *Generalization of the Fierz-Pauli Action*, *Phys.Rev.* **D82** (2010) 044020, [arXiv:1007.0443].

[279] D. Bettoni, S. Liberati, and L. Sindoni, *Extended LCDM: generalized non-minimal coupling for dark matter fluids*, *JCAP* **1111** (2011) 007, [arXiv:1108.1728].

[280] J. Cembranos, A. Dobado, and A. L. Maroto, *Dark geometry*, *Int.J.Mod.Phys.* **D13** (2004) 2275–2280, [hep-ph/0405165].

[281] J. Cembranos, A. Dobado, and A. L. Maroto, *Cosmological and astrophysical limits on brane fluctuations*, *Phys.Rev.* **D68** (2003) 103505, [hep-ph/0307062].

[282] J. Cembranos, A. Dobado, and A. L. Maroto, *Brane world dark matter*, *Phys.Rev.Lett.* **90** (2003) 241301, [hep-ph/0302041].

[283] M. Andrews, K. Hinterbichler, J. Khoury, and M. Trodden, *Instabilities of Spherical Solutions with Multiple Galileons and SO(N) Symmetry*, *Phys.Rev.* **D83** (2011) 044042, [arXiv:1008.4128].

[284] T. Clemson, K. Koyama, G.-B. Zhao, R. Maartens, and J. Valiviita, *Interacting Dark Energy – constraints and degeneracies*, *Phys.Rev.* **D85** (2012) 043007, [arXiv:1109.6234].

[285] X. ming Chen, Y. Gong, E. N. Saridakis, Y. Gong, and E. N. Saridakis, *Time-dependent interacting dark energy and transient acceleration*, arXiv:1111.6743.

[286] **Particle Data Group** Collaboration, K. Nakamura *et. al.*, *Review of particle physics*, *J.Phys.G* **G37** (2010) 075021. *http://pdg.lbl.gov*.

[287] D. F. Mota and D. J. Shaw, *Evading Equivalence Principle Violations, Cosmological and other Experimental Constraints in Scalar Field Theories with a Strong Coupling to Matter*, *Phys.Rev.* **D75** (2007) 063501, [hep-ph/0608078].

[288] J. Noller, *Derivative Chameleons*, arXiv:1203.6639.

[289] R. M. Wald, *General Relativity*, .

[290] J. G. Williams, S. G. Turyshev, and D. H. Boggs, *Progress in lunar laser ranging tests of*

relativistic gravity, *Phys.Rev.Lett.* **93** (2004) 261101, [gr-qc/0411113].

[291] P. Brax, C. Burrage, and A.-C. Davis, *Shining Light on Modifications of Gravity*, arXiv:1206.1809.

[292] C. van de Bruck and G. Sculthorpe, *Modified Gravity and the Radiation Dominated Epoch*, arXiv:1210.2168.

[293] N. Metropolis, A. W. Rosenbluth, M. N. Rosenbluth, A. H. Teller, and E. Teller, *Equation of state calculations by fast computing machines*, *J. Chem. Phys.* **21** (1953) 1087–1092.